Investigating Translaminar Signaling from Layer 5 Pyramidal Subpopulations to Layer 2/3 in Somatosensory Cortex.

Alexander von Klemperer



Thesis submitted for the degree of Doctor of Philosophy

Oriel College

University of Oxford

Hilary term 2021

Page intentionally left blank

Abstract

Information processing in the mammalian cortex is achieved via a precise arrangement of synaptic connections between different neuronal subtypes. The excitatory neurons of the cortex are arranged in a laminar manner across six layers and form specific intralaminar and translaminar connections with one another. In addition, these excitatory neurons interact with a series of inhibitory interneuron subtypes, such that the relative levels and timing of excitatory and inhibitory synaptic transmission determine how information is processed by the cortical network. This thesis examines the translaminar signaling from layer 5 (L5) to layer 2/3 (L2/3) of cortex. Considered the principal output layer, L5 is populated by intratelencephalic (IT) and pyramidal tract (PT) pyramidal neurons, which form long-range projections to other cortical and subcortical regions, respectively. These long-range axons of L5 pyramidal neurons also branch locally and form ascending collaterals that extend to more superficial layers, including L2/3. An unanswered question in the field, is what sorts of translaminar signals do these local collaterals deliver.

I have used the mouse somatosensory cortex in order to address this question. In the first series of experiments, transgenic mice expressing the optogenetic activator, channelrhodopsin-2 (ChR2), were used to stimulate a non-specific population of L5 pyramidal neurons. This was shown to elicit both monosynaptic excitation and disynaptic inhibition within L2/3, and to modulate the action potential activity of L2/3 pyramidal neurons *in vitro* and *in vivo*. I then used retrograde labelling strategies in order to distinguish between IT and PT L5 pyramidal neurons, revealing that the long-range target of the L5 neuron is associated with morphological differences in its local ascending collaterals. To investigate whether the functional consequences, I used a retrograde viral system to deliver ChR2 to each of the projection-defined L5 subtypes. Patch clamp recordings revealed that IT L5 neurons evoked robust excitation but little inhibition within L2/3. In contrast, PT L5 neurons elicited significant levels of synaptic inhibition, which was shown to result from the selective targeting of L2/3 parvalbumin-expressing interneurons. Finally, I was able to demonstrate that this differential recruitment of excitation and inhibition by the L5 subtypes results in opposing modulatory effects upon L2/3 pyramidal neuron activity *in vitro* and during sensory-driven input *in vivo*.

The work supports growing evidence that L5 plays a significant role in modulating ongoing local cortical activity. It also suggests that projection-defined L5 subpopulations provide opposing translaminar signals to L2/3, which could be important for sensory processing, sensory-motor integration and synaptic plasticity.

Dedicated to Nivi, my parents and Nick without whose support this never would have been possible.

Statement of originality

I declare that the work in this thesis is entirely my own and I clearly acknowledge where others have made contributions. David Lohse and Alexios Vourvoukelis, working under my supervision as masters students, assisted with immunohistochemistry and analysis of imaged tissue used in Chapter 4. Alexios Vourvoukelis also assisted with the collection and processing of electrophysiological recordings made in Chapter 4. Kashif Mahfooz assisted with the collection of electrophysiology recordings used in Chapter 3 and Chapter 5. Joram van Rheede assisted with the collection of *in vivo* recordings and development of data analysis pipeline in Chapter 6. This work has not been submitted for any other degree or qualification at this or any other institution.

Acknowledgments

I would first like to express my immense gratitude towards my supervisor Colin. I have learnt such an incredible amount from him both academically as a scientific role model but also as a mentor. His infectious enthusiasm for science, remarkable insights and incredible generosity with time will always be appreciated. I will forever be indebted for the support he has shown me. I would also like to thank my co-supervisor Tommas for sharing his knowledge, skill and expertise with me.

I would also like to thank the entire Akerman lab, whose members both past and present truly are a special group of people. Everyone in the lab was always willing to help with the development of ideas, and were always willing sharing a wealth of experience. Working with them made every day a fun experience that I looked forward to. The lab zoom quizzes and Christmas dinners helped to lighten what was an otherwise bleak 2020. An additional thank you to the members of the Magill and Somogyi labs for the shared equipment and expertise.

I would like to thank my funders, both the Rhodes trust and the Clarendon scholarship. It was the financial support of these scholarships which made this experience possible. Through the social support of the Rhodes scholarship that I was able to meet a number of my closest friends in Oxford.

No work in this thesis would have been possible without the hard work and dedication of the department of pharmacology support staff. They truly kept everything running and effortlessly made up for any shortfall in my own organization and logistic skills.

A special thank you to the members of the Biomedical service animal care team. It was always incredibly reassuring knowing that our mice were being cared for by such a compassionate and professional team of people.

Both Merton and Oriel colleges provided me with a college base for my time in Oxford. The latter employed me as a Junior Dean, a position in which I worked with the wonderful college welfare team. Thank you to the other junior deans and to Oliver for your camaraderie in what could be an emotionally tricky job.

My friends in Oxford truly made this a special experience. Doing everything together, from college dinners, early morning runs, workouts, travel and exploring the continent has enriched the last four years beyond belief. Support too, through Zoom writing and debriefing sessions significantly improved the thesis writing time.

Finally I cannot begin to express my thanks for the love and support of my family and Nivi. Without you, there is no way that I would have been able to reach the point of submitting this thesis. The silly pups, Gizmo and Skye also deserve special mention for keeping me sane while writing up in social isolation.

Table of Contents

Abstract I
Statement of originality IV
Acknowledgments V
List of figures 5
List of abbreviations 7
Chapter 1 : Introduction 9
General organization of mammalian neocortex 10
The laminar structure of cortex 11
The columnar structure of cortex 12
The mouse barrel cortex as a model of cortical organization 13
Decoding fine scale excitatory columnar connectivity 17
General patterns of Excitatory connectivity 18
Understanding cortical circuitry through cell classification 21
IT and PT projection-defined layer 5 pyramidal neurons 27
Inhibition in cortex 31
Excitatory and inhibitory interplay in cortical circuits. 34
How somatosensory information is processed by these circuits 39
Aims of the thesis 41
Chapter 2 : Materials and methods 43
General strategies for the restricted expression of genetic tools 43
Animals and General strategy for the restriction of genetic tools 44
Viruses and plasmids 46
In utero electroporation 47
Postnatal injections 47
Acute brain slice preparation and in vitro recording conditions 49
Analysis of in vitro electrophysiological recordings 51
Histological analyses 52
Image acquisition and analysis 53
In vivo preparation and recording conditions 54
In vivo stimulus protocols and data analysis 55
Statistics 57
Chapter 3 : The influence of layer 5 input upon layer 2/3 of mouse somatosensory cortex 59
Introduction 59

Aims 61
Results 61
Discussion 72
Chapter 4 : Examining axon ascending collaterals from projection-defined L5 pyramidal neuron subtypes 77
Introduction 77
Aims 80
Results 80
Discussion 93
Using retrograde labelling to target projection-defined subtypes of L5 pyramidal neurons 93
IT and PT L5 pyramidal neurons show morphological differences in their axon ascending collaterals 94
Validating retrograde viral tools for functional studies of projection-defined L5 subtypes in S1 96
Chapter 5 : Projection-defined L5 subtypes differentially recruit local inhibitory circuits in L2/3 99
Introduction 99
Aims 101
Results 101
Discussion 119
Functional differences in the ascending connectivity of projection-defined L5 subtypes 119
Ascending collaterals from L5 pyramidal neurons differentially recruit local L2/3 interneurons 121
Ascending collaterals from L5 PT^{thal} pyramidal neurons target PV interneurons in L2/3 122
Chapter 6 : Functional effects of ascending input from projection-defined L5 subtypes to l2/3 125
Introduction 125
Aims 128
Results 128
Discussion 138
Chapter 7 : Discussion 143
Summary of the main findings 143
Methodological considerations 145
Acute slice electrophysiology 145
The use of ChR2 to stimulate specific neuronal subpopulations 146
In vivo electrophysiology 150
Implications of the findings 152
Implications for our understanding of L5 local circuitry 152
How might local L5 circuitry be established? 155

Potential functions for distinct translaminar L5 to L2/3 signals 157
Signal processing implications for distinct translaminar L5 to L2/3 signals 158
Parallel information processing streams with distinct translaminar L5 to L2/3 signals 159
Distinct translaminar L5 to L2/3 communication as 'feedback' signals 162
Concluding remarks 165
Chapter 8 : References 167

Page intentionally left blank

List of figures

Figure 1.1 Organization of the mouse barrel cortex 6
Figure 1.2 Cortical information is processed through stereotypical connections between neuronal subtypes. 19
Figure 1.3 IT and PT pyramidal neurons in L5 are distinct neuronal subtypes. 28
Figure 1.4 Cortical excitation and inhibition is matched but can result in different E/I ratios for components of cortical circuitry. 38
Figure 2.1 General strategies for the restricted expression of genetic tools. 45
Figure 3.1 Transgenic mouse model for investigating the effects of L5 input to L2/3 in primary somatosensory cortex 62
Figure 3.3 L5 elicits monosynaptic excitation and disynaptic inhibition in L2/3 pyramidal neurons 64
Figure 3.4 L5 inputs modulate the spiking of L2/3 pyramidal neurons 66
Figure 3.5 Examining the effects of L5 input upon whisker-evoked L2/3 responses 69
Figure 3.6. L5 has a net inhibitory effect upon whisker-evoked L2/3 responses 71
Figure 4.1 Using retrograde labelling to target subpopulations of L5 pyramidal neurons 81
Figure 4.2 Long-range projection-defined L5 pyramidal neurons exhibit distinct electrophysiological characteristics 84
Figure 4.3 Axonal reconstructions of target-defined L5 pyramidal neurons reveal local collaterals ascending to supragranular layers. 88
Figure 4.4 The branching and bouton density of local ascending collaterals suggest functional differences between L5 subpopulations 89
Figure 4.5. Retrograde AAVs allow for the delivery of genetic tools to projection-defined L5 pyramidal neurons. 91
Figure 4.6 Retrograde AAVs restrict ChR2 expression to L5 pyramidal neuron subpopulations defined by their long-range projections 92
Figure 5.1 PT L5 pyramidal neurons recruit L2/3 inhibitory circuits more efficiently than IT L5 pyramidal neurons 103
Figure 5.2 L2/3 responses reflect input from local L5 pyramidal neurons 106
Figure 5.3 L5 pyramidal neurons recruit L2/3 inhibitory interneurons 108
Figure 5.4 Recording from of L2/3 PV-expressing interneurons 110
Figure 5.5 Electrophysiological and connectivity characteristics of L2/3 PV-expressing interneurons 111
Figure 5.6 PT^{thal} L5 pyramidal neurons provide greater excitatory drive to L2/3 PV-expressing interneurons 113
Figure 5.7 Recording from L2/3 SST-expressing interneurons 115
Figure 5.8 Electrophysiological and connectivity characteristics of L2/3 SST-expressing interneurons 116
Figure 5.9 L5 pyramidal neurons provide little excitatory drive to L2/3 SST-expressing interneurons 118
Figure 6.1 Ascending collaterals from IT and PT L5 pyramidal neurons generate distinct E/I dynamics in L2/3 127
Figure 6.2 Ascending collaterals from IT and PT L5 pyramidal neurons exert opposing effects on L2/3 pyramidal neuron spiking 132
Figure 6.3 Evaluating the effects of projection-defined L5 pyramidal subtypes upon whisker-evoked L2/3 spiking activity 134
Figure 6.4 IT L5 pyramidal neurons augment concurrent whisker input to L2/3 136
Figure 6.5 PT L5 pyramidal neurons inhibit subsequent whisker input to L2/3 137
Figure 7.1 PT and IT L5 pyramidal neurons deliver opposing E/I signals to L2/3 154

Page intentionally left blank

List of abbreviations

Acronym	Expanded
E/E+I	Peak EPSC/(Peak EPSC+IPSC) an estimate of Excitation/Inhibition ratio.
EPSC	Excitatory Post synaptic Current
EPSP	Excitatory Post synaptic Potential
IPSP	Inhibitory Post synaptic potential.
Kyn	Kynurenic acid
L1-6	Cytoarchitectonic cortical Layers 1-6
LFP	Local Field potential.
PSTH	Peristimulus Time Histogram
PT	Pyramidal tract type Layer 5 pyramidal neurons
PT^{thal}	Pyramidal tract type Layer 5 pyramidal neurons projecting to ipsilateral Thalamus.
Pyr	Pyramidal neurons.
rAAV2retro	Adeno Associated virus 2 engineered for retrograde transport
SST	Somatostatin expressing inhibitory interneurons.
Vm	Membrane potential measured in mV
Im	Membrane injected current measured in pA.
PTX	Picrotoxin
[supra-]granular	Above and inside the L4 (L1-4)
Ai32	A mouse line in which Cre- inducible Channelrhodopsin is expressed in all neocortical neurons.
Ai9	A mouse line in which Cre- inducible TdTomato reporter is expressed in all neocortical neurons.
AMPA	α-amino-3-hydroxy-5-methyl-4-isoxazolepropionic acid
AP	Action potential
ChR2	Channelrhodopsin
Cre	Cre recombinase
DAP	Depolarizing After potential.
fAHP	fast After Hyperpolarizing Potential
Floxed-ChR2	Cre recombinase dependent Channelrhodopsin 2
GABA	Gamma aminobutyric Acid
Granular	Inside the cortical L4
Infragranular	Below cortical L4 (L5+6)
IPSC	Inhibitory Post synaptic Current
IT	Intratelencephalic type Layer 5 pyramidal neurons
IT^{contra}	Intratelencephalic type Layer 5 pyramidal neurons projecting to contralateral cortical areas
IT^{ipsi}	Intratelencephalic type Layer 5 pyramidal neurons projecting to ipsilateral cortical areas
IUE	In Utero Electroporation

LED	Light Emitting Diode
M1	Primary Motor cortex
PV	Parvalbumin expressing inhibitory interneurons.
RBP4-Cre	A transgenic mouse line which expresses Cre exclusively in cortical Layer 5 pyarmidal neurons.
S1	Primary Somatosensory cortex
Supragranular	Above cortical L4, (L1-3)
Thal	Thalamus

Chapter 1 : Introduction

Understanding the neural and circuit level principles that underpin the functions of cortex is a fundamental goal of neuroscience. It has long been understood that key to cortical information processing is the arrangement of fine scale synaptic connectivity between multiple neuronal cell types. To provide the necessary context to this thesis, I will first introduce our general understanding of cortical organization. I will explain how the columnar and laminar organization of cortex are thought to divide into fundamental units of computation, and why the mouse barrel cortex has become a popular experimental model to interrogate questions regarding cortical processing. I will outline how our understanding of the broad patterns of excitatory connectivity emerged and led to the influential idea of a 'canonical' circuit for information flow through cortex. I will then explore how advances in methods over the last 20 years have revealed increasing diversity and complexity in terms of cortical neuron types and their synaptic connectivity patterns.

Given the focus of this thesis, I will pay particular attention to the intratelencephalic (IT) and pyramidal tract (PT) projection neurons found in layer 5 (L5) of cortex. These excitatory neurons are considered to be the primary output neurons of cortex as they send long-range axons to other regions of the brain, acting as the relay for information that leaves a cortical column. I will explain how these L5 neuronal subtypes differ morphologically and functionally, and will describe the fact that these neurons also form local synaptic connections with neurons within the same region of cortex, via axonal collaterals that branch from their long-range axonal projections. These local collaterals represent a route for the information that is being delivered to other regions of the brain, to be simultaneously delivered to local neurons in different cortical layers. The experimental work within this thesis will examine translaminar signaling via these local collaterals from L5 to layer 2/3 (L2/3).

To understand the impact of these translaminar signals, it is also necessary that I introduce the role of inhibitory interneurons in cortical circuits. Our understanding of cortical interneurons is another area that has advanced remarkably over the last 20 years and I will review our current understanding of the diversity and function of cortical interneurons neurons, including how the interplay between excitatory and inhibitory synaptic signals is important for cortical computations. Having established that important questions remain unanswered regarding the nature of translaminar signaling from L5 to L2/3, I will outline the experimental aims of this thesis.

General organization of mammalian neocortex

The cerebral cortex is one of the most prominent features of the mammalian brain and is concerned with the processing of information, cognition and behavior. As with other parts of the central nervous system, the cortex has been classified into distinct regions that exhibit functional specificity. This was first demonstrated empirically by the separate work of Paul Broca, Carl Wernicke and Hughlings Jackson. The former two neurologists studied how damage to specific regions of cortex could lead to disruption of language and thus expressive or receptive aphasia (Berker et al., 1986; Broca, 1861; Wernicke, 1969). Whereas Hughlings Jackson was an epileptologist who demonstrated that when epileptic activity spreads across cortex, corresponding seizure activity spreads to different muscle groups in what is now known as a 'Jacksonian march' (Jackson, 1867, 1868; York III & Steinberg, 2011).

The functional specification of cortical areas appears to be conserved across mammals (Kaas, 2011) and can be broadly subdivided as follows: sensory areas, motor areas and association areas. Even at this broad level, there are already clear differences in neuronal connectivity that correlates with functional specification. Sensory areas of cortex receive input from sensory receptors in the peripheral nervous system via thalamic nuclei. Subsequent stepwise processing of these signals through primary, secondary and higher sensory cortical areas is thought to underlie the construction of a sensory percept.

In contrast, motor areas of cortex characteristically have long-range outputs to motor neurons in the spine, which convey signals to muscular motor units and allow an action to be performed. Primary motor cortex receives input signals from surrounding secondary and associative motor regions, which are involved in the planning and coordinating of motor actions. Meanwhile, association areas of cortex receive a wide range of inputs from surrounding cortex to enable higher cognitive functions, such as planning or decision making.

A fundamental challenge in neuroscience has been to understand the building blocks that allow functionally distinct regions of cortex to process such apparently different types of information. Ramon y Cajal is credited as the first to propose that neurons act as discrete units, but with highly specific interconnection that could function as a 'network' (Glickstein, 2006; y Cajal, 1891, 1911). Meanwhile, the first links between functional specification and cytoarchitectonic structure were made by Brodmann, who recognized differences in the number and shapes of neurons in different cortical areas. He was able to generate a map of fifty two 'areas' that roughly correspond to functional specialization and is still used today (Brodmann, 1907, 1909, 1914).

The laminar structure of cortex

Whilst there may be differences between the numbers and proportions of neuronal subtypes in cortical regions, there are also general organizational principles. The mammalian neocortex is predominantly composed of six layers (Adesnik & Naka, 2018; Brodmann, 1907, 1914; Guy & Staiger, 2017; Kaas, 2011; Kandel et al., 2013). This laminar structure is defined broadly by characteristic density, size and distribution of excitatory neuronal subtypes. The most superficial layer, layer 1 (L1), is almost devoid of cell bodies aside from infrequent inhibitory neurons, and mainly consists of the axonal and dendritic projections of neurons found in other layers. Layer 2 and 3 (L2/3) are often grouped together and consist of highly numerous medium sized pyramidal excitatory neurons(van Aerde & Feldmeyer, 2015).

These L2/3 pyramidal neurons are one of the most numerous cell types in the brain and provide interareal connections both within the same hemisphere, and to the opposite hemisphere via the corpus callosum(Aronoff et al., 2010; Gilbert & Kelly, 1975; Wise & Jones, 1977). Layer 4 (L4) consists of densely packed spiny stellate excitatory neurons and is often referred to as 'granular cortex'(Lübke et al., 2000). More superficial layers are therefore referred to as 'supragranular', whilst deeper layers are referred to as 'infragranular'(Wise & Jones, 1977). L4 is often thought to be the principal sensory input layer, as it is most conspicuous in sensory cortical regions and is strongly innervated by thalamocortical projections from so-called 'first order' thalamic nuclei that convey sensory information(Michael Armstrong-James & Fox, 1987; Chmielowska et al., 1989; Sermet et al., 2019; Woolsey & Van der Loos, 1970). Layer 5 (L5) is often considered the principal output layer of cortex(Feldmeyer, 2012; van Aerde & Feldmeyer, 2015). It consists of characteristic large pyramidal neurons whose long apical dendrites extend radially through other layers of cortex(Le Bé et al., 2006; Ramaswamy & Markram, 2015; Wang et al., 2018). These neurons have long-range axonal projections either to other cortical regions or to subcortical structures such as thalamus, striatum, midbrain nuclei or the spinal cord (Deschênes et al., 1994; Feldmeyer, 2012; Gilbert & Kelly, 1975; Hattox & Nelson, 2007a; Killackey et al., 1989; Wise & Jones, 1977). Finally L6 consists of a diverse group of excitatory neurons that project to both thalamus and other cortical regions(Gilbert & Kelly, 1975; Lam & Sherman, 2010; Wise & Jones, 1977).

The columnar structure of cortex

Cortex is also organized into multiple vertical 'columns', which are oriented orthogonal to the pial surface and span the layers. Columns were first described by Vernon Mountcastle and have since been proposed as a basic unit of cortical computation(Mountcastle, 1957, 1997). The initial evidence came from Mountcastle's experiments testing responsiveness to distinct somatosensory stimuli, where he observed that neurons would selectively respond to only one type of stimulus. These responsive neurons were arranged in vertical columns that were perpendicular to the brains surface and included all cortical layers

(Mountcastle, 1957). These ideas were extended by the seminal work of Hubel and Weisel in visual cortex (Hubel & Wiesel, 1959, 1977). They revealed that groups of neurons arranged perpendicular to the pial surface had similar response properties to simple visual stimuli and that recording from surrounding regions showed a systematic variation in both orientation tuning and ocular dominance. In contrast, neurons arranged parallel to the pial surface differed significantly in their stimulus selectivity. The finding that neurons with similar responses are organised into columns has been replicated in multiple studies and appears to be a general feature across species (Mountcastle, 1997). One notable exception to this is the rodent visual cortex, in which, the spatial layout of similarly selective neurons shows little clear organisation, often termed a 'salt and pepper distribution'(Bonin et al., 2011; Espinosa & Stryker, 2012).

The mouse barrel cortex as a model of cortical organization

A relatively small number of experimental models have become the mainstay for studying the organizational principles of cortex and the rodent primary somatosensory cortex (S1) remains one of the best studied systems. The importance of this sensory modality for the rodent, plus the clear structural and functional correspondence between the sensory periphery and cortical representations, has made this an attractive model. And, when combined with the development of transgenic mouse technologies, neuroscientists have been able to apply an increasing array of tools to probe cortical circuitry (Madisen et al., 2012).

Rodent S1 receives input from peripheral somatosensory receptors, which then undergoes local filtering and transformation before being passed to 'higher' cortical regions such as secondary somatosensory cortex (S2) (Aronoff et al., 2010). S1 is organized in a highly somatotopic manner, such that defined regions of S1 correlate with sensory input from specific contralateral body parts, and the region referred to as 'barrel cortex' receives input from the contralateral whiskers (**Fig. 1.1A**).

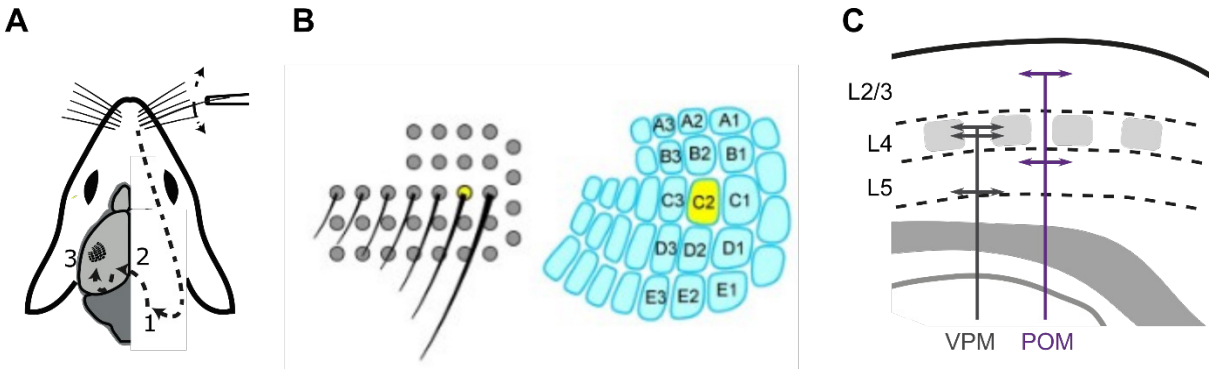


Figure 1.1 Organization of the mouse barrel cortex

(A) Whisker deflection results in activation of mechanoreceptors and the transduced signals are passed to contralateral trigeminal nuclei in the brainstem and spine (1). Neurons in these nuclei synapse onto thalamocortical neurons in thalamic nuclei (2) and these then project to the barrel region of primary somatosensory cortex (S1) (3). **(B)** The barrel cortex is highly somatotopically-organised, with barrels spatially arranged in a manner that corresponds to the whisker from which each barrel receives its principal input. **(C)** The thalamic inputs to barrel cortex are from the ventral posteromedial thalamic nucleus (VPM) and the posterior medial thalamic nucleus (POm). These correspond to the so called lemniscal and paralemniscal pathways and are functionally segregated and interdigitating within S1. Figure modified from (Petersen, 2007).

The thalamorecipient L4 of barrel cortex exhibits distinct 'barrels' (**Fig. 1.1B**) that represent a density of principal neurons around a less dense centre (Van der Loos & Woolsey, 1973; Woolsey & Van der Loos, 1970). In a series of seminal experiments, it was shown that each barrel receives strong input from a single principal whisker (Simons, 1978; Welker, 1971), and that the arrangement of the barrels corresponds somatotopically to the arrangement of whiskers on the whisker pad. Between each barrel is a 'septa', which is less structured and appears to receive more contextual information regarding multiple whisker stimuli (Alloway, 2008).

A feature that has made this region attractive for study is that the radial portion of cortex demarked by each barrel can be considered a column, providing a clearly defined unit in keeping with Mountcastle's definition (Mountcastle, 1957, 1997). Sensory information in the barrel cortex flows from mechanoreceptors in the whisker pad via the trigeminal nerve to synapse onto second order neurons in trigeminal nuclei (Alloway, 2008).

These secondary neurons then target thalamic nuclei, where thalamocortical neurons are stimulated to relay information to the barrel cortex. There are three principal information streams, which are organized in anatomically distinct pathways and convey different sensory information to the cortex. These are the 'lemniscal', 'paralemniscal' and 'extralemniscal' pathways (**Fig. 1.1C**).

The lemniscal pathway arises from whisker sensory afferents that project to the principal and spinal trigeminal nuclei, then thalamocortical neurons in the ventral posteromedial thalamic nucleus (VPM) of the thalamus (Pierret et al., 2000; Veinante et al., 2000). Principal neurons located in L4 barrels and deeper L5 (referred to as L5b) within the barrel column, are highly thalamorecipient from the VPM (Constantinople & Bruno, 2013; Lu & Lin, 1993; Sermet et al., 2019; Wimmer et al., 2010). Throughout this pathway, neurons are organized into structures that convey the somatotopic organization of the whisker inputs, referred to as 'barrelettes' in the principal sensory trigeminal and spinal trigeminal nuclei (P. M. Ma, 1991), 'barreloids' in VPM (Pierret et al., 2000), and 'barrels' in S1 (Woolsey & Van der Loos, 1970).

The paralemniscal pathway in contrast, arises from sensory afferents to the interpolar spinal trigeminal nucleus (M. N. Williams et al., 1994). Neurons in this nucleus then project to the posterior medial thalamic nucleus (POm) (Veinante et al., 2000) and notably the somatic structure of barreloids and barrelettes are absent from this pathway. Within barrel cortex, the POm inputs appear to interdigitate with VPM inputs, specifically targeting more superficial L5 (referred to as L5a) and L2/3, with greatest density of projections in the septa (Audette et al., 2018; Lu & Lin, 1993; Schoonover et al., 2014; Sermet et al., 2019; Zhang & Bruno, 2019). Finally, the extralemniscal pathway originates as a highly somatotopically organized caudal subdivision of the nucleus interpolaris of the spinal trigeminal nucleus, and passes through a ventrolateral portion of the VPM to septal barrel cortex and secondary somatosensory nucleus (Pierret et al., 2000). This pathway has been less studied than the other two, and the following sections will therefore focus on the lemniscal and paralemniscal pathways.

In keeping with the anatomical distinction between lemniscal and paralemniscal pathways, these two information streams are also thought to convey different whisker sensation information. The lemniscal pathway relays information to a specific barrel regarding stimulation of the single principal whisker (M Armstrong-James et al., 1992; Michael Armstrong-James & Fox, 1987; Diamond et al., 1992). Within barrel cortex, the shortest latency responses following stimulation of a single whisker are routed via VPM thalamic inputs to L4 and L5b (M Armstrong-James et al., 1992; Constantinople & Bruno, 2013). Subsequent responses are then seen in other layers and spread to surrounding cortex. The paralemniscal pathway meanwhile, conveys information regarding the movement of multiple surrounding whiskers to a wider group of septal neurons, which therefore have less specific receptive fields (Petersen, 2007).

It should be noted that these two interdigitating streams of information in the barrel cortex provide an interesting example of the interplay between the columnar and laminar organization of cortex. There still exists segregation of information from the lemniscal and paralemniscal pathways in the layers above and below the barrels and septa, despite the lack of clear barrel structures (Shepherd & Svoboda, 2005). There must, however, be embedded circuitry that allows for the integration of these streams and the pyramidal neurons of L2/3 and, in particular, L5 represent plausible candidates to mediate this integration, thanks to their complex dendritic structures that span multiple layers. Following local columnar processing, long-range projection neurons from L2/3 and L5 then pass the sensory information both to other regions of cortex and to subcortical structures. Relevant cortical target structures include ipsilateral S2, contralateral S1 and a strong reciprocal connectivity to primary motor cortex (M1) (Aronoff et al., 2010; Mao et al., 2011; Yamashita et al., 2018). Long-range axonal projections from L5 pyramidal neurons can also target thalamus, including POm (Mease et al., 2016a, 2016b), as well as deeper structures such as trigeminal nuclei, basal pontine and spinal nuclei (Alloway, 2008; Aronoff et al., 2010).

Decoding fine scale excitatory columnar connectivity

Having introduced the significance of regional and columnar organisation of cortex, a major question arises, which is how does laminar (i.e. radial) cortical organisation enable cortex to perform its computations? Decades of work on the nature of sensory perception had suggested that a hierarchical organisation of feedforward connections is computationally very powerful. For instance, evidence from the visual system supported a hierarchical structure in the sense that inputs are first filtered by neurons that carry out simple feature detection, which are then transformed and encoded by more complex neurons (Hubel & Wiesel, 1962). From this backdrop came the idea of a 'canonical circuit' within cortex, comprised of stereotypical feedforward excitatory connections between the different cortical layers(Rodney J Douglas et al., 1989; Rodney J Douglas & Martin, 2004). This was consistent with early evidence for a general model of laminar connectivity in which thalamic input drives sequential, feedforward activity (Gilbert, 1983). First, thalamic inputs project to L4, which in turn outputs to L2/3, then L2/3 projects to L5, and then L5 outputs to other cortical and subcortical regions (M Armstrong-James et al., 1992; Binzegger et al., 2004; R J Douglas & Martin, 1991; Lefort et al., 2009). Whilst this incarnation of the canonical circuit has proved to be overly simplistic, the idea that fine scale circuit motifs underpin cortical computations has remained extremely influential. In this section, I will first introduce the sorts of experimental methods that have been used to describe fine scale cortical circuitry, as these have determined the types of data that have been collected. I will then provide a short review of our current understanding of fine scale cortical circuits, with a focus on S1 and some of the gaps in our knowledge that have motivated the experimental work in this thesis.

Investigations into fine scale cortical connectivity have mainly relied upon three methodological approaches. The earliest intracortical circuits were based on anatomical reconstructions, which either assumed that the axons of pre-synaptic neurons only target the soma of post-synaptic neurons (Gilbert,

1983), or that wherever axons and dendrites overlap, there exists a connection. Whilst axo-dendritic overlap may be necessary, it is not sufficient for a connection, and these techniques were also unable to provide insight into the functional properties of connections. The application of paired whole cell patch clamp recordings in live tissue therefore represented a significant advance and provided some of the first evidence for direct and functional connections between two or more neurons. Whilst this technique has been instrumental in advancing our understanding of fine scale cortical circuits (Feldmeyer et al., 2002, 2006; Hardingham et al., 2010; Lefort et al., 2009), it has typically been used *in vitro* and so suffered from the fact that connections between neurons are severed in brain slice preparations, systematically decreasing the probability of detecting a connection as the distance between soma increases. Finally, a variety of stimulation methods have been used to evoke activity in defined pre-synaptic populations, typically combining with techniques such as whole cell patch clamp to record the post-synaptic effects. Within this category, methods such as glutamate uncaging have been successfully used to examine connectivity in acute slices (Dirk Schubert et al., 2001; Shepherd & Svoboda, 2005; X. Xu & Callaway, 2009). And more recently, the development of optogenetic methods based on channelrhodopsin-2 (ChR2), have made it possible to map the fine scale connectivity of genetically-defined neurons (Boyden, 2011; Boyden et al., 2005), with the important benefit that even cut pre-synaptic fibers can be stimulated (Ellender et al., 2019; Kätzel et al., 2011; Petreanu et al., 2007; Yamawaki & Shepherd, 2015).

General patterns of Excitatory connectivity

Through a combination of the above methods, the field has been systematically advancing our understanding of fine scale cortical circuitry. In doing so, this work has confirmed that some aspects of the original canonical cortical circuit, whereas other aspects of this circuit have been refined and/or refuted (**Fig. 1.2**).

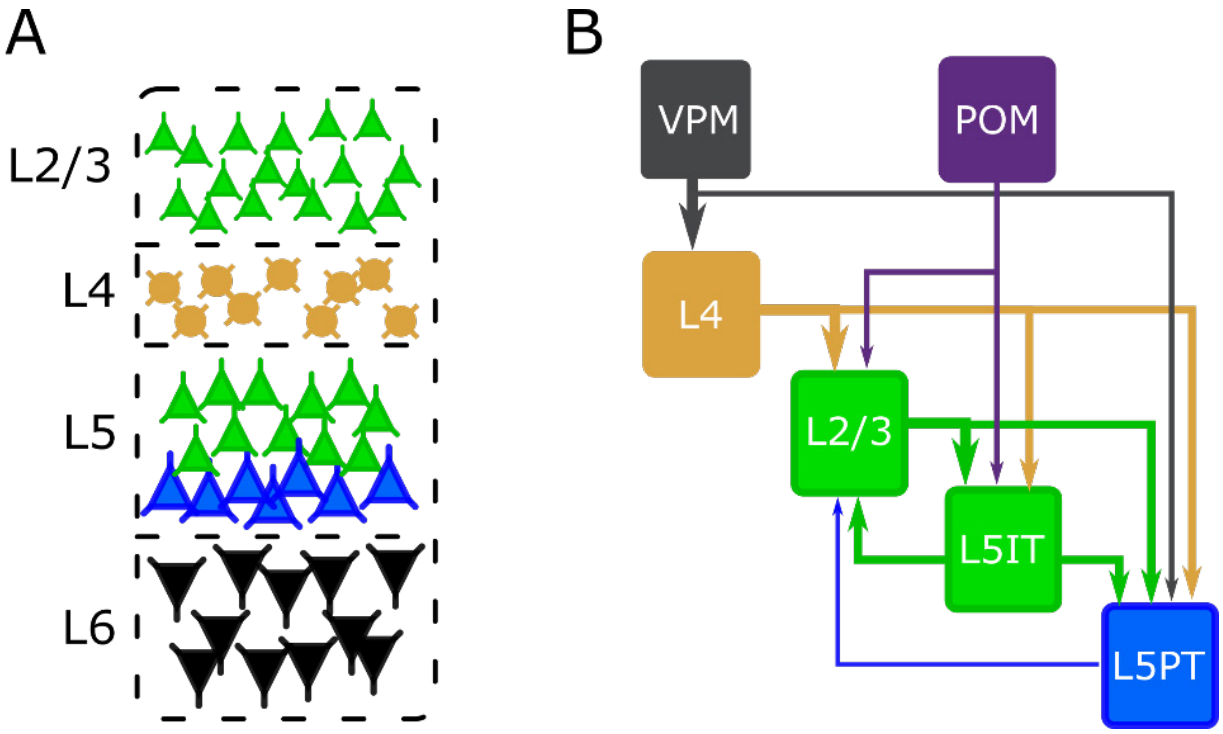


Figure 1.2 Cortical information is processed through stereotypical connections between neuronal subtypes.

(A) Cortical laminae are populated by a variety of projection defined excitatory subtypes. These include Intratelencephalic (IT) pyramidal neurons found in L2/3 and L5a (Green), Spiny stellate cells in L4, Pyramidal tract (PT) pyramidal neurons found in L5b (blue) and Cortico-Thalamic pyramidal neurons in L6. **(B)** Stereotypical connectivity patterns between subpopulations are often conceptualized as a series of feed forward information processing steps. Separate inputs from the Lemniscal and Paralemniscal pathways (VPM and POM thalamic nuclei respectively) are integrated by interdigitating thalamorecipient layers. Subsequent local intralaminar connectivity enable further information processing and long range outputs from IT and PT neurons in L2/3 and L5. Modified from (Adesnik & Naka, 2018)

For instance, there is compelling evidence from experimental stimulation of thalamocortical fibres that L4 receives strong excitatory inputs from thalamus, but it is also now clear that monosynaptic thalamic inputs can be detected in other cortical layers (Cruikshank et al., 2007, 2010; Petreanu et al., 2007) and particularly neurons in infragranular L5b and L6 (Constantinople & Bruno, 2013; Reyes-Puerta et al., 2015). Our appreciation of thalamic organization has also advanced, such that thalamocortical inputs are no longer seen as uniform, but rather differ in their targeting of cortical laminae in a manner that reflects

their status as either 'first order' (i.e. the first relay to cortex of a particular type of subcortical information) or 'higher' order (i.e. relaying information that has previously reached cortex) (Sherman and Guillery, 1998; Sherman, 2007; Audette et al., 2018; Sermet et al., 2019)**.** In mouse barrel cortex, these correspond to VPM and POm, respectively, and inputs from these two thalamic nuclei appear to interdigitate with one another across the laminar structure of cortex (Sermet et al., 2019; Shepherd & Svoboda, 2005) (**Fig. 1.2B**).

Fine scale connectivity studies have also shown that L4 neurons have strong intralaminar connectivity, as well as broadcasting excitation to other layers, in particular L2/3, without receiving reciprocal connections (Binzegger et al., 2004; Feldmeyer et al., 2006; Lefort et al., 2009; Shepherd & Svoboda, 2005). This is consistent with L4 functioning primarily as an input layer and it has been suggested that L4 may act as an amplifier of thalamic inputs, due to the high degree of reciprocal connectivity between thalamorecipient L4 neurons (Lefort et al., 2009; Dirk Schubert et al., 2003). L2/3 pyramidal neurons also form strong intralaminar connections (Feldmeyer et al., 2006; Hardingham et al., 2010; Lefort et al., 2009) and have been shown to provide monosynaptic excitation to neurons throughout superficial and deep L5, referred to as L5a and L5b (Adesnik & Scanziani, 2010; Hardingham et al., 2010; Lefort et al., 2009; Petreanu et al., 2007; Reyes & Sakmann, 1999; D Schubert et al., 2006) **(Fig. 1.2B)**. Although it should be noted that whilst these translaminar connections are significant, the amplitude of the post-synaptic responses and their connection probability can be lower than for some intralaminar connections (Lefort et al., 2009). L2/3 pyramidal neuron local projections can also spread beyond the bounds of the home column to surrounding columns (Adesnik & Scanziani, 2010; Lefort et al., 2009).

L5 continues to be considered the main output layer of cortex, due to the fact that the pyramidal neurons located throughout this layer form long-range axonal projections to multiple cortical and subcortical structures (Feldmeyer, 2012). However, feedforward models in which information is viewed as passing from L2/3 to L5, where it is then integrated and output to long-range targets, is increasingly seen as an

oversimplification of what L5 contributes to local cortical processing. Anatomical work has established that the long-range axons of L5 pyramidal neurons also branch locally and form ascending collaterals that synapse within L5 and extend to more superficial layers, including L2/3 (Oberlaender et al., 2011). As well as enabling L5 neurons to form intralaminar connections (Hardingham et al., 2010), these collaterals have been seen as a route for L5 neurons to signal across cortical layers (Binzegger et al., 2004; Oberlaender et al., 2011). Indeed, these local collaterals of long-range projections represent a route for the information that is being relayed to other regions of the brain, to be simultaneously fed back and influence neurons within the local cortical circuit. Consistent with this idea, recent optogenetic studies have confirmed that L5 pyramidal neurons can modulate activity throughout the cortical column (Adesnik & Scanziani, 2010; Beltramo et al., 2013; Vecchia et al., 2020). Despite their potential importance, the nature of local translaminar signaling from L5 to other cortical layers remains poorly understood. The overall objective of this thesis therefore, is to advance our understanding of translaminar signals relayed from L5 to L2/3. It is important to note there is an increasing recognition that the laminar architecture *per se* is less important than specific connectivity patterns between defined subpopulations of neurons whose preferred cortical depth location may have some overlap with traditionally defined layers(Guy & Staiger, 2017; Harris & Shepherd, 2015). To understand the potential impact of these translaminar signals, it is appropriate that I now review advances that have been made in classifying cortical neuronal subtypes, as well our current understanding of the diversity and roles of inhibitory interneurons within cortical circuits.

Understanding cortical circuitry through cell classification

Another area that has advanced remarkably over the last 20 years, has been the classification of cortical cell types. What has becoming increasingly clear, is that through an appreciation of neuronal subtype, comes a more complete understanding of cortical circuitry. Indeed, these two concepts may be converging, such that neuron type ultimately becomes defined by a neuron's synaptic connectivity

patterns. In this section, I will review some of the most important approaches that have been used to classify cortical cell types and I will introduce the idea that excitatory neuron subtypes can be classified according to their long-range projection targets, as this will be relevant for the experimental approaches in this thesis.

At the most fundamental level, cortical neurons can be split into those that are either glutamate-releasing excitatory neurons or GABA-releasing inhibitory neurons. These two groups, found throughout all layers, have distinct characteristics and embryonic origins (Marín & Müller, 2014). Excitatory neurons make up the majority of cortical neurons, with inhibitory neurons accounting for only about 20% of the total neuronal population (Meinecke and Peters, 1987). Original attempts to subclassify excitatory neurons used morphological characteristics. Such classification systems trace back to the original drawings of Ramon y Cajal (y Cajal, 1911), whose drawings and original classifications remain influential over 100 years later. Modern approaches to classify neurons have relied on three main properties: morphological, physiological and molecular features (Zeng & Sanes, 2017). Morphological studies have primarily focused upon axonal and dendritic reconstructions that describe branching patterns and shapes. Within cortex, the most common morphological classification distinguishes pyramidal neurons on the basis of their large apical spiny dendrite and pyramid shaped soma, from excitatory spiny stellate neurons found exclusively in L4, from inhibitory smooth neurons.

Classifying neurons according to their electrophysiological properties is based on the knowledge that neurons differ significantly in the type and distribution of ion channels on the soma, dendritic tree and axon initial segment (Connors & Gutnick, 1990). Most commonly, neurons can be referred to as regularly or irregularly spiking, intrinsically bursting or fast spiking. Each of these describes a specific pattern of action potentials, usually in response to injections of somatic current. These spiking pattern definitions have been associated with a number of both excitatory and inhibitory neuronal morphologies (Rudy et al., 2011; Dirk Schubert et al., 2001; Staiger et al., 2016; Tremblay et al., 2016; Wang et al., 2018). Such

intrinsic property differences are of noted functional importance as when acting together as a population, relative differences in spike rate or membrane properties can fundamentally change the network behaviour (Llinás, 2014).

Another major effort has been to subclassify neurons according to the protein and/or RNA that they express. Indeed a number of molecular markers have been associated with specific laminar cell types. For instance *Cux1, Cux2,* and *Lhx2* are all molecular markers associated with supragranular layers, while *Rorβ* locates to L4 and *Opn3* and *Ctip2* are markers of L5 neurons (Molyneaux et al., 2007). It is however, unlikely that a single gene defines functionally-related populations of cortical neurons, rather the expression of a set of genes is likely to determine the functional properties of a neuronal class (Deneris & Hobert, 2014; Holmberg & Perlmann, 2012). Whilst molecular markers have been identified via methods such as immunolabelling and *in situ* hybridisation, more recent methods have made use of increasingly high throughput transcriptomic approaches (Tasic et al., 2016). Molecular-genetic methods for identifying cell types have the advantage of allowing the generation of transgenic mouse lines to target specific cell types. With the development of systems such as Cre driver lines, in which Cre recombinase is expressed under the control of cell-specific gene promoters (Gerfen et al., 2013), a highly flexible toolbox now exists for the identification and manipulation of specific neuronal subtypes (Daigle et al., 2018).

It is important to note however, that most modern efforts to define neuronal subtypes combine information relating to cell morphological, electrophysiological and molecular characteristics, as well as incorporating features of their connectivity to other cells. Such a multidimensional and functional approach to neuronal classification incorporates a sense of how a particular neuron type influences other neurons within a network. Indeed, one definition proposed by Peter Somogyi, defined neuronal cell type as a group of neurons that deliver identical neuroactive substances to a matching range of post-synaptic targets and with the same temporal patterns (Somogyi & Klausberger, 2005). By this logic, neurons with similar patterns of connectivity (assuming all other characteristics are also similar) are likely to therefore

play similar roles within the local circuit (Seung & Sümbül, 2014). This functional perspective on neuronal subtype emphasises the importance of considering the synaptic targets of cortical neurons, both locally and in terms of long-range projections.

Throughout cortex, subpopulations of excitatory neurons can be defined by the targets of their long-range axonal projections. The first subpopulation defined by long-range projection are commonly referred to as intratelencephalic projection neurons (IT), as they project to other cortical regions and bilateral striatum. IT neurons can be found predominantly in L2/3 and L5 and are associated with the Sat2b molecular marker (Feldmeyer, 2012; Harris & Shepherd, 2015; Tasic et al., 2018). These neurons are principally responsible for interareal connectivity both ipsilaterally, and are the only neurons to project contralaterally via the corpus callosum and anterior commissure. L4 spiny stellate neurons can also be classed as IT neurons, but these neurons only project within local cortex and do not target more distant structures (Harris & Shepherd, 2015). Some IT type projection neurons can also be found in L6 (Yamawaki & Shepherd, 2015).

The second subpopulation defined by their long-range projection target are pyramidal tract projection neurons (PT), which project to subcortical structures such as the spine, thalamus, trigeminal nucleus and striatum (Feldmeyer, 2012; Harris & Shepherd, 2015; Tasic et al., 2018). PT neurons are found predominantly in deep L5 and are associated with the expression of Fezf2 and Ctip2. Finally, the third subpopulation defined by their long-range projection target are cortico-thalamic projection neurons (CT), which can be found in L6 and project primarily to thalamus (Feldmeyer, 2012; Harris & Shepherd, 2015; Tasic et al., 2018).

The recognition of long-range projection target as an important feature for classifying cortical cell type and function has existed since some of the earliest anatomical descriptive work .

The first such studies of long-range projection targets used tracers that would be transported retrogradely along the axon. Initially, horseradish peroxidase (Kristensson & Olsson, 1971a, 1971b) and fluorogold

(Schmued & Fallon, 1986) were used to identify neurons projecting to a particular injection site. More recently, the development of retrograde tracing tools that minimally disrupt the neuronal physiology have been combined with techniques such as whole cell patch clamping, and used to study how a neuron's intrinsic electrophysiological characteristics (Hattox & Nelson, 2007b), local connectivity (Brown & Hestrin, 2009), and activity during behaviour, all correlate with the long-range projection target of that neuron (Yamashita et al., 2013). The development of fluorescently tagged choleratoxin subunit B, as a highly efficient retrograde tracer, has made this a popular tool in in *vitro* physiology (Conte et al., 2009b, 2009a).

The use of viral vectors for such retrograde tracing studies has also proven attractive, as this opens the possibility for the delivery of genetic tools to study and/or manipulate a projection-defined subpopulation. Whilst the use of different viral vectors to deliver optogenetic tools have allowed for significant specificity in the manipulation of neuronal subpopulations, viral vectors with a high degree of retrograde transport remained difficult to use (Mao et al., 2011; Nagel et al., 2003; Petreanu et al., 2007, 2009). Rabies virus is a well-known neurotropic viral vector, that shows a high degree of retrograde transport, although concerns regarding the virulence of the rabies virus have limited its use (Schnell et al., 2010). Efforts have been made to modify the rabies virus to improve safety (Reardon et al., 2016) and these have been used to manipulate subpopulations of L5 and L6 pyramidal neurons on the basis of their long-range projection in motor cortex (Kiritani et al., 2012; Yamawaki & Shepherd, 2015). Canine adenovirus 2 (CAV2) is another virus that shows a high degree of retrograde transport and has quickly become popular in the evaluation of neuronal projections (Junyent & Kremer, 2015). However, CAV2 is limited in the size of genetic tools that can be delivered and there have been some concerns regarding toxicity (Piersanti et al., 2013; Simão et al., 2016).

Recombinant adeno-associated viruses (rAAVs) have increasingly been identified as effective, safe vectors for genetic tools in research (Lanciego & Wouterlood, 2020), but rAAVs are not known to exhibit selective retrograde transport. Recently however, a recombinant AAV type 2 was developed specifically to exhibit a high degree of retrograde transport efficiency (Tervo et al., 2016). Using a process of guided evolution, the viral capsid gene was enriched to promote retrograde transport. An initial diverse library of viral capsid gene variants were injected into the hindbrain and substantia nigra in order to target long-range projections from glutamatergic neurons in the cerebellum and GABAergic neurons in the striatum, respectively. By recovering viral capsid genes from the cerebellum and striatum, the most effective variants for retrograde transport were identified. The error prone polymerase chain reaction (PCR) was then used to introduce further variation into the capsid gene and repetition of this process ensured selection of Capsid genes with increasingly more efficient retrograde transport. The resulting 'rAAV2retro' was then demonstrated to be effective at the retrograde delivery of a number of genetic tools. Following the development of rAAV2retro, this tool has been used to manipulate specific projection-defined subpopulations of neurons (Li et al., 2020; Tervo et al., 2016).

In the experimental work in this thesis, I make significant use of these retrogradely transported viral tools in order to target projection-defined subpopulations of L5 pyramidal neurons. More specifically, I am able to efficiently deliver Cre-dependent ChR2 to L5 pyramidal neurons based on their long-range axonal projection target. This allows me to explore the local post-synaptic connectivity of these subpopulations, without the need for simultaneous patch clamp recordings across layers. Crucially, the use of the retrogradely transported viral tools confers specificity by defining the L5 subpopulations based on their axonal projection target, rather than previous strategies that have tended to rely upon biases in the locations of L5 neuronal soma.

IT and PT projection-defined layer 5 pyramidal neurons

Having introduced the classification of cortical neuronal subtypes, including the definition of subtype according to the target of long-range axonal projections, this section focuses upon the specific examples of IT and PT projection-defined L5 pyramidal neurons, as these play a central role in this thesis. Distinct morphological, electrophysiological and molecular characteristics are all associated with IT and PT L5 pyramidal neuron types (**Fig. 1.3**). Firstly, within L5 these neurons show differences in their typical soma position. PT neurons are most densely located in deeper L5b, whilst IT neurons are found throughout L5, but are preferentially associated with L5a (Aronoff et al., 2010; Feldmeyer, 2012; Oswald et al., 2013).

Often where unequivocal projection tracing is not possible, such as in the identification of units in extracellular recordings, L5a and L5b are used as a proxy to try to distinguish IT and PT subtypes. These neuronal subtypes also exhibit distinct dendritic morphological characteristics (Gao & Zheng, 2004; Naka & Adesnik, 2016; Oswald et al., 2013; Ramaswamy & Markram, 2015; Wang et al., 2018). PT neurons are associated with a 'thick-tufted' dendritic morphology consisting of a large primary apical dendritic often with numerous distal tufts and extensive ramification in L1 (Gao & Zheng, 2004; Oswald et al., 2013; Ramaswamy & Markram, 2015; Wang et al., 2018). In contrast, IT neurons tend to be 'thin/slender tufted' with a more narrow apical dendrite that lacks distal tufts and may be more limited in its superficial extension (Gao & Zheng, 2004; Le Bé et al., 2006; Oswald et al., 2013; Wang et al., 2018).

The differences between these two projection-defined subpopulations also extend to intrinsic electrophysiological characteristics. Experiments that have used retrograde labelling to identify and then record from IT and PT neurons have reported that PT L5 neurons are more likely to exhibit burst firing and little spike rate adaptation (**Fig. 1.3**).

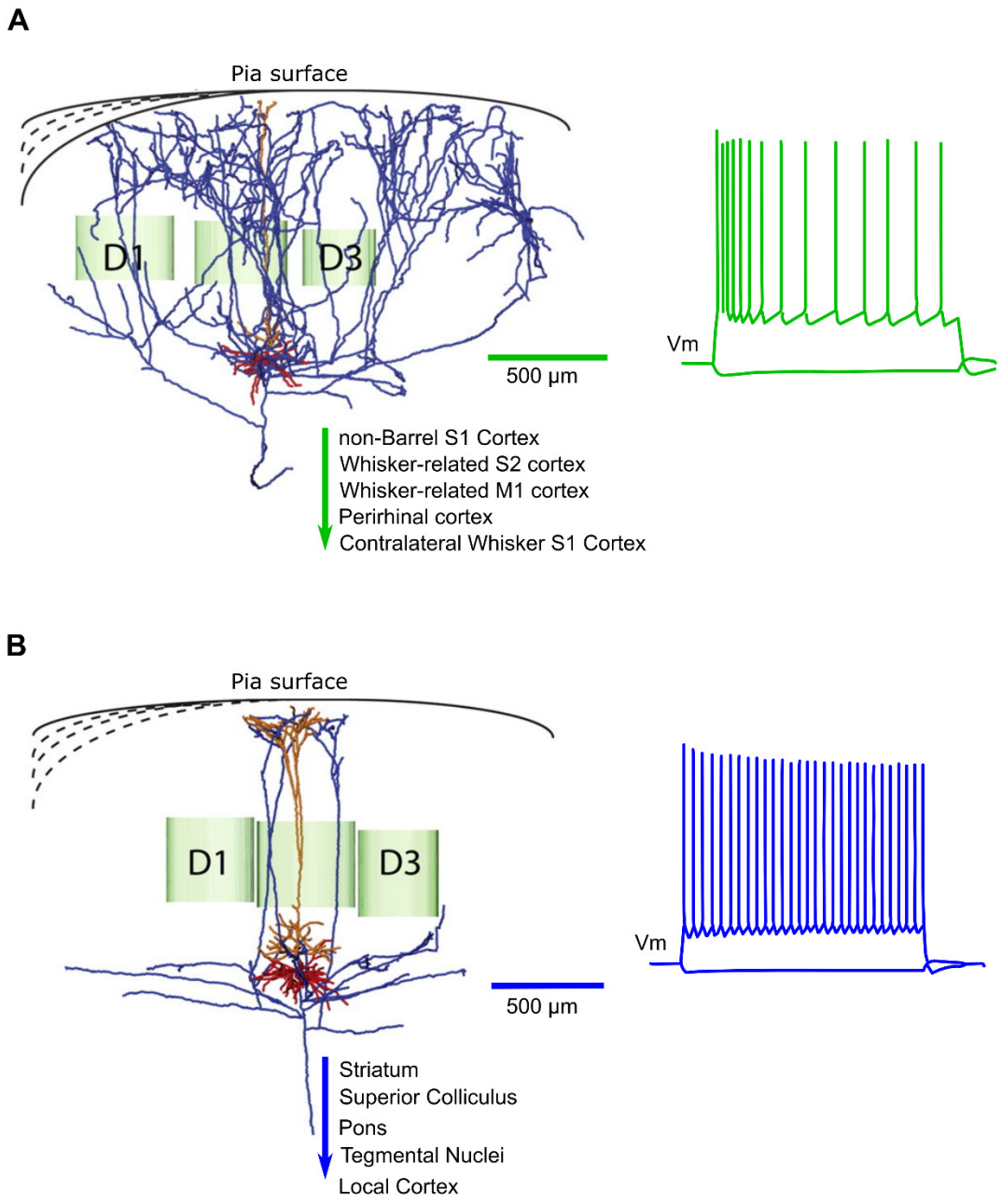


Figure 1.3 IT and PT pyramidal neurons in L5 are distinct neuronal subtypes.

(**A**) An example reconstructed IT L5 pyramidal neuron illustrating the elaborate branching of local ascending intracortical axonal collaterals (left). Axons are blue, dendrites are red. These neurons have long-range projections to other cortical areas. Electrophysiological recordings reveal that IT L5 neurons show a characteristic action potential firing pattern with prominent spike rate adaptation (right). (**B**) An example reconstructed PT L5 pyramidal neuron demonstrating more restricted intracortical ascending collaterals (left). These neurons have long-range projections to subcortical structures. The characteristic action potential firing of a PT L5 pyramidal neuron shows little spike rate adaptation (right). Figure modified from (Feldmeyer, 2012; Hattox & Nelson, 2007b; Oberlaender et al., 2011).

Whereas IT L5 neurons show more regular spiking patterns with significant spike rate adaptation (Guan et al., 2015; Hattox & Nelson, 2007b; E. J. J. Kim et al., 2015; Le Bé et al., 2006). Differences in the action potential firing of IT and PT L5 neurons are thought to reflect a different expression and distribution of voltage-gated ion channels (Hattox & Nelson, 2007b; Ramaswamy & Markram, 2015). In particular, PT L5 neurons are associated with the expression of hyperpolarization-activated cation (HCN) channels, known to mediate an inward current when the membrane is significantly hyperpolarized (I_h), and resulting in so called 'sag' potentials (Guan et al., 2015; Ramaswamy & Markram, 2015; Robinson & Siegelbaum, 2003). These channels are thought to contribute to the burst firing characteristic of these neurons, and to modulate somatodendritic integration mechanisms (Robinson & Siegelbaum, 2003). IT and PT L5 neurons also differ in the expression of molecular markers and the development of transgenic mice has allowed for further characterization of these subtypes (E. J. J. Kim et al., 2015). Genetic manipulations have demonstrated the importance of certain key genes on the PT or IT phenotype in cortex. By knocking out the *fezf2* transcription factor, subcortically-projecting pyramidal neurons in L5 failed to demonstrate their typical long-range targeting and began to also show electrophysiological characteristics that were typically associated with IT L5 neurons(Lodato et al., 2011).

Efforts to examine the local connectivity of IT and PT L5 neurons also suggest differences in the local synaptic networks that these neurons form. IT and PT L5 neurons appear to integrate different excitatory inputs, being more likely to receive input from higher-order and first-order thalamic nuclei, respectively (Bureau et al., 2006; Diamond et al., 2008; Feldmeyer, 2012; Guo et al., 2020; Petersen, 2007, 2019; Sherman, 2007). In the barrel cortex, this equates as VPM inputs to PT L5 and POm inputs to IT L5. Further evidence for subtype specificity is that the long-range project target correlates with different local connectivity patterns. Hestrin and Brown first demonstrated through paired recordings of retrogradely labelled neurons, that cortico-striatal L5 pyramidal neurons formed higher rates of connectivity than other

L5 projection neurons (Brown & Hestrin, 2009; Le Bé et al., 2006). They also demonstrated that IT L5 neurons exhibit a connectivity bias towards PT L5 neurons. Interestingly, evidence for such selective subnetworks between target-defined projection neurons and a preference for feedforward connectivity from one subpopulation to another, has also been provided in frontal cortex (Morishima & Kawaguchi, 2006), L5 and L6 pyramidal neurons of motor cortex (Kiritani et al., 2012; Yamawaki & Shepherd, 2015), as well as between L2/3 pyramidal neurons with different cortical targets (M.-H. Kim et al., 2018).

As was mentioned previously, L5 pyramidal neurons communicate locally via the collaterals that branch from their main, long-range axonal projection. Previous studies have reconstructed the local axonal tree of putative IT and PT neurons (identified on the basis of dendritic morphology and electrophysiological characteristics) (Delaine D Larsen, 2008; Narayanan et al., 2017; Oberlaender et al., 2011; Staiger et al., 2016; Wang et al., 2018). Thick-tufted neurons (putative PT) have been shown to possess predominantly infragranular local axonal connections, with slender ascending connections that cross superficial layers, but remain within the same cortical column (**Fig. 1.3**). In contrast, thin-tufted neurons (putative IT) possess highly elaborate ascending axonal branches that have significant lateral extension to surrounding columns. This anatomical evidence hints at functional differences, although there remains a paucity of data directly mapping the local axonal collateral morphology onto the long-range projection targets of these neurons.

The possibility that there are significant differences in the translaminar output from IT and PT L5 neurons is also supported by results from glutamate uncaging experiments. These studies have shown that in addition to receiving strong excitatory inputs from L2/3, the reciprocal excitatory connectivity from L5 to L2/3 appears to differ depending on the position within L5, with more superficial L5 showing stronger excitatory connectivity to L2/3 (Bureau et al., 2006; Feldmeyer, 2012; Lefort et al., 2009; Shepherd &

Svoboda, 2005; Staiger et al., 2015). However, these glutamate uncaging experiments would be susceptible to slice-related damage of the translaminar projections, and they did not distinguish between L5 neurons based on their long-range projection targets. It is well described that cortical excitatory connectivity is in fact characteristically sparse and there exists a low probability of connection between any two cells either within a layer or across layers(Thomson & Bannister, 2003). These sparse connections are not the results of a random or probabilistic process, neurons show significant selectivity in their post synaptic target.(Brown & Hestrin, 2009; Kampa et al., 2006; M.-H. Kim et al., 2018; T. Kim et al., 2016; Kiritani et al., 2012; Lefort et al., 2009; Silberberg & Markram, 2007; Yamawaki & Shepherd, 2015).

A further unexplored aspect is whether the local L5 axons preferentially target L2/3 interneurons, which would alter how this signal modulates L2/3 activity. As a result, there remain a series of unanswered questions about the nature of translaminar signaling from L5 subtypes to L2/3.

Inhibition in cortex

To understand the impact of these translaminar signals, it is also necessary that I introduce the role of inhibitory interneurons in cortical circuits. Our understanding of cortical interneurons is another area that has advanced remarkably over the last 20 years and I will review our current understanding of the diversity and function of cortical interneurons, including how the interplay between excitatory and inhibitory synaptic signals is important for cortical computations.

The chief source of cortical inhibitory signaling are GABAergic interneurons that can be found across all 6 Layers. Whilst interneurons represent only approximately 20% of the cortical neuronal population, a diversity of cellular subtypes have been identified (Markram et al., 2004; Somogyi & Klausberger, 2005; Tremblay et al., 2016). As with excitatory neurons, continuing efforts are being made to classify these neurons on the basis of morphological, electrophysiological and molecular characteristics (Ascoli et al.,

2008). In structures such as the hippocampus, successful classification systems have been described that map molecular and functional diversity onto broad classes based on somatic location and dendritic arbor structure (Klausberger & Somogyi, 2008; Somogyi & Klausberger, 2005). However, due to the intermingling of intraneuronal cell types across all layers of varying cytoarchitectonic structure, cortical classification systems that start with broad molecular differences have been more successful. It has been identified that almost all cortical interneurons express one of three proteins; the calcium-binding protein parvalbumin (PV), the neuropeptide somatostatin (SST), or the ionotropic serotonin receptor 5HT3a (5HT3aR) (SooHyun Lee et al., 2010; Rudy et al., 2011; Tasic et al., 2016).

Parvalbumin-expressing (PV) interneurons are overall the largest interneuron population in cortex and can be divided into two distinct morphological groups (Hu et al., 2014; X. Xu & Callaway, 2009). The first group are chandelier cells, named after the characteristic 'candle stick' appearance of their axons (DeFelipe et al., 2013) and also known as axo-axonic interneurons due to their specific targeting of the axon initial segment of pyramidal neurons (Y Kawaguchi & Kubota, 1997). Meanwhile, basket cells are the more numerous sub group of PV interneurons and provide perisomatic inhibition (Hu et al., 2014; Y Kawaguchi & Kubota, 1997). Electrophysiologically, basket cells have a characteristic high firing rate with little spike rate adaptation leading to these cells being referred to as 'fast spiking' (McCormick et al., 1985). PV interneurons can be found throughout all layers of cortex and have broad dendritic and axonal arborising domains. Within all layers of cortex, PV interneurons have been found to form dense non-specific connectivity with almost all neighboring pyramidal neurons (Packer & Yuste, 2011). In addition to this within-layer connectivity, translaminar axonal projections have been described specifically from infragranular PV interneurons to pyramidal neurons in more superficial layers (Bortone et al., 2014; Buchanan et al., 2012).

In contrast to PV interneurons, somatostatin-expressing (SST) interneurons have been shown to selectively target the dendritic domain of local pyramidal neurons (Y Kawaguchi & Kubota, 1996, 1997; Wang et al., 2004). Another key difference between SST interneurons and other inhibitory interneurons is that while the excitatory synapses onto most interneuron subtypes undergo varying degrees of depression, synapses onto SST interneurons are strongly facilitating (Pouille & Scanziani, 2004; Silberberg & Markram, 2007). This means that SST interneurons are optimally recruited by trains of pre-synaptic inputs, a phenomenon known as frequency dependent disynaptic inhibition (Silberberg & Markram, 2007). Within SST interneurons there is increasing evidence for multiple morphological subclassifications (Riedemann, 2019). One well known group is the Martinotti type SST interneurons found predominantly in L2/3 and L5 (DeFelipe et al., 2013; L. Gentet, 2012; Naka & Adesnik, 2016). These interneurons characteristically have ascending axonal arbors that target L1, as well as significant local axonal arbors (Y Kawaguchi & Kubota, 1996; Wang et al., 2004). Non-Martinotti type SST interneurons share many characteristics with the Martinotti type, but crucially lack L1 targeting axonal arbors (Tremblay et al., 2016). A number of spiking patterns have been associated with SST interneurons, which include low threshold spiking, regular spiking, or burst spiking (Y Kawaguchi & Kubota, 1996; Kubota, 2014; Riedemann, 2019; H. Xu et al., 2013). SST interneurons in L5 have been described with a high firing rate, but with typically far greater spike rate adaptation than PV interneurons.

Ionotropic serotonin receptor-expressing (5HT3aR) interneurons constitute about 30% of all cortical interneurons and are thought to be more diverse than either PV or SST interneurons (Tremblay et al., 2016). One clear distinction between the groups of interneurons is their embryonic origin. Whilst PV and SST interneurons are derived from the medial ganglionic eminence before migrating to their final locations in cortex, 5HT3aR interneurons are derived from the caudal ganglionic eminence (Butt et al., 2005; Miyoshi et al., 2010; Q. Xu et al., 2004). 5HT3aR interneurons are most richly found in the supragranular

layers and comprise the vast majority of neurons in L1 (SooHyun Lee et al., 2010; X. Xu et al., 2010). These interneurons can be divided into those that also express vasoactive intestinal peptide (VIP) and those that do not. VIP interneurons typically display a bipolar or multipolar dendritic morphology and have been reported to receive inputs from multiple cortical layers (Y Kawaguchi & Kubota, 1996, 1997) and are associated with an irregular spiking pattern (SooHyun Lee et al., 2010). Of particular note, VIP interneurons appear to specifically target other interneuron subtypes and thus have been implicated in cortical disinhibitory motifs (Karnani et al., 2016). In addition to VIP interneurons, other 5HT3aR interneurons include neurogliaform cells that are noted for their characteristic multipolar morphology; and non-VIP expressing, cholecystokinin- expressing (CCK) interneurons (DeFelipe et al., 2013; Y Kawaguchi & Kubota, 1997).

Excitatory and inhibitory interplay in cortical circuits.

Due to the small size of depolarizing unitary excitatory potentials in cortex, for a neuron to reach threshold and generate an action potential, a number of incoming excitatory inputs must sum together. Inhibitory inputs may counteract this depolarization and thus shape the neuronal output. Importantly, inhibitory inputs can reduce neuronal output not only through hyperpolarization, but via a 'shunting' effect. This is due to the opening of $GABA_A$ receptors and the resultant drop in the post-synaptic neuron's input resistance. In accordance with Ohm's law, this results in a reduced membrane potential change for a given current input to the neuron and as such a shift in the neuron's input/output relationship (Cardin et al., 2008; Ferguson & Cardin, 2020). Depending on its subcellular location, strength and timing, an interneuron's input can exert different degrees inhibition upon post-synaptic action potentials. Inhibitory inputs located at the neuronal soma or axon initial segment are likely to result in a more profound effect, than Inhibitory inputs on dendritic processes (Roux & Buzsáki, 2015; Tremblay et al., 2016).

Inhibitory interneurons are embedded in repeated circuit motifs, which enable the interneuron to influence activity at both an individual neuron and network level. These inhibitory circuits exist in the brain to provide stability to, and modulation of, excitatory neuron populations. They can be broadly divided into 'feedforward' or 'feedback' circuit motifs. Disynaptic feedforward inhibitory circuits are particularly prevalent in cortex. In such circuits, excitatory pre-synaptic axons that target principal neurons, also target a local inhibitory neuronal population that provides inhibition to the principal neurons (Cruikshank et al., 2007, 2010; Jouhanneau et al., 2018; Roux & Buzsáki, 2015). Therefore, increasing the excitatory input to the principal neurons also increases recruitment of the inhibitory population. Within cortex the majority of such disynaptic feedforward inhibitory circuits are mediated by PV interneurons (Bruno & Simons, 2002; Cruikshank et al., 2007, 2010; Inoue & Imoto, 2006; Swadlow & Gusev, 2002). In such a feedforward circuit, several mechanisms ensure the reliable recruitment of inhibition, including larger and more efficient synaptic connections onto inhibitory neurons and lower threshold to action potential and relatively depolarized resting membrane potential in the PV interneurons (Cruikshank et al., 2007, 2010; Fanselow et al., 2008; Jouhanneau et al., 2018; Stokes & Isaacson, 2010). Thus, under physiological conditions, disynaptic feedforward excitation can be tightly temporally coupled to incoming excitatory inputs (Roux & Buzsáki, 2015).

One of the best described disynaptic feedforward inhibitory circuits is found in L4 (Bruno & Simons, 2002; Cruikshank et al., 2007, 2010; Inoue & Imoto, 2006; Swadlow & Gusev, 2002). Excitatory pre-synaptic thalamocortical axons synapse onto L4 excitatory neurons, but the same axons have a higher connection probability to local PV interneurons. In addition, the thalamocortical synapses onto the PV interneurons are stronger (Cruikshank et al., 2007, 2010; Sermet et al., 2019), a feature mediated by the clustering of multiple synaptic contacts and a high quantal release of neurotransmitter (Bagnall et al., 2011; Hull et al., 2009). These features, along with the arrangement of the circuit motif, mean that very few inputs are

required to drive a PV interneuron to action potential threshold and thus provide powerful inhibition onto neighboring neurons. Such PV interneuron-mediated feedforward inhibitory circuits are also observed as part of translaminar signals across cortical layers (Helmstaedter et al., 2008; House et al., 2011; X. Xu & Callaway, 2009). Disynaptic feedforward inhibition mediated by SST interneurons has also been described. Due to the facilitating nature of the excitatory synapses to SST interneurons, this motif is known as frequency dependent disynaptic inhibition (Naka & Adesnik, 2016; Silberberg & Markram, 2007).

In contrast, feedback inhibitory circuits are those in which action potential discharges from excitatory population drives an inhibitory population, which then synapses back onto the original excitatory population (Miles, 1990). These inhibitory connections may even extend beyond the local column and thus input onto neuronal populations that did not provide the initial source of excitation, in what is referred to as 'lateral inhibition' (Helmstaedter et al., 2008; Kätzel et al., 2011). For instance, it has been shown that rapid recruitment of L2/3 PV interneurons by optogenetic stimulation of local pyramidal neurons can attenuate the firing of neighboring pyramidal neurons (Avermann et al., 2012). This is due to the fact that both SST and PV interneurons form dense divergent connectivity with surrounding local principal neurons (Fino & Yuste, 2011; Packer & Yuste, 2011). Finally, inhibitory interneurons may also form preferential connections with other inhibitory interneurons, resulting in so-called disinhibitory circuits. One of the best examples of such a motif is that mediated by VIP interneurons (Karnani et al., 2016). The first evidence of such disinhibitory circuits arose from the hippocampus (Acsády et al., 1996) and it has subsequently been described in L2/3 of the cortex (Staiger et al., 2004). Thanks to the use of optogenetic techniques using Cre driver lines, it has been proposed that VIP inhibition of SST interneurons and thus disinhibition of pyramidal neurons is a general feature of superficial layers of cortex (Soohyun Lee et al., 2013; Pfeffer et al., 2013; Pi et al., 2013).

One of the consequences of these inhibitory motifs, is that they generate a tight coupling between excitation and inhibition. This coupling has been demonstrated *in vivo* where even simple sensory stimuli result in closely associated excitatory and inhibitory synaptic activity in somatosensory (Okun & Lampl, 2008; Swadlow, 2003; Wilent & Contreras, 2005), auditory (Anderson et al., 2000; Monier et al., 2003) and visual cortex (Tan et al., 2004; Wu et al., 2008). As such, it has been shown that increases in excitation are met with proportional increases in inhibition (Moore et al., 2018; Xue et al., 2014). This has led to the concept of excitation/inhibition balance or 'E/I balance' (**Fig. 1.4**) (Isaacson & Scanziani, 2011; Wehr & Zador, 2003; Wilent & Contreras, 2005; Xue et al., 2014).

Importantly, whilst there may be an overall matching between excitation and inhibition, the exact temporal nature of this is crucial to circuit function. Indeed, for any effective spike transfer to occur, there must be transient imbalances in E/I(Roux & Buzsáki, 2015). It is perhaps not surprising therefore, that the E/I ratio can differ across different projections (**Fig. 1.4**) (Adesnik, 2018; Sempere-Ferràndez et al., 2019; Yamawaki & Shepherd, 2015; Yang & Sun, 2018). One example of this was demonstrated by Adesnik and Scanziani who used optogenetic tools to gradually increase activity across different layers of cortex (Adesnik & Scanziani, 2010). They found that the resulting oscillatory activity recruited matched excitatory and inhibitory conductances, but the E/I ratio varied across layers.

Further evidence that E/I ratios vary comes from the visual system, where the E/I ratio depends upon the point in the information processing hierarchy. Feedforward connections from lower order cortical regions show the strongest recruitment of PV interneurons and the lowest E/I ratios. Whereas feedback connections from higher order regions show the least inhibitory recruitment and therefore highest E/I ratios (D'Souza et al., 2016).

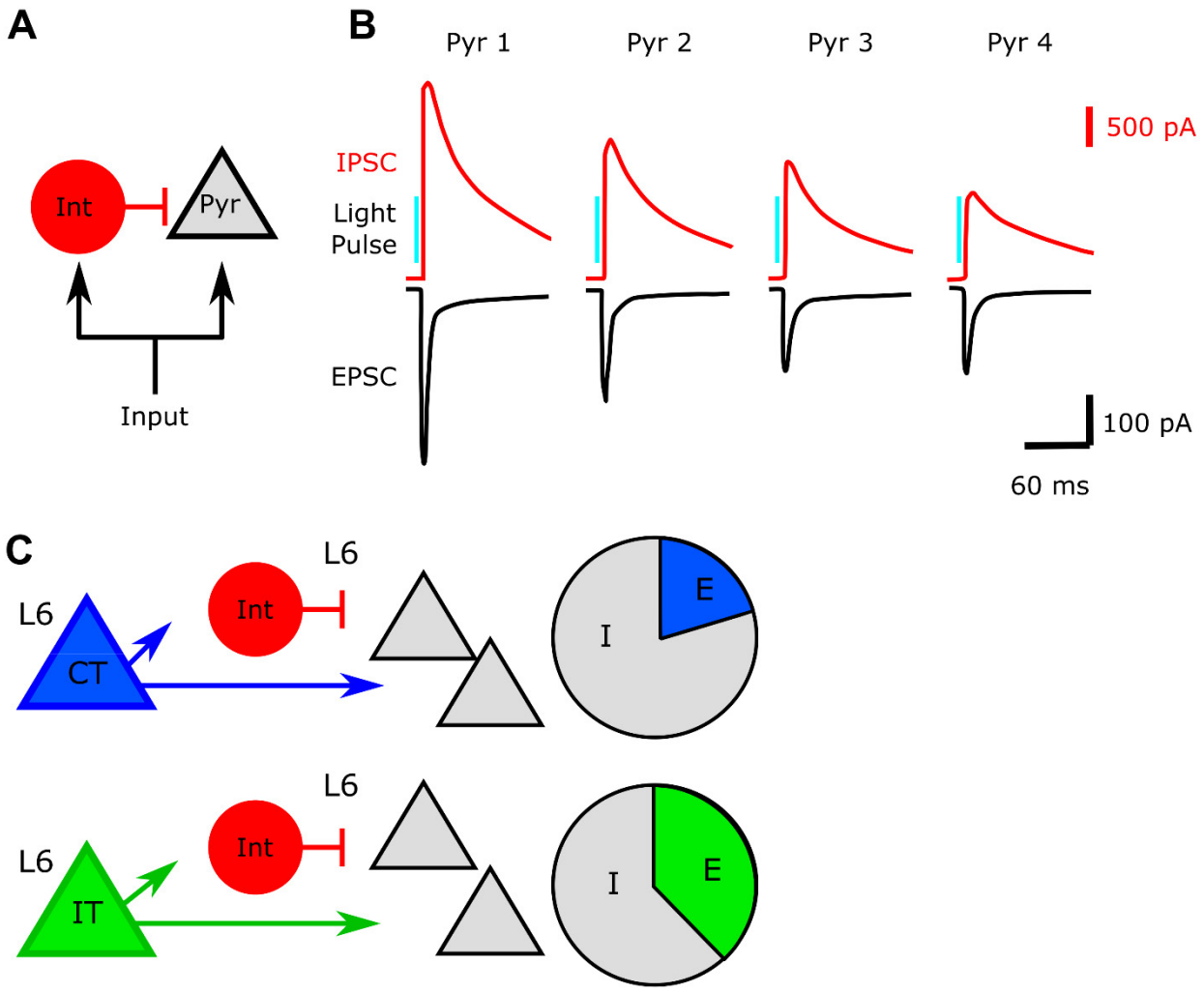


Figure 1.4 Cortical excitation and inhibition is matched but can result in different E/I ratios for components of cortical circuitry.

(A) Representation of feedforward disynaptic recruitment of inhibition. An excitatory input results in monosynaptic excitation of a pyramidal neuron population ('Pyr') as well as a neighboring population of inhibitory interneurons ('Int'). Such excitation efficiently brings the interneuron population to threshold and thus results in the recruitment of disynaptic inhibition on Pyr. (**B)** Across four L2/3 pyramidal neurons, optogenetic stimulation of L4 results in the recruitment of a level of disynaptic inhibition that is proportional to the evoked excitation. **(C)** E/I ratios can vary across different projections and circuits. For example, it has been shown that within Layer 6 the relative recruitment of inhibition by L6 CT neurons is greater than that of L6 IT neurons. This results in different E/I ratios being recruited when these neurons are stimulated. Modified from (Xue et al., 2014; Yamawaki & Shepherd, 2015).

Previous studies that have investigated the connectivity of ascending collaterals from infragranular layers to L2/3 using glutamate uncaging or similar techniques were unclear on whether the sources of inhibition overlapped well with the strongest sources of excitation (Kätzel et al., 2011; Meng et al., 2017; X. Xu et al., 2016). Whilst such studies suggested sublaminae differences in inhibitory motifs (Kätzel et al., 2011), or preferential targeting of L2/3 interneuron subtypes (Dantzker & Callaway, 2000), it remains unresolved how these correlate with specific projection-defined excitatory subtypes.

How somatosensory information is processed by these circuits

Given the focus of this thesis on the interplay between L2/3 and L5 pyramidal neurons, I will briefly explore how these neurons may play different functional roles in the coding and processing of somatosensory information.

Whilst broad subnetworks of L2/3 pyramidal neurons can receive subthreshold inputs, action potential firing in this layer is characteristically sparce(Harris & Mrsic-Flogel, 2013; Petersen & Crochet, 2013). In experiments where the activity of L2/3 pyramidal neurons were recorded during whisker driven behavior, the majority of neurons in this layer were 'silent' while a sparse subset drove almost all activity recorded in this layer. Firing rates in the active neurons were lower than those seen in L5(O'Connor et al., 2010; Sakata & Harris, 2009). It is thought that this sparse coding activity is enforced by a high level of ongoing inhibition in the layer(Mateo et al., 2011). One of the advantages of such sparse coding enforced by a strongly balanced E/I is that it allows for the maximum energy efficiency of information carried by each spike(Sengupta et al., 2013). This sparse coding regime however may be broken by a high velocity sharp whisker deflections (which may be of behavioral significant during texture discrimination), resulting in a wide spread high frequency response(Ranjbar-Slamloo & Arabzadeh, 2016).

In contrast L5 pyramidal neurons have higher rates of firing and follow a dense coding regime(Harris & Mrsic-Flogel, 2013; O'Connor et al., 2010). This may be important for the broadcasting of information to long range targets with high fidelity (Harris & Mrsic-Flogel, 2013). In L5 , and in particular L5 PT, neurons appear to have a wide sensory tuning to whisker inputs(C P J De Kock et al., 2007). Whisker stimulation responses tend to be coded with high fidelity in specific highly responsive pyramidal neurons in L5b (PT) , whilst spread of excitatory activity to neighboring columns appears to originate with a higher latency from L5a (IT)(C P J De Kock et al., 2007; Lefort et al., 2009; Reyes-Puerta et al., 2015). The interaction between ongoing activity in L5 pyramidal subpopulations and sparse sensory evoked spiking in L2/3 mediated by ascending collaterals and local inhibitory circuits remains unclear.

Aims of the thesis

Having introduced the relevant background and concepts underlying cortical synaptic circuitry, I am now in a position to articulate the main aims of my thesis and how it sets out to advance our understanding of translaminar signaling from L5 pyramidal subpopulations to L2/3, using the mouse somatosensory cortex as an experimental system.

We have seen that whilst L5 receives excitatory inputs from L2/3, there also exist reciprocal connections from L5 to L2/3. These are mediated by the local collaterals of L5 axons, but how they modulate activity in L2/3 remains poorly understood. **The aim of Chapter 3** is to begin to address this by recording from L2/3 pyramidal neurons *in vitro* and using optogenetic techniques to stimulate a non-specific population of L5 pyramidal neurons. Using a similar strategy *in vivo*, I will also explore how L5 modulates L2/3 responses to physiologically relevant sensory input.

Previous evidence suggests that different L5 neuronal subtypes can differ in terms of their local ascending axonal collaterals, which project radially and enter L2/3. **The aim of Chapter 4** is to examine whether L5 subtypes that are distinguished by their long-range axonal projection targets, also show differences in their local ascending collaterals. More specifically, retrograde labelling methods will be used to target IT and PT L5 pyramidal neurons, which will then be compared in terms of their intrinsic electrophysiological and axonal morphologies. Building upon these retrograde labelling techniques, I will also establish virus-mediated delivery of optogenetic tools to projection-defined L5 subtypes.

Whilst previous work has explored aspects of excitatory connectivity between L5 and L2/3, it remains unclear what translaminar signals IT and PT L5 pyramidal neurons transmit via their ascending axonal collaterals. Using the retrograde optogenetic tools developed in the previous chapter, **the aim of Chapter 5** is to determine the E/I signals that IT and PT L5 pyramidal neurons transmit to L2/3 pyramidal neurons.

In doing so, these experiments will establish which local interneuron subtypes are recruited by the ascending collaterals of IT and PT L5 pyramidal neurons.

In the intact brain, L2/3 neurons exhibit sparse activity and are believed to be strongly influenced by synaptic inhibition. But it is unknown how translaminar signals from IT and PT L5 pyramidal neurons modulate the activity of individual L2/3 pyramidal neurons. **The aim of Chapter 6** is to investigate how the differential recruitment of L2/3 inhibition by IT and PT L5 neurons, modulates spiking activity in L2/3 pyramidal neurons. This will be examined in brain slices *in vitro* and then using an *in vivo* preparation to investigate the effects upon sensory-driven responses.

Chapter 2 : Materials and methods

General strategies for the restricted expression of genetic tools

In order to explore the role of L5 pyramidal neurons in local cortical circuitry, a number of strategies were employed to restrict the expression of genetic tools such as the optogenetic activator, ChR2, and the fluorescent reporter, TdTomato (TdTom; **Fig 2.1**). Mice in which ChR2 is restricted to L5 pyramidal neurons were generated by crossing the *Rbp4-Cre* mouse line in which Cre recombinase (Cre) is expressed in L5 pyramidal neurons (details below), with the Ai32 reporter line that expresses ChR2 in a Cre-dependent manner (**Fig 2.1A**). Meanwhile, subpopulations of L5 pyramidal neurons could be studied through the use of stereotaxically-targeted viral injections into *Rbp4-Cre* mice. Injections with an Adeno-associated virus engineered for retrograde transport (rAAV2retro; details below) allowed for the selective, Cre-dependent expression of ChR2 in only those L5 pyramidal neurons that both expressed Cre and had long-range axonal projections to the injection site (**Fig 2.1B**). Similar expression patterns were also achieved in wild-type mice via *in utero* electroporation (IUE) of a DNA plasmid that expresses Cre-recombinase (details below), followed by targeted injection of rAAV2retro into the contralateral hemisphere. In this case, ChR2 was only expressed unilaterally and in those neurons that had both been electroporated and had long-range axonal projections to the injection site in the contralateral hemisphere. Finally, to perform fluorescently-targeted recordings from L2/3 interneurons whilst optically activating a subpopulation of L5 pyramidal neurons, 'triple' transgenic mouse lines were generated. This involved crossing the *Rbp4-Cre* mouse line with a second line in which Cre is expressed in a defined interneuron population, and a third line that expresses TdTom in a Cre-dependent manner. This resulted in TdTom expression in both L5 pyramidal neurons and the interneuron population of interest (**Fig 2.1C**). Through the use of targeted rAAV2retro injections into these triple transgenic animals, it was again possible to achieve selective ChR2 expression

in those L5 pyramidal neurons that both expressed Cre and had long-range axonal projections to the injection site. In tissue from these animals interneurons of interest in L2/3 could then be identified for targeted recordings through the selective expression of TdTom.

Animals

All animals were bred, housed and used in accordance with the UK Animals (Scientific Procedures) Act (1986). Experiments that relied upon restricting transgene expression to Layer 5 (L5) pyramidal neurons were performed with the *Rbp4-cre* transgenic mouse line (031125-UCD, GENSAT), in which a Cre recombinase (Cre) expression cassette is inserted at the initiating ATG codon of the first coding exon of the Retinol Binding Protein 4 (Rbp4) gene (Gerfen et al., 2013; Gong et al., 2007). A subset of experiments achieved channelrhodopsin-2 (ChR2) expression throughout L5 **(Fig2.1 A)** by crossing the *Rbp4-cre* line with the Ai32 line (012569, The Jackson Laboratory) that uses the CAG promoter to express ChR2 fused to enhanced yellow fluorescent protein (ChR2(H134R)-EYFP), in a Cre-dependent manner(Madisen et al., 2012). These mice were referred to as '*Rbp4-Cre/Ai32*' and were used for *in vitro* and *in vivo* studies at 12-16 weeks (3-4 months) of age.

Experiments that involved targeted recordings from fluorescently-labelled interneurons were performed in triple transgenic mice created by first crossing either the PV^{Cre} line (008069, The Jackson Laboratory) or the SST^{Cre} line (013044, The Jackson Laboratory)(Taniguchi et al., 2011), with the Ai9 transgenic line (007909, The Jackson Laboratory) that use the CAG promoter to express the red fluorescent protein, TdTomato, in a Cre-dependent manner(Madisen et al., 2010). The PV^{Cre} line uses the endogenous parvalbumin (*PV*) promoter/enhancer elements to direct Cre expression to *PV*-expressing cells. The SST^{Cre} line uses the endogenous somatostatin gene (*SST)* promoter/enhancer elements to direct *Cre* expression to SST-expressing cells.

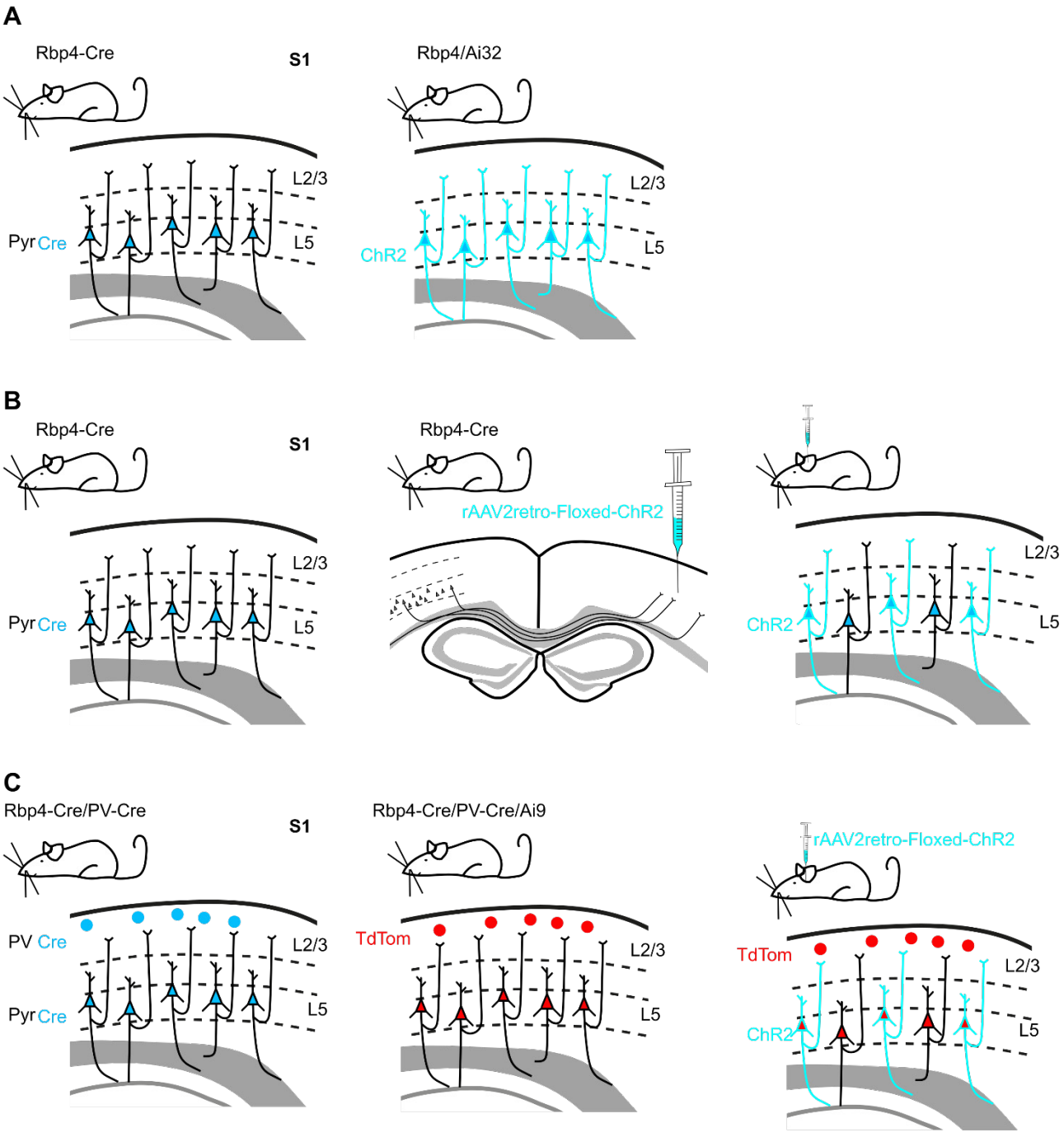


Figure 2.1 General strategies for the restricted expression of genetic tools.

(A) *Rbp4-Cre* mice express Cre recombinase selectively in L5 pyramidal neurons (l*eft*). To restrict ChR2 expression to L5 pyramidal neurons, *Rbp4-Cre/Ai32* mice were generated by crossing *Rbp4-Cre* mice with *Ai32* mice in which Channel rhodopsin-2 (ChR2) – EYFP is expressed in a Cre dependent manner (*Right*).

The resultant mice were then crossed with the *Rbp4-cre* line to generate triple transgenic lines (referred to as '*PV-Cre/Rbp4-Cre/Ai9'* and '*SST-Cre/Rbp4-Cre/Ai9*') in which floxed viral tools could also be expressed in L5 pyramidal neurons. In utero electroporation (IUE) experiments were carried out on time-mated C57BL/6 wild type mice, in which females were checked for plugs daily and the day of the plug was considered embryonic day 0.5 (E0.5).

Viruses and plasmids

The retrograde delivery of floxed ChR2 made use of a recently engineered adeno-associated virus (AAV) that is optimized for efficient retrograde transport(Tervo et al., 2016). The retrograde AAV encoded floxed ChR2-EYFP under the control of the elongation factor 1 *alpha (*EF1a) *promoter, is r*eferred to as 'rAAV-Floxed-ChR2', and obtained from Addgene (20298-AAVrg; AAVrg-EF1a-double floxed-hChR2(H134R)-EYFP-WPRE-HGHpA). IUE used a plasmid expressing Cre recombinase fused with the red fluorescent protein, mCherry, under the control of a CAG promoter (referred to as 'CAG-Cre'). CAG-Cre was made by Dr Louise Kay who replaced green fluorescent protein (GFP) in CAG-GFP (16664, Addgene) with Cre-mCherry.

Figure 2.1 Continued from opposite.

(B) A projection-defined L5 subpopulation was targeted by performing a stereotaxic injection of a retrogradely transported rAAV2retro encoding Cre-dependent ChR2 into a defined region of the brain (*middle;* contralateral S1 in this example). Following retrograde transport, ChR2 was expressed in only those L5 pyramidal neurons that both expressed Cre and had long-range axonal projections to the injection site (*right*). **(C)** To record from L2/3 interneurons whilst optically activating a subpopulation of L5 pyramidal neurons, 'triple' transgenic mouse lines were generated. *Rbp4-Cre* mice were first crossed with mice expressing Cre in a defined interneuron population, such that Cre was expressed in both L5 pyramidal neurons and the interneuron population of interest (*left;* in this example parvalbumin-expressing interneurons, '*PV-Cre*'). These mice were then crossed with the *Ai9* line that expresses TdTom in a Cre-dependent manner, resulting in TdTom expression in both the interneuron population and L5 pyramidal neurons (*middle*). Through the use of targeted rAAV2retro injections into these triple transgenic animals, it was again possible to achieve selective ChR2 expression in those L5 pyramidal neurons that both expressed Cre and had long-range axonal projections to the injection site. Meanwhile, L2/3 interneurons could be targeted for recording based on their expression of TdTom (*right*).

In utero electroporation

Time-mated pregnant dams with embryos aged 13 days (E13) were anaesthetized with isoflurane. The depth of anaesthesia was assessed by monitoring respiration rate and the pedal withdrawal reflex. Surgery was performed in a laminar flow hood and the animals were positioned on a heating pad to maintain body temperature. Buprenorphine (Alstoe Animal Health) and metacam (Boehringer Ingelheim) were administered preoperatively, and Viscotears (Alcon) was applied to protect both corneas during the procedure. The abdomen was shaved and sterilized using a chlorhexidine based solution. A midline laparotomy incision exposed the uterine horns and provided access for targeted injections into the embryos. 1 μL of CAG-Cre DNA (at a concentration of 3-4 μg/μL and mixed with 0.03 % Fast Green in phosphate buffer) was injected intraventricularly into each embryo using a pulled micropipette, inserted through the uterine muscle and amniotic sac. The anode of a platinum Tweezertrode (Genetronics) was Placed outside of the uterine muscle, over the dorsal telencephalon of the embryo. Five 42 V pulses (each 50 ms duration, separated by 950 ms) were applied using an Eltro Square Porator (ECM830, BTX Harvard Apparatus). After electroporating the embryos, the uterus was replaced within the abdomen, the cavity filled with warm sterile phosphate buffered saline (PBS) and the abdominal muscle and skin incision were closed with prolene sutures. Animals were left to recover in a heated recovery box for 10 minutes and then moved to a clean cage. Bupenorphine was administered as post-operative analgesia two hours after the surgery, followed by meloxicam 24 hours after the surgery.

Postnatal injections

Mice aged 6 weeks were anaesthesized with isoflurane (Zoetis), placed on a heating pad and positioned in a stereotaxic frame (Kopf), where they were secured using bilateral ear bars in the external auditory meatus. Bupenorphine was administered subcutaneously preoperatively and Viscotears were applied

bilaterally to protect corneas. The skin over the cranium was shaved and Emla cream (AstraZeneca) applied. The skin was then sterilized using a chlorhexidine based solution and a midline incision was made from the interpupillary line to the interaural line. A small craniotomy (< 1 mm^2) was performed at predefined stereotaxic coordinates using a high speed dental drill (H.MH-170, Foredom). A pulled glass micropipette (Blaubrand IntraMARK) was used to inject either cholera toxin subunit B (CTB) conjugated with Alexafluor-488 (CTB-488, Thermo Fisher Scientific) or rAAV-Floxed-ChR2 at predefined stereotaxic coordinates relative to bregma and depths relative to the pial surface. Injections were made at a rate of 33 nL/min. rAAV-Floxed-ChR2 was injected into one of three anatomical targets: the left primary motor cortex (LM1), right primary somatosensory cortex (RS1), or left posterior medial nucleus (POm) of the thalamus (LThal), as follows. For LM1, 300-660 nL was injected at a depth of 500 µm from the pial surface, 1 mm anterior and 1.1-1.5 mm lateral of bregma. For RS1, 300-900 nL was injected at a depth of 500 µm from the pial surface, 1.0-1.5 mm posterior and 2.5-3.0 mm lateral of bregma. For LThal, 300-660 nL was injected at a depth of 2.5-3.0 mm from the pial surface, 2.1 mm posterior and 1.4 mm lateral of bregma. The pipette was maintained in place for an additional 5-10 minutes before slow withdrawal. The craniotomy was then covered and the skin closed using 6-0 Vicryl sutures. Intraoperative losses were replaced with subcutaneous normal saline and animals were recovered in a heated chamber. Following injections with rAAV-Floxed-ChR2, animals were maintained for > 4 weeks to optimize levels of viral expression and were studied *in vitro* or *in vivo* at 12-24 weeks (3-6 months). Injections with CTB-488 were performed at the same co-ordinates, but with adjusted volumes. For LM1 and RS1, 300-460 nL of CTB-488 was injected. For LThal, 200-330 nL of CTB-488 was injected. Following injections with CTB-488, animals were maintained for >1 week, before being used for *in vitro* brain slice experiments at 8-12 weeks (2-3 months).

Acute brain slice preparation and in vitro recording conditions

To prepare acute brain slices, mice were anaesthetized with isoflurane and decapitated. The head was rapidly cooled using ice cold cutting solution containing in mM (75 sucrose, 80 NaCl, 1.25 $NaH_2PO_4.2H_20$, 26 $NaHC0_3$, 2.5 KCL, 20 glucose, 0.5 $CaCl_2$ and 4 $MgCl_2$; at pH 7.2-7.4), which had been bubbled with carbogen gas (95 % O_2/5 % CO_2). Coronal slices (350-400 µm thick) of primary somatosensory cortex were generated with a vibrating microtome (Microm HM650V) at ice cold temperatures. Slices were immediately transferred to a submerged recovery chamber containing artificial cerebrospinal fluid (aCSF) comprising in mM (119 NaCl, 1.25 $NaH_2P0_4.2H_20$, 26 $NaHC0_3$, 2.5 KCL 10 glucose, 2 $CaCl_2$, 2 $MgCl_2$ and 5 ascorbic acid; at 305 mOsm and pH 7.2-7.4) and continuously bubbled with carbogen gas. Slices were rested for at least one hour before starting recordings, during which they were held at 35°C for the first 30 minutes and then cooled to room temperature. Once transferred to the recording chamber, slices were continuously perfused with aCSF at 28-32 °C at a rate of 2-3 ml/min and bubbled with carbogen gas. In a subset of experiments, fibres passing through L4 were cut by making an incision with a fine micro-knife of 1-2 mm length, between L5 and L2/3, and directly below (i.e. ventral to) the recorded L2/3 neurons. The effectiveness of these transections was confirmed visually during the recordings and then post-hoc using confocal microscopy.

Patch pipettes were pulled from standard wall borosilicate glass capillaries (Warner Instruments) to achieve a tip resistance of 3-6 MΩ. For voltage clamp experiments, pipettes were filled with internal solution containing in mM (126 Cs-gluconate, 10 HEPES, 1.5 $MgCl_2.6H_20$, 4 Mg_2ATP 0.4 Na-GTP, 10 Na-phosphocreatine, 2 QX-314-Cl and 2 EGTA; at 292 mOsm and pH 7.3). For current clamp experiments, patch pipettes were filled with a solution containing in mM (128 K-gluconate, 4 KCl, 4 Mg_2ATP, 0.3 Na-GTP, 10 Na-phosphocreatine and 10 HEPES; at 292 mOsm and pH 7.3). Biocytin (0.2-0.5 %; Sigma-Aldrich) was added to the internal solution for cell filling and morphological reconstruction. Recordings were performed using a MultiClamp 700B amplifier controlled by Multiclamp Commander software (Molecular

Devices) and acquired using Clampex 10.2 software (Molecular devices). Slices were visualized via 10x and 60x objectives using video assisted infrared differential interference contrast imaging (DIC) on a BX51WI microscope (Olympus).

Recordings were performed from pyramidal neurons in L2/3 or L5 of primary somatosensory cortex, which was identified by the direct visualization of barrels and characteristic location relative to anatomical landmarks under DIC. Cortical layers were identified based on cell sizes, cell density and depth from pia. In a number of experiments, recordings were made from pairs of neurons comprising a L2/3 pyramidal neuron and a neighbouring fluorescently-labelled interneuron (mean pair distance 50 ± 6 μm). In addition to fluorescence, interneuron identity was confirmed from characteristic electrophysiological intrinsic properties. Neuronal pairs were recorded simultaneously, except for 6 pairs that were recorded sequentially with minimal delay. Access resistance was calculated in voltage clamp configuration, from the fast current transients following repeat square wave voltage steps of -10mv. Neurons were accepted if they exhibited an access resistance below 35 MΩ, which changed less than 30 % over the course of the recording. Neurons with a depolarized membrane potential (> -45 mV) or significant negative leak current, were excluded. Excitatory post-synaptic currents (EPSCs) were measured at the reversal potential for inhibitory post-synaptic currents (IPSCs; -60 mV). IPSCs were measured at the reversal potential for EPSCs (+10 mV). For optical stimulation of ChR2, blue light was delivered via an LED positioned immediately below the recording chamber. LED pulse duration (1-3ms) was optimized for each neuron and delivered at 20 s intervals, with a minimum of 10 sweeps for both the EPSC and the IPSC recordings at a particular light intensity. For further analysis the maximum amplitude of each current were used for further analysis ("peak EPSC" and "peak IPSC") . Where possible, different light intensities were used to sample a neuron's excitation/inhibition ratio (E/I ratio) across a range of input levels. The light intensity that recruited a peak EPSC amplitude closest to a target amplitude were used for further matched comparisons of E/I ratio. This was selected to best explore monosynaptic connectivity and limit unwanted polysynaptic recruitment.

Light intensity ranged from 5-80mW/mm^2 recorded at the tissue edge closest to the LED. To standardize the activation of ChR2-expressing fibres in current clamp recordings, the LED settings were determined by first recording light-evoked EPSCs in voltage clamp. Monosynaptic connectivity between simultaneously recorded neuronal pairs was assessed in current clamp by eliciting brief trains of action potentials (spikes) in the putative pre-synaptic neuron with suprathreshold somatic current pulses (3 x 10 ms), and recording the membrane potential of the putative post-synaptic neuron. This was repeated 10 times for each putative connection and the sweeps averaged to determine if a post-synaptic response was present. In a subset of experiments, EPSC and IPSC amplitudes were recorded before and after the addition of picrotoxin (PTX; 100µM) , kynurenic acid (Kyn; 1 µM) or CNQX (10µM) to the recording solution.

Analysis of in vitro electrophysiological recordings

Electrophysiological recordings were analysed using custom-written scripts in MATLAB (R2017b/R2019a, MathWorks). Subsequent statistical analysis was performed in Prism (Version 8, GraphPad). For light-evoked currents and potentials, the first sweep was discarded to eliminate the potential effects of hysteresis between recordings. Leak currents or resting membrane potentials were subtracted so that responses reflected the relative change from baseline. E/I ratio was calculated as the peak EPSC / (peak EPSC + peak IPSC). Matched comparisons used light levels that elicited an equivalent peak EPSC amplitude, so that E/I ratios were compared across similar levels of excitatory input. For animals expressing rAAV-Floxed-ChR2, the matched peak EPSC amplitude was ~50 pA. Meanwhile, in *Rbp4-Cre/Ai32* transgenic animals, the matched peak EPSC amplitude was ~250pA. In current clamp recordings, the peak excitatory post-synaptic potential (EPSP) was defined as the maximum membrane potential recorded within 100 ms of the light pulse, and the peak inhibitory post-synaptic potential (IPSP) was defined as the minimum membrane potential within 200 ms following the peak EPSP. Membrane resistance was calculated in

voltage clamp configuration, from the stable current change following repeat square wave voltage steps of -10mv.

Action potential (AP) input-output curves were generated in current clamp by injecting a series of somatic current steps (minimum step = -200 pA, Δ step = +50 pA, step duration 500 or 1000 ms). Intrinsic properties were calculated at the first suprathreshold current injection. AP threshold (i.e. spike threshold) was defined as the membrane potential at which the first derivative first exceeded 20 mV/ms. AP height was defined as the membrane potential difference between AP threshold and the peak of the AP. AP half width was defined as the time between the upstroke and downstroke at AP half-height. The fast afterhyperpolarizing potential (fAHP) was defined as the minimum membrane potential immediately following the peak of the AP, relative to AP threshold. The depolarizing after potential (DAP) was defined as the peak depolarization that followed the fAHP within 70ms. The sag was determined from the first negative current step at which the membrane potential reached -100 mV and was defined as the maximum hyperpolarization (maxHP), minus the steady-state hyperpolarization. Spike rate was calculated as the total number of action potentials measured over the total time of the current step and adaptation index was calculated from the slope of the linear fit of interspike intervals (ISIs) plotted in temporal order (excluding the first two ISIs). For example, an adaptation index of 0.1 translated to a 10 % mean increase in ISIs between successive spikes.

Histological analyses

Brain slices were fixed in 4 % paraformaldehyde in PBS (pH 7.4) for at least 24 hours at 4°C. The tissue was then blocked in PBS containing 0.3 % Triton X-100 (Sigma-Aldrich) and 10 % normal goat serum (NGS; Thermo Fisher Scientific) for 1 hour at RT. For soma counts, a double immunolabelling protocol was performed for GFP (to boost the ChR2-EYFP signal) and NeuN (to detect neuronal nuclei). Slices were incubated overnight at 4°C in PBS containing 0.3 % Triton X-100 and 1 % NGS, plus anti-GFP (1:1000, rabbit;

Thermo Fisher Scientific, CAT# A-11122, RRID:AB_221569) and anti-NeuN (1:250, mouse; Millipore CAT# MAB377, RRID:AB_2298772) primary antibodies. Slices received three 10 minute washes in PBS and were then incubated overnight at 4 °C in PBS containing 0.3% Triton X-100 and anti-rabbit Alexa Fluor 488 (1:500, goat; Thermo Fisher Scientific, CAT# A-11034, RRID:AB_2576217) and anti-mouse Alexa Fluor 568 (1:500, goat; Thermo Fisher Scientific, CAT# A-21124, RRID:AB_2535766) secondary antibodies. For neuronal reconstructions, biocytin-filled cells were visualized using streptavidin fluorescent conjugated antibodies. Slices were processed as above, but using subsets of the following as primary antibodies: anti-GFP to boost EYFP signal (1:1000, chicken; Aves Lab, CAT# GFP-1020, RRID:AB_10000240), anti-RFP to boost TdTomato signal (1:500, rat; Chromotek, CAT# 5f8-100, RRID:AB_2336064), Alexa Fluor 488 streptavidin (1:1000; Life Technologies, CAT# S32354, RRID:AB_2315383), Alexa Fluor 594 streptavidin (1:1000; Life Technologies, CAT# S32356) and Alexa Fluor 680 streptavidin (1:1000; Life Technologies, CAT# S21378), in combination with the following secondary antibodies, as required: anti-chicken Alexa Fluor 488 (1:500, goat; Thermo Fisher Scientific, CAT# A-11039, RRID:AB_142924) and anti-rat Alexa Fluor 594 (1:500, donkey; Thermo Fisher Scientific, CAT# A-21209, RRID:AB_10561522). To delineate cortical layers and regions, slices were counter-stained with the nuclear marker 4',6-diamidino-2-phenylindole (DAPI, 1:1000 in PBS, Sigma-Aldrich, CAT# **D9542**) and then mounted on slides with VECTASHIELD mounting medium (Vector Laboratories, CAT# H-1000, RRID:AB_2336789).

Image acquisition and analysis

Fluorescence images were acquired with an LSM 880 confocal microscope (Zeiss) equipped with 488 nm, 561 nm and 633 nm lasers, plus a 10x air objective and 20x water-immersion objective (W Plan-Apochromat, NA 1.0), and an integrated motorized XY stage. For assessing fluorescence across brain regions, low power images were generated using the tiling function in the ZEN acquisition software (Zeiss, RRID:SCR_013672) and were then aligned with the corresponding section from a stereotaxic mouse brain

atlas (Franklin & Paxinos, 2007). For soma counts, cells and layers were manually identified and their position relative to the pia and white matter was determined. To generate radial fluorescence profiles through cortex, a custom script was used to draw a line from the pia to white matter, along which was calculated relative fluorescence levels. The reconstruction of axon morphologies was performed on biocytin-filled neurons and used all visible axonal processes within the local region of cortex, through all dimensions of the brain slice. Damaged neurons that lacked axonal processes exiting L5 were excluded from further analysis. Reconstructed neurons were traced using the Fiji image analysis software (Longair et al., 2011) (Schindelin et al., 2012) and the 'Simple Neurite Tracer' plugin. Cortical layers were identified and overlaid on the images by registering DAPI images and confocal images with the 'Line ROI' and 'Landmark Correspondences' plugins. The reconstructed axon and bouton locations were skeletonized and processed using custom written scripts, making use of the 'natverse' (https://natverse.github.io/) neuroanatomical packages (Bates et al., 2020). The locations of pre-synaptic boutons were identified as regions of interest (ROIs). Each bouton's interbouton interval (IBI) was defined as the mean of the distances to the preceding and subsequent boutons along the axon.

In vivo preparation and recording conditions

Animals were weighed and anaesthesia was induced with isoflurane (3 %) and then maintained by urethane injection (1.3-1.8g/kg, Sigma-Aldrich). Isoflurane levels were reduced to zero following the initial craniotomy and electrode placement. No recordings were made until 30 min following the cessation of isoflurane. A subcutaneous injection of glycopyrrolate (0.04mg/kg, Wyeth LLC) was administered to minimize respiratory secretions. The surgical and recording area were sterilized using 70 % ethanol and distel disinfectant (Tristel), and the surgical procedure was carried out under aseptic conditions. Animals were continually supplied with oxygen (0.1 L/min) throughout surgery and recordings. Anaesthetic depth was confirmed by monitoring animal vital signs as well as for the absence of spontaneous movements. A

trimmer was used to remove fur from the head, and the area was sterilized with iodine solution. Marcaine (Hospera) was applied topically for local analgesia. Animals were positioned in a stereotaxic frame (Stoelting), the head stabilized with ear bars and body temperature maintained via a regulated heat mat (FHC). A single incision was made anterior-posterior through the skin overlying the skull, the periosteum retracted and the skull surface scraped dry with a scalpel. A pneumatic dental drill (H.MH-170, Foredom) was used to perform a 2 x 2 mm craniotomy, centred over the left primary somatosensory cortex (coordinates: 3.0 mm lateral and 1.5 mm posterior of bregma). The bone flap was removed and saline-soaked spongostan (Ethicon) applied to the dura mater to prevent any bleeding. Recordings used a 32-channel linear probe (A32, NeuroNexus). To identify probe placement post-mortem, electrodes were repeatedly submerged in a DiI lipophilic dye solution (Thermo Fisher) and allowed to air dry before use. During recordings, the probe was inserted into the cortex at a 30 degree angle, to a depth of 1 mm. The probe was connected to an acquisition board (Open Ephys) using a NPD36 connector (Omnetics) and a RHD2132 amplifier board (Intan) which acquired and digitised the signal at 30kHz.

In vivo stimulus protocols and data analysis

Stimulus protocols were generated using custom-written scripts in MATLAB and delivered via a Pulse Pal (Open Ephys). To stimulate individual whiskers, a single whisker was inserted into a piece of capillary glass, which was attached to a piezoelectric waver (Piezo Technics) clamped to a manoeuvrable swivel arm and operated via a piezo amplifier (E-650, Physik Instrumente). For optogenetic stimulation, brief light pulses (3-5ms duration) were delivered from a blue LED (473nm, Farnell), positioned directly above the brain surface. A range of LED intensities were used (light values 3-47mW/mm^2), so that the level of L5 activity could be matched across animals. All stimulus protocols were repeated for at least 25 sweeps.

Data were analysed using custom scripts written in MATLAB. Data were band-pass filtered (300 - 6000 Hz) to analyse multiunit activity (MUA), and low-pass filtered (<300 Hz; second order Butterworth filter) to

analyse local field potentials (LFPs). LFP traces were further filtered using a 50 Hz notch filter to ensure complete absence of any electrical noise. MUA was detected from negative deflections whose peaks were greater than four times the standard deviation of the filtered signal. To avoid undue influence from physiological signals or artifact transients, this standard deviation was estimated by dividing the median absolute value of the trace by 0.6745 (Quiroga et al., 2004). The location of layer 4 was estimated by locating the channel with the largest short-latency negative LFP deflection in response to a whisker stimulus (Einevoll et al., 2013; Kajikawa & Schroeder, 2011; Yamamura et al., 2017). Layer 5 activity was sampled from the channels 50-300 microns below the channel of the layer 4 sink. Only those animals exhibiting a statistically significant light-evoked spiking response in L5 (in time window of 7ms until 30ms following light stimulus onset, compared to baseline) were included in the analysis (one-tailed, two-sample t-test between the post-opto time windows and baseline windows of equal length for all trials, $P < 0.05$). To identify putative single units, spike sorting was performed with the Kilosort algorithm (M Pachitariu et al., 2016).Putative regular spiking units in L2/3 and upper L4 (from 25 microns below the peak L4 channel upwards) were identified and included for further analysis. Only units exhibiting a whisker-evoked response (defined as a minimum spike probability of 20% across all trials in the 5-50ms window following stimulus in the control condition) were subjected to further analysis. In accordance with previous work, threshold values were used to exclude fast-spiking neurons. Units with a spike trough-to-peak time of less than 0.5 ms, and a spike width (between the points that crossed 10% of peak deflection) less than 0.25 ms, were excluded as putative fast-spiking neurons (Barthó et al., 2004; Okun et al., 2015; Rojas-Piloni et al., 2017). To evaluate light-evoked modulation of the whisker response, spike rates were calculated for the 5-50 ms following whisker stimuli. To calculate a light-induced change in spike rate, data from whisker-light paired stimuli was compared with whisker-only stimuli The population of putative fast-spiking neurons was not sufficiently large to compare activity modulation across different cell populations.

Statistics

Statistical analysis was performed in MATLAB and Prism. Data was tested for normality using the Kolmogorov-Smirnov, Shapiro-Wilk and D'Agostino and Pearson tests as appropriate, and data sets found to be significantly non-normal by any of these tests ($p < 0.05$) were treated as non-parametric. Appropriate parametric or non-parametric test were then performed. All data is displayed as mean ± standard error of the mean, unless otherwise stated. A level of statistical significance was assumed at $\alpha = 0.05$.

Page intentionally left blank

Chapter 3 : The influence of layer 5 input upon layer 2/3 of mouse somatosensory cortex

Introduction

Cortical columns comprise of a series of stereotypical connections within and between cortical layers. This has led to the influential idea of a 'canonical microcircuit', which incorporates consistent patterns of synaptic connectivity and represents a fundamental unit for information flow through cortex (Rodney J Douglas et al., 1989; Rodney J Douglas & Martin, 2004; Harris & Shepherd, 2015). At the same time however, it is widely acknowledged that cortical connectivity defies a simple feedforward excitatory model. Indeed, reciprocal connectivity between networks, either in different cortical areas or layers within a column, is increasingly being recognized as an important component underlying cortical computations (Ayaz et al., 2019; Guo et al., 2020; Harris & Mrsic-Flogel, 2013; Yasuo Kawaguchi, 2017). Of particular interest to this thesis, is the interaction between cortical Layer 2/3 (L2/3) and Layer 5 (L5) pyramidal neurons.

L2/3 pyramidal neurons are one of the most numerous cell types in the brain, forming highly specific subnetworks and playing an important role in sensory processing (Harris & Mrsic-Flogel, 2013; Petersen & Crochet, 2013). L2/3 receives strong excitatory input from L4, which, as the major thalamorecipient layer, is often classed as the principal input layer in somatosensory cortex. L5 meanwhile, is often classed as the principal output layer (Feldmeyer, 2012). L5 pyramidal neurons integrate incoming signals from the local cortical circuit as well as distant networks, and then project the results of this neuronal integration through dense action potential coding to long range targets such as other cortical regions or subcortical

structures (Brumberg et al., 1999; Rodney J Douglas & Martin, 2004; Feldmeyer, 2012; Harris & Mrsic-Flogel, 2013; Lefort et al., 2009; Reyes-Puerta et al., 2015).

Within the canonical microcircuit, it has been well described that L2/3 pyramidal neurons make excitatory connections onto L5 pyramidal neurons (Feldmeyer, 2012; Harris & Mrsic-Flogel, 2013; Harris & Shepherd, 2015; Mao et al., 2011; Petreanu et al., 2009). However, the axons of L5 pyramidal neurons that project to long-range targets are also known to have collaterals that form local intracortical reciprocal connections with L2/3 (Feldmeyer, 2012; Lefort et al., 2009; Oberlaender et al., 2011; Shepherd & Svoboda, 2005; Staiger et al., 2015). The exact role that these ascending collaterals from L5 pyramidal neurons may play in shaping local cortical activity, and in particular ongoing processing in L2/3, remains unclear. Recent work suggests that L5 may play an important role in passing information to surrounding cortical columns (Lefort et al., 2009; Oberlaender et al., 2011), determining slow wave oscillations (Beltramo et al., 2013) or sensory perception (Vecchia et al., 2020).

A fundamental feature of cortical circuits is the near-simultaneous recruitment of inhibition that accompanies excitatory inputs (Isaacson & Scanziani, 2011). This inhibitory recruitment is often matched to the level of excitation, which results in an excitation/inhibition (E/I) balance (Xue et al., 2014) that can vary depending on the particular source of input (Adesnik, 2018; Sempere-Ferràndez et al., 2019; Yang & Sun, 2018). The E/I ratio determines how a particular input will shape the activity of the target post-synaptic neuron, as the E/I ratio determines the integration of synaptic inputs, input-output functions and, in the context of sensory processing, spatial and temporal feature selectivity of the post-synaptic neuron (Atallah et al., 2012; Isaacson & Scanziani, 2011; Okun & Lampl, 2008; Pouille et al., 2009; Pouille & Scanziani, 2001; Swadlow & Gusev, 2002; Wehr & Zador, 2003). Some work has suggested that translaminar connectivity from L5 to L2/3 may be excitatory and facilitatory (Adesnik, 2018; Adesnik & Scanziani, 2010). However, it has also been recognized that there exist strong inhibitory motifs from L5 to L2/3 (Kätzel et al., 2011) and that L5 can efficiently recruit local inhibition throughout the column (Vecchia

et al., 2020). Thus, whilst the excitatory connectivity from L2/3 to L5 is well established, the role that potential reciprocal connectivity from L5 ascending collaterals may play in local cortical information processing remains unclear. There is a paucity of data on how these connections functionally recruit inhibition and modulate L2/3 activity both *in vitro* and *in vivo.*

Aims

The aims of this chapter were as follows:

1. To characterize the functional connectivity between L5 and L2/3 in terms of both monosynaptic excitation and the recruitment of inhibition.
2. To assess how input from L5 may modulate ongoing activity in L2/3.
3. To assess how input from L5 influences responses to physiologically relevant stimuli *in vivo.*

Results

To evaluate functional connectivity from L5 to L2/3, I used a transgenic strategy that afforded the selective optogenetic stimulation of L5 pyramidal neurons. *Rbp4-Cre/Ai32* mice were generated by crossing *Rbp4-cre* mice in which Cre recombinase (Cre) is restricted to L5 pyramidal neurons, with *Ai32* mice in which channelrhodopsin-2 (ChR2)-EYFP is expressed in a Cre-dependent manner (**Fig 3.1A)**. Acute cortical brain slices were then prepared from primary somatosensory cortex at 12-16 weeks (3-4 months) of age and L2/3 pyramidal neurons were targeted for whole cell patch clamp recordings. By clamping the L2/3 pyramidal neuron at the reversal potential for ionotropic glutamate receptors and gamma-aminobutyric

Figure 3.1 continued from opposite

(B) Example EPSCs (at -60 mV) and IPSCs (at +10 mV) recorded from the same L2/3 pyramidal neuron in response to light stimulation of L5. **(C)** Example recordings from a single neuron demonstrating how different light intensities were used to sample a neuron's excitation/inhibition ratio (E/I ratio) across a range of input levels. The single pair of EPSC and IPSC recordings from the level of light stimulation which recruited Excitatory currents closest to a target size (~ 200pA) were chosen for further analysis **(D)** Across a population of L2/3 neurons, peak EPSC amplitude positively correlated with peak IPSC amplitude (n = 40 neurons; Spearman's correlation coefficient, r = 0.55, p = 0.0002). Line indicates the line of best fit, constrained to pass through the origin. Peak EPSC amplitude was smaller than peak IPSC amplitude (EPSC: 239 ± 10 pA versus IPSC: 652 ± 83 pA, Wilcoxon matched-pairs signed rank test, W = 662, p < 0.0001). **(E)** The peak EPSC/(peak EPSC + peak IPSC) for the input from L5-to-L2/3 was biased towards inhibition (0.370 ± 0.034, One sample Wilcoxon signed rank test, W = -490, p = 0.0007).

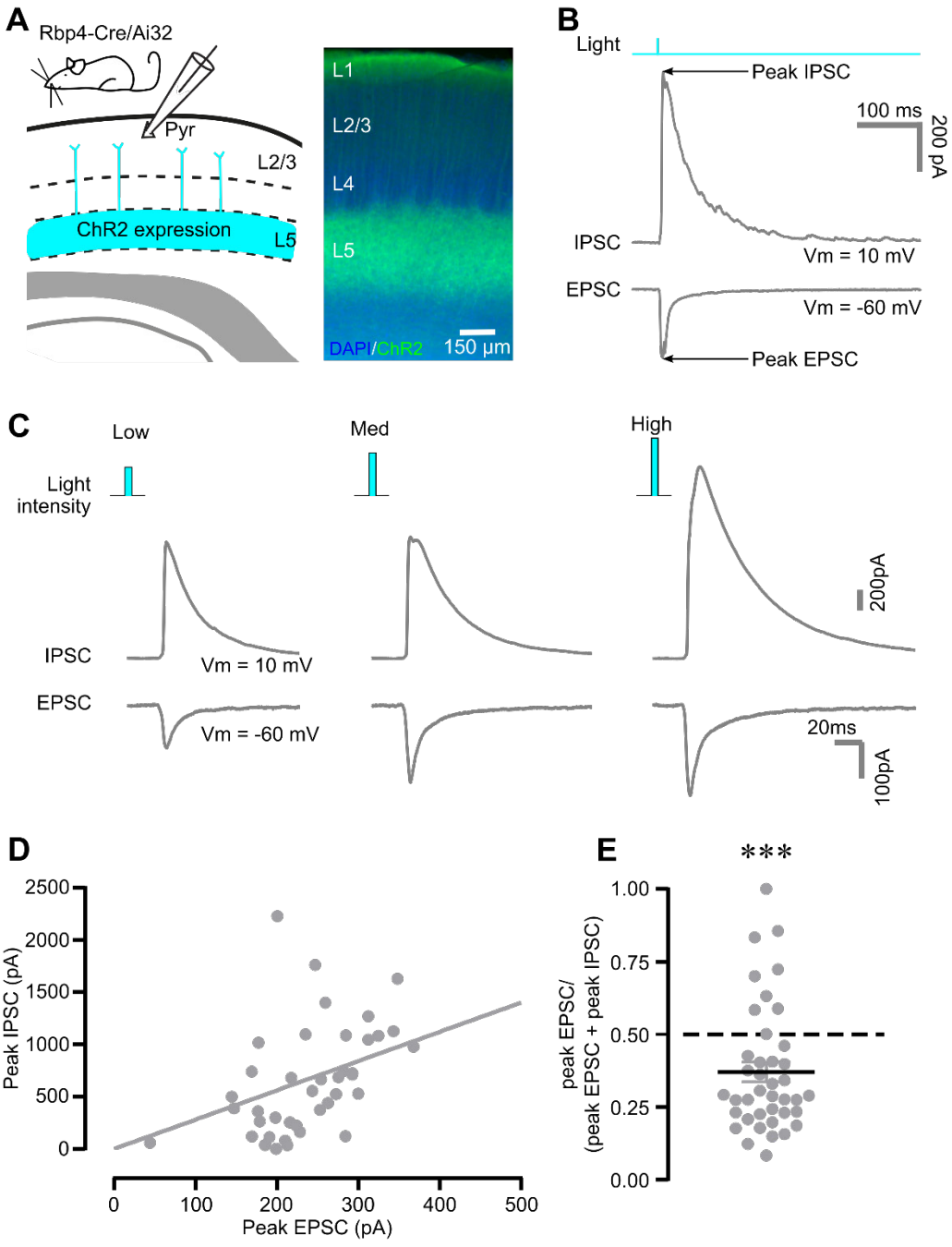


Figure 3.1 Transgenic mouse model for investigating the effects of L5 input to L2/3 in primary somatosensory cortex

A) Experimental design for studying the functional effects of L5 input to L2/3 pyramidal neurons (*left*). Rbp4-Cre/Ai32 mice were generated by crossing *Rbp4-cre* mice in which Cre recombinase (Cre) is restricted to L5 pyramidal neurons, with *Ai32* mice in which channelrhodopsin-2 (ChR2)-EYFP is expressed in a Cre-dependent manner. Acute brain slices were prepared from primary somatosensory cortex at 12-16 weeks (3-4 months) of age. L2/3 pyramidal neurons were targeted for whole cell patch clamp recordings, whilst L5 neurons were stimulated with brief pulses of blue light (473 nm; 1-3 ms). Example image of fixed tissue illustrating ChR2-EYFP expression in L5 (*right)*. Cortical layers were delineated with the nuclear marker, DAPI.

acid receptor type A ($GABA_A$) receptors, I could record light-evoked excitatory post-synaptic currents (EPSCs) and inhibitory post-synaptic currents (IPSCs) within the same cell (**Fig 3.1B).** For the purpose of further analysis the maximum amplitude of each current were used ("Peak EPSC" and "Peak IPSC"). L5 neurons were stimulated with brief pulses of blue light (473 nm; 1-3 ms), whose intensity could be varied across recordings. For each neuron, where possible, multiple light intensities were recorded (**Fig 3.1 C)** and then currents recorded from the intensity which evoked Excitation closest to a target amplitude were chosen for further analysis. This generated a range of peak EPSC amplitudes in the L2/3 pyramidal neuron (n = 40 neurons; minimum peak EPSC was 44 pA and maximum was 368 pA), whose delay was consistent with a monosynaptic excitatory connection from L5. For this range of light-evoked EPSCs, there was a positive Correlation between the L2/3 neuron's peak EPSC amplitude and peak IPSC amplitude elicited by the same L5 stimulation (**Fig 3.1D;** Spearman's coefficient, r = 0.55, p = 0.0002). This is consistent with the idea that the level of synaptic inhibition is related, or 'matched', to the level of synaptic excitation(Xue et al., 2014). Under these recording conditions, the peak IPSC amplitude was larger than the peak EPSC (peak EPSC of 239 ± 10 pA versus peak IPSC of 652 ± 83 pA; Wilcoxon matched-pairs signed rank test $p < 0.0001$). As a result, the E/I ratio (calculated as peak EPSC/(peak EPSC + peak IPSC)) was below equality and had a value of 0.37 ± 0.03, indicating a significant role for inhibition in mediating L5's functional effect upon L2/3 (**Fig 3.1E**; , One sample Wilcoxon signed rank test, p = 0.0007). I next examined the circuit underlying the functional effects of L5 upon L2/3 pyramidal neurons. The recruitment of disynaptic inhibition is a common motif in cortex, whereby monosynaptic excitatory inputs to a layer or region are able to recruit interneurons that then elicit their inhibitory effects upon the post-synaptic population (**Fig 3.2A**; (Cruikshank et al., 2007, 2010; Swanson & Maffei, 2019)).

Figure 3.2 ***Continued from opposite***

(E) The latency from light pulse to synaptic current onset was shorter for EPSCs than IPSCs (n= 12 neurons, 5.13 ± 0.40 ms for EPSCs versus 7.26 ± 0.66 ms for IPSCs; Wilcoxon matched-pairs signed rank test, W = -78, p = 0.0005). **(F)** Example current clamp recording of a L2/3 pyramidal neuron's membrane potential (V_m) following light stimulation of L5 inputs. An EPSP in the L2/3 neuron is immediately followed by a hyperpolarizing IPSP. **(G)** EPSP and IPSP peak amplitudes for a population of L2/3 pyramidal neurons (n = 5 neurons, mean Peak EPSP was 14.3 ± 2.3 mV and mean Peak IPSP was 4.5 ± 1.1 mV).

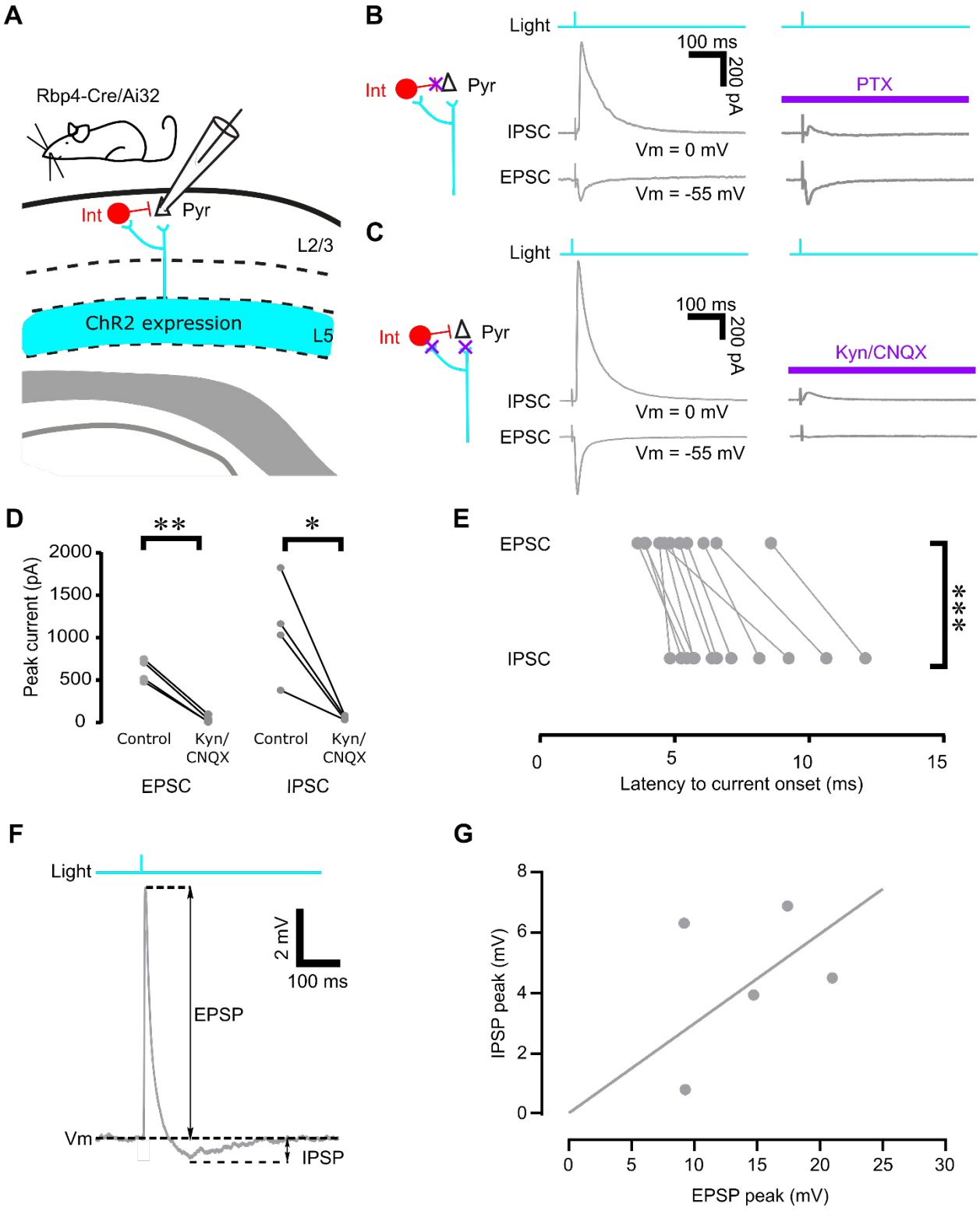


Figure 3.2 L5 elicits monosynaptic excitation and disynaptic inhibition in L2/3 pyramidal neurons

(A) Experimental setup in which whole cell patch clamp recordings were performed from L2/3 pyramidal neurons in slices from Rbp4-Cre/Ai32 mice. **(B)** Example light-evoked EPSCs and IPSCs recorded from a L2/3 pyramidal neuron under control conditions (left) and in the presence of the $GABA_A$ receptor blocker, picrotoxin ((PTX; 50µM) right). **(C)** Example light-evoked EPSCs and IPSCs under control conditions (left) and in the presence of a glutamate receptor blocker (right), kynurenic acid (Kyn; 1 µM) or CNQX (10µM). **(D)** Blockade of glutamate receptors substantially reduced both the peak EPSC current (n = 4 neurons; 613 ± 67 pA in control versus 40 ± 20 pA in Kyn/CNQX; Paired t-Test (3) = 11, p = 0.0014) and peak IPSC current (n = 4 neurons, 1100 ± 296 pA in control versus 54 ± 13 pA in Kyn/CNQX; Paired t-Test (3) = 3.6, p = 0.035).

To investigate whether disynaptic inhibition underlies the activity observed in L2/3 pyramidal neurons following L5 stimulation, I performed a series of pharmacological manipulations. First, I confirmed that adding the $GABA_A$ receptor blocker picrotoxin (PTX; 100µM) to the superfusate was able to effectively abolish the IPSCs (n = 4 neurons; **Fig 3.2B**).

Next, I established that the IPSCs observed in L2/3 pyramidal neurons following L5 stimulation were dependent upon excitatory synaptic inhibition, in keeping with a disynaptic inhibitory motif. Adding antagonists of ionotropic glutamate receptors to the superfusate in the form of kynurenic acid (Kyn; 1 µM) or CNQX (10µM) reduced, by approximately 95%, both the peak EPSC (Paired t-Test, p = 0.0014) and the peak IPSC (Paired t-Test, p = 0.035) elicited by L5 stimulation (**Fig 3.2D**; n = 4 neurons peak EPSC was 613 ± 67 pA under control conditions versus 40 ± 20 pA in Kyn/CNQX; peak IPSC was 1100 ± 296 pA under control conditions versus 54 ± 13 pA in Kyn/CNQX).

A further feature of disynaptic inhibition is that the onset of the inhibition is delayed relative to the onset of the monosynaptic excitation (Isaacson & Scanziani, 2011). Consistent with this, the latency to the onset of the light-evoked EPSC in the L2/3 pyramidal neuron following light-activation of L5 was shorter than the onset of the IPSC, and on a timescale consistent with a synaptic delay (**Fig 3.2E**; n= 12 neurons ; latency to EPSC onset was 5.1 ± 0.40 ms and latency to IPSC onset was 7.26 ± 0.66 ms Wilcoxon matched-pairs signed rank test, p = 0.0005). Finally, by performing current clamp recordings I was able to assess the net effect of L5 stimulation upon the membrane potential of the L2/3 pyramidal neuron. In all cases, a depolarizing excitatory post-synaptic potential (EPSP) was followed by a delayed hyperpolarizing inhibitory post-synaptic potential (IPSP) (**Fig 3.2F-G**; relative to the neuron's resting membrane potential, the peak EPSP amplitude was 14.3 ± 2.3 mV and the peak IPSP amplitude was 4.5 ± 1.1 mV). Having established that L5 pyramidal neurons elicit monosynaptic excitation and disynaptic inhibition, one comparing alternate sweeps on which L5 was either not stimulated ('Control') or L5 was stimulated with a brief (1-3ms) light pulse which immediately preceded the onset of the current step ('Light'; **Fig 3.3A**).

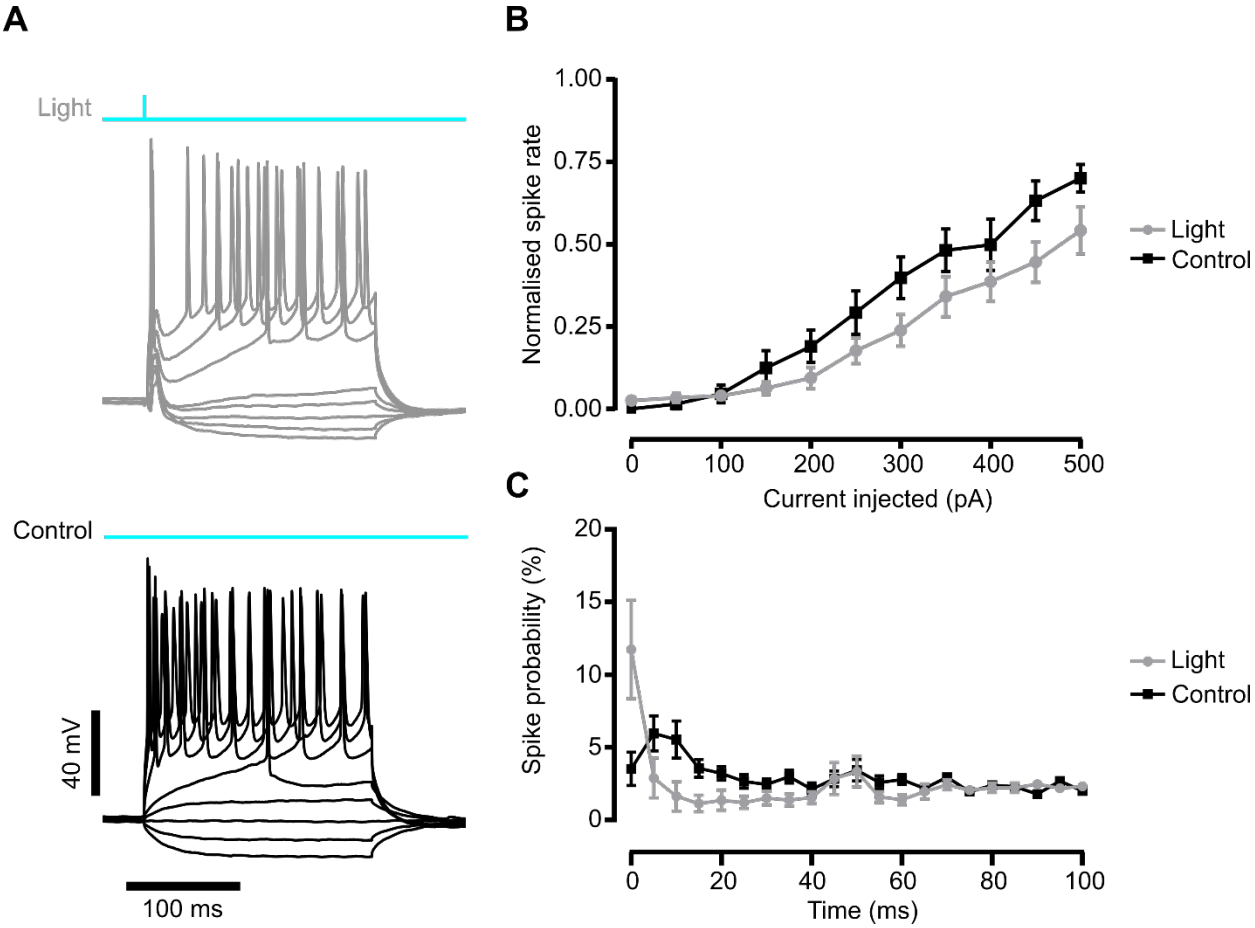


Figure 3.3 L5 inputs modulate the spiking of L2/3 pyramidal neurons

(A) Current clamp recordings were used to assess the influence of L5 input on L2/3 pyramidal neurons. Spiking activity in the L2/3 neuron was elicited by somatic injection of current steps (50 pA increments) under control conditions ('Control'; top) or on alternate trials during which ChR2-expressing L5 inputs were stimulated at the start of the somatic current step ('Light'; bottom). Light pulse(1-3 ms) onset immediately preceded the onset of the somatic current step. **(B)** Photostimulation of L5 inputs reduced the total number of spikes and caused a rightward shift in the input-output curve of the L2/3 neurons, consistent with a net inhibitory effect (n = 9 neurons; Mixed effects ANOVA $F(10,150) = 2.76$, $p = 0.0037$). **(C)** Spike probability as a function of time. Data are combined across all current steps and 0 ms represents the onset of the current step. Spike times were significantly modulated by L5 stimulation (n =9 neurons; two-way ANOVA $F(49,784) = 3.72$, $p < 0.0001$). L5 input increased the probability of an early spike (0-5 ms bin; Sidak's multiple comparisons, $p < 0.0001$) and decreased the probability subsequent spikes (5-10 ms and 10-15 ms bins, Sidak's multiple comparisons test, $p = 0.069$ and $p < 0.0001$, respectively).

This confirmed that L5 can modulate the spiking of L2/3 pyramidal neurons (**Fig 3.3B-C)**. Slopes of the IO curves were significantly different (Linear Regression, Light = 0.0011 ± 0.00009, R^2 =0.61) with a decrease in spike output in the light-stimulated condition (n = 9 neurons; F(1,184) = 9.25, p = 0.0027). This is in keeping with gain modulation typically seen in the recruitment of strong local inhibition (Atallah et al., 2012; Ferguson & Cardin, 2020; Nieus et al., 2014). Interestingly, when the L2/3 pyramidal neuron was close to spike threshold (i.e. ≤ 50 pA injected somatic current), L5 stimulation generated a modest increase in spike rate, consistent with an excitatory effect (**Fig 3.3B**; Wilcoxon matched pairs, signed rank test, W = -29, p = 0.047). Similarly, examination of spike probability during the somatic current steps revealed that L5 stimulation was associated with an increased probability of an early spike (**Fig 3.3C**), 0-5 ms after the start of the somatic current step (Sidak's multiple comparisons , p < 0.0001), but a more sustained decrease in spike probability over subsequent time bins (e.g. 5-10 ms and 10-15 ms after the start of the somatic current step; Sidak's multiple comparisons , p < 0.0069 and p < 0.0001, respectively). Having established how L5 inputs can modulate the spiking activity of L2/3 pyramidal neurons *in vitro*, I next set out to examine how L5 modulates responses to a physiologically-relevant whisker stimulus *in vivo.* To evaluate this, I performed multiunit recordings with a 32-channel linear electrode probe inserted orthogonally to the pial surface of the left barrel cortex(Brumberg et al., 1999) of anaesthetized head-fixed *Rbp4-cre/Ai32* mice (**Fig 3.4A-C**; (Brumberg et al., 1999)). A piezoelectric wafer was used to stimulate the principal whisker corresponding to the barrel that had been targeted for recording. Meanwhile L5 pyramidal neurons in the vicinity of the recording site were photostimulated using an LED (473nm), positioned just above the surface of the brain (**Fig 3.4D**). To relate recording sites to cortical laminae, whisker-evoked local field potential (LFP) minima were used to identify the center of L4 (**Fig 3.4E;** (Einevoll et al., 2013; Okun et al., 2015)). Thus for all recordings it was possible to distinguish putative supragranular and infragranular signals.

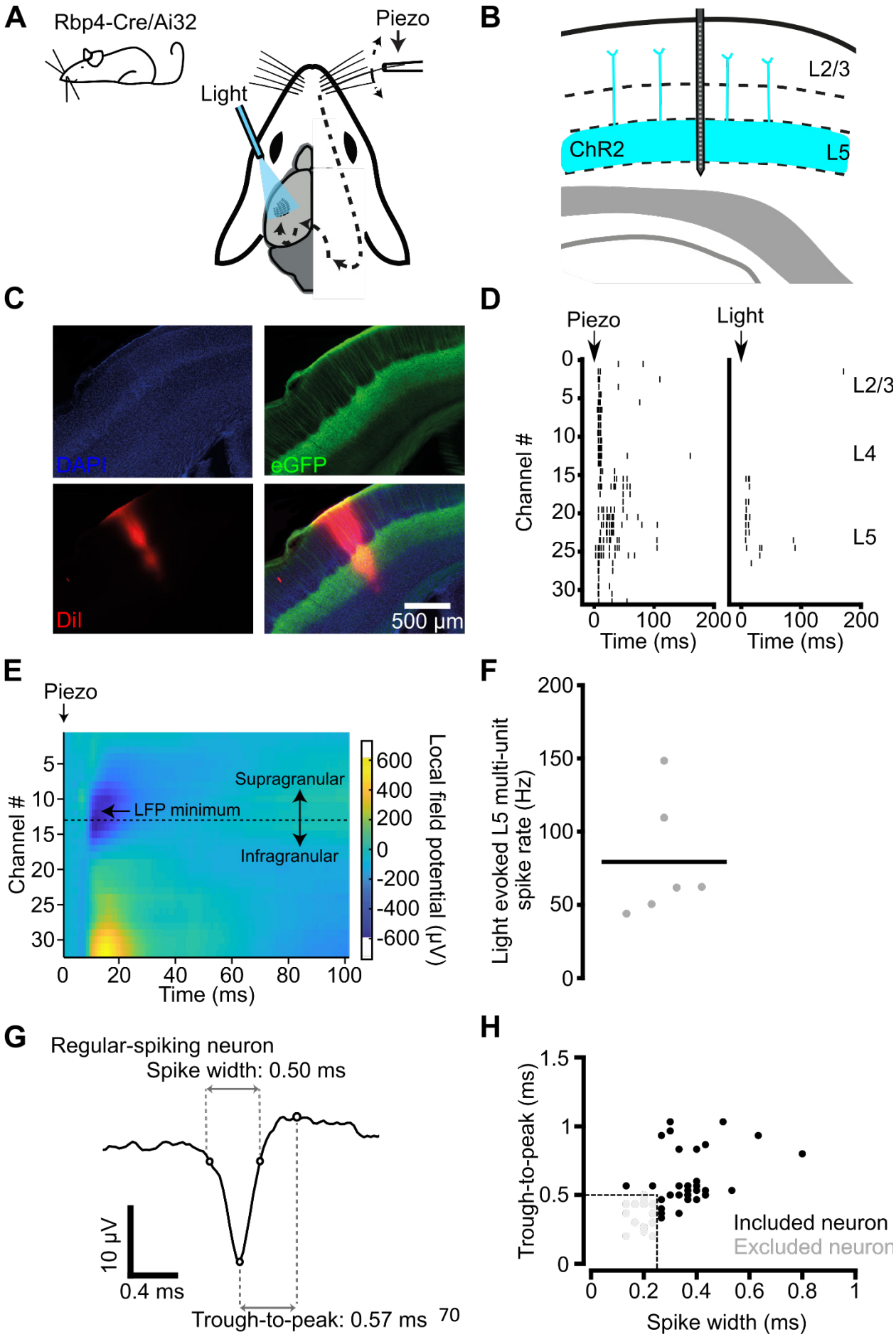
As expected, brief light pulses (5 ms) caused an increase in infragranular multiunit spiking activity, which was consistent with the expected depth of L5 and could be used to confirm successful activation (**Fig 3.4F,** n = 6 animals; Δ spike rate compared to spontaneous levels of 79.41 ± 16.7 Hz, Wilcoxon Signed rank test , W = 21, p = 0.031). To identify single units, spike sorting was performed with the 'KiloSort' algorithm (M Pachitariu et al., 2016) and putative regular spiking neurons within L2/3 and upper L4 were identified based on their spike properties (**Fig 3.4G-H;** (Reyes-Puerta et al., 2015)). Only neurons exhibiting a significant whisker-evoked response were subject to further analysis (minimum spike probability increase of 10% across all trials in the 5-30ms window following stimulus in the control condition).

Using this *in vivo* preparation I was able to assess the effects of L5 activation upon whisker-evoked responses in supragranular barrel cortex. To assess the influence of L5 upon incoming sensory input, the time of whisker stimulation was systematically varied with respect to L5 activation, over a timescale based on the L5-to-L2/3 responses observed *in vitro* (time intervals of 0, 10, 50 and 100 ms; **Fig 3.5A-B**). Whisker responses were measured over the 5-30 ms window following the whisker stimulus, which corresponds to the time of maximal response (Reyes-Puerta et al., 2015). Paired stimulations were compared to a control condition in which only the whisker stimulus was delivered (**Fig 3.5C**). All conditions that paired L5 activation and whisker stimulation showed a net decrease in the whisker-evoked response (n = 37 neurons from 6 animals; **Fig 3.5D-G)**. Simultaneous stimulation of the whisker with L5 (i.e. 0 ms interval) reduced the whisker-evoked response of supragranular neurons by 10.2 ± 3.4 Hz (Wilcoxon signed rank test , p = 0.0025, **Fig 3.5D**).

The response to whisker stimulation 10 ms after L5 activation also reduced the whisker-evoked response in supragranular neurons, by 11.5 ± 3.3 Hz (Wilcoxon signed rank test p = 0.0025, **Fig 3.5E**). Meanwhile, stimuli 50 ms (**Fig 3.5F**) or 100 ms (**Fig 3.5G**) after L5 activation also showed decreases in the whisker-evoked response in supragranular neurons (50 ms: -12.9 ± 3.2 Hz , Wilcoxon signed rank test, p = 0.0001; 100 ms : -6.7 ± 2.6 Hz , Wilcoxon signed rank test, p = 0.0204). These data demonstrate that L5 activity is associated with a net inhibitory effect upon incoming sensory inputs to the supragranular layers of barrel cortex.

Figure 3.4 Examining the effects of L5 input upon whisker-evoked L2/3 responses

(A) Experimental design in which *in vivo* extracellular recordings were performed in anaesthetized *Rbp4-Cre/Ai32* mice. Recordings were performed from left barrel cortex, whilst the corresponding principal whisker was stimulated using a piezo-electric wafer and L5 was activated by delivering brief pulses of blue light at the recording site (473 nm; 5 ms). **(B)** A 32-channel linear probe was used to record multiunit spiking activity and LFPs across cortical layers. **(C)** Post-mortem epifluorescence confirmed the position of the DiI coated electrode, relative to the L5 ChR2-expression. Cortical layers were independently delineated with DAPI. **(D)** Example raster plots showing spiking responses to whisker stimulation ('Piezo') and photostimulation of L5 ('Light') for channel positions corresponding to different depths through cortex. **(E)** Representative profile of the LFP amplitude relative to the time of whisker stimulus, for different channel depths along a recording probe. The depth of putative L4 was established using the LFP minimum. All units located superficial to this depth were classified as supragranular, whilst units below were classified as infragranular. **(F)** Light-evoked responses in L5 were assessed from the light-evoked increase in multiunit spiking activity over spontaneous levels (n = 6 animals, mean Δ spike rate = 79 ± 17 Hz). **(G)** The activity of individual neurons was determined by spike sorting and putative regular spiking units were included based on the temporal properties of their spikes. **(H)** Units that met waveform criteria for regular spiking neurons were included in further analysis (n = 38 units from 6 animals).


A
Rbp4-Cre/Ai32
Piezo
Light
B
L2/3
ChR2
L5
C
DAPI
eGFP
DiI
500 µm
D
Piezo
Light
Channel #
L2/3
L4
L5
Time (ms)
Time (ms)
E
Piezo
Channel #
LFP minimum
Supragranular
Infragranular
Local field potential (µV)
Time (ms)
F
Light evoked L5 multi-unit spike rate (Hz)
G
Regular-spiking neuron
Spike width: 0.50 ms
10 µV
0.4 ms
Trough-to-peak: 0.57 ms
H
Trough-to-peak (ms)
Included neuron
Excluded neuron
Spike width (ms)

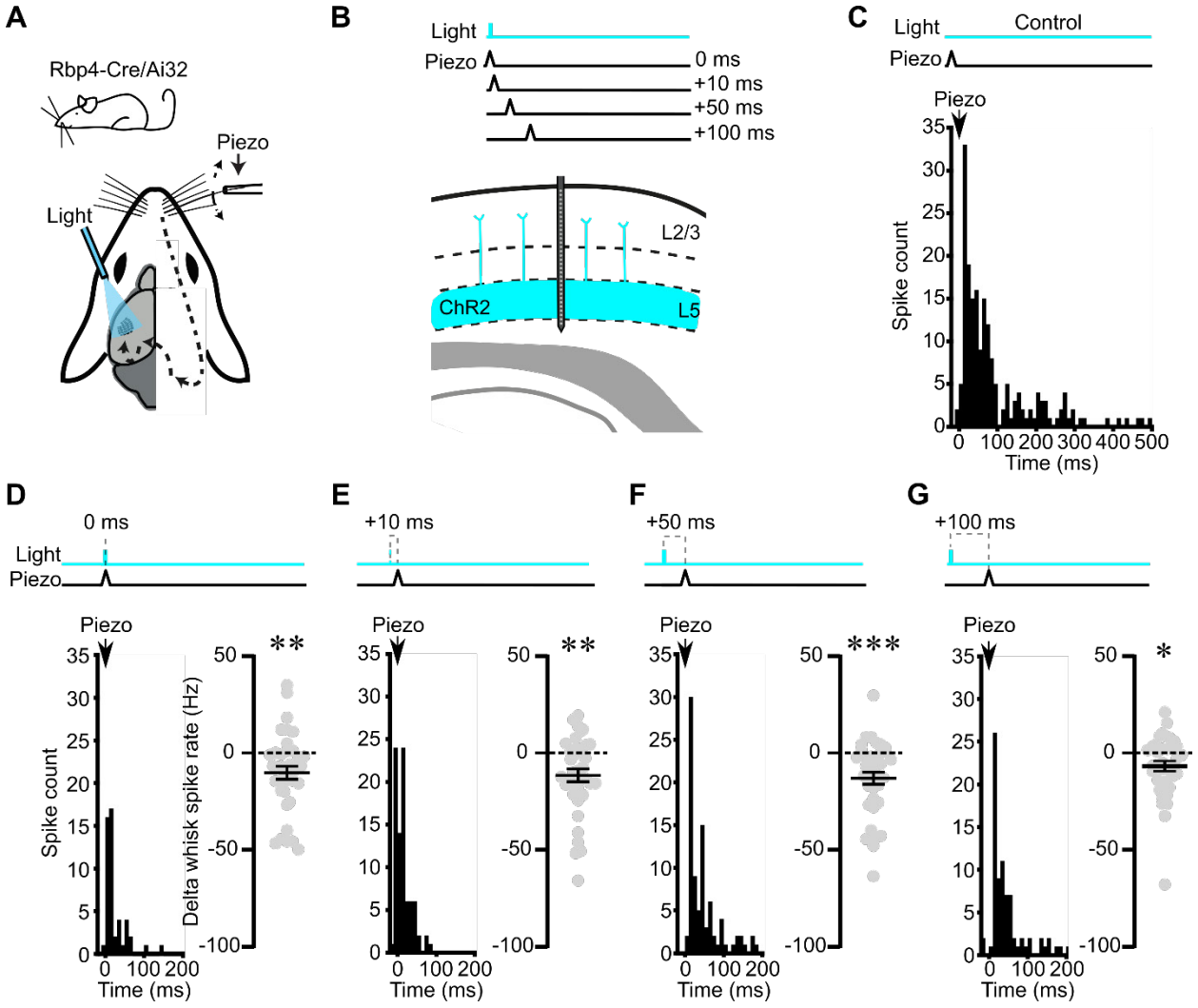


Figure 3.5 L5 has a net inhibitory effect upon whisker-evoked L2/3 responses

(A) Experimental design in which *in vivo* recordings were performed in anaesthetised Rbp4-Cre/Ai32 mice. **(B)** The relative timing of whisker stimulation ('Piezo') and L5 stimulation ('Light') were systematically varied to assess the impact of L5 upon whisker-evoked responses at 0, 10, 50 and 100 ms intervals. The spiking activity of neurons were recorded via a 32-channel linear probe, as in Figure 4. **(C)** Example peristimulus time histogram (PSTH) shows a putative L2/3 neuron's response to a control whisker stimulus (i.e. not paired with a light stimulus). **(D)** PSTH from the same neuron as in 'C' (left), shows the spiking activity when L5 was stimulated at the same time as the whisker (i.e. 0 ms interval). For a population of neurons (right, n = 37 neurons), the whisker-evoked response was reduced by simultaneous L5 activity (delta spike rate compared to control was -10.2 ± 3.4 Hz, one sample Wilcoxon signed Rank test, W= -391, p = 0.0025). **(E)** PSTH from the same neuron as in 'C' (left), shows the spiking activity when L5 was stimulated 10 ms before the whisker (i.e. 10 ms interval). Whisker-evoked responses were reduced at this stimulus interval (delta spike rate from control was -11.5 ± 3.3 Hz , one sample Wilcoxon signed rank text, W = -391, p = 0.0025). **(F)** PSTH from the same neuron as in 'C' (left), shows spiking activity when L5 was stimulated 50 ms before the whisker. Whisker-evoked responses were reduced at this stimulus interval (delta spike rate from control was -12.9 ± 3.2 Hz, one sample Wilcoxon signed rank test, W = -483 , p = 0.0001). **(G)** PSTH from the same neuron as in 'C' (left), shows spiking activity when L5 was stimulated 100 ms before the whisker. Whisker-evoked responses were reduced at this stimulus interval (delta spike rate from control was -6.7 ± 2.6 Hz, One sample Wilcoxon signed rank test, W = -305, p = 0.0204).

Discussion

In this chapter I have used an optogenetic strategy to investigate the functional effects of L5 upon L2/3 in mouse somatosensory cortex. The data support the conclusion that L5 pyramidal neurons can form direct monosynaptic excitatory connections, and recruit disynaptic inhibition, onto L2/3 pyramidal neurons. *In vitro* pharmacological experiments in combination with voltage clamp recordings confirmed that the recruitment of $GABA_A$ receptor mediated inhibition was dependent upon glutamatergic transmission. This is in accordance with a disynaptic circuit and argues against monosynaptic inhibitory connections to L2/3, at least from the ChR2-expressing L5 population.

These observations are consistent with a well-recognized motif in cortical circuits, whereby a direct excitatory input elicits a fast excitation, followed by synaptically-delayed inhibition. I was able to demonstrate that the two components of this response are positively correlated in the sense that L2/3 pyramidal neurons receiving stronger L5 excitatory input, also receive stronger disynaptic inhibition, in keeping with previous evidence that cortical neurons tend to exhibit matched excitation and inhibition (Xue et al., 2014). Under the recording conditions used here, the IPSC amplitudes were significantly larger than the EPSCs, resulting in a relatively low E/I ratio for the input from L5 to L2/3. My work contributes to the general observation that the recruitment of L5 through can modulate ongoing activity in L2/3 through the recruitment of varying degrees of local inhibition (Adesnik, 2018; Adesnik & Scanziani, 2010; Beltramo et al., 2013; Vecchia et al., 2020). This may be of importance in a number of columnar computations.

At this point, my findings do not offer insight as to which interneurons mediate this disynaptic inhibition in the L5-to-L2/3 circuit. Three interneuron subtypes classified by marker expression are responsible for mediating almost all network inhibition in L2/3: parvalbumin (PV), somatostatin (SST) and the ionotropic serotonin receptor 5HT3a (5HT3aR) expressing interneurons (L. Gentet, 2012; Rudy et al., 2011).

It is well established that L2/3 pyramidal neurons form dense interconnectivity with PV and SST interneurons (Fino & Yuste, 2011; Packer & Yuste, 2011). However, prior studies have reported that PV interneurons play a significant role in mediating the fast synaptic inhibition that is recruited to match excitation, in a similar manner to that observed here (Moore et al., 2018; Xue et al., 2014). I would therefore hypothesize that the PV interneuron population makes a major contribution to the inhibitory post-synaptic responses that I recorded. At the same time, my data do not distinguish whether these are local L2/3 interneurons or L5 interneurons that display translaminar connectivity (Buchanan et al., 2012; Naka & Adesnik, 2016).

The relationship between a neuron's synaptic inputs and its action potential output is fundamental to neuronal computation. My *in vitro* current clamp recordings demonstrate that the disynaptic recruitment of inhibition by L5 serves to modulate the input-output relationship of L2/3 pyramidal neurons. Previously it has been shown that shunting inhibition can generate 'divisive' gain effects, which alter the slope of the of the input-output curve (Mitchell & Silver, 2003) and increase a neuron's dynamic range (Pouille et al., 2009). Whilst this mechanism has typically been associated with tonic inhibition, there is evidence that strong phasic synaptic inhibition can modulate neuronal gain (Nieus et al., 2014), supporting the idea that L5 elicits an effective inhibition of L2/3. At the same time, my current clamp recordings revealed effects consistent with a monosynaptic excitatory component, as there was a detectable increase in the L2/3 pyramidal neuron's spike probability immediately following L5 activation. Such an effect is consistent with the idea of temporal gating of spiking activity through millisecond differences in the timing of excitatory and inhibitory membrane transients (Kremkow et al., 2010). In summary therefore, the *in vitro* data revealed a bimodal nature to the L5 input to L2/3, whereby an early excitatory signal is overtaken by a robust inhibition.

Using an anaesthetized *in vivo* preparation, I then investigated how L5 inputs might influence sensory-evoked activity in the supragranular layers of barrel cortex. To interpret these recordings it was important to differentiate the activity of putative fast-spiking interneurons and local pyramidal neurons. Whilst a classification method such as a cluster analysis of the features of the recorded units would be ideal for this task, I was limited by the number of high quality responsive units. This is consistent with the relatively sparse activity levels observed in the supragranular layers of cortex (Harris & Mrsic-Flogel, 2013). Therefore, to maximize the chance of analyzing the responses of regular spiking pyramidal neurons, threshold values for spike trough-to-peak time and spike width were selected in keeping with prior literature (Barthó et al., 2004; Okun et al., 2015; Rojas-Piloni et al., 2017).

As the major output layer, L5 spiking reflects the culmination of synaptic integration throughout the cortical column. This spiking output is relayed via the axons of L5 pyramidal neurons to long-range targets throughout the brain, but is also delivered locally via axonal collaterals that extend to the supragranular layers(Oberlaender et al., 2011). To investigate how this local 'feedback' modulates incoming sensory input, my experiments examined the effect of activating L5 prior to whisker stimulation. Activating L5 pyramidal neurons between 0 and 100 ms before whisker stimulation resulted in a pronounced inhibition of the sensory-evoked spiking activity in supragranular layers. At a general level, this supports the *in vitro* observation that L5 elicits a robust inhibition of L2/3. Under the *in vivo* recording conditions however, the inhibitory effects appeared to be more dominant, to the extent that simultaneous activation of L5 (i.e. 0 ms interval) had a pronounced inhibitory effect upon the whisker response. Interestingly, recent experiments in which L5 was activated shortly after whisker stimulation also revealed a pronounced inhibitory effect on the local cortical column (Vecchia et al., 2020).

The fact that an excitatory component was not evident *in vivo* may therefore reflect a greater dominance of inhibitory circuits in the intact brain, particularly as strong inhibition is thought to underlie sparse activity in upper cortical layers (Harris & Mrsic-Flogel, 2013; Petersen & Crochet, 2013). Alternatively, these observations may reflect the spatiotemporal aspects of optogenetically activating a large population of L5 neurons. Indeed, a limitation of these experiments is that whilst the strategy affords selective activation of L5 pyramidal neurons, it does not distinguish between the different subpopulations of L5 pyramidal neuron (Harris & Shepherd, 2015). Therefore having established that L5 can indeed influence activity in supragranular layers, I next set about exploring the contribution of different L5 subpopulations. This is explored in the next chapters of my thesis.

Page intentionally left blank

Chapter 4 : Examining axon ascending collaterals from projection-defined L5 pyramidal neuron subtypes

Introduction

Throughout cortex, excitatory pyramidal neurons can be defined by their long-range projections as either intratelencephalic ('IT') - those that project to other cortical regions and bilateral striatum, or pyramidal tract ('PT') - those that project to subcortical structures such as the spine, thalamus, trigeminal nucleus and striatum (Feldmeyer, 2012; Harris & Shepherd, 2015; Tasic et al., 2018). I will refer to these as 'projection-defined' subtypes. L5 is often classed as the principal output layer of cortex (Feldmeyer, 2012) and within L5 these two subtypes of pyramidal neuron have been well described, with clear differences in morphology, intrinsic electrophysiological properties, connectivity patterns and soma position with the layer. PT neurons are most densely located in deep infragranular L5b, whilst IT neurons are found throughout L5 but are preferentially located in L5a (Oswald et al., 2013) (Aronoff et al., 2010; Feldmeyer, 2012). Often, where unequivocal projection tracing is not possible, such as in the identification of units in extracellular recordings, L5a or L5b is used as a shorthand to indicate these two subtypes.

Dendritic morphology is also frequently used to differentiate subtypes of L5 pyramidal neurons. IT and PT projection-defined subgroups have been associated with characteristic morphological patterns (Gao & Zheng, 2004; Naka & Adesnik, 2016; Oswald et al., 2013; Ramaswamy & Markram, 2015; Wang et al., 2018). PT neurons are strongly associated with a 'thick tufted' dendritic morphology consisting of a large primary apical dendrite, with numerous distal tufts and extensive ramification in L1 (Gao & Zheng, 2004; Oswald et al., 2013; Ramaswamy & Markram, 2015; Wang et al., 2018). In contrast, IT neurons tend to be

'thin/slender tufted' neurons with a slim apical dendrite that lacks distal tufts that may be more limited in superficial laminar extension (Gao & Zheng, 2004; Le Bé et al., 2006; Oswald et al., 2013; Wang et al., 2018).

In a now classic study, Hattox and Nelson found that long-range axonal projection target was associated with characteristic intrinsic electrophysiological properties of L5 pyramidal neurons (Hattox & Nelson, 2007b). A number of subsequent studies have repeatedly demonstrated that PT neurons are more likely to show narrow action potentials (APs) with prominent afterpotentials, and burst firing with little spike rate adaptation. In contrast, IT neurons are more likely to have wider AP half widths, less prominent afterpotentials and greater spike rate adaptation (Guan et al., 2015; Hattox & Nelson, 2007b; E. J. J. Kim et al., 2015; Le Bé et al., 2006). Such action potential differences are likely mediated by differences in the expression of various voltage-gated ion channels (Hattox & Nelson, 2007b; Ramaswamy & Markram, 2015). PT neurons have been associated with the expression of hyperpolarization activated cation (HCN) channels, which are known to mediate an inward current when the membrane is significantly hyperpolarized (I_h), resulting in so called 'sag' potentials (Guan et al., 2015; Ramaswamy & Markram, 2015; Robinson & Siegelbaum, 2003). These are thought to play a role in the burst firing characteristic of PT neurons and to modulate somatodendritic integration (Robinson & Siegelbaum, 2003).

PT and IT L5 subpopulations also integrate different excitatory inputs, suggesting that they may be involved in different streams of information processing (Bureau et al., 2006; Diamond et al., 2008; Feldmeyer, 2012; Guo et al., 2020; Petersen, 2007, 2019; Sherman, 2007). In the somatosensory system, the first order ventral posteromedial thalamic nucleus (VPM) preferentially inputs to L4 of barrel cortex, as well as infragranular L5b and L6. In contrast, the higher order posterior medial thalamic nucleus (POm) preferentially inputs to L5a as well as L2/3. It has similarly been shown in visual cortex, that PT neurons

receive greater input from the dorsolateral geniculate nucleus - a first order thalamic nucleus. Whereas IT neurons receive a greater proportion of their excitatory input from secondary thalamic nuclei (E. J. J. Kim et al., 2015).

A key aspect to understanding the role neuronal subtypes play in cortical information processing is determining the intracortical connections that the neurons form. It has been shown that L5 PT and IT neurons participate in distinct subnetworks through their local intralaminar connectivity (Brown & Hestrin, 2009; Le Bé et al., 2006). These L5 pyramidal neurons have also been shown to modulate activity throughout the cortical column via their local axons that form ascending collaterals (Adesnik, 2018; Beltramo et al., 2013; Lőrincz et al., 2015; Vecchia et al., 2020). To investigate these ascending axonal collaterals, previous studies have reconstructed the local axonal tree of putative PT and IT neurons (identified on the basis of dendritic morphology and intrinsic electrophysiological properties) (Delaine D Larsen, 2008; Narayanan et al., 2017; Oberlaender et al., 2011; Staiger et al., 2016; Wang et al., 2018). The axon collaterals of thick tufted neurons have been shown to form dense infragranular connections as well as slender ascending collaterals that remain within the local column. In contrast, thin tufted neurons have more elaborate ascending axonal branches that extend through the local column and into neighboring columns (Delaine D Larsen, 2008; Narayanan et al., 2017; Oberlaender et al., 2011; Staiger et al., 2016; Wang et al., 2018). However, there remains a paucity of evidence that directly relates the local axon collateral morphology to the long-range projection targets of a L5 neuron. Furthermore, despite the apparent differences, we lack an understanding of how different local axonal morphology translates into functional effects upon local cortical computations. An exciting development in this regard, is the recent engineering of viral vectors that are optimized for retrograde transport (Tervo et al., 2016) and generate new opportunities to deliver molecular tools to projection-defined subpopulations (Li et al., 2020).

Aims

The aims of this chapter were as follows:

1) To identify L5 pyramidal neuron subtypes on the basis of their long-range projection targets.
2) To characterize the local ascending axon collaterals of projection-defined L5 subtypes.
3) To establish the use of retrograde viral tools for performing functional studies of projection-defined L5 subtypes.

Results

L5 pyramidal neurons influence local cortical processing via their ascending axon collaterals. To quantitatively describe these axon collaterals for projection-defined L5 subtypes, I first set about targeting L5 pyramidal neuron subtypes on the basis of their long-range axonal projections. To do this, intracranial injections of cholera toxin subunit B conjugated with Alexafluor 488 (CTB-Alexa 488) were performed in mice at 6 weeks of age (**Fig 4.1A;** see Chapter 2 for details). CTB-Alexa 488 is a highly sensitive retrograde tracer (Conte et al., 2009a, 2009b; Lanciego & Wouterlood, 2020) and has been used previously to investigate the intrinsic electrophysiological properties of neurons based on their long-range projections (Rojas-Piloni et al., 2017; Yamashita et al., 2013). Injection sites were chosen such that PT neurons projecting to thalamus (PT^{thal}) and IT neurons projecting to ipsilateral and contralateral cortex (IT^{ipsi} and IT^{contra}, respectively) would be targeted (see Chapter 2 for details).

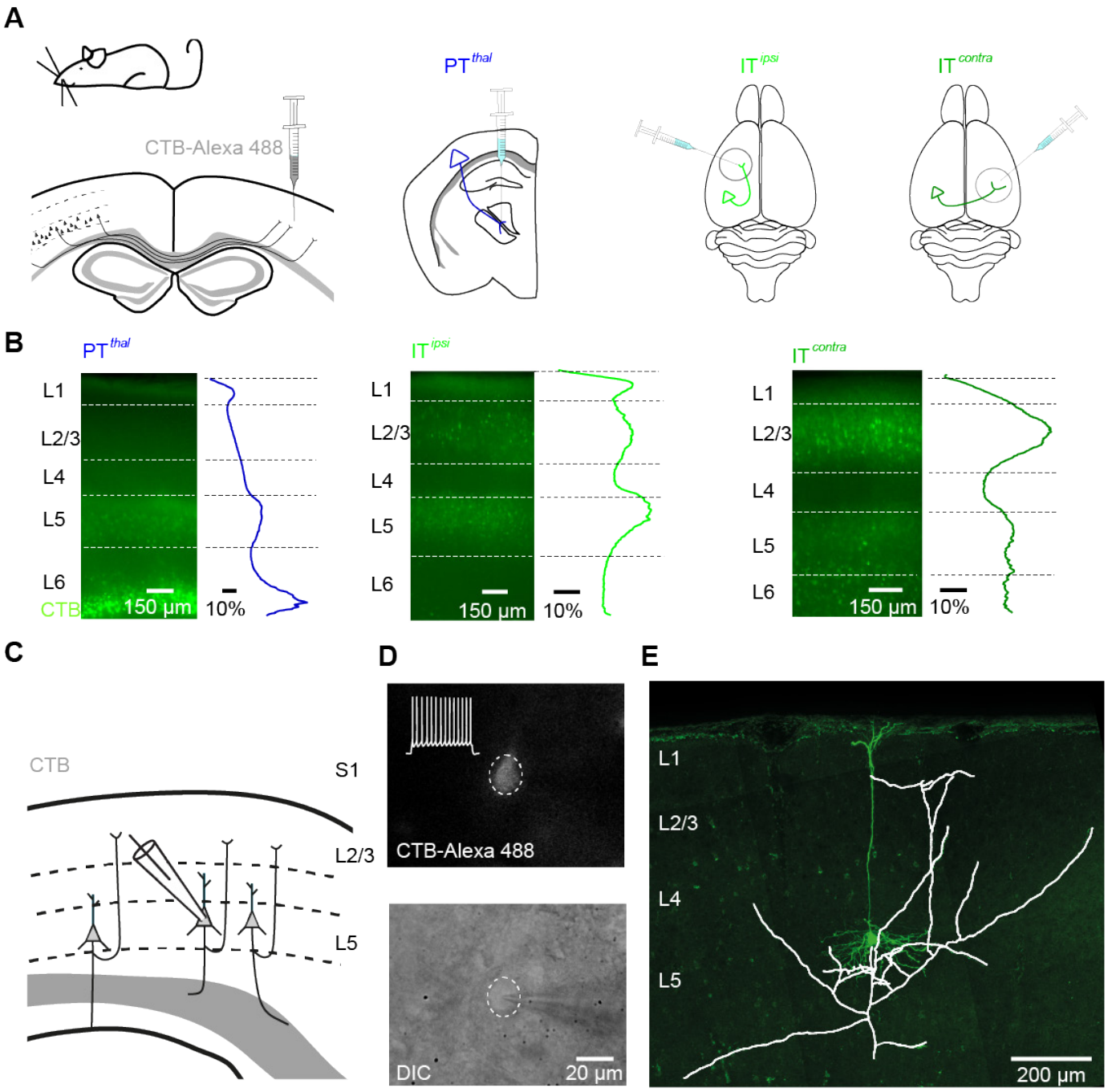


Figure 4.1 Using retrograde labelling to target subpopulations of L5 pyramidal neurons

(A) The fluorescent retrograde tracer, cholera toxin subunit B conjugated with Alexafluor 488 (CTB-Alexa 488), was injected into either the left thalamus, the left primary motor cortex (M1), or the right primary somatosensory cortex (S1), in order to retrogradely label pyramidal tract-type pyramidal neurons that project to the thalamus (PT^{thal}), or intratelencephalic-type pyramidal neurons projecting to either ipsilateral (IT^{ipsi}) or contralateral (IT^{contra}) cortex, respectively. **(B)** Epifluorescence images showing retrograde labelling of CTB-Alexa 488 in left S1 (LS1) following injections targeting each of the subpopulations of projection neurons in 'A'. Corresponding fluorescence intensity profiles indicate the relative proportion of retrograde labelling across the cortical layers. Soma of PT^{thal} neurons were mainly located in L5 and L6, whilst soma of IT^{ipsi} and IT^{contra} neurons were mainly located in L2/3 and L5.

When the animals were sacrificed and the brains sectioned at least one week after the injection, CTB-Alexa 488 labelling was present in the soma of pyramidal neurons in primary somatosensory cortex (S1) (**Fig** 4.**1B**). The laminar distribution of these neurons was in keeping with previously described patterns, i.e. neurons that send long-range projections to subcortical structures such as thalamus were found to have their soma in deeper layers (L5b or L6) of S1. Meanwhile, neurons that project to other cortical regions were observed to have their soma in both L2/3 and L5a (Aronoff et al., 2010; Feldmeyer, 2012).

To further validate the retrograde labelling and generate morphological reconstructions of the local axons of projection-defined of L5 subtypes, acute coronal brain slices of S1 (350-400 μm thick) were generated from animals that had received targeted CTB-Alexa 488 injections. Whole cell patch clamp recordings were used to confirm the intrinsic electrophysiological properties and the L5 neurons were filled with biocytin to recover axonal morphology (**Fig 4.1C-D**). After completing each recording the brain slice was fixed, the biocytin signal amplified with a fluorescent streptavidin antibody, and the axonal processes of the neuron underwent confocal imaging and morphological reconstruction (**Fig 4.1E**). This analysis pipeline therefore made it possible to relate a L5 pyramidal neuron's long-range axonal target, to the detailed morphology of the same axon's local ascending collaterals.

Figure 4.1 ***Continued from opposite***

(C) Acute brain slices were prepared and retrogradely-labelled fluorescent L5 pyramidal neurons in LS1 were targeted for whole cell patch clamp recording. The intrinsic electrophysiological properties were characterized and the neuron was filled with biocytin for subsequent morphological reconstructions. **(D)** Example of a retrogradely labelled CTB-Alexa 488 L5 pyramidal neuron, which was targeted for recording using the fluorescence signal (top) and DIC signal (bottom). Inset trace shows the neuron's spiking activity in response to a depolarizing current step. **(E)** Confocal image of a biocytin filled L5 IT^{ipsi}, with post-hoc reconstructed axon overlaid (white lines).

First, I assessed the intrinsic electrophysiological properties of PT^{thal}, IT^{ipsi} and IT^{contra} L5 pyramidal neurons (**Fig 4.2A**). By injecting a suprathreshold somatic current into retrogradely-labelled neurons, the characteristics of AP's could be assessed in each of the three subpopulations. In particular, the fast after-hyperpolarization (fAHP) and depolarizing after potential (DAP) were quantified as these have previously been reported to be larger in PT^{thal} neurons (Hattox & Nelson, 2007b) (**Fig 4.2B**). I found clear differences between the three subpopulations in AP Height (**Fig 4.2C**), AP half-width (**Fig 4.2D**), fAHP amplitude (**Fig 4.2E**) and DAP amplitude (**Fig 4.2F**).

Figure 4.2 ***Continued from opposite***

(D) Subpopulations also differed in AP half-width (Kruskal-Wallis test = 17.08, p = 0.0002). PT^{thal} had a more narrow AP half-width than either IT^{ipsi} (p = 0.0003) or IT^{contra} (p = 0.03) neurons. There was no difference between the IT subpopulations (p > 0.99, Dunn's multiple comparison tests). PT^{thal} (n = 21 neurons) AP half-width was 0.54 ± 0.02 ms, IT^{ipsi} (n = 12 neurons) was 0.74 ± 0.06 ms and IT^{contra} (n = 8 neurons) was 0.66 ± 0.03 ms. **(E)** The amplitude of the fast after hyperpolarization potential (fAHP) also differed between the three subpopulations (Kruskal-Wallis test = 12.62, p = 0.0018). Subsequent multiple comparisons revealed that PT^{thal} had larger fAHP amplitudes than IT^{ipsi} (p = 0.0026), but not larger than IT^{contra} (p = 0.078). fAHP amplitude was not different between the IT subpopulations (p > 0.999, Dunn's multiple comparison tests). PT^{thal} (n = 21 neurons) fAHP amplitude was 7.52 ± 0.64 mV, IT^{ipsi} (n = 12 neurons) was 2.18 ± 1.18 mV and IT^{contra} (n = 8 neurons) was 3.49 ± 1.54 mV. **(F)** The amplitude of the depolarizing after potential (DAP) was different between the subpopulations (Kruskal-Wallis test = 18.7, p <0.0001). PT^{thal} had larger DAP than both IT^{ipsi} (p = 0.0001) and IT^{contra} (p = 0.039) neurons. DAP amplitude was not different between the two IT subpopulations (p = 0.92, Dunn's multiple comparison tests). PT^{thal} (n = 21 neurons) DAP amplitude was 2.26 ± 0.32 mV , IT^{ipsi} (n = 12 neurons) was 0.30 ± 0.18 mV and IT^{contra} (n = 8 neurons) was 0.90 ± 0.42 mV. **(G)** Example traces from current clamp recordings showing action potential firing response to a 1 s depolarizing current step. **(H)** Spike rate in response to injected current steps was similar across the three subpopulations (repeated measures ANOVA F(34,595) = 1.17, p = 0.24). **(I)** Subpopulations differed in their rate adaptation ratio (AR) (Kruskal-Wallis test 27.62, p <0.0001). Spike trains in PT^{thal} neurons were non-adapting, with a significantly lower AR than both IT^{ipsi} (p < 0.0001) and IT^{contra} (p <0.0001) neurons. AR was not different between the two IT subpopulations (p >0.999, Dunn's multiple comparison tests). PT^{thal} AR ratio was -0.002 ± 0.002, IT^{ipsi} was 0.043 ± 0.018 and IT^{contra} was 0.07 ± 0.035. **(J)** In response to hyperpolarizing currents, the sag (expressed as percentage of the maximum hyperpolarization of the plateau potential) was different between the subpopulations (Kruskal-Wallis test = 8.2, p = 0.017). Subsequent analysis revealed that PT^{thal} showed a larger sag than IT^{ipsi} (p = 0.048), but not IT^{contra} (p = 0.083). There was no difference between IT populations (p > 0.999, Dunn's multiple comparison tests). PT^{thal} (n = 21 neurons) sag was 17.4 ± 1.4 %, IT^{ipsi} (n = 12 neurons) was 12.1 ± 1.5 % and IT^{contra} (n = 7 neurons) was 12.4 ±3.1 %.

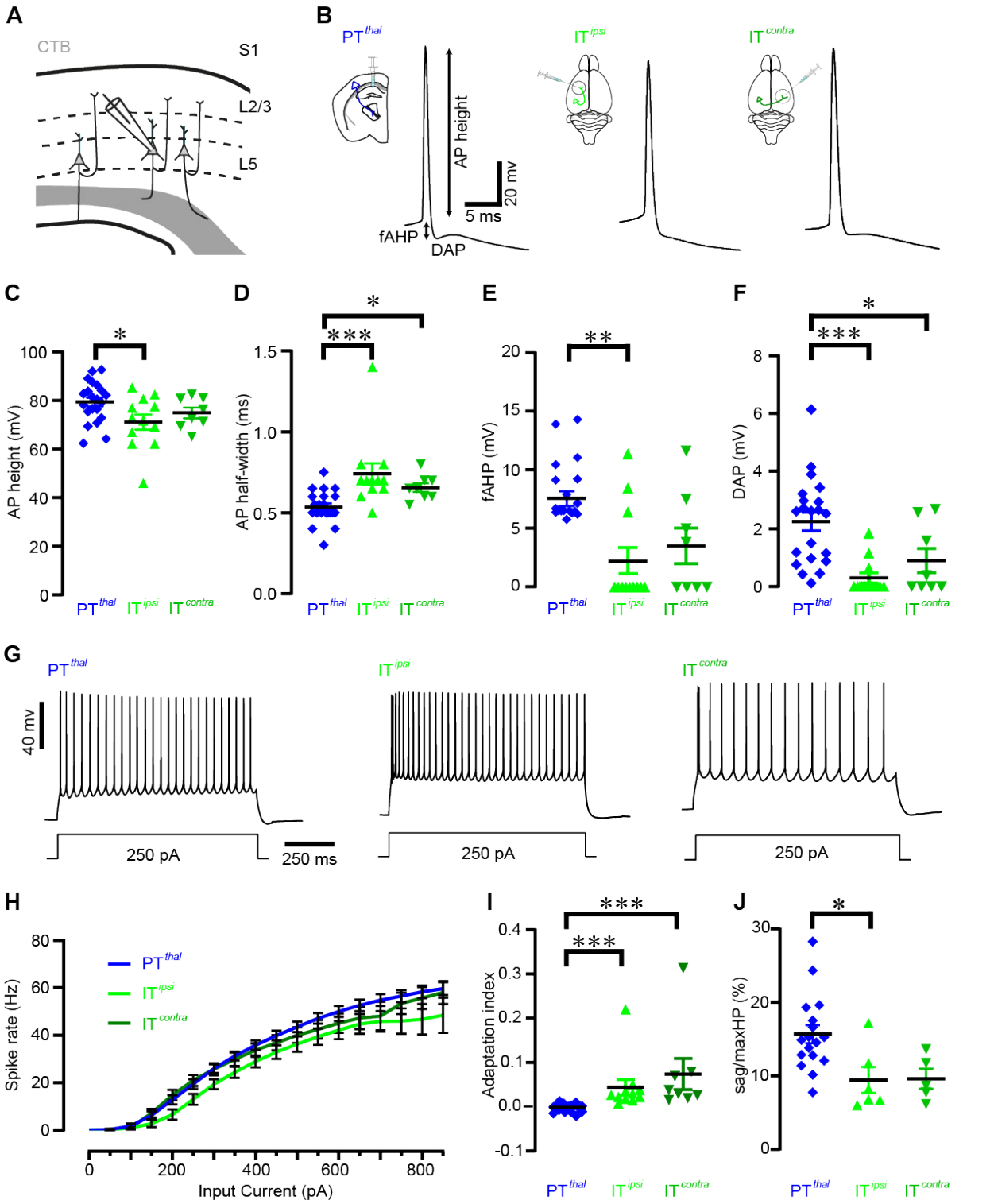


Figure 4.2 Long-range projection-defined L5 pyramidal neurons exhibit distinct electrophysiological characteristics

(A) Following retrograde labelling with CTB-Alexa 488, PT^{thal}, IT^{ipsi} or IT^{contra} L5 pyramidal neurons in S1 were targeted for whole cell patch clamp recordings *in vitro*. **(B)** Example current clamp recordings revealed the features of action potentials (APs) in PT^{thal}, IT^{ipsi} and IT^{contra} L5 pyramidal neurons. **(C)** The projection-defined subpopulations differed in their AP height (one-way ANOVA $F(2,38) = 3.43$, $p = 0.043$), with subsequent comparisons revealing that PT^{thal} neurons had greater AP height than IT^{ipsi} ($p = 0.041$), but not IT^{contra} ($p = 0.41$), and no difference between the two IT populations ($p = 0.41$, Holm-Sidak's multiple comparisons). PT^{thal} ($n = 21$ neurons) AP height was 79.4 ± 1.8 mV, IT^{ipsi} ($n = 12$ neurons) was 71.2 ± 3.2 mV and IT^{contra} ($n = 8$ neurons) was 75.0 ± 2.2 mV.

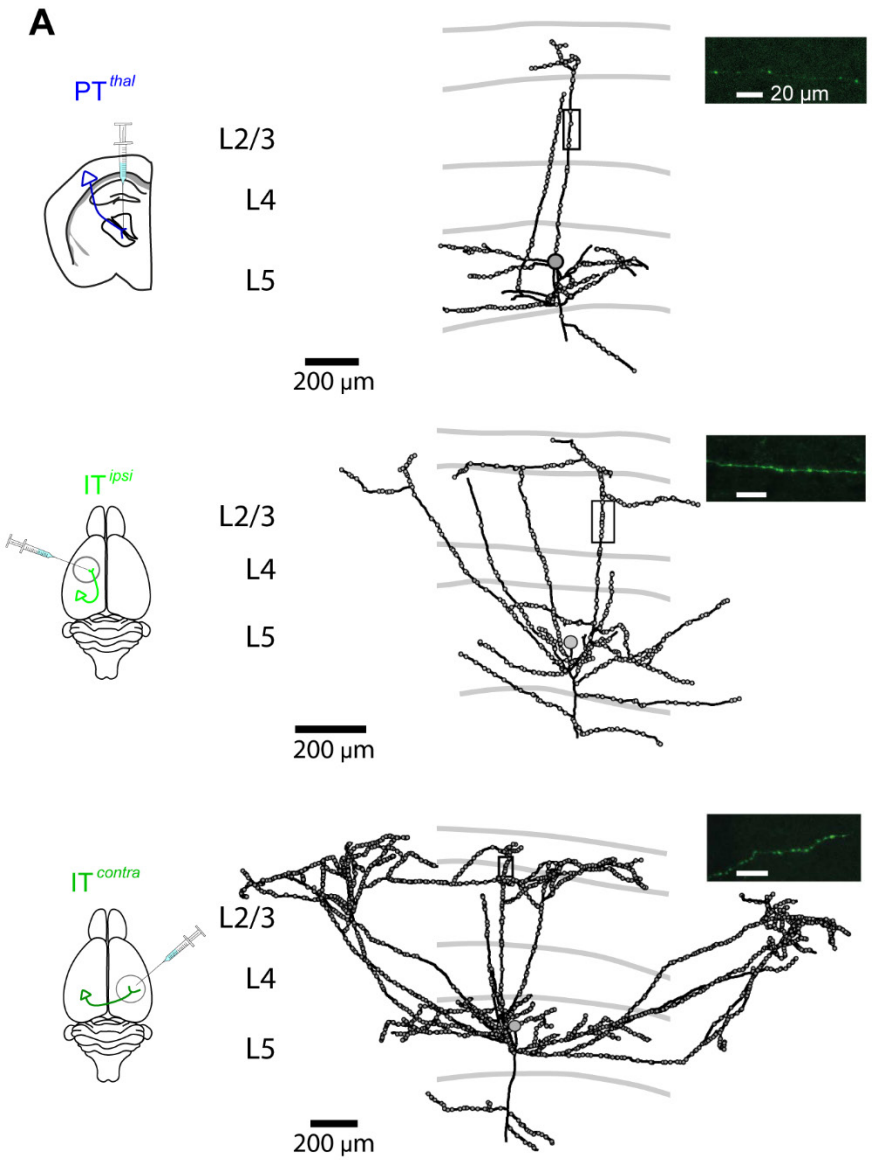
Subsequent multiple comparisons analyses revealed that PT^{thal} neurons had narrower APs than either of the IT subpopulations (PT^{thal} AP half-width was 0.54 ± 0.02 ms, IT^{ipsi} was 0.74 ± 0.06 ms and IT^{contra} was 0.66 ± 0.03 ms) and AP height was greater in PT^{thal} neurons than in IT^{ipsi} neurons (PT^{thal} AP height was 79.43 ± 1.81 mV, IT^{ipsi} was 71.16 ± 3.16 mV and IT^{contra} was 74.95 ± 2.21 mV). The DAP was larger in PT^{thal} neurons than either of the other two groups (PT^{thal} DAP amplitude was 2.26 ± 0.32 mV, IT^{ipsi} was 0.30 ± 0.18 mV and IT^{contra} was 0.90 ± 0.42 mV) and the fAHP was larger in PT^{thal} neurons than in IT^{ipsi} neurons (PT^{thal} fAHP amplitude was 7.52 ± 0.64 mV, IT^{ipsi} was 2.18 ± 1.18 mV and IT^{contra} was 3.49 ±1.54 mV). Sample sizes are stated in the figure legend. L5 pyramidal neuron subtypes have also been distinguished in terms of their patterns of AP spiking activity. By injecting somatic suprathreshold depolarizing currents, I was able to assess both the input-output spiking functions and stable spiking characteristics of the three subpopulations (**Fig 4.2G**). Whilst I found no difference in terms of the input-output function (**Fig 4.2H**), PT^{thal} neurons showed less spike adaptation than the IT^{ipsi} or IT^{contra} neurons, where the adaptation index was defined as the change in interspike interval (ISI) between successive APs in a train. PT^{thal} neuron spike adaptation was -0.002 ±0.002, IT^{ipsi} was 0.043 ± 0.018 and IT^{contra} was 0.07 ± 0.035 (**Fig 4.2I**).The final distinguishing property was the sag potential (**Fig 4.2J**), which was defined (see Chapter 2 for details) as the difference between the peak and steady-state membrane potential during a hyperpolarizing current step, expressed as a percentage of the peak hyperpolarization (Ramaswamy & Markram, 2015).

The subpopulations showed a difference in sag amplitude and subsequent multiple comparisons analyses revealed greater sag in PT^{thal} compared to IT^{ipsi} neurons. PT^{thal} sag/maxHP was 17.39 ± 1.36 %, IT^{ipsi} was 12.10 ± 1.51 % and IT^{contra} was 12.41 ± 3.05 %. Sample sizes are stated in the figure legend.

Having characterized the intrinsic electrophysiological differences between the projection-defined subpopulations, I next set about quantifying the morphology of the neurons' local axonal arbors within S1. Confocal images of the biocytin-filled PT^{thal}, IT^{ipsi} and IT^{contra} neurons were used to reconstruct the morphology of the ascending collaterals and to locate pre-synaptic boutons along the local axons

(**Fig 4.3A**). Previous axonal morphology studies have subclassified L5 populations according to their dendritic morphology (e.g. thick- or thin-tufted) or intrinsic electrophysiological properties (Narayanan et al., 2017; Oberlaender et al., 2011; Staiger et al., 2016; Wang et al., 2018). Whilst these features are associated with the L5 neuron's projection target, my data represent the first quantitative description of the collaterals that branch from the same long-range axon that defines the subtype. In keeping with previous descriptions of 'thick tufted' and 'thin/sparse tufted' L5 pyramidal neurons, I observed differences in the total intracortical axon length. PT^{thal} neurons had the least amount of axon in S1, whilst IT^{contra} had the greatest (**Fig 4.3B**). PT^{thal} axon length was 5.79 ± 1.14 mm, IT^{ipsi} was 9.37 ± 7.65 mm, and IT^{contra} was 15.94 ± 4.18 mm. However, all three subpopulations had axon collaterals that reached the supragranular layers and the percentage of collateral that was located in the supragranular layers did not differ between the three subtypes (**Fig 4.3C**; PT^{thal} proportion in supragranular layers was 27.18 ± 8.88 %, IT^{ipsi} was 31.19 ± 6.33 % and IT^{contra} was 47.38 ± 2.34 %). Sample sizes are stated in the figure legend.

Given the interest in L5-to-L2/3 connectivity, the axon collaterals reaching the supragranular layers were further characterized by documenting the location of individual pre-synaptic boutons. The first observation was that the L5 subtypes differed in the degree to which the collaterals extended laterally from the central axis of the neuron, as defined by a radial line drawn along the apical dendrite from soma to pia (**Fig 4.4A**). The collaterals of PT^{thal} neurons showed limited lateral spread from the central axis, whereas IT neurons exhibited more elaborate arbors that extended greater distances from the central axis of the neuron. As a consequence, the pre-synaptic boutons of IT^{ipsi} neurons, and to a greater extent IT^{contra} neurons, were located further from the central axis than for PT^{thal} neurons (**Fig 4.4B**; PT^{thal} mean bouton lateral distance was 179.6 ± 4.2 µm, IT^{ipsi} was 248.5 ± 3.9 µm and IT^{contra} was 498 ± 6.4 µm). This was in accordance with previous descriptions of L5 pyramidal neuron subtypes (Narayanan et al., 2017; Oberlaender et al., 2011)**.** I next assessed bouton density in the supragranular layers, by calculating each bouton's mean interbouton distance (**Fig 4.4C**). Bouton density was lower for PT^{thal} collaterals in the


A
PT thal
L2/3
L4
L5
200 µm
20 µm
IT ipsi
L2/3
L4
L5
200 µm
IT contra
L2/3
L4
L5
200 µm
B
Total axon length (mm)
25
20
15
10
5
0
*
PT thal
IT ipsi
IT contra
C
Supra
Gran
Infra
Proprotion of axon length (%)
100
75
50
25
0
PT thal
IT ipsi
IT contra

supragranular layers than for collaterals from either IT population (**Fig 4.4D**). PT^{thal} interbouton density was 15.75 ± 0.57 µm, IT^{ipsi} was 14.74 ± 0.3876 µm and IT^{contra} was 12.51 ± 0.17 µm. In summary therefore, whilst both PT^{thal} and IT extended a similar proportion of their local collaterals to the supragranular layers within S1, the IT ascending collaterals exhibited greater lateral spread and a higher density of pre-synaptic boutons. These structural differences in ascending collaterals suggest that the projection-defined L5 subtypes exert different functional effects upon local cortical activity and resulting information processing.

One of the challenges in understanding L5's contribution to cortical processing is that it has proved difficult to selectively control the activity of projection-defined pyramidal neurons. An exciting development in this regard has been the engineering of viral vectors that are optimized for retrograde transport and can be used to deliver optogenetic tools to projection-defined neurons (Tervo et al., 2016).

Figure 4.3 Axonal reconstructions of target-defined L5 pyramidal neurons reveal local collaterals ascending to supragranular layers.

(A) Cartoons (left) indicate the long-range injection target used to retrogradely label PT^{thal}, IT^{ipsi} or IT^{contra} L5 pyramidal neurons in S1. Neuronal drawings (centre) represent two-dimensional projections of the reconstructed local axonal collaterals of a retrogradely-labelled L5 pyramidal neuron in S1, with the soma (large circle), pre-synaptic boutons (small circles) and cortical layers as per DAPI staining (transparent grey lines) indicated. Inserts (right) are confocal images of the boxed section of the axon. **(B)** Total axonal length differed between the three subpopulations (one-way ANOVA $F(2,16) = 4.5$, $p = 0.028$). PT^{thal} neurons had significantly shorter axons than IT^{contra} ($p = 0.028$). Neither PT^{thal} compared to IT^{ipsi}, nor IT^{ipsi} compared to IT^{contra} were significantly different ($p = 0.55$, $p = 0.18$, Tukey's multiple comparison tests). PT^{thal} (n = 7 neurons) axonal length was 5.8 ± 1.1 mm, IT^{ipsi} (n = 6 neurons) was 9.4 ± 7.7 mm and IT^{contra} (n = 6 neurons) was 15.9 ± 4.2 mm. **(C)** Proportion of ascending axonal collaterals in supragranular ('Supra') versus granular ('Gran') versus infragranular ('Infra') layers. There was a significant interaction between subpopulation and the proportion of axon in the different layers (two-way ANOVA, $F(4,32) = 3.1$ $p = 0.029$). There was no difference in the proportion of axon in supragranular layers between the three subpopulations (Tukey's Multiple Comparisons, $p = 0.9$, $p = 0.17$, $p = 0.10$). The proportion of PT^{thal} supragranular axon was 27.2 ± 8.9 %, IT^{ipsi} was 31.2 ± 6.3 % and IT^{contra} was 47.4 ± 2.3 %.

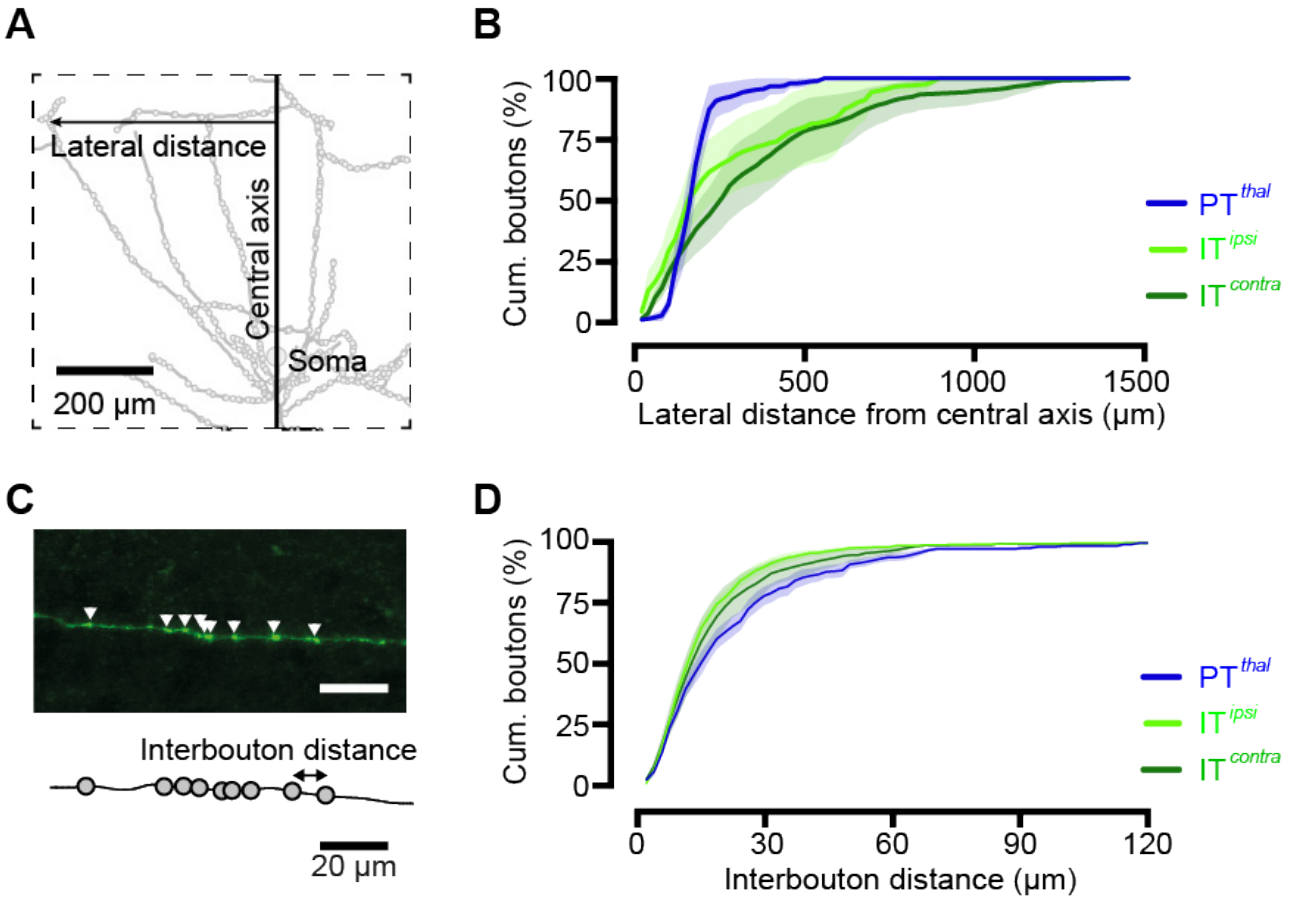


Figure 4.4 The branching and bouton density of local ascending collaterals suggest functional differences between L5 subpopulations

(A) Example trace illustrating how the lateral distance of each bouton was measured from the central radial axis of the ascending axonal collateral. **(B)** Cumulative distribution of lateral bouton distances for ascending collaterals in the supragranular layers. The lateral distribution of boutons differed across the three subpopulations of L5 pyramidal neurons (Kruskal-Wallis test = 785.3, $p < 0.001$). Boutons belonging to PT^{thal} (n = 437, 179.6 ± 4.2 µm) were closer to the central axis than those belonging to IT^{ipsi} (n = 2307, 248.5 ± 3.9 µm) or IT^{contra} (n = 3279, 498 ± 6.4 µm). A difference was also observed between the two IT subpopulations (Dunn's Multiple comparisons, $p < 0.0001$ in all cases). Accounting for within-cell variation, there was a significant interaction between L5 subpopulation and the lateral spread of boutons, with boutons from PT^{thal} neurons remaining closer to the central axis than those from IT^{ipsi} or IT^{contra} neurons (two-way repeated measures ANOVA, $F(144,1152) = 1.94$, $p<0.0001$). **(C)** Example confocal image (top) of a section of axon illustrating boutons (white arrowheads). The corresponding reconstruction of the same region (bottom), with boutons (grey circles) and the calculation of interbouton distance indicated. **(D)** Cumulative distribution of the mean interbouton distance on reconstructed axons in the supragranular layers. Interbouton distances differed significantly between the subpopulations (Kruskal-Wallis test = 45.56, $p < 0.0001$). Subsequent comparisons revealed that all three subpopulations were different from one another (Dunn's multiple comparisons, $p < 0.05$ in all cases). PT^{thal} interbouton distance was 15.75 ± 0.57 µm, IT^{ipsi} was 14.74 ± 0.39 µm and IT^{contra} was 12.51 ± 0.17 µm . Accounting for within-cell variation, there was a significant interaction between subpopulation and interbouton distance, with PT^{thal} neurons exhibiting the largest interbouton distance (two-way repeated measures ANOVA $F(28,1024) = 1.3$, $p = 0.018$).

To explore whether these retrograde viral tools could be used to selectively target projection-defined L5 subpopulations in S1, an experimental design was developed in which *Rbp4-cre* mice expressing Cre recombinase in L5 received a targeted intracranial injection of a retrograde AAV encoding Cre-inducible ChR2 (rAAV-Floxed-ChR2) (**Fig 4.5A**). This Cre-dependent strategy was designed to restrict ChR2 expression to L5 pyramidal neurons that possess a long-range axonal projection to the site of injection. Indeed, when rAAV-Floxed-ChR2 injections were targeted to either the left thalamus, left M1, or right S1 of *Rbp4-Cre* mice at 6 weeks of age, this resulted in the robust expression of ChR2 in L5 neurons in left S1 (**Fig 4.5B**). Animals were maintained for > 4 weeks after injection in order to maximize viral expression.

A series of validation experiments were conducted to provide the foundation for employing this strategy in subsequent chapters of this thesis. Single optical plane confocal images were taken of the respective region of interest in 350µm thick brain slices and ChR2 expressing soma were quantified as follows. First, to confirm the retrograde transport of the viral vector, I evaluated labelling in animals that had received an injection into a subcortical target. In all cases, somatic expression of ChR2 was restricted to neurons in cortex and was never observed at the subcortical injection site (**Fig 4.6A**). Second, I confirmed that injections intended to target PT^{thal}, IT^{ipsi} and IT^{contra} all resulted in ChR2 expression in S1. Consistent with what is known about the density of connectivity to the injection site (Aronoff et al., 2010; Guo et al., 2020), the number of retrogradely labelled cells expressing ChR2 found in S1 varied across injection site (**Fig 4.6B**) PT^{thal} (n = 6 slices from 2 animals) had 11.67 ± 1.41 cells per slice, IT^{ipsi} (n = 5 slices from 2 animals) had 9.2 ± 1.77 cells and IT^{contra} (n = 10 slices from 3 animals) had 5.5 ± 0.5 cells. Third, I confirmed that ChR2-expressing neurons were restricted to L5 of S1 for the three subpopulations (**Fig 4.6C**). PT^{thal} showed 97% restriction to L5, IT^{ipsi} showed 100% restriction to L5 and IT^{contra} showed 93% restriction to L5. Finally, evaluating the soma position of the retrogradely-labelled ChR2-expressing cells within L5 revealed that PT^{thal} neurons were significantly deeper (i.e. further from pia) than either of the IT subtypes (**Fig 4.6D**).

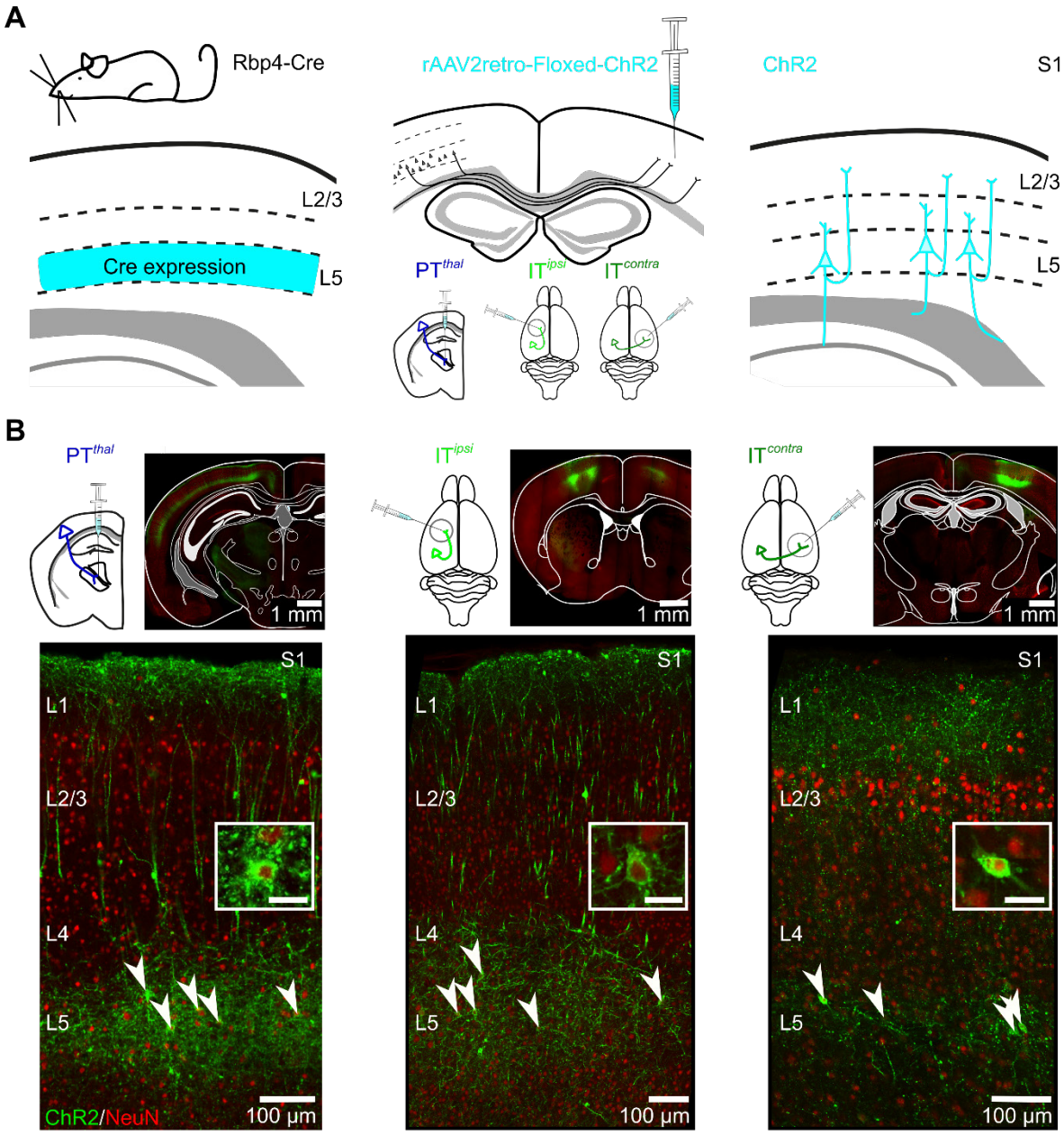


Figure 4.5. Retrograde AAVs allow for the delivery of genetic tools to projection-defined L5 pyramidal neurons.

(A) Rbp4-Cre mice expressing Cre recombinase in L5 pyramidal neurons (left) were injected with an adeno-associated virus that is optimized for retrograde transport and encoded floxed ChR2 (rAAV-Floxed-ChR2; centre). Injections were made in either left thalamus, left M1 or right S1, in order to target PT^{thal}, IT^{ipsi} and IT^{contra} L5 pyramidal neurons, respectively. Within left S1 therefore, ChR2 expression is restricted to the L5 pyramidal neuron subpopulation that projects to the injection site (right). **(B)** Examples are shown for each of the three L5 pyramidal neuron subpopulations (left to right). Cartoons show the long-range target of the L5 subpopulation. Low magnification confocal images show expression at the injection site. High magnification confocal images show ChR2 expression (green signal) in PT^{thal}, IT^{ipsi} and IT^{contra} L5 pyramidal neurons (arrowheads) within left S1. Layer boundaries were demarcated by NeuN staining of neuronal nuclei (red signal). Boxed insets show individual ChR2-expressing L5 pyramidal neurons (scale bar of inset, 20 µm).

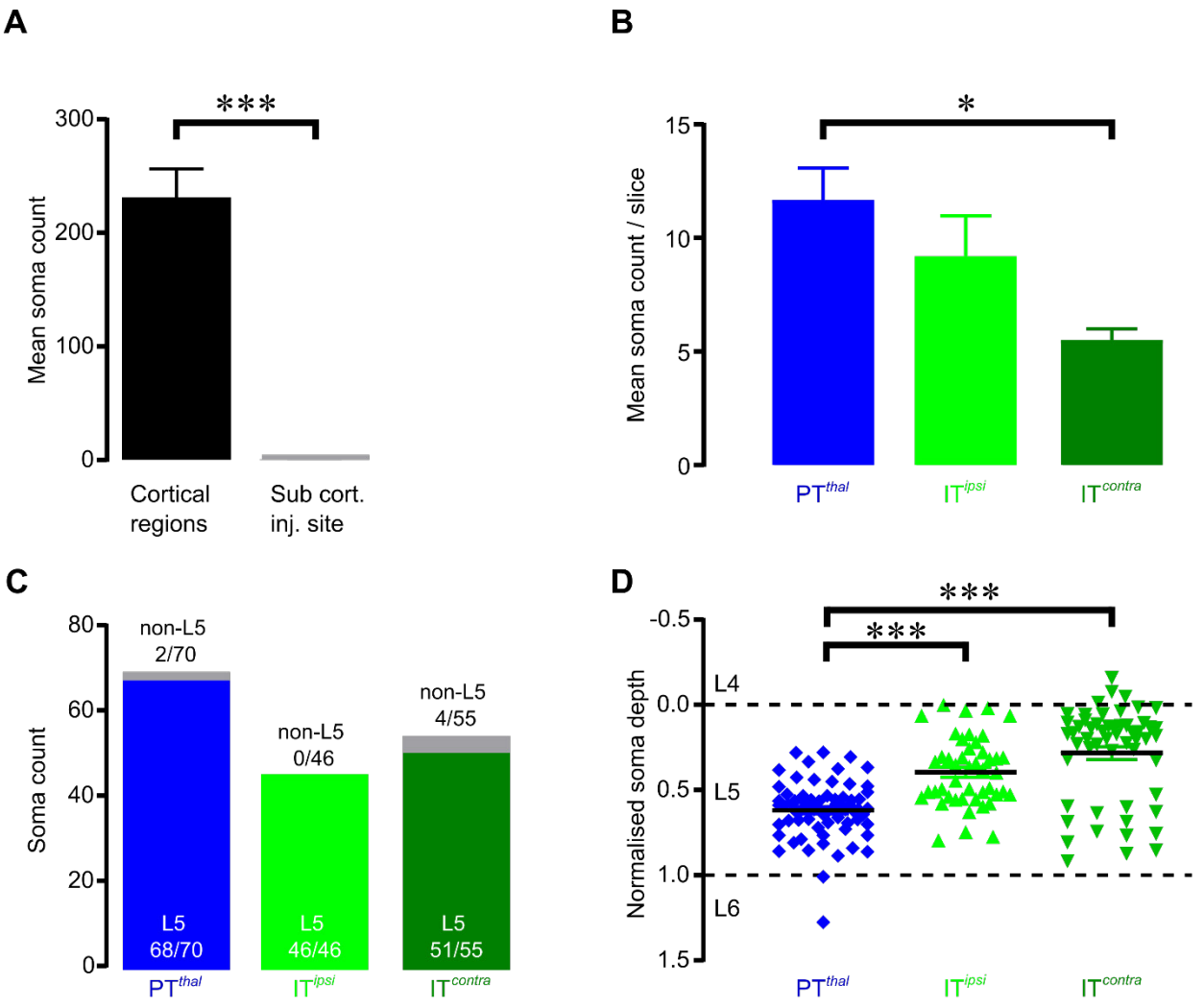


Figure 4.6 Retrograde AAVs restrict ChR2 expression to L5 pyramidal neuron subpopulations defined by their long-range projections

(A) Consistent with retrograde transport, ChR2-expressing cells were only evident in cortex following a subcortical injection (n = 4 animals; 231.3 ± 25.07 ChR2-expressing cells in cortex, compared to 0.75 ± 0.75 in subcortical regions; unpaired t-test, t(6) = 9.2 , p < 0.0001). **(B)** Mean soma counts in LS1 differed following injections targeting PT^{thal}, IT^{ipsi} and IT^{contra} L5 pyramidal neurons (Kruskal-Wallis test = 9.38, p = 0.0043). Subsequent multiple comparisons revealed that the number of soma was larger for PT^{thal} than IT^{contra} (p = 0.013). There was no difference between PT^{thal} and IT^{ipsi} (p = 0.12), or between the two IT subpopulations (p >0.999, Dunn's multiple comparison tests). PT^{thal} (n = 6 slices from 2 animals) soma count was 11.7 ± 1.4 cells, IT^{ipsi} (n = 5 slices from 2 animals) was 9.2 ± 1.8 cells and IT^{contra} (n = 10 slices from 3 animals) was 5.5 ± 0.5 cells. **(C)** ChR2-expressing cells were restricted to L5 of cortex (PT^{thal} n = 70 cells from 2 animals, IT^{ipsi} n = 46 cells from 2 animals and IT^{contra} n = 55 cells from 3 animals). **(D)** The soma depth within L5 of ChR2-expressing cells was different depending on long range projection target (Kruskal-Wallis test = 52.6, p <0.001). The soma of PT^{thal} neurons were significantly deeper than either IT^{ipsi} (p < 0.0001) or IT^{contra} (p < 0.0001) neurons. PT^{thal} soma depth within L5 was 0.62 ± 0.02 normalised units, IT^{ipsi} was 0.40 ± 0.03 normalised units and IT^{contra} was 0.28 ± 0.04 normalised units. The two IT subpopulations were not significantly different (p = 0.31, Dunn's multiple comparison tests).

PT^{thal} normalised soma position within L5 was 0.62 ± 0.02, IT^{ipsi} was 0.40 ± 0.03 and IT^{contra} was 0.28 ± 0.038. This is again in keeping with the reported soma distribution for PT and IT subpopulations (Anastasiades, Marlin, et al., 2018; Aronoff et al., 2010; Feldmeyer, 2012; Gao & Zheng, 2004; Mao et al., 2011).

Discussion

Using retrograde labelling to target projection-defined subtypes of L5 pyramidal neurons

The first aim of this chapter was to define subpopulations of L5 pyramidal neurons on the basis of their long-range projections. The interest in studying projection-defined neuronal subtypes is well established in the field and the use of tracers such as horseradish peroxidase (Kristensson & Olsson, 1971a, 1971b) and fluorogold (Schmued & Fallon, 1986) have been used to study the anatomy of long-range projections since the 1980's. More recently however, retrograde tracing tools that minimally disrupt neuronal physiology have been combined with techniques such as whole cell patch clamp recording to determine how the intrinsic electrophysiological properties (Hattox & Nelson, 2007b), local connectivity (Brown & Hestrin, 2009) and *in vivo* activity (Yamashita et al., 2013) relate to the long-range projection target of a neuron. One such tool that has been particularly powerful is fluorescently conjugated CTB (Conte et al., 2009b, 2009a). I was able to inject this tool into cortical regions and subcortical targets known to receive strong connectivity from S1 cortex (Aronoff et al., 2010), and thereby identify S1 L5 pyramidal neurons projecting to those sites.

The data collected on the intrinsic electrophysiological properties of the retrogradely-labelled neurons provided validation of this approach for distinguishing L5 pyramidal neuron subtypes. In keeping with previous studies, I found that IT neurons showed significant spike rate adaptation, whereas this property was mostly absent in PT neurons (Hattox & Nelson, 2007b; Oswald et al., 2013). Previous work has also revealed that PT neurons tend to have narrower AP's than IT neurons (Guan et al., 2015; Le Bé et al., 2006)

and a key finding by Hattox and Nelson was that fAHP and DAP were larger in PT than in IT neurons (Hattox & Nelson, 2007b). I was able to replicate these findings in my experiments. It is perhaps worth noting here that the amplitude of fAHP and DAP are likely to be related and therefore not independent parameters. For instance, a number of IT neurons did not exhibit any depolarization immediately following the action potential (i.e. zero DAP) and therefore did not exhibit any fAHP. Finally, another PT neuron characteristic identified in the literature, and which I also observed, was a more pronounced sag potential compared to IT neurons (Guan et al., 2015; E. J. J. Kim et al., 2015; Oswald et al., 2013). Interestingly, I did not find significant differences in the neuronal firing rate in response to depolarizing currents, which has been observed in some previous studies (Hattox & Nelson, 2007b). It is not known what underlies this difference, although factors such as the exact temperature of the recordings can influence neuronal firing patterns (Oswald et al., 2013). In summary, my data were able to replicate a series of predicted differences in intrinsic electrophysiological properties that are associated with L5 pyramidal neuron subtypes and thereby confirmed the effective retrograde-labelling of the desired subpopulations.

IT and PT L5 pyramidal neurons show morphological differences in their axon ascending collaterals

Prior work examining the local axonal projections of L5 pyramidal neurons has suggested potential differences between IT and PT neurons(Delaine D Larsen, 2008; Oberlaender et al., 2011) . Here I was able to reconstruct the ascending local intracortical collaterals of axons from retrogradely-labelled L5 neurons. This enabled me to demonstrate that all subpopulations have local axonal projections to the supragranular layers, where I observed clear differences between the projection-defined subpopulations. Whilst the proportion of axonal total length present in supragranular layers was not different, the morphology of these local arbors was different. IT neurons had greater axonal length than PT neurons and showed a high degree of lateral spread with elaborate branching. This is in keeping with published work in which a retrograde rabies virus was used and neurons in S1 projecting to either contralateral S1, or one of two subcortical targets, were reconstructed (Delaine D Larsen, 2008). The reconstructed neurons were

not quantified in this previous study, but visual inspection of the example data suggests that IT neurons showed greater ascending branch length and lateral branching. Other studies drew similar conclusions when reconstructing 'thick tufted' and 'thin tufted' L5 pyramidal neurons as a proxy for PT and IT neurons, including reconstructions from neurons labelled *in vivo* rather than in brain slices (DeLaine D Larsen & Callaway, 2006; Narayanan et al., 2017; Oberlaender et al., 2011; Wang et al., 2018).

In the context of L5-to-L2/3 connectivity, I observed differences in the pre-synaptic boutons in the supragranular layers, with the two IT populations showing a higher density and greater lateral distribution than the PT^{thal} neurons. Previous studies are somewhat unclear on this aspect, with some reporting a similar difference (Wang et al., 2018) and others not (Oberlaender et al., 2011). It should also be noted that I found previously undescribed differences in axonal morphology between the two IT subpopulations (IT^{ipsi} compared to IT^{contra}). There is evidence that the particular cortical region to which a L5 IT neuron projects may further distinguish this subpopulation (Yamashita et al., 2013) and differences have been reported between PT neurons depending on their particular long-range target (Rojas-Piloni et al., 2017). Thus a more fine-grained examination of IT and PT axonal morphology based on their particular long-range targets represents a possible direction for future work.

As may have become clear, there is not always consistency in how IT and PT neurons have been identified in the literature. Dendritic morphology has often been used to classify L5 neurons, with the assumption then made about the long-range axonal projections. This may have contributed to apparent contradictory results. For example, one study defined L5 pyramidal neurons as regular spiking (RS) or regular bursting (RB) based on their *in vitro* recordings, yet it is unclear how these characteristics map onto the PT and IT dichotomy. Interestingly, this particular study failed to find the same intrinsic electrophysiological differences as other studies cited above (e.g. AP width, fAHP amplitude) and reported different morphological features of the local axons (Staiger et al., 2016). It was for this reason that I used a projection-defined definition and focused on features that have been found to robustly distinguish the L5

subtypes of interest. Having validated electrophysiological differences between the neurons, I was then able to demonstrate differences in the axon ascending collateral morphology. Whilst these differences are consistent with many aspect of the literature, this is the first time to my knowledge that a quantification of the local axon collaterals of projection-defined L5 subtypes has been performed.

Validating retrograde viral tools for functional studies of projection-defined L5 subtypes in S1

The differences in axonal morphology and intrinsic electrophysiology suggest that PT and IT L5 pyramidal neurons play different roles in local cortical information processing. For instance, it has been suggested on the basis of their axonal branching, that IT neurons may preferentially share information to surrounding columns, which could be particularly important in integrating contextual information during sensory perception (Hawkins et al., 2017). Functional studies of L5a and L5b pyramidal neurons suggest that this could be the case (Reyes-Puerta et al., 2015). However, until recently the ability to manipulate projection-defined subtypes of L5 pyramidal neurons has been very difficult. Previous experimentation often relied on either direct electrical stimulation or the use of techniques such as glutamate uncaging. However, viral-mediated delivery of optogenetic tools offers more precise spatial and temporal control over defined subpopulations (Mao et al., 2011; Nagel et al., 2003; Petreanu et al., 2007, 2009). And, with the recent development of viral vectors optimized for retrograde transport, there are exciting opportunities to selectively manipulate projection-defined subpopulations of neurons (Li et al., 2020; Tervo et al., 2016).

By delivering a retrograde AAV encoding Cre-inducible ChR2 to specific locations, I was able to express ChR2 in the projection-defined L5 subpopulations of interest. Evaluating subcortical injection sites confirmed that the virus exhibits a high degree of retrograde transport following transduction. I also confirmed that the expression of ChR2 from the retrograde AAV was restricted by the expression of Cre recombinase in L5 of cortex, thus ensuring that experiments would not be contaminated by expression

outside of L5, such as in L2/3 following a cortical injection or L6 following a thalamic injection. Given the varying degree of long-range connectivity from S1 to other cortical regions and thalamic nuclei (Aronoff et al., 2010; Guo et al., 2020; Sherman, 2007, 2016), it is perhaps unsurprising that the number of ChR2-expressing S1 neurons varied according to the injection target. Finally, the somatic position of ChR2-expressing neurons within L5 reflected those typically associated with IT and PT neurons (Anastasiades, Marlin, et al., 2018; Aronoff et al., 2010; Feldmeyer, 2012; Gao & Zheng, 2004; Delaine D Larsen, 2008; Mao et al., 2011; Oswald et al., 2013), providing validation that the retrograde AAV targeted the subpopulations of interest.

In conclusion, this chapter has established the ability to target three projection-defined subpopulations of L5 pyramidal neurons in S1: PT^{thal}, IT^{ipsi} and IT^{contra}. I was able to reproduce subtype differences in intrinsic electrophysiological properties and thus validate my retrograde labelling of these subpopulations. I was then able to reconstruct the local axonal morphology of these neurons and determine subtype-related differences in the ascending collaterals. Whilst all three subpopulations show local projections to supragranular layers, IT neurons exhibit a greater axonal length, lateral branching and density of pre-synaptic boutons compared to PT neurons. Finally, I used the same injection strategy to deliver retrogradely transported viral tools, which resulted in the selective expression of ChR2 in these L5 subpopulations. This provides a foundation for functional studies into the role that these neuronal subtypes play in modulating local cortical information processing, which I begin in the following chapter.

Page intentionally left blank

Chapter 5 : Projection-defined L5 subtypes differentially recruit local inhibitory circuits in L2/3

Introduction

L5 is often considered the principal output layer of cortex. L5 pyramidal neurons can be subclassified as either intratelencephalic (IT), or pyramidal tract (PT) subtypes, depending on whether their long-range projections target either other cortical regions or subcortical structures, respectively. In addition to their long-range targets, the axons of L5 pyramidal neurons form ascending intracortical collaterals, through which the L5 neuron can signal locally to post-synaptic neurons in different cortical layers. Whilst supragranular L2/3 pyramidal neurons are known to provide significant excitatory input to L5 (Feldmeyer, 2012; Lefort et al., 2009), our knowledge remains limited about the role of reciprocal connectivity via the ascending collaterals from L5 to L2/3. More specifically, it is unclear whether L5 IT and PT subpopulations provide different reciprocal input.

An initial step in addressing this question is to quantify the functional connection strength between L5 subpopulations and different cortical layers. Early key experiments made use of tools such as laser scanning photostimulation via glutamate uncaging to investigate the connection strength from L5 to L2/3 (Dantzker & Callaway, 2000; Feldmeyer, 2012; Lefort et al., 2009; Meng et al., 2017; Staiger et al., 2015; X. Xu et al., 2016; Yoshimura et al., 2005). In such studies, the glutamate was converted with brief flashes of light from a chemically 'caged' form, to a bioavailable neurotransmitter in a spatially localized manner. This was repeated across a grid pattern overlaid on an acute cortical slice, such that the release of glutamate would be sufficient to cause underlying neurons to spike. The resulting post-synaptic currents could be measured from a neuron of interest (e.g. a L2/3 pyramidal neuron) and used to determine the

functional connectivity strength. Later studies have used a similar strategy with optogenetic tools such as channelrhodopsin-2 (ChR2) to explore the contribution of genetically-defined populations(Kätzel et al., 2011; Kätzel & Miesenböck, 2014). Such studies provided some of the first measures of functional connectivity between cortical layers, confirming that L5 receives strong excitatory inputs from L2/3, but also revealing reciprocal excitatory connectivity for different L5 sublaminae(Bureau et al., 2006; Feldmeyer, 2012; Lefort et al., 2009; Shepherd & Svoboda, 2005; Staiger et al., 2015). L5a showed stronger excitatory connectivity to L2/3 pyramidal neurons than L5b. Interestingly, in mouse primary somatosensory (S1) barrel cortex, the strength of connectivity from L5 to L3 was in some instances greater than that of L4 to L2/3, which is considered the principal input to L2/3 according to classical canonical circuits. In particular, those L2/3 pyramidal neurons that were found over the barrel septa had strong excitatory inputs from L5a, with very limited inputs from L4(Bureau et al., 2006). As has been mentioned, L5 IT and PT neurons have distinct (though not absolute) laminar depth preference definitions (Bureau et al., 2006; Constantinople & Bruno, 2013; Shepherd & Svoboda, 2005; X. Xu & Callaway, 2009). IT neurons are most often found in superficial L5a, whilst PT neurons are often found in L5b. Thus by using laminar depth of input as a proxy for neuronal subtypes, inferences can be made about the likely strength of excitatory connectivity from IT and PT L5 pyramidal neurons to L2/3.

In evaluating these interlaminar connections, it is important to not only consider the strength of the monosynaptic excitatory component. The recruitment of disynaptic inhibition that is tightly coupled to monosynaptic excitation is a ubiquitous feature of cortical circuits(Isaacson & Scanziani, 2011; Xue et al., 2014). In supragranular layers, pyramidal neurons form dense reciprocal connections with parvalbumin-expressing (PV) interneurons that mediate fast perisomatic inhibition and with somatostatin-expressing (SST) interneurons that preferentially target the dendrites of pyramidal neurons (Fino & Yuste, 2011; L. Gentet, 2012; Packer & Yuste, 2011; Rudy et al., 2011; Tremblay et al., 2016). The disynaptic recruitment of these interneurons results in post-synaptic excitation that is rapidly followed by a proportional or

'matched' inhibition(Xue et al., 2014), resulting in an excitation/inhibition (E/I) ratio for a particular input. This E/I ratio can vary depending on the input source and is crucial for fundamental aspects of cortical information processing (Adesnik, 2018), such as controlling synaptic integration windows(Pouille & Scanziani, 2001), the temporal precision of spiking activity (Jouhanneau et al., 2018), gain control (Isaacson & Scanziani, 2011) and oscillatory activity(Adesnik & Scanziani, 2010).

Previous studies that have investigated functional connectivity from L5 to L2/3 have not addressed the relationship between the sources of excitation and inhibition(Kätzel et al., 2011; Meng et al., 2017; X. Xu et al., 2016). Furthermore, whilst sublaminae differences in inhibitory motifs and preferential targeting of L2/3 interneuron subtypes have been suggested(Dantzker & Callaway, 2000), it is unknown how these relate to PT and IT neurons. Having established a method to deliver ChR2 to projection-defined L5 subpopulations (Chapter 4), I was now in a position to selectively control the output of PT and IT L5 pyramidal neurons and assess their influence upon L2/3. In particular, I wished to explore how these subpopulations recruited local inhibitory circuits in relation to local excitation.

Aims

The aims of this chapter were as follows:

1. To determine L2/3 responses to ascending collateral input from different projection-defined L5 pyramidal neuron subtypes.
2. To determine the synaptic circuits underlying L2/3 responses to projection-defined L5 pyramidal neuron subtypes.
3. To determine which L2/3 interneuron subpopulations are recruited by projection-defined L5 pyramidal neuron subtypes.

Results

To investigate L2/3 responses to local input from L5 pyramidal neuron subtypes, I used a retrograde Adeno Associated Virus (AAV) strategy to express ChR2 in projection-defined L5 subpopulations in S1. As in

Chapter 4, the retrograde AAV encoding Cre-inducible ChR2 (rAAV-Floxed-ChR2) was injected into either the left thalamus, left M1, or right S1 of *Rbp4-Cre* mice at 6 weeks of age. The animals were maintained for > 4 weeks to maximize expression, resulting in the selective expression of ChR2 in PT^{thal}, IT^{ipsi} or IT^{contra} L5 pyramidal neurons in left S1 (**Fig 5.1A**). Acute slices were prepared from left S1 and whole cell recordings were combined with selective optogenetic activation of the L5 subpopulation. As expected, brief flashes of blue light (473 nm; 1-3 ms) elicited temporally controlled spiking activity in the L5 subpopulation of interest (**Fig 5.1B**). Having confirmed the effectiveness of ChR2 expression, whole cell patch clamp recordings were used to measure the responses of L2/3 pyramidal neurons to input from the defined L5 subtype (**Fig 5.1C**). To evaluate the recruitment of both excitatory and inhibitory circuits, EPSCs and IPSCs were isolated by clamping the L2/3 pyramidal neuron at the reversal potential for $GABA_A$ receptors (-60 mV) or glutamate receptors (10 mV), respectively (**Fig 5.1D;** Wehr and Zador, 2003; Xue et al., 2014).

By varying the intensity of the light pulses, comparable levels of L2/3 excitatory response were elicited for the three L5 subtypes. Under these conditions, it was observed that for a given excitatory input (peak EPSC amplitude), the recruitment of inhibition (peak IPSC amplitude) in the L2/3 pyramidal neuron was between 2 to 5 times larger when the L5 PT^{thal} subtype was stimulated, than when the L5 IT subtypes were stimulated (**Fig 5.1D-E**). This resulted in a lower E/I ratio in the L2/3 pyramidal neurons in response to L5 PT^{thal} (n = 17 neurons, Peak EPSC/(Peak EPSC+ Peak IPSC) of 0.23 ± 0.03) than to either L5 IT^{ipsi} (n = 20 neurons, Peak EPSC/ (Peak EPSC+ Peak IPSC) of 0.74 ± 0.08) or L5 IT^{contra} (n = 13 neurons, Peak EPSC/ (Peak EPSC+ Peak IPSC) of 0.84 ± 0.08; **Fig 5.1F**). Statistical analyses confirmed that the E/I ratio varied as a function of the L5 subtype (Kruskal-Wallis test = 30.82, $p < 0.0001$).

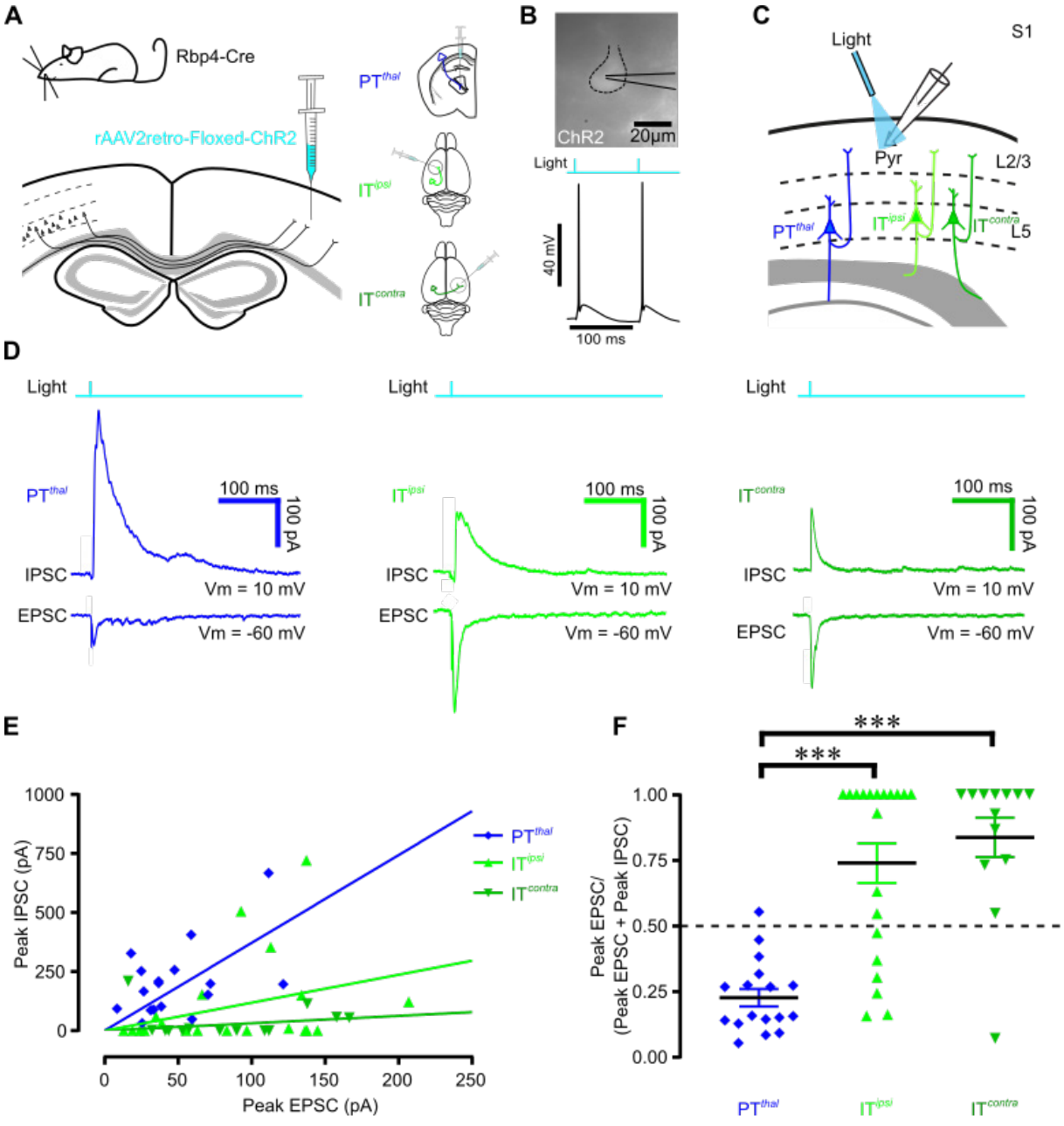


Figure 5.1 PT L5 pyramidal neurons recruit L2/3 inhibitory circuits more efficiently than IT L5 pyramidal neurons

(A) Rbp4-Cre mice received targeted injections of a retrograde AAV ('rAAV-Floxed-ChR2') into either left thalamus, left M1 or right S1, in order to target PT^{thal}, IT^{ipsi} and IT^{contra} L5 pyramidal neurons, respectively. **(B)** An example ChR2-expressing L5 pyramidal neuron that was targeted for electrophysiological recording in left S1 (top). The ChR2-expressing neuron made to spike (bottom) with brief pulses of blue light (473 nm; 1-3 ms; 'Light'). **(C)** Experimental design for studying functional connectivity from a projection-defined L5 subpopulation to L2/3. Pyramidal neurons in L2/3 of S1 were targeted for patch clamp recordings, whilst inputs from ChR2-expressing PT^{thal}, IT^{ipsi} or IT^{contra} L5 pyramidal neurons were photostimulated. **(D)** Example excitatory post synaptic currents (EPSCs) and inhibitory post synaptic currents (IPSCs) recorded from L2/3 pyramidal neurons following light activation of PT^{thal}, IT^{ipsi} or IT^{contra} L5 pyramidal neurons.

Subsequent multiple comparison analyses revealed that PT^{thal} neurons elicited a significantly lower E/I ratio than either IT^{ipsi} ($p < 0.0001$) or IT^{contra} ($p < 0.0001$) neurons, whilst the E/I ratio was not different between the two IT groups ($p = 0.182$, Dunn's multiple comparisons). Peak EPSC amplitude differed between the three subtypes (PT^{thal} peak EPSC was 48.3 ± 7.6 pA, IT^{ipsi} was 87.5 ± 12.0 pA and IT^{contra} was 84.2 ± 13.6 pA; Kruskal-Wallis test = 6.50, $p = 0.038$) although multiple comparisons did not detect a difference in any individual pairwise comparison (Dunn's multiple comparisons, $p > 0.05$ for all). Peak IPSC amplitude differed between the three subtypes (PT^{thal} peak IPSC 204.9 ± 37.6 pA, IT^{ipsi} was 105.3 ± 44.2 pA and IT^{contra} was 34.5 ± 17.5 pA; Kruskal-Wallis test = 16.08, $p = 0.0003$) and multiple comparisons revealed a pairwise differences between PT^{thal} and IT^{ipsi} ($p = 0.0030$), PT^{thal} and IT^{contra} ($p = 0.001$), but no difference between the IT groups ($p > 0.999$; Dunn's multiple comparisons).

In summary therefore, L5 subtypes elicit different response profiles in L2/3 pyramidal neurons, with PT^{thal} eliciting greater inhibition and IT input eliciting greater excitation. The working hypothesis was that these different L5-to-L2/3 signals are mediated by the ascending collaterals of the different L5 pyramidal neuron subtypes, which differentially recruit local interneurons within L2/3. To interrogate this hypothesis however, I considered two alternative explanations. First, I considered the possibility that the higher E/I ratio of IT subtypes actually reflects long-range L5 inputs from outside of S1, which could be associated with cortical injections but not subcortical injections. Second, I considered the possibility that the lower E/I ratio of PT^{thal} reflected a greater recruitment of L5 interneurons with ascending translaminar inhibitory

Figure 5.1 ***Continued from opposite***

(E) Scatter plot comparing the peak EPSC and peak IPSC in L2/3 pyramidal neurons following activation of either PT^{thal} (n = 17 neurons), IT^{ipsi} (n = 20 neurons) or IT^{contra} (n = 13 neurons) L5 pyramidal neurons**.** For comparable EPSC ampltiudes, PT^{thal} L5 neurons recruited larger IPSCs than IT L5 neurons. Lines of best fit for visualization purposes were constrained to pass through the origin. **(F)** This generated differences in the E/I ratio (peak EPSC / (peak EPSC + peak IPSC)) for the three L5 subpopulations (Kruskal-Wallis test = 30.82, $p < 0.0001$). PT^{thal} neurons elicited a lower E/I ratio in L2/3 than either IT^{ipsi} ($p < 0.0001$) or IT^{contra} ($p < 0.0001$) neurons. The E/I ratio was not different between the two IT groups ($p = 0.182$, Dunn's multiple comparisons). PT^{thal} E/I ratio was 0.23 ± 0.033, IT^{ipsi} was 0.74 ± 0.075 and IT^{contra} was 0.84 ± 0.075.

projections to L2/3 (Buchanan et al., 2012; Kätzel et al., 2011; Naka & Adesnik, 2016). I designed experiments to interrogate each of these possibilities.

The higher L2/3 E/I ratio of IT subtypes could reflect long-range axonal input from neurons close to the cortical injection sites, which have also been retrogradely labelled by rAAV-Floxed-ChR2 and could then be inadvertently activated when recording and stimulating in left S1 (Aronoff et al., 2010; Mao et al., 2011; Hafner et al., 2019; Sempere-Ferràndez et al., 2019). To address this, I used *in utero* electroporation (IUE) at E13 in order to drive Cre recombinase expression only in the left hemisphere of wild-type mice, timing the electroporation to preferentially target L5 and targeting the region that would become left S1 (see Chapter 2). Once these animals had developed to 6 weeks of age, they received a targeted injection of rAAV2retro-Floxed-Chr2 into contralateral (i.e. right) S1 (**Fig 5.2A**). As a result, only Cre-expressing L5 IT pyramidal neurons in left S1 (and not neurons close to the injection) expressed ChR2 (**Fig 5.2B**). Soma counts taken from single optical plane images (840 by 640 μm section) of representative cortex from each hemisphere of 350μm thick slices confirmed that ChR2-expression was restricted to the left hemisphere, which had been targeted for electroporation (**Fig 5.2C**).

Figure 5.2 ***Continued from opposite***

(C) The soma of ChR2-expressing IT^{IUE} L5 pyramidal neurons were restricted to left S1 (n = 4 animals; 8.5 ± 2.75 cells per 50 μm slice on the IUE side compared to 0.25 ± 0.25 cells on the injected side; unpaired t-test t = 3.0, p = 0.0245). **(D)** Example EPSC and IPSC recording from a L2/3 pyramidal neuron following activation of IT^{IUE} L5 pyramidal neurons. **(E)** Scatter plot of L2/3 responses shows that IT^{IUE} activation (n = 7 L2/3 neurons) elicited similar amplitude EPSCs and IPSCs to those following IT^{contra} activation (n = 13). In contrast, IT^{IUE} activation elicited smaller IPSCs than those elicited by PT^{thal} neurons (n = 17). Lines of best fit were constrained to pass through the origin. **(F)** These data generated differences in the E/I ratio across groups (Kruskal-Wallis Test, p < 0.0001). The E/I ratio following activation of IT^{IUE} was similar to the E/I for IT^{contra} (p > 0.9999) and higher than PT^{thal} (p = 0.0006, Dunn's multiple comparisons). The IT^{IUE} E/I ratio was 0.89 ± 0.11, IT^{contra} was 0.84 ± 0.08 and PT^{thal} was 0.23 ± 0.03.

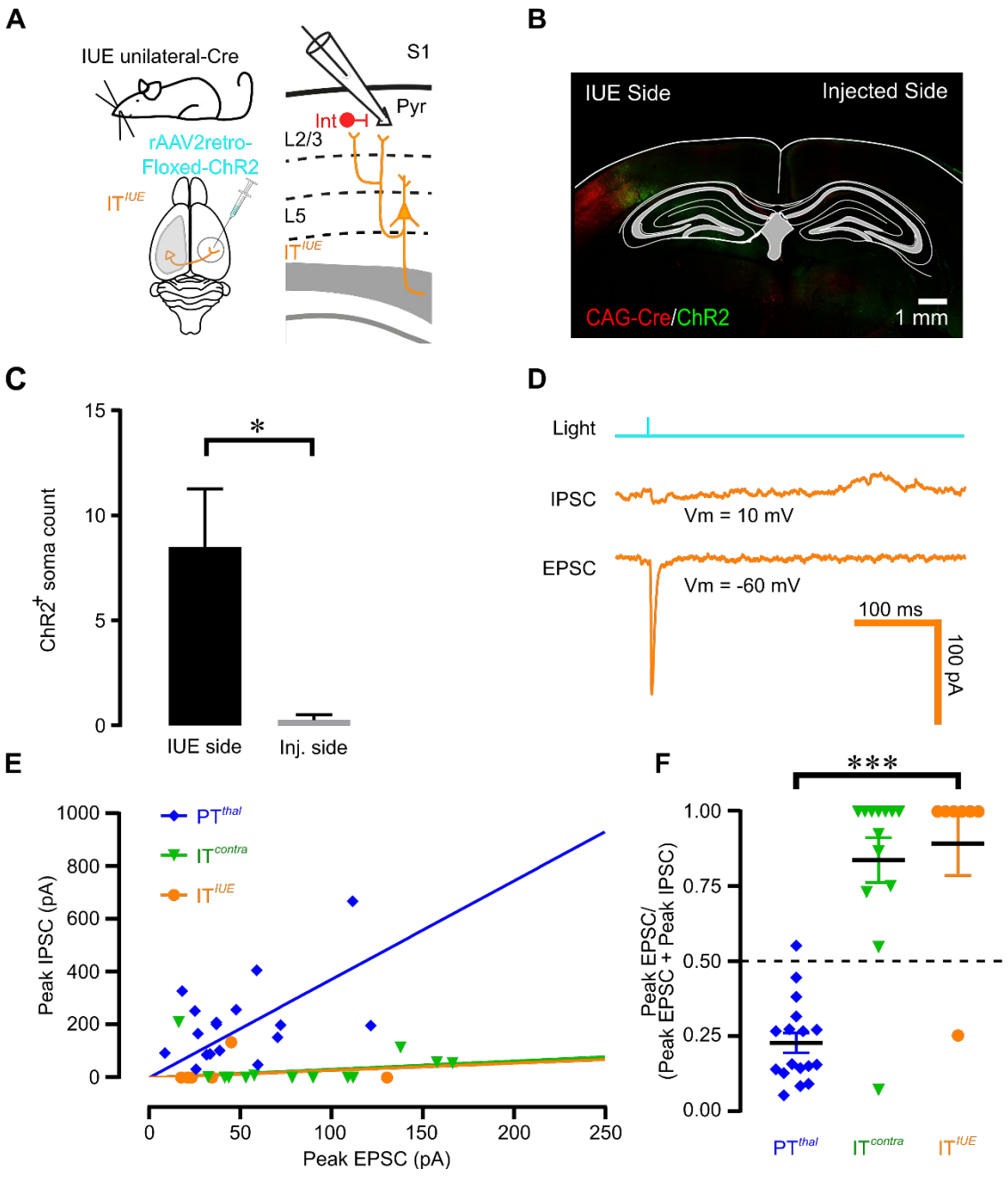


Figure 5.2 L2/3 responses reflect input from local L5 pyramidal neurons

(A) Wild type mice underwent *in utero* electroporation (IUE) at E13 to express Cre recombinase in L5 pyramidal neurons of left S1 (i.e. unilaterally). The plasmid expressed Cre recombinase fused with the red fluorescent protein, mCherry, under the control of the CAG promoter (referred to as 'CAG-Cre'). Upon reaching adulthood, rAAV-Floxed-ChR2 was injected into right S1, such that ChR2 would only be expressed in the Cre-expressing L5 neurons in left S1 that project a long-range axon to right S1. This population is referred to as IT^{IUE} L5 pyramidal neurons. Acute slices were prepared from left S1 and whole cell patch clamp recordings were performed from L2/3 pyramidal neurons. **(B)** Example confocal image shows Cre and ChR2 expression in the left hemisphere that underwent IUE. There was no ChR2 expression in the right hemisphere into which the retrograde AAV was injected.

Then acute brain slices were prepared from left S1, L2/3 pyramidal neuron were targeted for recording, and EPSCs and IPSCs recorded in response to the stimulation of the ChR2-expressing L5, which were referred to as IT^{IUE} L5 pyramidal neurons (**Fig. 2D**). The L2/3 excitation and inhibition elicited following stimulation L5 IT^{IUE} pyramidal neurons was comparable to that elicited by stimulation of IT^{contra} neurons in *Rbp4-cre* mice. For equivalent peak EPSC amplitudes, the IPSC recorded following L5 IT^{IUE} stimulation was smaller than when stimulating L5 PT^{thal} (**Fig 5.2E**). These data generated differences in the resulting E/I ratio across groups (**Fig 5.2F**; Kruskal-Wallis Test, $p < 0.0001$). The Peak EPSC/ (Peak EPSC+ Peak IPSC) ratios from IT^{IUE} (n = 7 neurons; 0.89 ± 0.11) were not different from IT^{contra} (n = 13 neurons, 0.84 ± 0.08; $p > 0.9999$) but were higher than PT^{thal} (n = 17 neurons, 0.23 ± 0.03; $p = 0.0006$, Dunn's multiple comparisons). These data support the conclusion that different L5-to-L2/3 signals are mediated by the ascending collaterals of local L5 pyramidal neuron subtypes.

Next, I considered the second alternative explanation, that the lower E/I ratio of PT^{thal} reflected a greater recruitment of L5 interneurons with ascending translaminar projections to L2/3, rather than the recruitment of interneurons within L2/3. Evidence for direct translaminar inhibitory connections from the infragranular layers to L2/3 has been reported (Kätzel et al., 2011; Buchanan et al., 2012; Bortone et al., 2014; Nigro et al., 2018) and therefore in principle, the lower E/I ratio of PT^{thal} could reflect a differential recruitment of infragranular translaminar-projecting interneurons that provide disynaptic inhibition to L2/3. To address this, ChR2 was expressed in PT^{thal} L5 pyramidal neurons as previously, but in the resulting acute brain slices the fibres passing through L4 were lesioned by making an incision above L5 **(Fig 5.3A**). This would sever any translaminar inhibitory projections, but still leave the ChR2-expressing axon terminals of PT^{thal} in L2/3 available for photostimulation (**Fig 5.3A-B**). Under these conditions, photostimulation still elicited a monosynaptic excitatory response that was followed by a much larger inhibitory response in the L2/3 pyramidal neuron (**Fig 5.3C-D**; n = 4 neurons from 4 slices, peak EPSC of 23.8 ± 9.4 pA compared to a peak IPSC of 144.0 ± 59.9 pA).

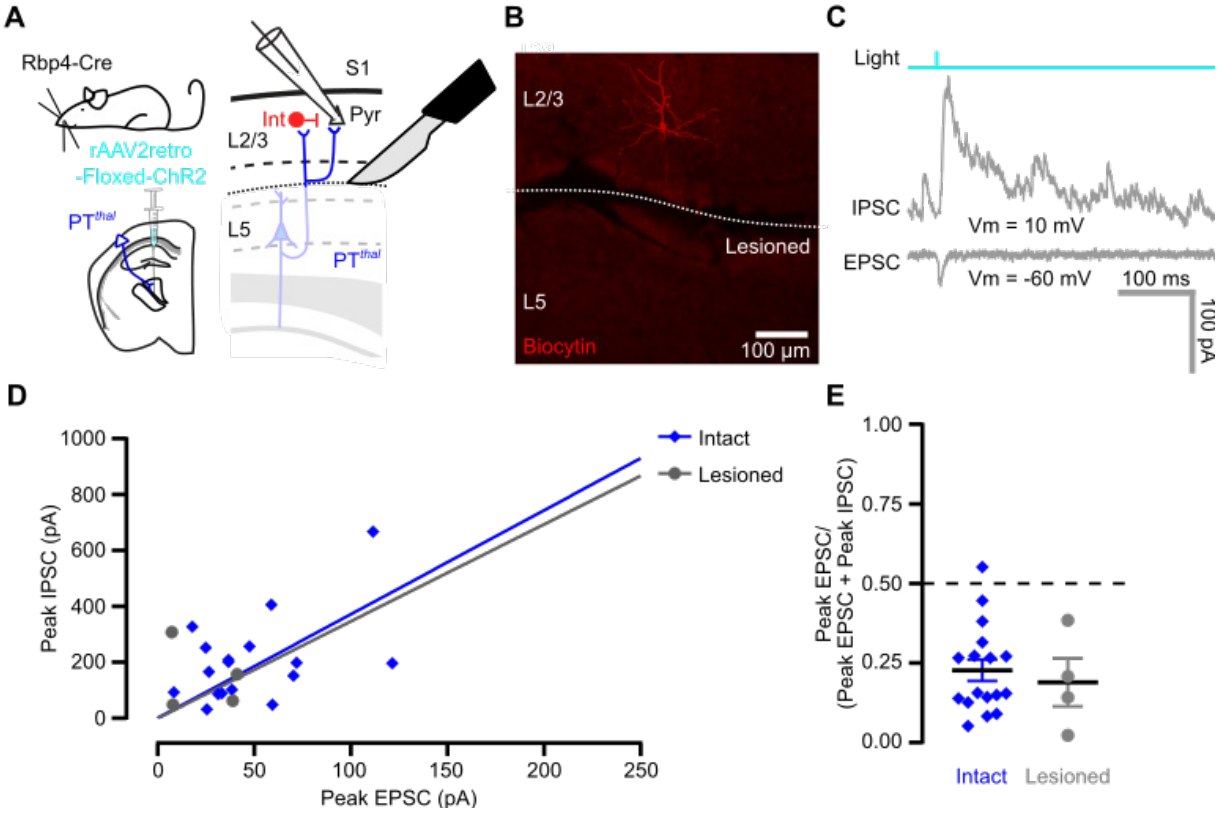


Figure 5.3 L5 pyramidal neurons recruit L2/3 inhibitory interneurons

(A) Experimental design to assess whether L5 pyramidal neurons recruit inhibitory neurons within L2/3. ChR2 was expressed in PT^{thal} L5 pyramidal neurons in S1 by injecting rAAV-Floxed-ChR2 into the thalamus of Rbp4-Cre mice. When acute cortical slices were prepared, fibres passing through L4 were lesioned by making an incision above L5, to leave the PT^{thal} axon terminals in L2/3. **(B)** Confocal imaging was used to confirm the effectiveness of the lesion (dashed line) and its location relative to the patched and biocytin-filled L2/3 pyramidal neuron. **(C)** Example EPSC and IPSC recording from a L2/3 pyramidal neuron following activation of ChR2-expressing PT^{thal} axon terminals in a lesioned slice. **(D)** Scatter plot of L2/3 responses shows that after lesioning the slice, photostimulation of ChR2-expressing PT^{thal} axon terminals elicited larger peak IPSCs than EPSCs (n = 4 neurons from 4 slices; peak IPSC of 144 ± 59.84 pA and peak EPSC of 23.8 ± 9.36 pA, Mann-Whitney test, p = 0.02), which were comparable to when the slice was intact. Lines of best fit were constrained to pass through the origin. **(E)** These data generated E/I ratios that were comparable when the slice was intact (n = 17, E/I ratio of 0.23 ± 0.033) and lesioned (n = 4, Peak EPSC/ (Peak EPSC+ Peak IPSC) ratio of 0.19 ± 0.075; t-test, p = 0.63).

Indeed, the PT^{thal} E/I ratio for the lesioned slices was similar to that in the intact slices (**Fig 5.3E**; Peak EPSC/ (Peak EPSC+ Peak IPSC) ratio from lesioned slices was 0.19 ± 0.08 and intact slices was 0.23 ± 0.03; t-test p = 0.63). These data support the conclusion that different L5-to-L2/3 signals are mediated by the differential recruitment of L2/3 interneurons by the ascending collaterals of L5 pyramidal neuron subtypes.

Having established that ascending collaterals of L5 subtypes differentially recruit local L2/3 interneurons, I next investigated whether this involves the selective targeting of specific L2/3 interneuron subpopulations. Whilst a variety of interneuron subpopulations exist, L2/3 pyramidal neurons receive dense inhibition primarily from two classes of inhibitory interneurons, which can be defined by the expression of parvalbumin (PV) or somatostatin (SST) (Fino & Yuste, 2011; Karnani et al., 2014; Packer & Yuste, 2011; Rudy et al., 2011). Experiments in the remainder of this chapter were designed to examine whether the ascending collaterals of L5 subtypes differentially recruit PV-expressing or SST-expressing L2/3 interneurons. Fast-spiking PV interneurons are known to play a role in mediating rapid perisomatic inhibition and balancing excitation (Xue et al., 2014; Moore et al., 2018). To examine L5 inputs to L2/3 PV interneurons, I used an experimental design based on a triple transgenic mouse line (*PV-Cre/Rbp4-Cre/Ai9*), in which PV interneurons express the red fluorescent protein tdTomato, whilst Cre recombinase in L5 also allows for ChR2 to be selectively expressed in either PT^{thal}, IT^{ipsi} or IT^{contra} L5 pyramidal neurons by injecting rAAV-Floxed-ChR2 into the relevant target structure (**Fig 5.4A-B**). This enables dual patch recordings to be made from a tdTomato-expressing L2/3 PV interneuron and a neighbouring, non-fluorescent L2/3 pyramidal neuron (**Fig 5.4A-C**). To first validate the experimental design, the electrophysiological characteristics of the PV interneurons were quantified and compared with the neighboring pyramidal neurons. The PV interneurons (n = 30) showed characteristic high firing rates and a lack of spike frequency accommodation in comparison with the pyramidal neurons (n = 15; **Fig 5.4D + Fig 5.5A**; Fanselow et al., 2008; Avermann et al., 2012; Gentet, 2012).

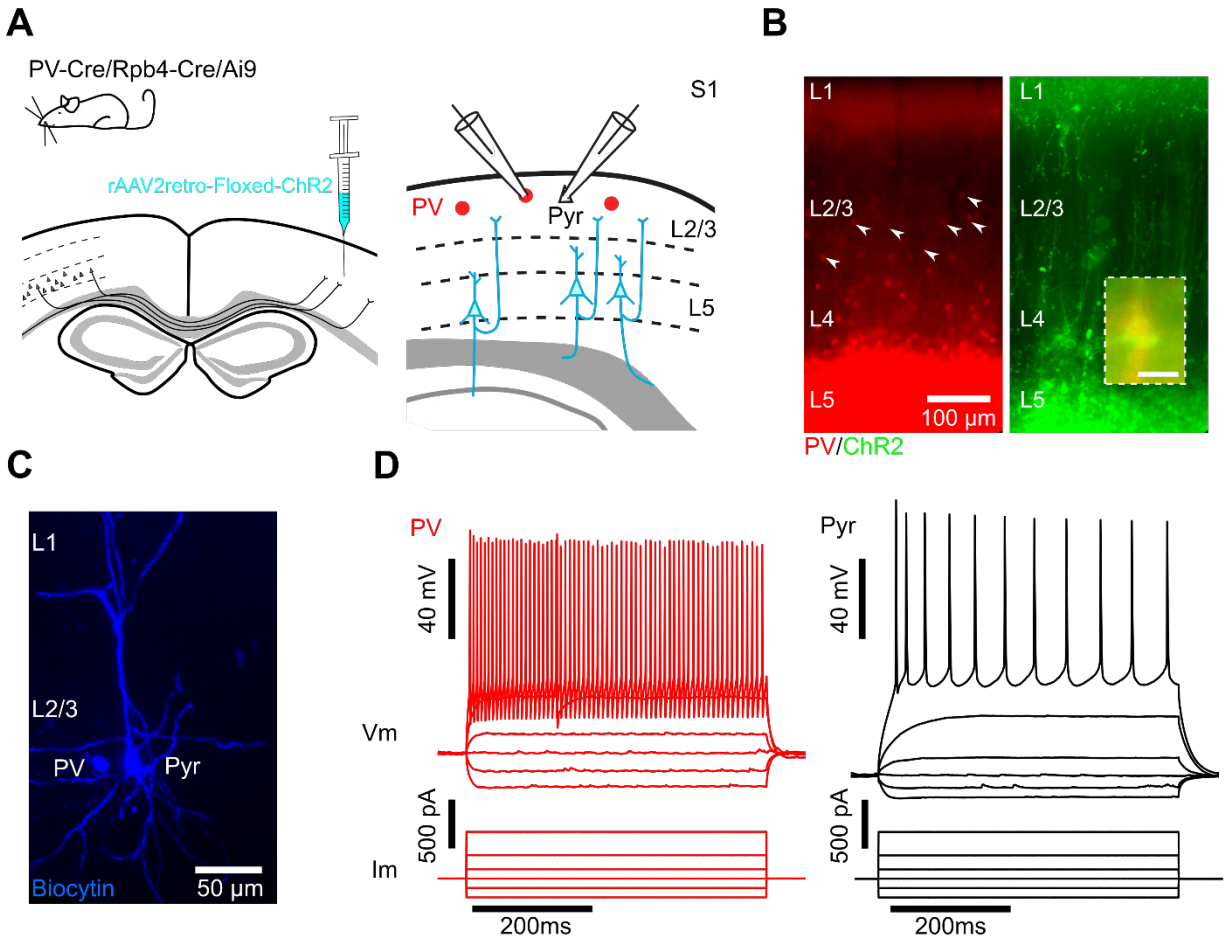


Figure 5.4 Recording from of L2/3 PV-expressing interneurons

(A) Experimental design for examining L5 input to L2/3 PV-expressing (PV) interneurons. The PV-Cre/Rbp4-Cre/Ai9 triple transgenic mouse line expresses tdTomato in PV interneurons, whilst L5 pyramidal neurons also express Cre recombinase and tdTomato. ChR2 was expressed in either PT^{thal}, IT^{ipsi} or IT^{contra} projecting L5 pyramidal neurons by injecting rAAV-Floxed-ChR2 into the relevant target structure (left). Acute slices were then generated from S1 and whole cell patch clamp recordings were performed from pairs of L2/3 neurons comprising a tdTomato-expressing PV interneuron and a neighbouring pyramidal neuron (right ; mean pair distance 50 ± 6 µm) . Neuronal pairs were recorded either simultaneously or sequentially (see Chapter 2 for details). **(B)** Example images of left S1 illustrating tdTomato-expressing PV interneurons in L2/3 (arrowheads) and ChR2-expressing L5 pyramidal neurons. Insert shows an individual pyramidal neuron expressing both tdTomato and ChR2 (scale, 20 µm). **(C)** Confocal image after histology showing a biocytin-filled L2/3 PV interneuron and L2/3 pyramidal neuron. **(D)** Example current clamp recordings from a L2/3 pair comprising a PV interneuron (left) and pyramidal neuron (right), showing the membrane potential (Vm) response to a series of 50 pA current steps (Im).

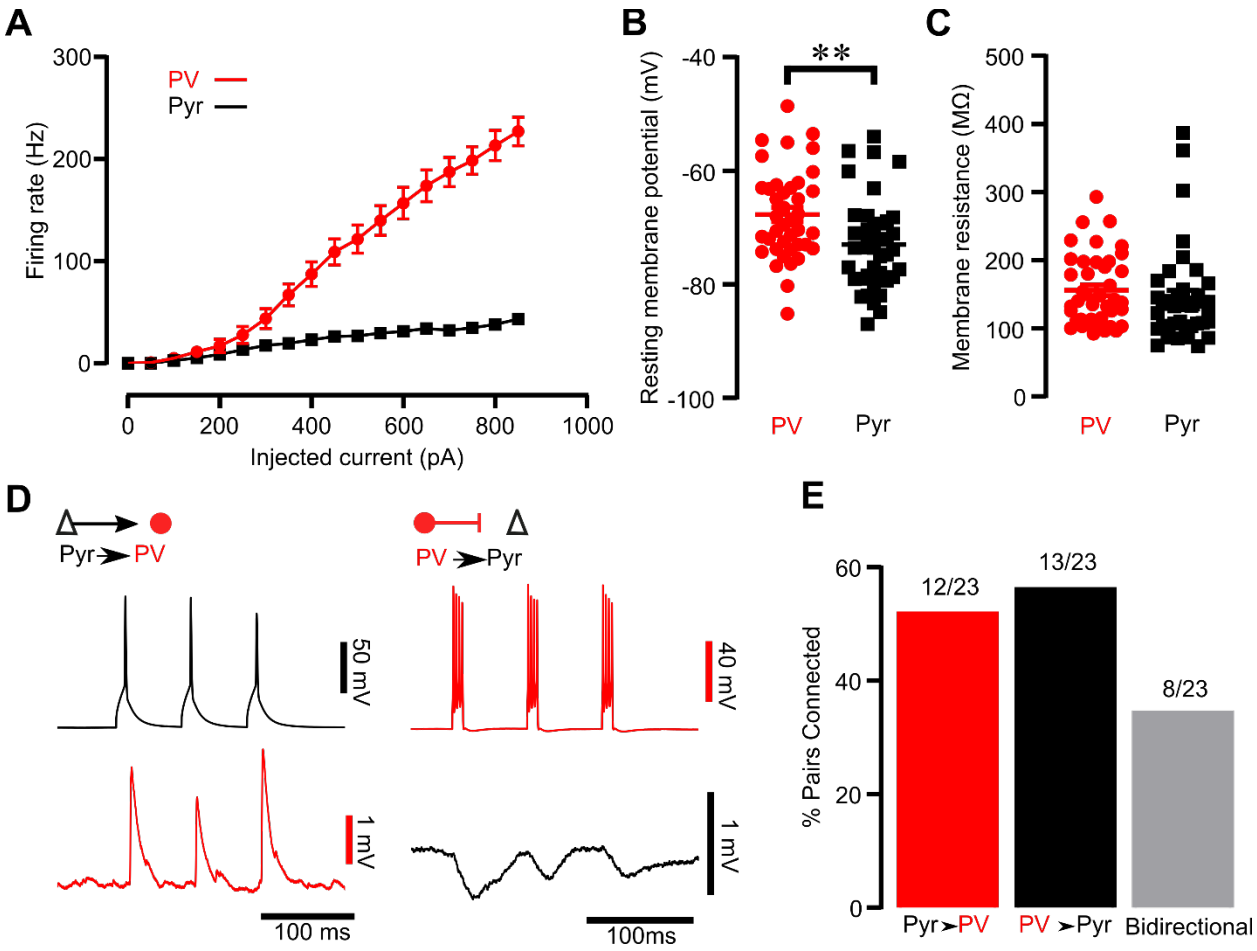


Figure 5.5 Electrophysiological and connectivity characteristics of L2/3 PV-expressing interneurons

(A) Input-output spiking curve illustrates that the PV interneurons (n = 30) exhibited higher firing rates than the pyramidal neurons (n = 15) in response to injected current (mixed effects model analysis $F(17, 600) = 36.31$, $p < 0.0001$). **(B)** PV interneurons exhibited more depolarized resting membrane potentials (-67.69 ± 1.25 mV) than the pyramidal neurons (-72.99 ± 1.30 mV; paired t-test $t(38) = 2.89$, $p = 0.0063$). **(C)** Membrane resistance was not different between the two neuronal populations. PV membrane resistance was 155.9 ± 8.01 MΩ and pyramidal neuron was 144.8 ± 10.67 MΩ (Wilcoxon Rank test $W = -225$, $p = 0.15$). **(D)** To assess monosynaptic connectivity between simultaneously recorded pairs of neurons, brief trains of action potentials were evoked in either the PV (left) or pyramidal (right) neuron, whilst putative post-synaptic responses were recorded in the other neuron. **(E)** A high proportion of PV-pyramidal neuron pairs showed either uni-directional or bi-directional monosynaptic connectivity.

Also in keeping with previous descriptions of L2/3 barrel cortex fast-spiking interneurons (Gentet et al., 2010; Avermann et al., 2012), the resting membrane potential of the PV interneurons was relatively depolarized compared to the pyramidal neurons (**Fig 5.5B,** PV resting membrane potential was -67.7 ± 1.3 mV, pyramidal was -73.0 ± 1.3 mV; paired t-Test t(38) = 2.89, p = 0.0063). The membrane resistance was not different between the PV interneurons and the pyramidal neurons (**Fig 5.5C;** PV membrane resistance was 155.9 ± 8.0 MΩ, pyramidal was 144.8 ± 10.7 MΩ; Wilcoxon Rank test W = -225, p = 0.15). Finally, synaptic connectivity between the L2/3 PV interneurons and pyramidal neurons was high, as expected (**Fig 5.5D**). 52% of PV interneurons received direct input from the pyramidal neuron, 57% of the pyramidal neurons received direct input from the PV interneuron, and 35% of pairs showed bidirectional connectivity (**Fig 5.5E**). These data validated the use of dual patch recordings to target a L2/3 PV interneuron and a neighboring, non-fluorescent L2/3 pyramidal neuron.

To compare the strength of input from L5 subtypes to L2/3 PV interneurons, ChR2 was selectively expressed in either PT^{thal}, IT^{ipsi} or IT^{contra} L5 pyramidal neurons by injecting rAAV-Floxed-ChR2 into the relevant target structure (**Fig 5.4A** and **Fig 5.6A**). Injections were performed at 6 weeks of age and the animals maintained for > 4 weeks to maximize expression. Acute brain slices were prepared from left S1 and dual recordings performed from a PV interneuron and neighboring pyramidal neuron, as described above. Light pulses were used to photostimulate either PT^{thal}, IT^{ipsi} or IT^{contra} inputs from L5 and the EPSC in the L2/3 pyramidal neuron was used to normalize the level of stimulation, so that the PV EPSC could be expressed relative to the EPSC of the neighboring pyramidal neuron (i.e. PV/Pyr ratio) (**Fig 5.6B**). Under these conditions, there was a pronounced difference between L5 subtypes in terms of the size of the monosynaptic excitatory response in the PV interneuron (Kruskal-Wallis, p = 0.022; **Fig 5.6B-D**).

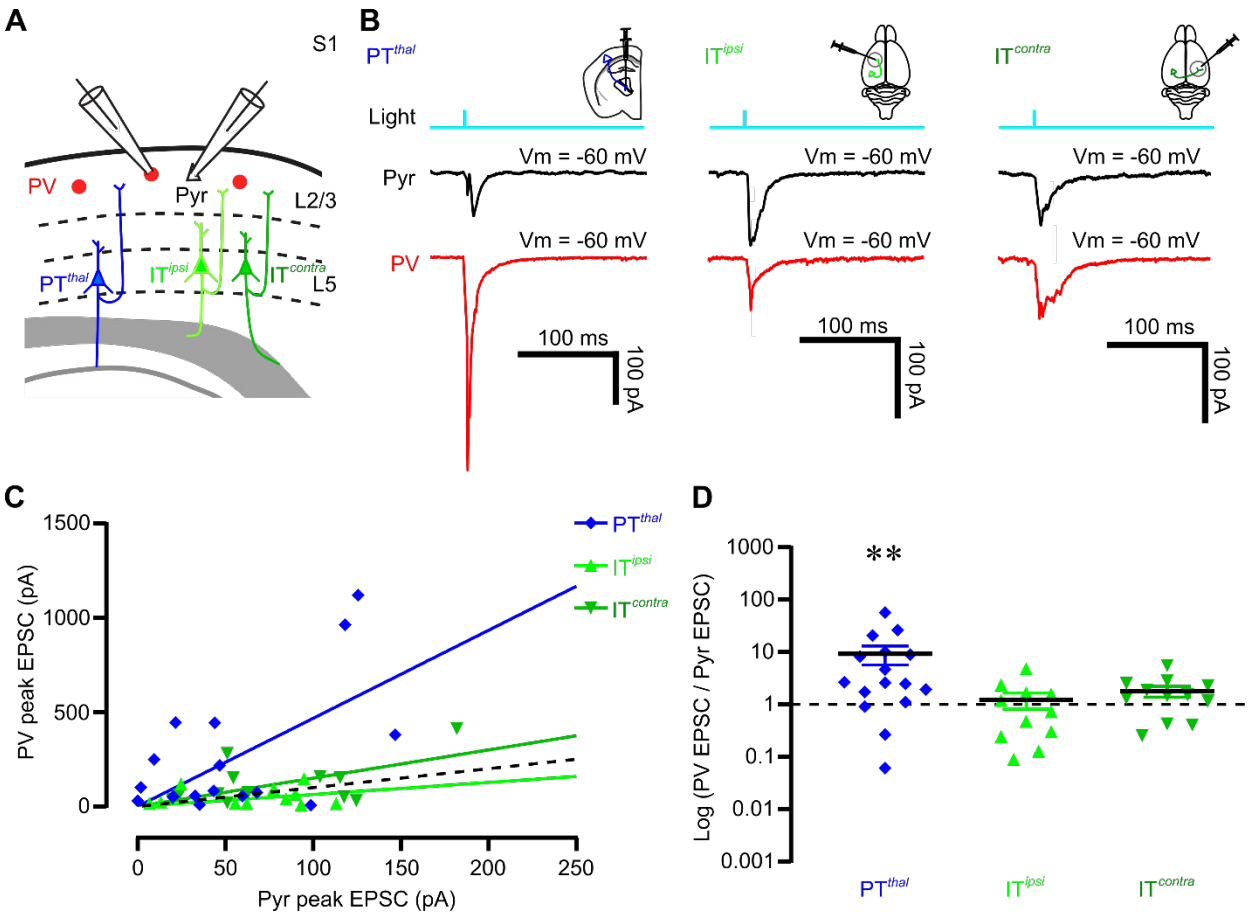


Figure 5.6 PT^{thal} L5 pyramidal neurons provide greater excitatory drive to L2/3 PV-expressing interneurons

(A) Experimental design for examining L5 input to L2/3 PV-expressing (PV) interneurons. Following injection with rAAV-Floxed-ChR2 such that ChR2 was expressed in either PT^{thal}, IT^{ipsi} or IT^{contra} L5 pyramidal neurons, dual recordings were performed from pairs of L2/3 neurons comprising a PV interneuron and a neighbouring pyramidal neuron in S1. **(B)** Example EPSCs recorded in L2/3 from pairs of PV (red trace) and pyramidal (Pyr; black trace) neurons in response to activation of either PT^{thal} (left), IT^{ipsi} (centre) or IT^{contra} (right) L5 pyramidal neurons. **(C)** Scatter plot comparing the L2/3 pyramidal neuron peak EPSC and the PV interneuron peak EPSC following activation of either PT^{thal} (n = 16 pairs), IT^{ipsi} (n = 11 pairs) or IT^{contra} (n = 12 pairs) L5 pyramidal neurons**.** When PT^{thal} neurons were activated, PV interneurons received stronger EPSCs than the neighbouring pyramidal neuron. The dashed line indicates equality and the lines of best fit were constrained to pass through the origin. **(D)** The ratio of PV EPSC to Pyr EPSC (i.e. the PV/Pyr ratio) differed significantly for the three L5 subpopulations (Kruskal-Wallis test, p = 0.02). The dashed line indicates equality. Activating PT^{thal} resulted in the highest PV/Pyr ratio in L2/3 (n = 16 pairs, 9.28 ± 3.65), which was significantly greater than equality (Wilcoxon signed rank, p = 0.0017) and consistent with strong excitatory drive from PT^{thal} to L2/3 PV interneurons. The L2/3 PV/Pyr ratio for IT^{ipsi} (n = 11 pairs, 1.2 ± 0.42) and IT^{contra} activation (n = 12 pairs, 1.79 ± 0.41) were not different from equality (Wilcoxon signed rank, p = 0.90 and p = 0.11, respectively), consistent with relatively weak excitatory drive from IT neurons to L2/3 PV interneurons. Subsequent multiple comparisons revealed a difference in the PV/Pyr ratio recorded for PT^{thal} and IT^{ipsi} (p = 0.02), but not between of PT^{thal} and IT^{contra} (p = 0.33) or between the two IT groups (p = 0.84, Dunn's multiple comparisons).

The PV/Pyr ratio of 9.2 ± 3.7 (n = 16 pairs) revealed a strong bias in excitatory drive from PT^{thal} to L2/3 PV interneurons, and was the only subtype that elicited a PV/Pyr ratio greater than equality (**Fig 5.6D**; Wilcoxon signed rank, p = 0.0017). In contrast, stimulation of IT^{ipsi} and IT^{contra} subtypes resulted in mean PV/Pyr ratios of 1.2 ± 0.4 (n = 11 pairs) and 1.8 ± 0.4 (n = 12 pairs), respectively, neither of which were different from equality (Wilcoxon signed rank, p = 0.90 and p = 0.11). These data suggest that PT^{thal} generate strong recruitment of L2/3 PV interneurons, which could underlie the differences in L5-to-L2/3 signals provided by the ascending collaterals of L5 pyramidal neuron subtypes.

Dendrite-targeting SST interneurons can also provide disynaptic inhibition to L2/3 pyramidal neurons (Silberberg and Markram, 2007). It was therefore important to evaluate the relative targeting of L2/3 SST interneurons by different L5 pyramidal neuron subtypes. Using a similar experimental design as for the PV interneurons, a triple transgenic mouse line (*SST-Cre/Rbp4-Cre/Ai9*) expressed tdTomato in SST interneurons and Cre recombinase in L5, which allowed for ChR2 to be selectively expressed in either PT^{thal}, IT^{ipsi} or IT^{contra} L5 pyramidal neurons by injecting rAAV-Floxed-ChR2 into the relevant target structure (**Fig 5.7A-B**). Neuronal pairs comprising a L2/3 SST interneuron and a neighbouring non-fluorescent L2/3 pyramidal neuron were then targeted for recording (**Fig 5.7A-C**). The experimental design was validated by confirming the electrophysiological characteristics of the SST interneurons compared with the pyramidal neurons. In keeping with previous characterization (Ma, 2006; Fanselow et al., 2008; Gentet et al., 2010; Fino and Yuste, 2011; Gentet, 2012), the L2/3 SST interneurons (n = 20) exhibited higher firing rates than the L2/3 pyramidal neurons (n = 19; **Fig 5.7D+ Fig 5.8A**). The SST interneurons also exhibited a more depolarized resting membrane potential (**Fig 5.8B**; SST resting membrane potential was -62.2 ± 1.7 mV, pyramidal was -75.6 ± 1.8 mV) and higher membrane resistance than local pyramidal neurons (**Fig 5.8C,** SST membrane resistance was 223 ± 18 MΩ, pyramidal was 142 ± 15 MΩ).

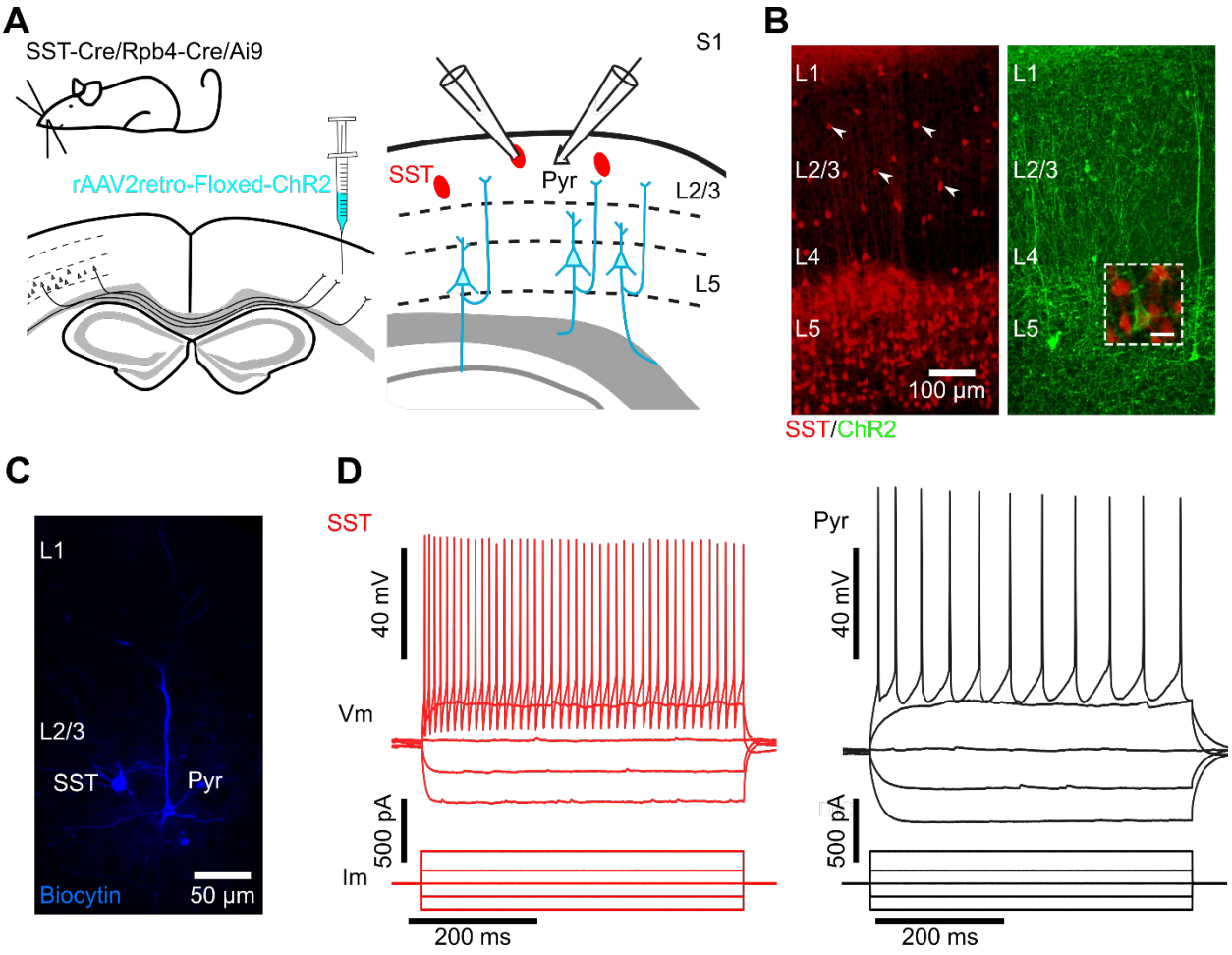


Figure 5.7 Recording from L2/3 SST-expressing interneurons

(A) Experimental design for examining L5 input to L2/3 SST-expressing (SST) interneurons. The SST-Cre/Rbp4-Cre/Ai9 triple transgenic mouse line expresses tdTomato in SST interneurons, whilst L5 pyramidal neurons also express Cre recombinase and tdTomato. ChR2 was expressed in either PT^{thal}, IT^{ipsi} or IT^{contra} projecting L5 pyramidal neurons by injecting rAAV-Floxed-ChR2 into the relevant target structure (left). Acute slices were then generated from S1 and whole cell patch clamp recordings were performed from pairs of L2/3 neurons comprising a tdTomato-expressing SST interneuron and a neighbouring (within 100 µm) pyramidal neuron (right). Neuronal pairs were recorded either simultaneously or sequentially (see Chapter 2 for details). **(B)** Example images of left S1 illustrating tdTomato-expressing SST interneurons in L2/3 (arrowheads) and ChR2-expressing IT^{ipsi} L5 pyramidal neurons. Insert shows an individual pyramidal neuron expressing both tdTomato and ChR2 (scale, 20 µm). **(C)** Confocal image after histology showing a biocytin-filled L2/3 SST interneuron and L2/3 pyramidal neuron. **(D)** Example current clamp recordings from a L2/3 pair comprising a SST interneuron (left) and pyramidal neuron (right), showing the membrane potential (Vm) response to a series of 50 pA current steps (Im).

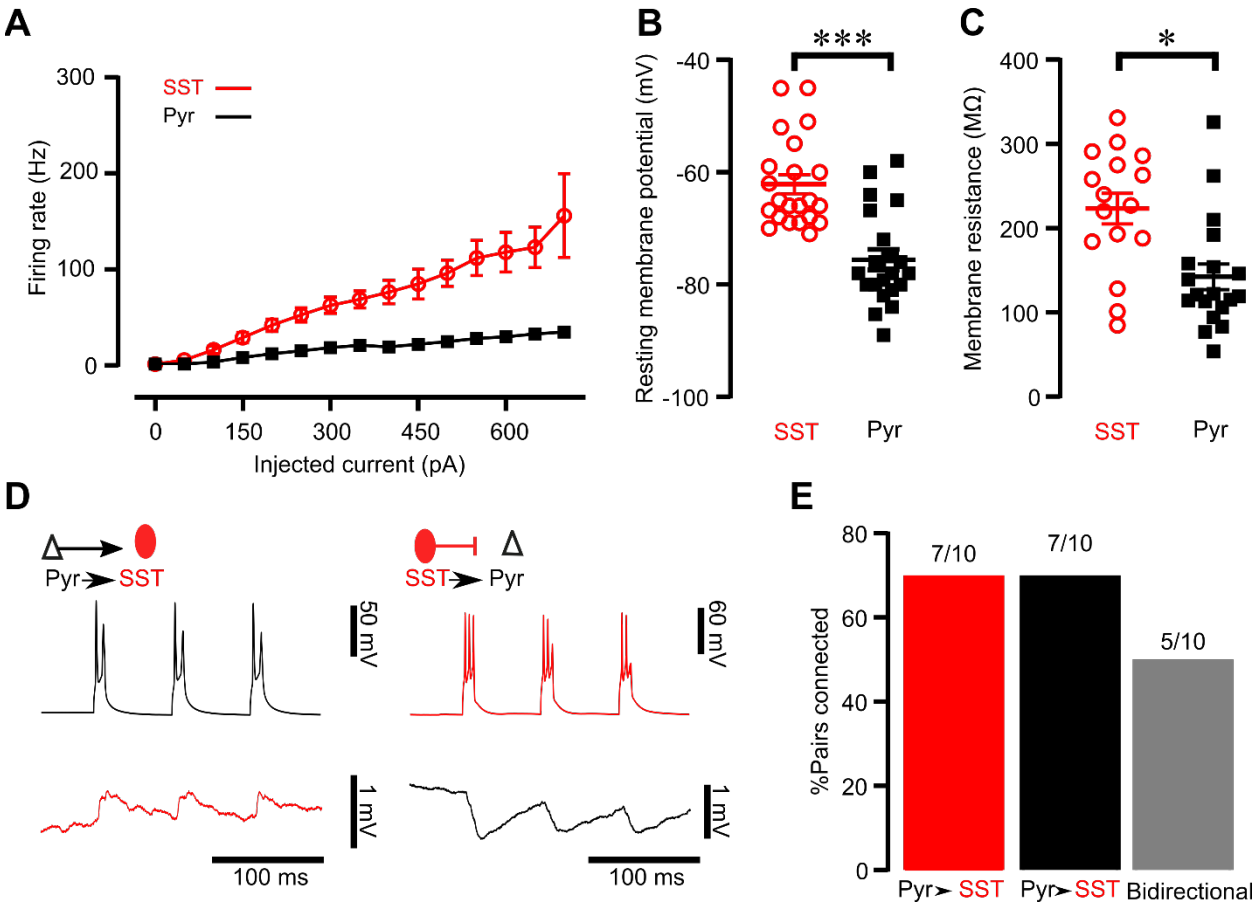


Figure 5.8 Electrophysiological and connectivity characteristics of L2/3 SST-expressing interneurons

(A) Input-output spiking curve illustrates that the SST interneurons (n = 20) exhibited higher firing rates than the pyramidal neurons (n = 19) in response to injected current (mixed effects model analysis $F(14,404) = 31.8$, $p < 0.0001$). **(B)** SST interneurons exhibited more depolarised resting membrane potentials (-62.17 ± 1.69 mV) than the pyramidal neurons (-75.59 ± 1.82 mV; Wilcoxon matched pairs signed rank test $W = -206$, $p < 0.0001$). **(C)** SST membrane resistance (223.2 ± 18.15 MΩ) was higher in SST interneurons than the pyramidal neurons (142.3 ± 15.16 MΩ; Wilcoxon matched pairs signed rank test $W = -86$, $p = 0.013$). **(D)** To assess monosynaptic connectivity, brief trains of action potentials were evoked in either the SST (left) or pyramidal (right) neuron, whilst putative post-synaptic responses were recorded in the other neuron. **(E)** A high proportion of SST-pyramidal neuron pairs showed either uni-directional or bi-directional monosynaptic connectivity.

As expected, synaptic connectivity between the L2/3 SST interneurons and pyramidal neurons was high (**Fig 5.8D**). 70 % of SST interneurons received direct input from the pyramidal neuron, 70 % of the pyramidal neurons received direct input from the SST interneuron, and 50 % of pairs showed bidirectional connectivity (**Fig 5.8E**). These data validated the use of dual patch recordings to target a L2/3 SST interneuron and a neighboring, non-fluorescent L2/3 pyramidal neuron.

To compare the strength of input from L5 subtypes to L2/3 SST interneurons, I adopted a similar design to that used for the PV interneurons (**Fig 5.7A**). ChR2 was selectively expressed in either PT^{thal}, IT^{ipsi} or IT^{contra} L5 pyramidal neurons by injecting rAAV-Floxed-ChR2 into the relevant target structure (**Fig 5.7A** and **Fig 5.9A**). Acute brain slices were prepared from left S1 and dual recordings performed from an SST interneuron and neighboring pyramidal neuron, as described above. Light pulses were used to photostimulate either PT^{thal}, IT^{ipsi} or IT^{contra} inputs from L5 and the EPSC in the L2/3 pyramidal neuron was used to normalize the level of stimulation, so that the SST EPSC could be expressed relative to the EPSC of the neighboring pyramidal neuron (i.e. SST/Pyr ratio) (**Fig 5.9B**). The first observation was that across the L5 subtypes, excitatory input to L2/3 SST interneurons was much lower than was observed to L2/3 PV interneurons. When expressed relative to the EPSC of the neighboring pyramidal neuron, the average SST/Pyr ratio was 0.27 ± 0.08 combined across the L5 subtypes (n = 21 pairs), which was considerably lower than the PV/Pyr ratio of 5.6 ± 2.0 (n = 31 pairs; Mann-Whitney test, $p < 0.0001$). Within the SST interneuron recordings, the SST/Pyr ratio was not above equality for any of the L5 subtypes (PT^{thal} SST/Pyr ratio was 0.32 ± 0.12, IT^{ipsi} was 0.17 ± 0.09 and IT^{contra} was 0.25 ± 0.11; n = 12, 5 and 4 pairs, respectively) and there was no difference between the subtypes (**Fig 5.9C-D**; Kruskal-Wallis test, $p = 0.72$). These data reveal a low level of L2/3 SST interneuron recruitment by all of the L5 subtypes, strengthening the conclusion that it is the strong recruitment of L2/3 PV interneurons by PT^{thal}, which underlies the differences in L5-to-L2/3 signals provided by the ascending collaterals of L5 pyramidal neuron subtypes.

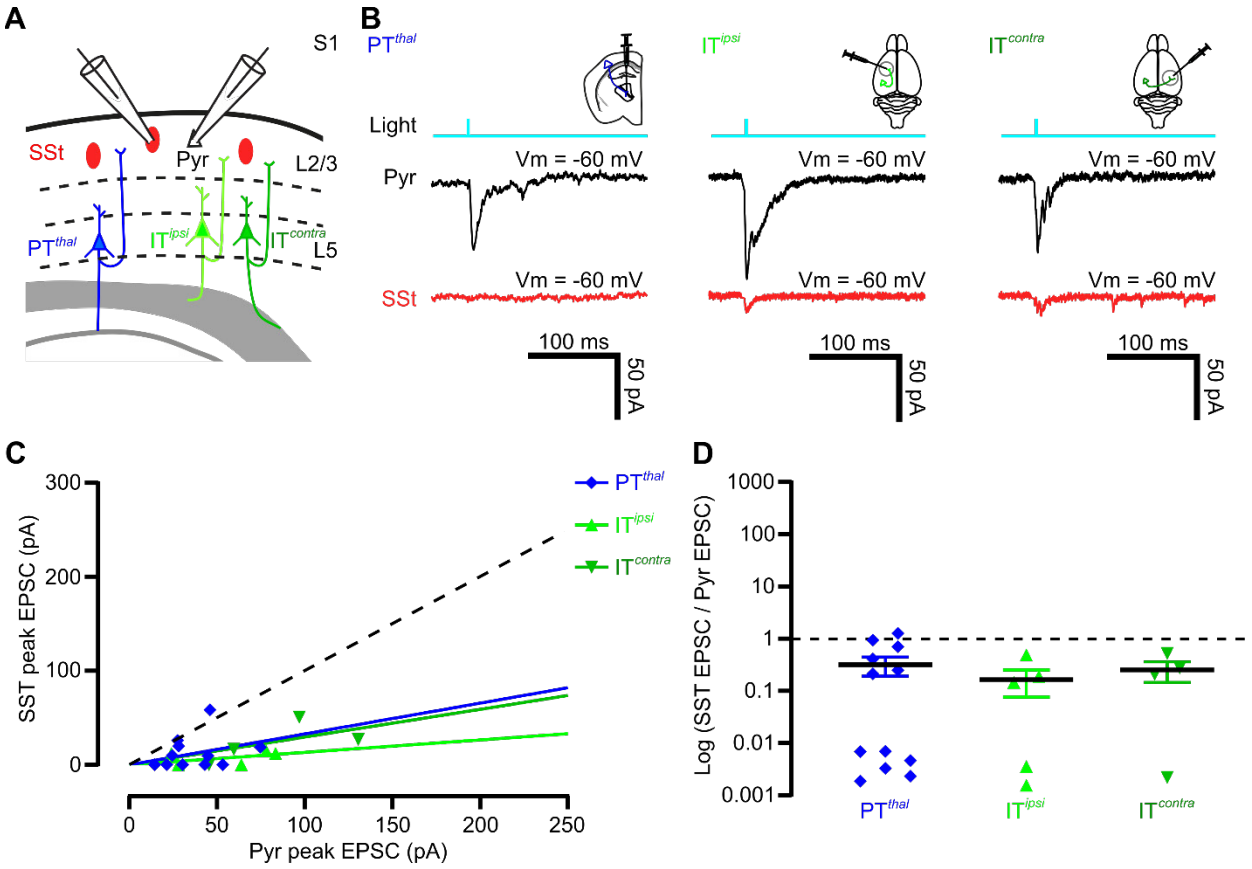


Figure 5.9 L5 pyramidal neurons provide little excitatory drive to L2/3 SST-expressing interneurons

(A) Experimental design for examining L5 input to L2/3 SST-expressing (SST) interneurons. Following injection with rAAV-Floxed-ChR2 such that ChR2 was expressed in either PT^{thal}, IT^{ipsi} or IT^{contra} L5 pyramidal neurons, dual recordings were performed from pairs of L2/3 neurons comprising a SST interneuron and a neighbouring pyramidal neuron in S1. **(B)** Example EPSCs recorded in L2/3 from pairs of SST (red trace) and pyramidal (Pyr; black trace) neurons in response to activation of either PT^{thal} (left), IT^{ipsi} (centre) or IT^{contra} (right) L5 pyramidal neurons. **(C)** Scatter plot comparing the L2/3 pyramidal neuron peak EPSC and the SST interneuron peak EPSC following activation of either PT^{thal} (n = 12 pairs), IT^{ipsi} (n = 5 pairs) or IT^{contra} (n = 4 pairs) L5 pyramidal neurons**.** For all L5 subtypes the EPSC elicited in the L2/3 SST interneuron was weaker than that elicited in the neighbouring pyramidal neurons. The dashed line indicates equality and the lines of best fit were constrained to pass through the origin. **(D)** The ratio of SST EPSC to Pyr EPSC (i.e. the SST/Pyr ratio) did not differ between the three L5 subpopulations (Kruskal-Wallis test, p = 0.72). The dashed line indicates equality. The SST/Pyr ratio was not greater than equality for any of the L5 subpopulations (PT^{thal}, n = 12 pairs, SST/Pyr ratio was 0.32 ± 0.12; IT^{ipsi}, n = 5 pairs, SST/Pyr ratio was 0.17 ± 0.09; IT^{contra}, n = 4 pairs, SST/Pyr ratio was 0.25 ± 0.11), consistent with weak excitatory drive from all L5 pyramidal neurons to L2/3 SST interneurons. Indeed, the PT^{thal} SST/Pyr ratio was significantly lower than equality (p = 0.0015), and whilst neither IT^{ipsi} nor IT^{contra} were different from equality (p = 0.063 and p = 0.13, respectively), the SST/Pyr ratio for the combined IT groups was below equality (p = 0.0039, Wilcoxon signed rank test in all cases).

Discussion

Functional differences in the ascending connectivity of projection-defined L5 subtypes

The first aim of this chapter was to establish the nature of L2/3 responses to ascending collateral input from projection-defined L5 pyramidal neuron subtypes, and thereby determine if the morphological differences identified in the preceding chapter are associated with differences in functional connectivity. Using an AAV engineered for retrograde transport as a vector for optogenetic tools, I examined the strength of both monosynaptic excitation and disynaptic inhibition from L5 to L2/3 pyramidal neurons. This revealed clear differences in the response profile of post-synaptic L2/3 pyramidal neurons, depending upon which pre-synaptic L5 subtypes were active. IT^{ipsi} and IT^{contra} L5 pyramidal neurons generated higher E/I ratios that favored excitation, whereas PT^{thal} L5 pyramidal neurons generated lower E/I ratios that favored inhibition of the L2/3 pyramidal neuron. To my knowledge, this is the first time that L5 to L2/3 signaling has been examined in terms of defining L5 neurons by their long-range projections, or in terms of the E/I signature elicited in L2/3. These observations suggest an important functional distinction in how L5 subtypes send reciprocal signals to L2/3, while simultaneously sending signals to their long-range targets.

Although previous related work has tended not to define L5 subpopulations based on their long-range projections, a number of descriptive studies of L5 to L2/3 connectivity are relevant to my findings. Consistent with my observations for example, glutamate uncaging and simultaneous patch clamp recordings have reported that compared to L5a, L5b provides less excitatory input to L2/3 pyramidal neurons (Dantzker and Callaway, 2000; Yoshimura et al., 2005; Lefort et al., 2009). In terms of the recruitment of L2/3 interneurons, one study observed that L5b inputs rarely form strong connections with L2/3 pyramidal neurons, but may form connections with local 'adapting' inhibitory interneurons (Dantzker & Callaway, 2000). Another study using glutamate uncaging to investigate inputs to L2/3 inhibitory

interneurons from different laminae identified excitatory input from neighboring L2/3, L4 and L5 (Xu and Callaway, 2009). Putative L2/3 fast-spiking interneurons were reported to receive excitatory input from both L5a and L5b, whilst some of the strongest excitatory inputs from L5a were to 'irregular spiking interneurons' (Xu and Callaway, 2009) - an electrophysiological subtype often associated with VIP-expressing interneurons (Karnani et al., 2016; SooHyun Lee et al., 2010; Tremblay et al., 2016).

In terms of understanding how different L5 subtypes signal to L2/3, my experimental design represents a refinement and advance upon previous work for several reasons. Firstly, questions have been raised regarding the classification of L5 pyramidal subtypes based on soma position, rather than projection target. While PT soma show a bias for L5b, and IT soma a bias for L5a, this is not an absolute demarcation. Neurons with IT characteristics can be found throughout L5b (Staiger et al., 2016) and PT neurons can be found in putative L5a (Rojas-Piloni et al., 2017). Secondly, previous studies of L5 to L2/3 signaling have generally used simultaneous patch clamp recordings and glutamate uncaging methods, which require the L5 soma and axon to remain intact. The preparation of acute brain slices severs axonal processes and this effect becomes more pronounced with distance, such as when one records across laminae. Thirdly, whilst glutamate uncaging has proven very powerful for circuit mapping, it has been noted that the method's spatial precision means that stimulation near laminar borders will activate neurons either side of the border, particularly when cells have dendritic arbors that cross laminae, as is the case for L4, L5a and L5b pyramidal neurons. The optogenetic strategy that I adopted defined L5 pyramidal subtypes based on their long-range projection target, was less likely to be compromised by the effects of acute slice preparation, and enabled me to quantify both the excitatory and inhibitory currents converging upon postsynaptic L2/3 pyramidal neurons. This has provided new insights into how L5 subtypes elicit E/I signatures in L2/3.

Ascending collaterals from L5 pyramidal neurons differentially recruit local L2/3 interneurons

The next aim of this chapter was to test the hypothesis that the different L5-to-L2/3 signals reflect the differential recruitment of local interneurons within L2/3, by ascending collaterals from the L5 subtypes. To test this hypothesis, I performed two control experiments. The first control experiment was designed to rule out the potential contribution of long-range axonal inputs from IT neurons, which may express ChR2 at the injection site. It has been shown that long-range inputs to S1 from other cortical regions can be disinhibitory and thus could influence the E/I ratio in L2/3. Through the use of *in utero* electroporation techniques, I was able to eliminate ChR2 expression at the IT injection site. Under these conditions, the E/I ratio in L2/3 pyramidal neurons remained strongly biased towards excitation, confirming that local IT ascending collaterals tend not to recruit interneurons in L2/3. The second control experiment was designed to test whether the strong inhibition associated with PT^{thal} reflected recruitment of interneurons within L5, which make translaminar inhibitory input to L2/3. Such a circuit motif could be mediated by L5 Martonotti cells, a subtype of SST interneuron known to exhibit translaminar connections (Naka and Adesnik, 2016), or by PV interneurons located in L5 with similar translaminar projections (Buchanan et al., 2012). By lesioning L4 and optically activating the L5 pyramidal neuron axons in L2/3, I was able to eliminate potential contributions of L5 interneurons. Under these conditions, PT^{thal} activation produced an E/I ratio in L2/3 that remained strongly biased towards inhibition, confirming that local PT^{thal} ascending collaterals recruit interneurons in L2/3. These control experiments strengthen the conclusion that the ascending collaterals of L5 subtypes differentially recruit L2/3 interneurons.

It is important to note that IUE can result in relatively widespread expression throughout the targeted hemisphere. Thus, in addition to L5 IT neurons within S1, it is possible that L5 IT neurons in other cortical regions may have also expressed Cre recombinase (such as S2 or M1). If these 'off-target' neurons both project to the injection site in contralateral S1 and possess a collateral to ipsilateral S1, they would be expected to contaminate the recordings in ipsilateral S1 barrel cortex. A significant contribution from

these off-target neurons seem unlikely, in part because of the sparse nature of IUE expression, but also because S1 shows particularly strong interhemispheric connectivity with contralateral S1 (Feldmeyer, 2012). Indeed, I observed very little ChR2 expression outside of S1 in the hemisphere that was targeted for IUE (**Fig 5.2**). Nevertheless, to further refine the experimental approach, future experiments could use viral-delivery of a ChR2 that is both Cre and Flippase (Flp) -dependent into ipsilateral S1 of Rbp-Cre mice (Fenno et al., 2014), and then an injection of a retrograde AAV encoding Flp into contralateral S1. This strategy would help to ensure that expression is restricted to S1 L5 pyramidal neurons that project to the contralateral S1. Although such an approach would have to address a potential drop in expression levels due to the requirement of two recombinase events.

Ascending collaterals from L5 PT^{thal} pyramidal neurons target PV interneurons in L2/3

The final aim of this chapter was to determine the nature of the L2/3 interneurons that are targeted by the ascending collaterals of L5 PT^{thal} pyramidal neurons. Towards this goal, I recorded from both PV interneurons and SST interneurons in L2/3, confirming the identity of the fluorescently-labelled interneurons through the recapitulation of intrinsic electrophysiological characteristics. Within L2/3, I found dense connectivity from both PV and SST interneurons to pyramidal neurons, in keeping with prior work (Fino and Yuste, 2011; Packer and Yuste, 2011). This supports the view that dense local networks of inhibition are recruited within L2/3, and that any differences in E/I ratios would most likely reflect differences in the relative strength of glutamatergic excitatory inputs to the local interneurons (Yang and Sun, 2018). In line with this hypothesis, I determined that L5 PT^{thal} preferentially target PV interneurons in L2/3, unlike either of the L5 IT subpopulations. Such a central role for PV interneurons is consistent with the fact that these neurons mediate fast perisomatic inhibition, which is likely to be a major contributor to inhibitory synaptic currents in whole cell recordings (Xue et al., 2014). Also in keeping with this observation, is recent evidence that PV interneurons are recruited following photostimulation of mixed populations of L5 pyramidal neurons (Vecchia et al., 2020), and my own finding that ascending

collaterals from each of the L5 pyramidal neuron subtypes provide relatively weak excitatory input to L2/3 SST interneurons. Although it is worth pointing out that excitatory inputs to SST interneurons typically facilitate to trains of input, which is an aspect that I did not investigate (Silberberg and Markram, 2007).

It should be noted that I observed a potentially interesting pattern of connectivity within the SST population. Whilst they received much less input than PV interneurons, SST interneurons appeared to exhibit a bimodal distribution in terms of their input strength from all L5 subpopulations. One apparent subpopulation of SST interneurons received negligible excitatory input from L5, whilst another subpopulation received a small, but measurable excitatory input from L5. Whilst the number of cells available for further analysis was limited, this represents a potential direction for further study. SST interneurons are often grouped broadly into 'Martinotti' and 'non-Martinotti' subtypes on the basis of their axonal projection to L1. Although recent work has demonstrated further diversity within the SST population in terms of morphology, the expression of genetic markers and electrophysiological properties (Gouwens et al., 2019; Mi et al., 2018; Tasic et al., 2016; Tremblay et al., 2016). Such diversity even within the Martinotti subpopulation has been associated with distinct patterns of translaminar input (X. Xu & Callaway, 2009). It should also be noted that interneuron populations are not distributed homogenously throughout L2/3 (Gouwens et al., 2019; Meyer et al., 2011) and that SST interneuron subtypes found in different layers have been associated with distinct roles (Muñoz et al., 2017). It would therefore be interesting to explore whether the degree of excitatory input from L5 pyramidal neurons is associated with particular subpopulations of SST based on their laminar depth, genetic and/or morphological characteristics.

At a general level, my findings extend previous work that has noted that the selective targeting of local inhibitory interneurons by a principal neuron can be correlated with the long-range projection targets of that principal neuron (Le Bé et al., 2006; Silberberg and Markram, 2007; Krook-Magnuson et al., 2012; Naka and Adesnik, 2016). The strong recruitment of PV interneurons by L5 PT^{thal}, but not by L5 IT, can

explain why inhibition dominates L5 PT to L2/3 signaling, whereas excitation dominates L5 IT to L2/3 signaling.

What role could such differences in the recruitment of L2/3 interneurons play in the local circuit? One aspect could be the delivery of different E/I signals, which are known to vary at different points in an information stream (D'Souza et al., 2016) and are suggested to underlie the gain control of a neuron's responsiveness to incoming signals (Isaacson and Scanziani, 2011). Whilst rapid recruitment of inhibition may match excitation at one point of a pathway (Xue et al., 2014), the E/I ratio varies across different cortical layers and from region to region (Adesnik, 2018; Yang and Sun, 2018; Sempere-Ferràndez et al., 2019). At the level of synaptic integration mechanisms, the low E/I signal and more efficient recruitment of perisomatic inhibition by PT ascending collaterals may narrow the integration window for incoming signals (Pouille and Scanziani, 2001), thus resulting in higher temporal precision for coding in supragranular cortex (Jouhanneau et al., 2018). In contrast, the high E/I signal and greater relative excitation elicited by IT ascending collaterals, could broaden temporal integration windows to L2/3, a feature suggested to play a role in gating plasticity (Williams and Holtmaat, 2019). To begin to address these possibilities, the next chapter explores the functional effects PT and IT L5 subtypes upon L2/3 spiking activity.

Chapter 6 : Functional effects of ascending input from projection-defined L5 subtypes to l2/3

Introduction

It is a well-recognized feature of cortical circuits that even simple sensory stimuli evoke both synaptic excitation and strongly correlated synaptic inhibition (Isaacson & Scanziani, 2011). This is true of somatosensory stimulation via the whisker system (Okun & Lampl, 2008; Swadlow, 2003; Wilent & Contreras, 2005), visual stimulation with drifting bars (Anderson et al., 2000; Monier et al., 2003) and auditory stimulation with simple tones (Tan et al., 2004; Wehr & Zador, 2003; Wu et al., 2008). The inhibition that is recruited is typically matched to excitation, such that as the level of excitatory input increases, there is a proportional increase in inhibition (Xue et al., 2014). However, the set point for E/I is not uniform (Adesnik, 2018; Yang and Sun, 2018; Sempere-Ferràndez et al., 2019). Studies in cortex have demonstrated that intralaminar circuits tend to recruit more lateral inhibition, resulting in a low E/I ratio. In contrast, translaminar inputs may have higher relative excitation and evoke increased activity in the local circuit (Adesnik and Scanziani, 2010; Adesnik, 2018). E/I ratios also vary depending on their point in the information stream. In the visual system for example, the E/I ratio varies between cortical regions, with relatively high E/I ratios associated with feedback pathways and relatively low E/I ratios associated with feedforward pathways (D'Souza et al., 2016).

The matching of inhibition to excitation and differences in E/I ratio are thought to underpin core features of cortical processing. One fundamental role is in determining the input-output, or "gain", of a neuron (Isaacson and Scanziani, 2011; Ferguson and Cardin, 2020), with greater relative inhibition being associated with a reduced slope in a neuron's input/output relationship (Isaacson & Scanziani, 2011; Mitchell & Silver, 2003; Nieus et al., 2014). The temporal relationship between excitatory and inhibitory

inputs is also crucial in the "temporal gating" of neuronal output (Kremkow et al., 2010). Closely time-locked excitation and inhibition leaves a narrow window for excitation to reach threshold (Swadlow, 2003; Wilent and Contreras, 2005), thus resulting in higher temporal precision for coding, as seen in supragranular somatosensory cortex (Jouhanneau et al., 2018). In contrast, delayed or reduced inhibition permits a wider integration window for incoming inputs (Pouille and Scanziani, 2001). This may serve to boost weak signals and regulate timing-sensitive processes, such as synaptic plasticity induction (Williams and Holtmaat, 2019; Zhang and Bruno, 2019). The relationship between excitation and inhibition is also thought to underpin receptive field structures, with the recruitment of greater local inhibition being associated with increased feature selectivity (Lee et al., 2012; Xue et al., 2014; Wilent and Contreras, 2005).

In the rodent somatosensory cortex, L2/3 pyramidal neurons exhibit low levels of spiking activity *in vivo*, consistent with a sparse coding regime that is enforced by strong inhibition (Mateo et al., 2011; Petersen and Crochet, 2013). In line with this model, the recruitment of local inhibition by translaminar input to superficial layers seems to be a general feature of cortex, which holds across sensory modalities and behavioral tasks (Tanke et al., 2018; Olsen et al., 2012; Bortone et al., 2014; Frandolig et al., 2019; Pauzin et al., 2019). Furthermore, recent work has provided the first direct evidence that global activation of L5 has a net inhibitory effect upon whisker-evoked responses in L2/3 of somatosensory cortex, consistent with the recruitment of local inhibition (Vecchia et al., 2020). The timing and source of excitation therefore seems particularly important in determining whether a L2/3 pyramidal neuron is able to escape its "blanket" of inhibition.

In the preceding chapter, I established that projection-defined L5 subtypes differ in the degree to which they recruit local inhibition within L2/3 (**Fig 6.1A**). PT^{thal} neurons efficiently recruit local inhibitory circuits in L2/3, through their targeting of local PV interneurons. In contrast, IT L5 pyramidal neurons elicit excitatory post-synaptic currents in L2/3 pyramidal neurons, without the recruitment of local

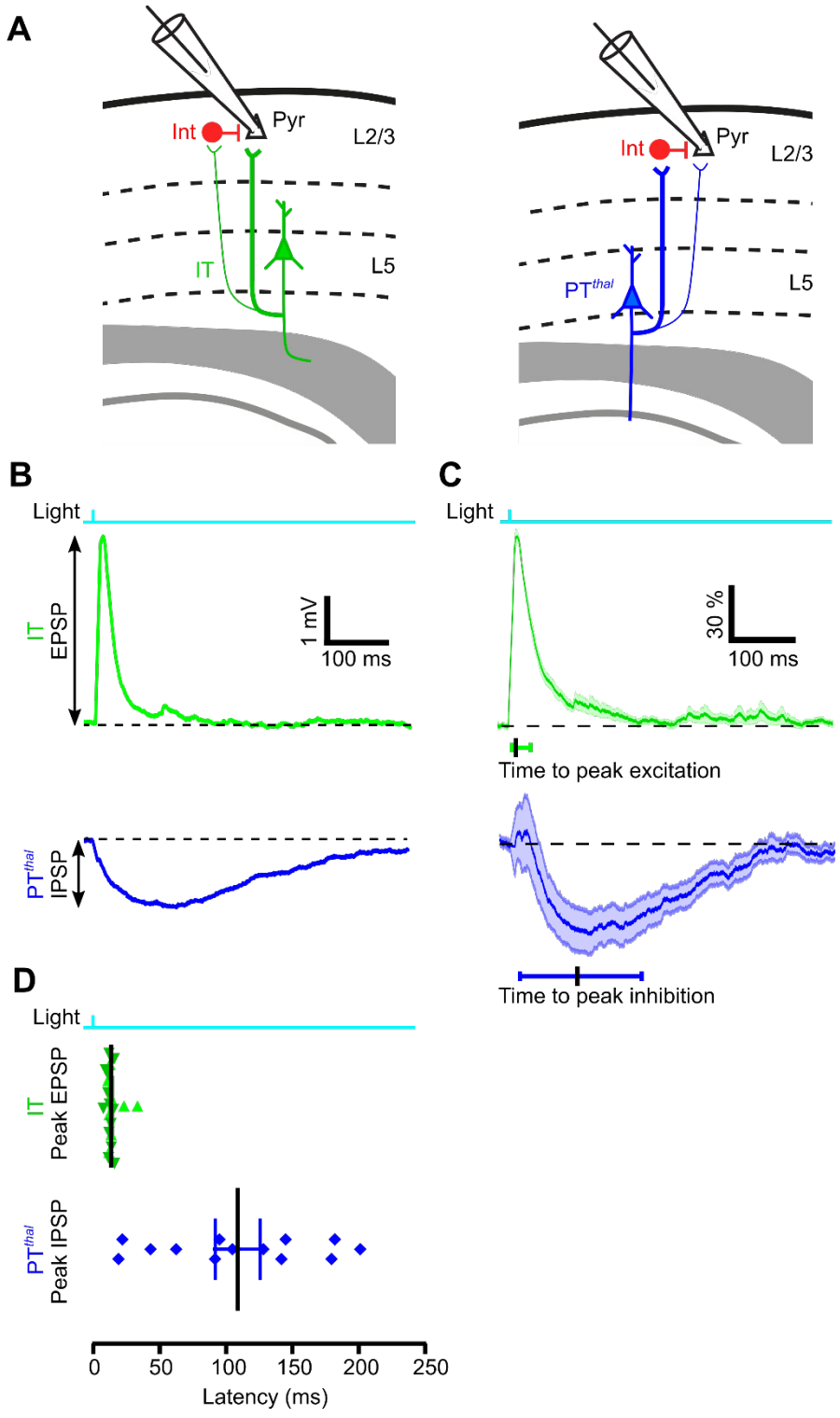


Figure 6.1 Ascending collaterals from IT and PT L5 pyramidal neurons generate distinct E/I dynamics in L2/3

(A) Cartoons summarizing previous observation and illustrating the experimental design. IT L5 pyramidal neurons are shown to provide stronger excitation to L2/3 pyramidal neurons (left), whilst PT L5 pyramidal neurons elicit stronger inhibition via local interneurons (right). In the current experiments, ChR2 was expressed in the relevant L5 subtypes by performing targeted injections of rAAV-Floxed-ChR2 into Rbp4-Cre mice. IT neurons of left S1 were targeted by injections into either left M1 or right S1 and the resulting data were combined. PT^{thal} were targeted by injections into left thalamus. Current clamp recordings were then performed from L2/3 pyramidal neurons in acute brain slices of left S1, whilst IT or PT^{thal} were stimulated with brief pulses of blue light (473 nm; 1-3 ms).

interneurons. These different L5 subtypes therefore deliver different E/I signals to L2/3 and are predicted to exert distinct effects upon the L2/3 pyramidal neuronal spiking activity, both in terms of timing and response to incoming sensory input. This chapter begins to explore the functional implications of this prediction.

Aims

The aims of this chapter were as follows:

1. To determine the effect of PT and IT L5 pyramidal neurons upon the membrane potential and spiking activity of L2/3 pyramidal neurons *in vitro*.
2. To establish an *in vivo* paradigm for investigating the effect of projection-defined L5 pyramidal subtypes upon whisker-evoked responses.
3. To compare the effect of PT and IT L5 pyramidal neurons upon incoming whisker input to L2/3 of primary somatosensory cortex.

Results

I first investigated the temporal profile of post-synaptic membrane potential dynamics in L2/3 pyramidal neurons following activation of ascending collaterals from IT and PT L5 pyramidal neuron subtypes. To explore this, I performed current clamp whole cell recordings from L2/3 pyramidal neurons and optically stimulated populations of either IT or PT neurons (**Fig 6.1A**). As in Chapter 5, projection-defined L5 subpopulations of S1 were transduced to express ChR2 using a retrograde AAV strategy.

Figure 6.1 ***Continued from opposite***

(B) Membrane potential (V_m) response of example L2/3 pyramidal neurons following stimulation of either L5 IT (top) or L5 PT^{thal} (bottom). **(C)** Normalised V_m responses were derived by averaging across a population of L2/3 pyramidal neurons following stimulation of either IT (n = 21 neurons; top) or PT^{thal} (n = 13 neurons; bottom), and used to calculate the time to peak excitation and inhibition, respectively. **(D)** The time to peak excitation following IT stimulation was short (13.5 ± 1.2 ms), whereas the time to peak inhibition following PT^{thal} stimulation was longer (108.9 ± 16.8 ms). Within the IT population, upright triangles indicate IT^{ipsi} stimulation, inverted triangles indicate IT^{contra} stimulation.

The retrograde AAV encoding Cre-inducible ChR2 (rAAV-Floxed-ChR2) was injected into either left M1, right S1 or the left thalamus of *Rbp4-Cre* mice at 6 weeks of age, resulting in the selective expression of ChR2 in IT^{ipsi}, IT^{contra} or PT^{thal} L5 pyramidal neurons in left S1. Data from IT^{ipsi} and IT^{contra} were combined and referred to as IT. The animals were maintained for > 4 weeks to maximize ChR2 expression and then acute slices were prepared from left S1. As predicted, when IT L5 pyramidal neurons were stimulated with brief flashes of blue light (473 nm; 1-3 ms), the membrane potential of the L2/3 pyramidal neuron exhibited a fast excitatory post-synaptic envelope, which occurred shortly after the light stimulus (**Fig 6.1B-C**). In contrast, PT^{thal} stimulation resulted in a more sustained inhibition of the L2/3 pyramidal neuron and the peak of this inhibitory envelope was more delayed compared to the light stimulus (**Fig 6.1B-C**). At a population level, the excitatory envelope elicited by IT L5 pyramidal neurons peaked at 13.5 ± 1.2 ms after the light stimulus (**Fig 6.1D**). Whereas the inhibitory envelope elicited by PT^{thal} pyramidal neurons peaked almost 100 ms later, at 108.9 ± 16.8 ms after the light stimulus (**Fig 6.1D**).

To investigate how these different E/I signals interact with the spiking activity of L2/3 pyramidal neurons, I used the same experimental arrangement but elicited action potentials in the L2/3 pyramidal neuron by injecting depolarizing somatic current (**Fig 6.2A**).

In the first experiment, I used a 200 ms somatic current step to reliably elicit a burst of spikes and compared alternating trials on which either the L5 subtype of interest was optically stimulated, or it was not stimulated (**Fig 6.2B**). Under these conditions, IT stimulation resulted in an increase in spike rate of 0.67 ± 0.20 Hz (one sample t-test, $p = 0.0034$) , whereas PT^{thal} stimulation resulted in the opposite effect and caused a decrease in spike rate of -1.67 ± 0.57 Hz (one sample t-test, $p = 0.0137$, **Fig 6.2C**). This observation is consistent with the idea that IT L5 pyramidal neurons deliver high E/I signals to L2/3, whereas PT^{thal} L5 pyramidal neurons deliver low E/I signals. The temporal aspects of the excitatory and inhibitory envelopes associated with IT and PT^{thal} inputs (**Fig 6.1**) also predicted timing differences in how the L5 subtypes might influence spiking activity in L2/3 pyramidal neurons. To explore this, I used a

paradigm in which optical stimulation of IT or PT^{thal} inputs was paired with a brief somatic current in the L2/3 pyramidal neuron. The amplitude of the L2/3 somatic current was adjusted to generate a spike on approximately 50% of trials, and the timing of the somatic current was either concurrent (i.e. 0 ms delay) or delayed (i.e. +100 ms delay), with respect to the L5 input. Concurrent pairing showed maximal alignment with the fast excitatory envelope associated with IT input, whilst the 100 ms delayed pairing showed maximal alignment with the inhibitory envelope associated with PT^{thal} input (**Fig 6.2D, F, H, J**). By interleaving control and optical stimulation trials, I was able to assess whether there was a change in the spike probability of L2/3 pyramidal neurons. IT stimulation that was concurrent with the somatic current produced a 59.8 ± 5.6 % increase in spike probability (**Fig 6.2D-E**). Whereas the same IT stimulation caused a 14.0 ± 4.2 % increase in spike probability when the somatic current was delivered 100 ms after the IT input (**Fig 6.2F-G**). In contrast, PT^{thal} stimulation that was concurrent with the somatic current produced only a 13.8 ± 12.1 % decrease in spike probability, whilst the same PT^{thal} stimulation caused a 24.4% ± 8.6 % decrease in spike probability when the somatic current was delivered 100 ms after the PT^{thal} input (**Fig 6.2H-K**). These experiments confirmed that ascending collaterals from projection-defined L5 subtypes exert distinct effects upon the spiking activity of L2/3 pyramidal neurons, and in a manner consistent with the temporal dynamics of the E/I signal delivered by the L5 subtype.

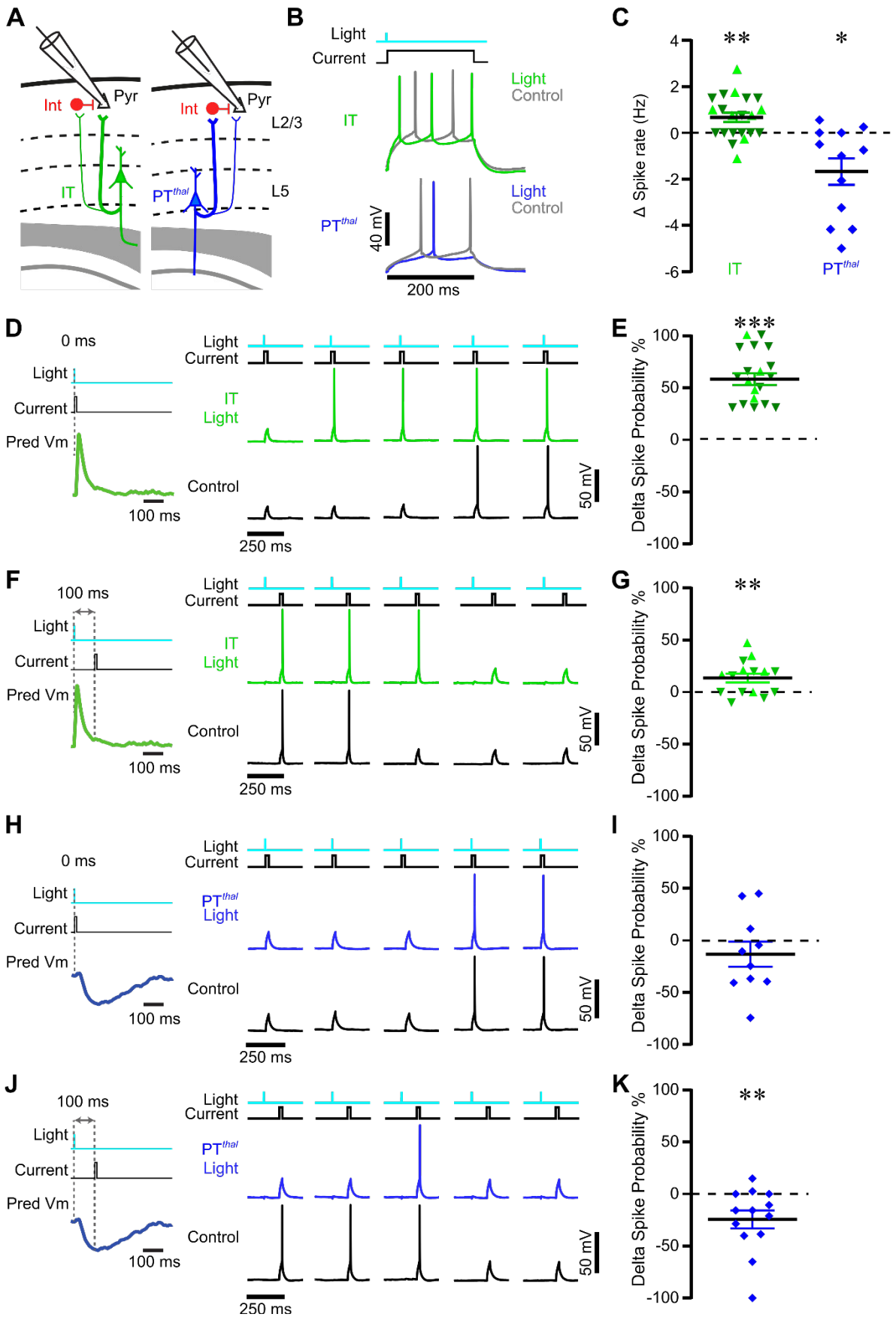

A
Int
Pyr
Int
Pyr
L2/3
IT
PT thal
L5
B
Light
Current
Light
Control
IT
PT thal
Light
Control
40 mV
200 ms
C
**
*
Δ Spike rate (Hz)
4
2
0
-2
-4
-6
IT
PT thal
D
0 ms
Light
Current
Pred Vm
100 ms
Light
Current
IT
Light
Control
50 mV
250 ms
E
***
Delta Spike Probability %
100
50
0
-50
-100
F
100 ms
Light
Current
Pred Vm
100 ms
Light
Current
IT
Light
Control
50 mV
250 ms
G
**
Delta Spike Probability %
100
50
0
-50
-100
H
0 ms
Light
Current
Pred Vm
100 ms
Light
Current
PT thal
Light
Control
50 mV
250 ms
I
Delta Spike Probability %
100
50
0
-50
-100
J
100 ms
Light
Current
Pred Vm
100 ms
Light
Current
PT thal
Light
Control
50 mV
250 ms
K
**
Delta Spike Probability %
100
50
0
-50
-100

Figure 6.2 Ascending collaterals from IT and PT L5 pyramidal neurons exert opposing effects on L2/3 pyramidal neuron spiking

(A) Current clamp recordings assessed the influence of IT and PT^{thal} L5 pyramidal neurons on the spiking of L2/3 pyramidal neurons. **(B)** Example recordings show L2/3 spiking to a depolarizing somatic current input ('Control'; grey) and alternate trials when the same depolarizing input was delivered concurrent with optogenetic stimulation ('Light') of either IT (green; top) or PT^{thal} (blue; bottom). **(C)** IT stimulation enhanced L2/3 spiking (n = 21 neurons; delta spike rate of 0.67 ± 0.20 Hz , one sample t-test, t(20) = 3.32, p = 0.0034). Whereas PT^{thal} stimulation decreased L2/3 spiking (n = 12 neurons; delta spike rate of -1.67 ± 0.57 Hz, one sample t-test, t(11) = 2.92, p = 0.0137). Within the IT population, upright triangles indicate IT^{ipsi} stimulation, inverted triangles indicate IT^{contra} stimulation. **(D)** Experimental design (left) in which L2/3 spiking was elicited on 50% of trials via a brief depolarizing current input (10 ms). Spiking responses were compared between these control trials and alternate trials when the same depolarizing input was delivered concurrent with IT L5 stimulation (i.e. delay of 0 ms). The predicted excitatory effect of IT stimulation on the L2/3 neuron's membrane potential is illustrated ('Pred Vm'). Example recordings (right) show spiking of a L2/3 neuron across five trials without IT stimulation (black; 'Control') and five trials with IT stimulation (green; 'Light'). **(E)** L5 IT caused a 59.8 ± 5.6 % increase in L2/3 spiking response to a concurrent depolarizing input (n = 19 neurons; one sample t-test, t(18) = 10.66, p < 0.0001). **(F)** The same experimental design, except the depolarizing current input was delivered with a 100 ms delay, subsequent to IT stimulation. **(G)** L5 IT caused a 14.0 ± 4.2 % increase in spiking response to a subsequent depolarizing input (n = 15 neurons; one sample Wilcoxon signed rank test, W = 60, p = 0.0049). **(H)** Same experimental design, except the depolarizing current input was delivered concurrent with PT^{thal} stimulation. The predicted inhibitory effect of PT^{thal} stimulation on the L2/3 neuron's membrane potential is illustrated ('Pred Vm'). **(I)** L5 PT^{thal} did not affect L2/3 spiking response to a concurrent depolarizing input (-13.8 ± 12.1 %; n = 10 neurons; one sample t-test, t(9) = 1.14, p = 0.28). **(J)** The same experimental design, except the depolarizing current input was delivered with a 100 ms delay, subsequent to PT^{thal} stimulation. **(K)** L5 PT^{thal} caused a 24.4 ± 8.6 % reduction in spiking response to a subsequent depolarizing input (n = 13 neurons; one sample Wilcoxon Signed Rank Test, W =-58, p = 0.0059).

To investigate these interactions in an *in vivo* context, I set out to test how the activity of projection-defined L5 subtypes influences L2/3 spiking activity to incoming whisker input in the primary somatosensory cortex. First, I established an experimental paradigm that would enable me to compare whisker-evoked responses following stimulation of defined L5 subtypes. Multiunit electrode recordings were performed from 32-channel linear probes inserted orthogonally to the pial surface of the left barrel cortex of anaesthetized *Rbp4-Cre* mice, in which ChR2 was expressed in a projection-defined L5 subtype via targeted injection of rAAV-Floxed-ChR2 (**Fig 6.3A**; Brumberg et al., 1999). Recordings could thus be performed from the barrel cortex of animals injected to target either IT L5 subtypes (**Fig 6.3B**) or the PT^{thal} subtype (**Fig 6.3C**). Viral injections were made at 6 weeks of age and the recordings were performed at 12-24 weeks. The ChR2-expressing L5 pyramidal neurons were stimulated by delivering brief pulses of blue light at the recording site (473 nm; 5 ms), whilst the corresponding principal whisker input was stimulated using a piezo-electric wafer (**Fig 6.3A**).

To distinguish recording channels along the length of the probe, the location of L4 was estimated by identifying the channel with the largest short-latency negative local field potential (LFP) deflection (i.e. sink) in response to a whisker stimulus (Kajikawa and Schroeder, 2011; Einevoll et al., 2013; Yamamura et al., 2017; **Fig 6.3D**).

Figure 6.3 ***Continued from opposite***

(B) Example data from an animal with ChR2-expressing IT L5 pyramidal neurons. The placement of the 32-channel linear recording probe was confirmed with DiI staining. Raster plots illustrate multiunit spiking responses to a whisker stimulus ('Piezo') or a light stimulus ('Light'). Each row on the raster corresponds to an individual channel on the recording probe and therefore reflects depth through cortex. **(D)** Example heat map of the mean LFP amplitude recorded in response to a whisker stimulus ('Piezo'), for different channels along the probe. The depth of L4 was established using the LFP minimum. **(E)** Levels of light-evoked L5 multiunit spiking activity were comparable between IT expressing animals (n = 7 animals; 33.5 ± 10.1 Hz) and PT^{thal} expressing animals (n = 8 animals; 37.5 ± 4.1 Hz; unpaired t-test, $t(13) = 0.38$, $p = 0.71$). Within the IT population, upright triangles indicate IT^{ipsi} stimulation, inverted triangles indicate IT^{contra} stimulation. **(F)** The activity of individual neurons was determined by spike sorting and putative regular spiking neurons were included based on the temporal properties of their spikes. **(G)** Neurons that met waveform criteria for regular spiking neurons were included in further analysis (n = 62 neurons from 15 animals).

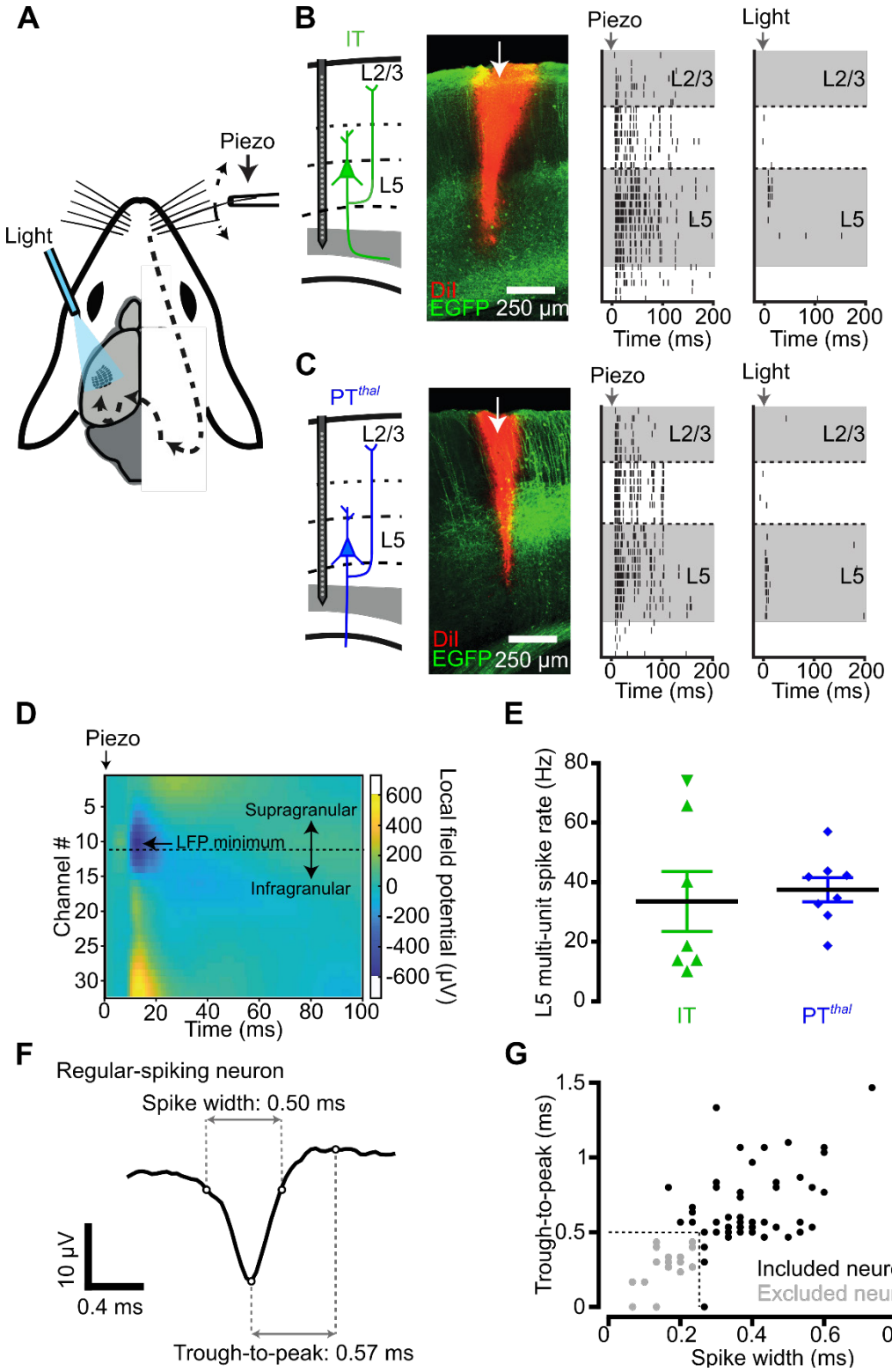


Figure 6.3 Evaluating the effects of projection-defined L5 pyramidal subtypes upon whisker-evoked L2/3 spiking activity

(A) Multiunit recordings were performed from the left S1 barrel cortex of anaesthetised Rbp4-Cre mice, in which ChR2 was expressed in projection-defined L5 subtypes via targeted injections of rAAV-Floxed-ChR2. ChR2-expressing L5 pyramidal neurons were stimulated by delivering brief pulses of blue light at the recording site (473 nm; 5 ms), whilst the corresponding principal whisker was stimulated using a piezo-electric wafer.

Activity in the supragranular layers, including L2/3, was sampled from above the L4 sink, whereas L5 activity was sampled from below the L4 sink (see Chapter 2). To make comparisons across different L5 subtypes, the light stimulus was adjusted at the start of a recording session so that comparable levels of L5 multi-unit activity were evoked (**Fig 6.3E**; PT^{thal} 37.5 ± 4.1 Hz versus IT 33.5 ± 10.1 Hz). Recordings from the supragranular layers under these conditions then underwent spike sorting using the Kilosort algorithm (Pachitariu et al., 2016) and analyses were restricted to regular-spiking units, which would are expected to include L2/3 pyramidal neurons (**Fig 6.3F-G**; Reyes-Puerta et al., 2015). Having established an *in vivo* paradigm, I examined how different L5 subtypes modulate the response of supragranular neurons to incoming whisker input. Optical stimulation of either IT or PT^{thal} ('Light') was paired with a single whisker stimulus ('Piezo'). Given the temporal dynamics of the excitatory and inhibitory envelopes associated with IT and PT^{thal} inputs to L2/3 (**Fig 6.1**), the timing of the whisker stimulus was either concurrent (i.e. +10 ms delay) or delayed (i.e. +100 ms delay), with respect to the L5 input (**Fig 6.4**). In each case, supragranular responses were compared to control conditions in which there was no optical stimulation of the L5 subtype. Based on my *in vitro* observations, I hypothesised that IT stimulation would enhance L2/3 spiking to whisker input, particularly when the whisker input is concurrent with L5 IT activity. Consistent with this hypothesis, I observed that IT stimulation that was concurrent with whisker stimulation resulted in a significant increase in the whisker-evoked spiking response in supragranular neurons (**Fig 6.4A-B**; delta firing rate of +4.1 ± 2.0 Hz, One sample Wilcoxon Signed rank test, $p = 0.044$). Whereas the same IT stimulation did not cause a significant increase in spike probability when the whisker stimulus was delivered 100 ms after the IT input (**Fig 6.4C-D;** delta firing rate of +3.1 ± 1.6 Hz , One sample t-test, $p = 0.0648$).

In contrast, I hypothesized that PT^{thal} stimulation would attenuate L2/3 spiking to whisker input, particularly if the whisker input occurred during the inhibitory envelope that follows L5 PT^{thal} activity.

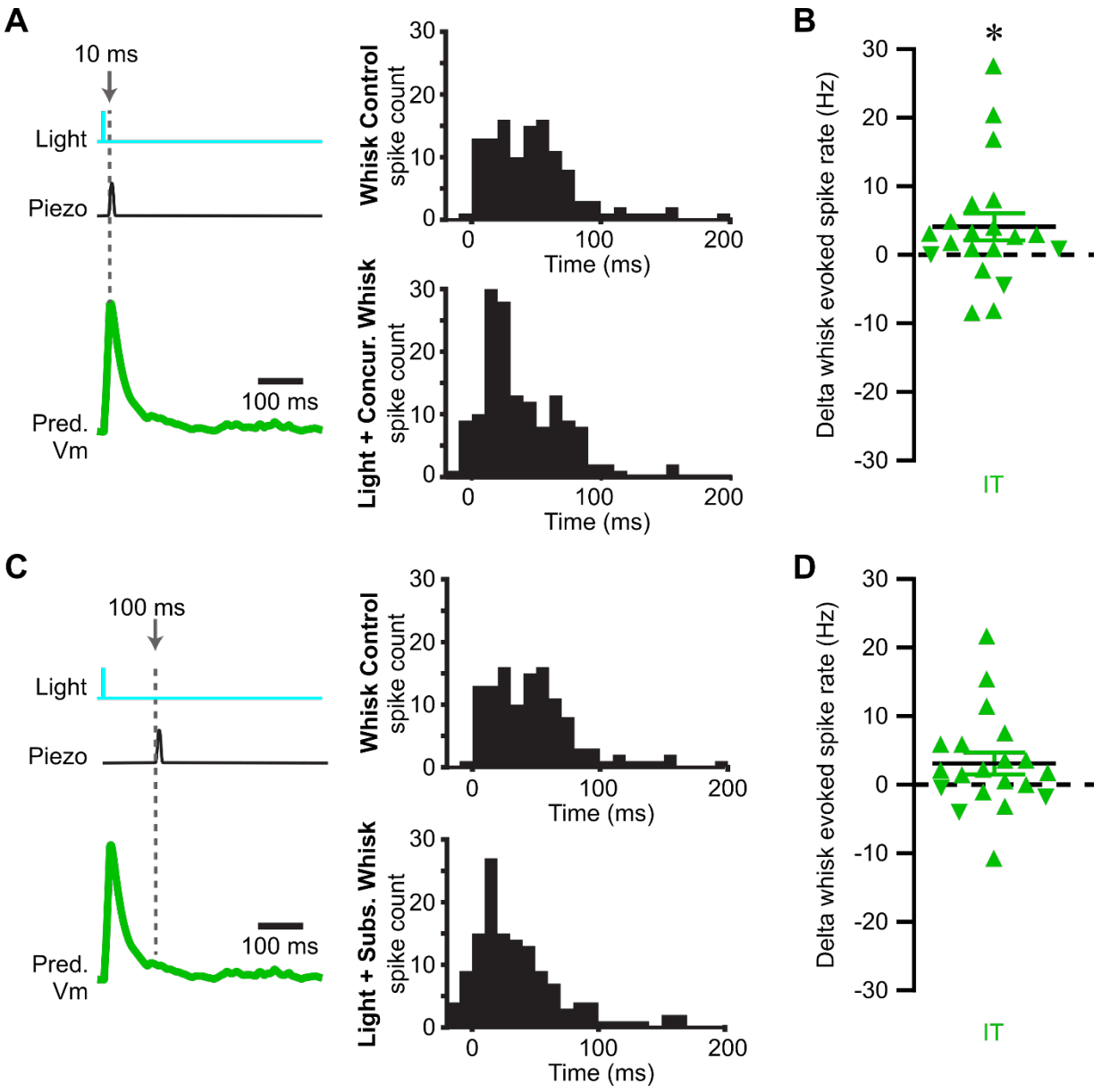


Figure 6.4 IT L5 pyramidal neurons augment concurrent whisker input to L2/3

(A) Experimental design (left) in which the whisker was stimulated ('Piezo') concurrently with IT L5 stimulation ('Light'; delay of 10 ms). The predicted excitatory effect of IT stimulation on L2/3 neuron membrane potential is illustrated ('Pred Vm'). Example PSTHs (right) show the whisk response of a single L2/3 neuron without IT stimulation ('Control'; top) and with concurrent IT stimulation ('Light + Concur. Whisk'; bottom). Each PSTH represents 50 trials. **(B)** Whisker input concurrent with IT stimulation resulted in an increase in the whisk-evoked spike rate of supragranular neurons (n = 20 neurons, +4.1 ± 2.0 Hz, One sample Wilcoxon Signed rank test W =108, p =0.044). Upright triangles indicate IT^{ipsi} stimulation, inverted triangles indicate IT^{contra} stimulation. **(C)** Experimental design (left) in which the whisker ('Piezo') was stimulated 100 ms subsequent to IT L5 stimulation ('Light + Subs. Whisk'; delay of 100 ms). Other conventions as in 'A'. **(D)** Whisker input subsequent to IT stimulation did not change the whisk-evoked spike rate (n = 20 neurons, +3.1 ± 1.6 Hz , One sample t-test t(19) =1.96, p =0.0648)

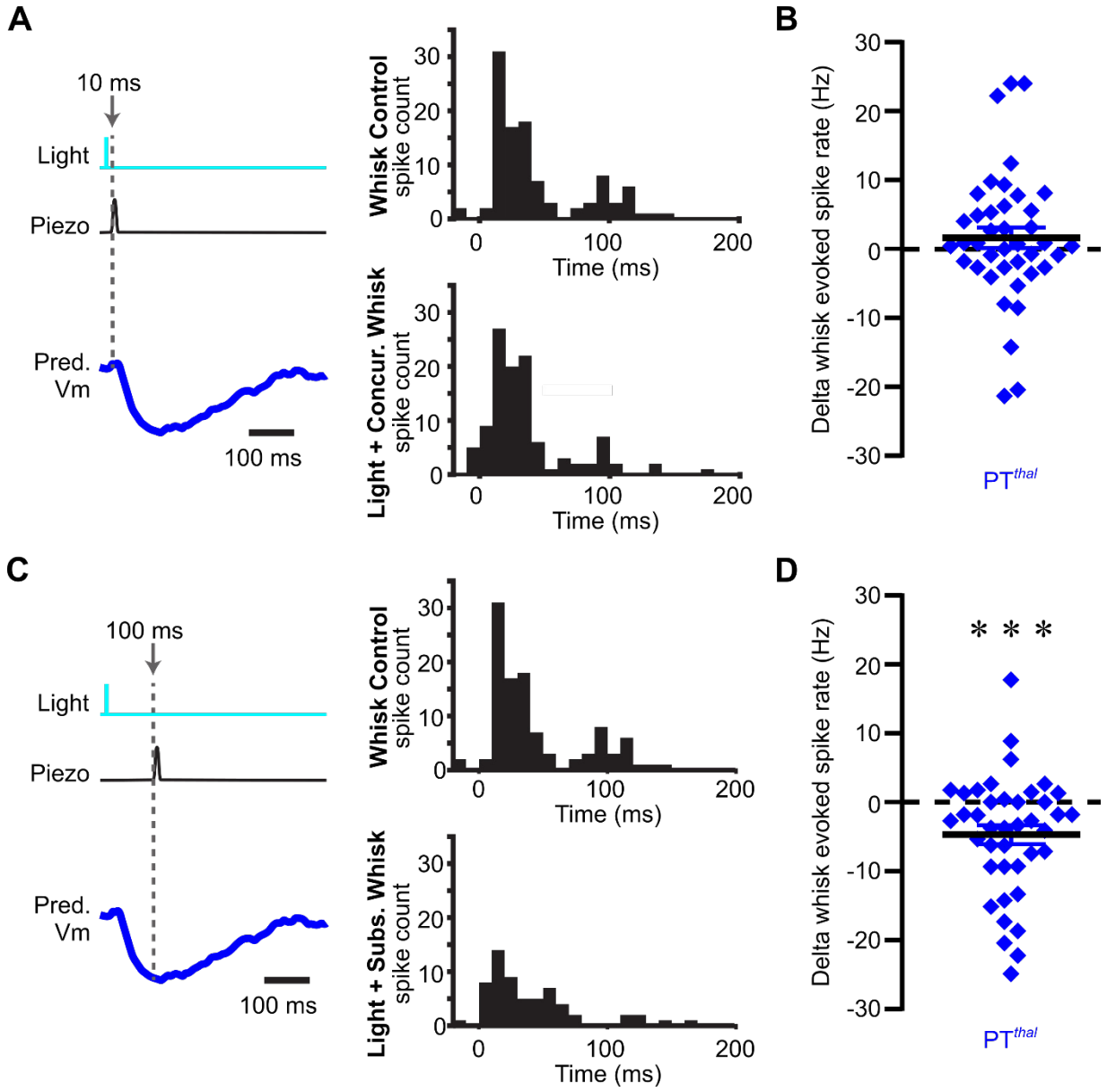


Figure 6.5 PT L5 pyramidal neurons inhibit subsequent whisker input to L2/3

(A) Experimental design (left) in which the whisker was stimulated ('Piezo') concurrently with PT^{thal} L5 stimulation ('Light'; delay of 10 ms). The predicted inhibitory effect of PT^{thal} stimulation on L2/3 neuron membrane potential is illustrated ('Pred Vm'). Example PSTHs (right) show the whisk response of a single L2/3 neuron without PT^{thal} stimulation ('Control'; top) and with PT^{thal} ('Light + Concur. Whisk'; bottom). Each PSTH represents 25 trials. **(B)** Whisker input concurrent with PT^{thal} stimulation did not change the whisk-evoked spike rate of supragranular neurons (n =40 neurons, +1.6 ± 1.5 Hz , One sample Wilcoxon Signed rank test W =177, p =0.238). **(C)** Experimental design (left) in which the whisker ('Piezo') was stimulated 100 ms subsequent to PT^{thal} stimulation ('Light + Subs. Whisk'; delay of 100 ms). Other conventions as in 'A'. **(D)** Whisker input subsequent to PT^{thal} stimulation resulted in a decrease in the whisk-evoked spike rate of supragranular neurons (n =40 neurons, -4.7 ± 1.4 Hz , One sample Wilcoxon signed rank test W= -488 , p =0.0004).

In line with this hypothesis, I observed that when PT^{thal} stimulation was concurrent with whisker stimulation, there was no net change in the whisker-evoked spiking response in supragranular neurons (**Fig 6.5A-B**, delta firing rate of +1.6 ± 1.5 Hz , p =0.238). Whereas, PT^{thal} stimulation caused a significant decrease in spike probability when the whisker stimulus was delivered 100 ms after PT^{thal} input (**Fig 6.5C-D**, delta firing rate of, -4.7 ± 1.4 Hz , One sample Wilcoxon signed rank test, p =0.0004). Therefore, the activity of projection-defined L5 subtypes can differentially modulate supragranular responses to incoming sensory stimuli, and in a manner consistent with the temporal dynamics of the E/I signal delivered by the L5 subtype: IT L5 pyramidal neurons augmented concurrent whisker input to L2/3 (**Fig 6.4**), whereas PT^{thal} L5 pyramidal neurons inhibited subsequent whisker input to L2/3 (**Fig 6.5**).

Discussion

Here I have demonstrated that differences previously ascribed to L5 subtypes in other chapters of this thesis, result in the differential modulation of L2/3 pyramidal neurons. I confirm *in vitro* that the E/I ratios estimated from voltage clamp recordings of post-synaptic currents, manifest as significant differences in the membrane potential dynamics of L2/3 pyramidal neurons following stimulation of different L5 subtypes. The net effects are that IT L5 pyramidal neurons deliver fast and high E/I signals to L2/3 pyramidal neurons, whereas PT^{thal} L5 pyramidal neurons deliver slow and low E/I signals to L2/3 pyramidal neurons. This is in line with the observations in Chapter 5, that IT L5 pyramidal neurons elicit excitatory post-synaptic currents in L2/3 pyramidal neurons, without the recruitment of local interneurons. Whereas PT^{thal} neurons efficiently recruit local inhibitory circuits in L2/3, through their targeting of local PV interneurons.

Whilst the effects upon membrane potential are suggestive, the importance of these L5 inputs increases if they are able to modulate spiking activity in the post-synaptic L2/3 neuron. In line with this, I was able to demonstrate that inputs from IT and PT L5 subtypes exert opposing effects upon the spike probability

of a L2/3 pyramidal neuron. In an *in vitro* preparation, I observed that activation of IT L5 pyramidal neurons increased spike probability in L2/3 pyramidal neurons, particularly when the IT activity was concurrent with other sources of excitation to the L2/3 neuron. In contrast, I observed that activation of PT^{thal} L5 pyramidal neurons decreased spike probability in L2/3 pyramidal neurons, particularly when other sources of excitation to the L2/3 neuron arrived after the PT^{thal} activity. Importantly, I was then able to take these predictions into an *in vivo* paradigm for studying spiking activity of neurons in the supragranular layers of somatosensory cortex, where I was demonstrate similar effects upon whisker-evoked spiking. L5 IT activity concurrent with whisker stimulation increased whisker-evoked spiking responses in supragranular neurons. Whereas L5 PT^{thal} activity inhibited supragranular neuronal responses to subsequent whisker input.

As in the rest of the thesis, the choice of statistical tests in the current chapter was based on the data's distribution, which was determined by normality testing (see Materials and Methods). This principled approach resulted in different tests being applied to the data examining the effect of IT stimulation upon whisker evoked responses (**Fig 6.4**). The data where whisker input was concurrent with IT stimulation (**Fig 6.4B**) failed normality testing and so a non-parametric test was applied that is more robust to outliers. Whereas the data where whisker input was delayed (**Fig 6.4D**) passed normality testing and so a parametric test was applied. It is important to reflect on the impact of this approach and the robustness of some of the observations. For instance, if one removes outlier points from the data where whisker input was concurrent with IT stimulation (**Fig 6.4B**), the resulting smaller population can pass a normality test and the appropriate parametric statistic no longer reaches statistical significance at an alpha level of 0.05. In contrast, the effects associated with PT^{thal} are more robust (**Fig 6.5**), in the sense that the conclusions remain the same regardless of whether the appropriate non-parametric test is applied, or a parametric test is applied after outlier removal. This suggests that conclusions on the effect of IT stimulation would benefit from collecting further data, or from improving the responsivity measures so

that they address sources of variability, such as by calculating the proportional changes in spike rate, or incorporating potential fluctuations in the network's state across the recordings.

As alluded to in the introduction, L2/3 is thought to use a sparse coding regime that is enforced by local recruitment of inhibition (Mateo et al., 2011; Harris and Mrsic-Flogel, 2013; Petersen and Crochet, 2013). It was therefore unclear whether the differences in E/I ratio that I recorded *in vitro*, would significantly alter *in vivo* responses to sensory input. Interestingly, it has been proposed that rare, large excitatory inputs to individual L2/3 pyramidal neurons could outweigh local inhibition and result in an action potential (Petersen & Crochet, 2013). The low levels of inhibition recruited in my experimental paradigm following L5 IT neuron stimulation and subsequent facilitation of whisker responses suggest that these neurons may mediate such excitatory inputs. Another instance where sparse coding transiently breaks down in L2/3 is following a sharp, high-velocity whisker stimulation (Ranjbar-Slamloo and Arabzadeh, 2016), which is thought to be involved in texture discrimination. As L5 IT neurons are thought to receive contextual information from the paralemniscal circuit during whisker sensation (Diamond et al., 2008; Feldmeyer, 2012), it is possible that this L5 subpopulation plays a key role in such brief periods of dense L2/3 coding.

At the same time, the increased recruitment of inhibition through stimulation of PT L5 pyramidal neurons could be important for local whisker perception. The recruitment of fast perisomatic inhibition is thought to play a role in shaping the receptive fields of somatosensory neurons. The relative activation of this L5 subpopulation during sensory processing could enhance feature selectivity of these neurons, particularly under conditions of high background noise (Sengupta et al., 2013). Indeed, a recent optogenetic study revealed that activation of all L5 pyramidal neurons recruits robust inhibition in supragranular layers and thus shortens or "sharpens" whisker responses in L2/3 (Vecchia et al., 2020). Such sharpening improved a perception-based behavioral task, whilst the silencing of L5 over the same time period worsened performance. Although this study did not distinguish different L5 subtypes, it did test predictions in an

awake preparation. It is therefore important to remember that my *in vivo* recordings were performed under anesthesia, which could alter coding regimes and relative levels of excitation and inhibition in L2/3 (Petersen and Crochet, 2013). It would therefore be interesting to examine L5 subtype effects in an awake behaving mouse.

An important aspect of the subtype-specific L5-to-L2/3 signaling examined here, is that the effects of L5 PT and IT output exhibit different kinetics in L2/3. The peak of the excitatory envelope in L2/3 occurred approximately 10 ms after L5 IT activation, which is consistent with the delay expected of an opsin-evoked monosynaptic response and typical membrane time constant. Meanwhile the peak of the inhibitory envelope occurred approximately 100 ms after L5 PT^{thal} activation. Whilst an inherent delay is expected for disynaptic inhibitory circuits, synaptic delays are typically on the order of milliseconds (Pouille et al., 2009; Cruikshank et al., 2010; Isaacson and Scanziani, 2011), suggesting the involvement of additional mechanisms for L5 PT^{thal}, such as sustained spiking of the PV interneurons or the recruitment of slower acting $GABA_B$ receptors(McClellan & Twyman, 1999)(McClellan & Twyman, 1999)(McClellan & Twyman, 1999)(McClellan & Twyman, 1999)(McClellan & Twyman, 1999)(McClellan & Twyman, 1999)(McClellan & Twyman, 1999)(McClellan & Twyman, 1999)(McClellan & Twyman, 1999)(McClellan & Twyman, 1999). I explored the L5-to-L2/3 signaling over a limited range of timing intervals. Under natural conditions, the activity of the different L5 subtypes would be expected to vary continuously and be independently controlled by inputs that selectively target the different L5 subpopulations (Harris & Mrsic-Flogel, 2013; Lefort et al., 2009; Reyes-Puerta et al., 2015). The fact that the L5 subtypes could be recruited at different times and to different degrees, adds further diversity in terms of how L5 subpopulations could regulate L2/3.

In conclusion, the findings of this chapter reveal that projection-defined L5 pyramidal neuron subpopulations can deliver opposing E/I signals to L2/3, which are able to modulate spiking activity of L2/3 pyramidal neurons both *in vitro* and *in vivo*. This heterogeneity within L5-to-L2/3 signaling represents a mechanism for bidirectionally modulating responses to physiologically-relevant whisker input, which could be important for sensory processing and computations within the cortical column.

Chapter 7 : Discussion

This thesis set out to investigate the role of translaminar signaling from L5 pyramidal subpopulations to L2/3, using S1 as a model system. I will begin this general discussion by summarizing the main findings of each of the results chapters.

Summary of the main findings

In Chapter 3, I investigated the potential role of ascending axonal collaterals from a non-specific population of L5 pyramidal neurons, to L2/3 pyramidal neurons of S1. I showed through the optogenetic activation of L5 that the ascending collaterals elicited both monosynaptic excitation and a feedforward disynaptic inhibitory circuit onto L2/3 pyramidal neurons. I then showed that the feedforward inhibition recruited by L5 could modulate the output of L2/3 pyramidal neurons. *In vitro,* the activation of L5 shifted the input-output curves for L2/3 pyramidal neurons in keeping with the recruitment of significant inhibition. I also found *in vivo*, that stimulation of this non-specific L5 population resulted in the net inhibition of a physiologically-relevant whisker response in the supragranular layers of S1.

In Chapter 4, I set about examining the contribution of specific intratelencephalic (IT) and pyramidal tract (PT) L5 pyramidal neuron subpopulations. I used retrograde tracing to label these L5 subpopulations on the basis of their long-range projection targets and showed that the morphology of the ascending collaterals correlates with the target of the long-range axon. PT neurons exhibited slender ascending collaterals that remained close to the home column of the neuron, whereas the ascending collaterals of IT neurons demonstrated elaborate branching patterns that extended laterally. Finally, I established a method for selectively controlling the activity of projection-defined pyramidal neurons, by delivering a

retrograde AAV encoding Cre-inducible ChR2 to IT and PT neurons. This method provided the basis for the final two results chapters of the thesis.

In Chapter 5, I demonstrated that optical stimulation of PT L5 neurons elicited significant levels of synaptic inhibition in L2/3 pyramidal neurons. In contrast, IT L5 stimulation at a comparable level evoked excitation, but little inhibition in L2/3. This resulted in a significantly higher E/I ratio when IT L5 neurons were stimulated, compared to when PT L5 neurons were stimulated. A series of control experiments determined that the inhibitory currents were mediated by PT L5 pyramidal neurons forming a disynaptic inhibitory circuit with local L2/3 inhibitory interneurons. Using dual patch recordings from neuronal pairs comprising a L2/3 interneuron and a L2/3 pyramidal neuron, I showed that PT L5 neurons provided stronger excitatory input to L2/3 PV interneurons than the IT L5 subpopulation. By comparison, L5 input to L2/3 SST interneurons was weak.

Finally, in Chapter 6 I explored whether the ascending collaterals of L5 subpopulations play distinct roles in sensory processing. Given the relative recruitment of L2/3 inhibition by these two subpopulations, it was predicted that IT L5 neurons would exert an excitatory effect upon the L2/3 pyramidal neurons, whilst PT L5 neurons would exert a net inhibitory effect. I was able to demonstrate that in keeping with these predictions, L2/3 spiking in response to a depolarizing somatic current injection was increased by IT L5 stimulation, but decreased by PT L5 stimulation. The peak effects of these two subpopulations followed distinct temporal envelopes, broadly consistent with a monosynaptic excitation and disynaptic recruitment of inhibition. The excitation in L2/3 evoked by IT L5 neurons peaked at approximately 10 ms, whereas the inhibition evoked by PT L5 neurons reached peak hyperpolarisation at approximately 100 ms. I then tested the effect of these two subpopulations on modulating whisker responses in an *in vivo* preparation. These experiments demonstrated that IT L5 activity that is concurrent with a whisker stimulus, results in an excitatory effect upon supragranular whisker responses. In contrast, PT L5 activity inhibits supragranular neuronal responses to subsequent whisker input.

Methodological considerations

Before discussing the possible implications of my findings, I will first explore some of the methodological considerations that should be taken into account when interpreting the results.

Acute slice electrophysiology

In many of the experiments performed in this thesis, I relied upon the use of acute cortical slices in order to perform whole cell patch clamp recordings. The preparation of acute brain slices for electrophysiological recordings has been a key method for understanding cellular and subcellular neurophysiology, as well as synaptic circuitry during development and in the adult (Colbert, 2006; Buskila et al., 2014). Acute slice preparation does, however, have some significant limitations that need to be considered. Firstly, the process of preparing a slice will inevitably result in trauma to the tissue. This can lead to both cell death and disruption of circuit anatomy. Neurons located closest to the slice surface are the most vulnerable to cell death, which typically occurs shortly after the slicing process (Khurana and Li, 2013). Another limitation of this technique is that although attempts can be made to mimic the extracellular environment found in vivo, it is highly likely that certain chemical constituents will be different from those found in the intact brain (Khurana and Li, 2013). In particular, the metabolic and oxygen demand of neurons is likely to differ, which may influence both the cellular and network physiology observed *in vitro* (Ivanov and Zilberter, 2011). Finally, slice preparation disrupts synaptic connections to surrounding cortex and more distant structures. Whilst methods have been developed to preserve specific pathways, such as slicing at an optimal angle to preserve fibres (Agmon & Connors, 1991), this remains a significant difference compared to *in vivo* preparations.

Whilst the limitations of acute slice electrophysiology should be considered, the many advantages of this technique including the ability to visualize and target specific neuronal subtypes, the stability of recordings, and the easy application of pharmacological agents, were all important aspects of my

experiments. I was able to optimize cell health by allowing the neurons to rest before patching, adding ascorbic acid to the recovery solution and warming slices to physiological levels during the recovery period (Rice, 1999; Colbert, 2006; Khurana and Li, 2013; Ting et al., 2018). I also only recorded from neurons that appeared visibly healthy and whose membrane potential was not depolarized upon breakthrough into whole cell mode. Through the use of optogenetic techniques, I could stimulate even cut pre-synaptic fibers of ChR2-expressing neurons, and therefore did not have to rely upon fibres being intact from pre-synaptic soma. I was also able to simultaneously record from neuronal pairs and demonstrate population level differences in input from L5 by normalizing to the excitation received by local pyramidal neurons. Thus, I was able to systematically explore the underlying synaptic circuitry through a combination of pharmacological, optogenetic and anatomical techniques. Whilst such techniques are possible to apply *in vivo*, they remain technically demanding and are associated with low throughput. On balance therefore, the use of acute slices was an important and justified part of my experimental strategy.

The use of ChR2 to stimulate specific neuronal subpopulations

ChR2 was used to evoke translaminar signaling from L5 subpopulations to L2/3 neurons. The use of ChR2 is an incredibly powerful technique as it allows precise temporal stimulation of a defined neuronal population (Boyden, 2011; Boyden et al., 2005). However, there are a number of limitations to this technique that must be considered. For example, it has been well described that the variant of ChR2 used in my experiments cannot reliably evoke neuronal action potentials at high frequencies (40 Hz and above). This is particularly dependent on the light pulse history, as the recovery of ChR2 following inactivation is relatively slow (Lin et al., 2009; Gunaydin et al., 2010; Berndt et al., 2011). When considered at a population level, this could lead to variability in both the size of monosynaptic excitatory inputs and recruitment of disynaptic inhibition.

To control for these properties of ChR2, I used a low frequency stimulus protocol and short pulses that avoided long-term changes to the synapses under study (see Chapter 2). Nevertheless, it is the case that this stimulus pattern would be predicted to favor high-efficiency synapses, which exhibit synaptic depression. This would mean that my recordings may have been biased against detecting facilitating synapses, such as those that mediate frequency-dependent recruitment of SST interneurons (Pouille and Scanziani, 2004; Silberberg and Markram, 2007). Other studies have used ramps of increasing light intensity to recruit activity within a ChR2-expressing population (Adesnik and Scanziani, 2010; Adesnik, 2018). Whilst this may recruit different forms of frequency-dependent inhibition, the close proximity and interconnected nature of IT and PT L5 subpopulations may make it difficult to isolate effects using these sorts of stimuli. Looking forwards, this issue may be addressed by making use of ChR2 variants with improved kinetics (Gunaydin et al., 2010).

Other possible pitfalls associated with circuit mapping include the fact that ChR2 activation may synchronize populations of neurons in a non-physiological manner. Such recruitment could result in the activation of polysynaptic activity from off-target sites that synapse onto the neuron being recorded (Anastasiades, Marques-Smith, et al., 2018). The timing and amplitude of excitatory currents I observed were in keeping with monosynaptic stimulation. However, future work could make use of agents such as tetrodotoxin and 4-aminopyradine to block action potentials and thus isolate the direct activation of synapses by ChR2. Such experiments would provide further evidence that the excitatory connections from L5 Pyramidal neurons to L2/3 neurons are monosynaptic (Petreanu et al., 2009). A final limitation of the strategy is that ChR2 does not provide definitive control of the pre-synaptic axon's spiking pattern (Gunaydin et al., 2010). As a consequence, the probability of monosynaptic connections and the quantal strength of synaptic connections cannot be assessed. As an alternative, simultaneous patch clamp recordings could be used to assess the monosynaptic connections between small groups of neurons (Hardingham et al., 2010; Lefort et al., 2009), although such recordings are technically demanding. Given

the low probability of connection between excitatory neurons within cortex, this would also be a low throughput alternative and sensitive to slice-related damage to the axons between neurons, particularly when assessing interlaminar connectivity.

Whilst the limitations of using ChR2 in circuit mapping are acknowledged, this technique provided several important experimental advantages to the current study. By using ChR2 expression in specific neuronal populations, I was able to stimulate the cut fibers of ChR2 neurons and minimize confounds caused by the slicing procedure. In addition, I was able to limit stimulation in a highly cell-specific manner, by restricting stimulation to neurons located in L5 and whose long-range axons projected to a particular injection site. This was achieved by using transgenic mice in which Cre recombinase expression was restricted to L5, thus avoiding misexpression in neurons from other layers. Furthermore, I performed several control experiments to exclude the influence of viral transduction at the injection site. Whilst I did not explore frequency-dependent recruitment of inhibition, I was able to demonstrate clear differences in the monosynaptic targeting of L2/3 PV interneurons. As well as differences in the monosynaptic input from L5 to L2/3 PV and SST interneurons.

Any interpretation of experiments that use optogenetic tools to manipulate activity within a cortical circuit must take into account differences in opsin expression across the target populations. Expression of ChR2 delivered through viral vectors can show significant variation even between slices from the same brain (Mao et al., 2011). In my studies of L5 subtypes, ChR2 was selectively expressed in L5 pyramidal neurons that were defined by their long-range axonal projections. There are known anatomical differences in the density of such axonal projections (e.g. the POm thalamic nucleus is densely innervated by multiple regions of cortex (Guo et al., 2020)). This was likely to lead to variation in the number of ChR2-expressing L5 neurons between injection sites. In my experimental design, I therefore sought to control for this by normalizing measurements to a matched physiological output from the ChR2-expressing population. In voltage clamp and current clamp recordings, a variety of light intensities were used to stimulate ChR2-

expressing neurons such that the light-evoked monosynaptic EPSCs were matched across populations (see Chapter 2 and Chapter 5) and inhibition was compared under the same conditions. In experiments where recordings were made from L2/3 inhibitory interneurons, responses were normalized to the monosynaptic excitatory input to a neighboring L2/3 pyramidal neuron. By matching and normalizing in this way, I controlled for variation in the number of ChR2-expressing axonal fibres. In all in-vivo experiments, the LED intensity was again varied such that the light-evoked increase in multi-unit activity measured in L5 was comparable between the subpopulations (see Chapter 6).

Further *in vivo* experimental work could complement the findings described here through the use of inhibitory opsins or non-optogenetic manipulations. Inhibitory opsins, such as Halorhodopsin or Archaerhodopsin, could be used to silence the L5 pyramidal neuron subpopulations of interest (Boyden, 2011; Chow et al., 2012). Such silencing experiments would demonstrate how reduced activity in a L5 subpopulation affects whisker responses or even the processing of somatosensory information during a behavioral task (Vecchia et al., 2020). These experiments would also be more robust to polysynaptic activation of downstream targets. Finally, the use of other genetically-targetable manipulations of neural activity, such as chemogenetic tools, could complement the optogenetic approaches by affording more sustained manipulations of the L5 subpopulations (Roth, 2016).

In summary, whilst there are limitations to the use of ChR2, I was able to explore the function of translaminar signaling from L5 to L2/3 in a manner that was robust to axonal damage. I was also able to control for differences in expression by normalising to the excitatory input or population level activity, to make meaningful comparisons between different neuronal subpopulations.

In vivo electrophysiology

As mentioned above, *in vivo* preparations can be a powerful tool to complement acute slice physiology. I was able to use an *in vivo* model of the whisker system to test a series of predictions from slice experiments. The *in vivo* method involved performing extracellular recordings with a multiunit electrode in anesthetized mice. It should first be noted that the anesthetic agent and depth of anesthesia can fundamentally change the responsiveness of cortical tissue to sensory stimulation, as well as modulate the dynamics of cortical layer interactions (Erchova et al., 2002; Devonshire et al., 2010; Pachitariu et al., 2015; Sellers et al., 2015). It has been shown that under urethane anesthesia, cortical activity can become organized into correlated 'bursts'. This effect can increase with anesthetic depth and influence whisker responsiveness in barrel cortex (Erchova et al., 2002). Another point to consider is that long-range circuits remain intact *in vivo*, and whilst this is an important advantage, it also brings issues. For instance, it has been reported that PT L5 neurons can drive thalamic activity in POm (Mease et al., 2016a, 2016b) and there exist cortico-thalamocortical loops between S1 and POm (Guo et al., 2020). It remains unclear to what extent the optogenetic activation of PT neurons recruited these loops *in vivo* or how they may interact with the sensory responses that were measured.

Whilst these sorts of limitations are often associated with *in vivo* recordings, this technique allowed me to observe population level differences in the modulation of supragranular neuronal sensory-evoked responses. I minimized the effects associated with anesthesia by using a lower dose of urethane. In part, this was achieved by first inducing the animal with isoflurane, which could be rapidly cleared from the animal's system once an appropriate maintenance dose was achieved (see Chapter 2). Anesthetic choice also helped to optimize the recording of *in vivo* sensory responses. It has been observed that urethane results in less 'burstiness' and more successful spike sorting than ketamine-based anesthetic protocols (Pachitariu et al., 2015; Hildebrandt et al., 2017). Future experiments could be performed in awake head-

fixed, or behaving animals, this would however bring the interesting challenge of distinguishing how brain state, attention or motor activity, might interact with the effects of L5 translaminar signaling.

One of the drawbacks of extracellular recordings is that it is challenging to determine the specific cell-types that are being recorded. To maximize the chance of analyzing regular spiking pyramidal neurons, the temporal spiking properties of individual units was used to remove putative fast-spiking interneurons from the population. As one of the predictions from the *in vitro* experiments is that fast-spiking PV interneurons are differentially targeted by the L5 subpopulations, it would also have been interesting to investigate how these putative fast-spiking interneurons are recruited *in vivo*. Unfortunately, the number of these units was too limited to warrant a separate analysis here, but this remains an interesting direction for future study. In pursuing this question, it would be advantageous to use a method where there was high confidence in the sub-type identify of the recorded neuron. For example, one could imagine using multiphoton-guided *in vivo* patch clamp recordings from fluorescently-labelled interneurons, or genetically-encoded fluorescent reporters of spiking activity expressed by defined interneuron populations. Such methods may bring other compromises, such as limited throughput or reduced temporal resolution, but may ultimately offer better insight into the modulation of specific interneuron cell types by L5 pyramidal subpopulations.

In summary, the use of multiunit electrode recordings allowed me to observe activity across the local cortical column. In this way I could physiologically monitor the response in L5 to light stimulation, at the same time as assessing whisking responses in supragranular neurons. I was able to isolate multiple units and therefore assess population effects, which would have been difficult if I had used *in vivo* whole cell recordings, for example.

Implications of the findings

Having considered some of the methodological limitations and how these were mitigated, I will now explore some of the key implications of my results. I will explore how my data relates to other studies that have described similar forms of fine scale cortical circuitry and I will consider mechanisms that may be responsible for generating such cell-type specific circuits. I will then explore how the different E/I signals conveyed by these subpopulations may influence cortical operations. In particular, I will consider their potential role in synaptic integration, parallel information processing streams, and how information carried by the ascending collaterals may operate as a local 'feedback' signal.

Implications for our understanding of L5 local circuitry

L5 pyramidal neurons provide the principal output of the cortical column, but any complete description of cortex must also consider how these neurons regulate local activity. My findings provide general support for previous evidence that L5 play an important role in translaminar signaling across the cortical column. Several functional studies have revealed that L5 may provide important translaminar signals to superficial L2/3. For example, two studies investigating the role of ramping L5 activity suggested that translaminar signaling from L5 to L2/3 can contribute to oscillatory activity (Adesnik, 2018; Adesnik & Scanziani, 2010). Such spread of excitation under this stimulation paradigm may be transferred to surrounding columns by the elaborate branching pattern of L5 thin tufted (IT) ascending axonal collaterals (Oberlaender et al., 2011). In recent work, pulsed activation of ChR2-expressing L5 pyramidal neurons recruited significant local inhibition throughout the cortical column, which was shown to be important for a somatosensory discrimination task (Vecchia et al., 2020).

My first set of experiments described in Chapter 3 support these general findings. I observed that L5 activation serves to recruit significant local inhibition in L2/3, decreasing net L2/3 spiking levels both *in vitro* and *in vivo*. Increasing L5 activity resulted in a robust inhibition of subsequent whisker-evoked spiking

activity in the supragranular layers, for at least 100 ms. However, as I demonstrated in subsequent experiments, L5 pyramidal neurons represent a heterogenous population, which can be subclassified according to the long-range targets of their axons. This led to a major contribution of my work, which is the observation that IT and PT L5 pyramidal neurons differ significantly in their local translaminar signaling and elicit opposing E/I signals in L2/3 pyramidal neurons. Whilst ascending collaterals from IT L5 pyramidal neurons elicit excitatory effects in L2/3, PT L5 pyramidal neurons elicit inhibitory effects due to their selective targeting of L2/3 PV interneurons. These findings are summarized in **Fig. 7.1** and raise the questions: how unique is such selective targeting and what mechanisms may be responsible for establishing this connectivity?

A number of previous studies have suggested that PT and IT neurons may exhibit different connectivity with excitatory and inhibitory neuronal subtypes (Krook-Magnuson et al., 2012; Le Bé et al., 2006; Naka & Adesnik, 2016; Silberberg & Markram, 2007; Yamawaki & Shepherd, 2015).

Such subtype-specific targeting has been shown to manifest as greater connectivity between L5 neurons depending on their long-range projection targets (Brown and Hestrin, 2009; Kiritani et al., 2012; Yamawaki and Shepherd, 2015). Specific targeting has also been described between L5 pyramidal neurons and specific interneuron populations. One of the best described examples is the targeting of large Martinotti cells by PT L5 neurons, which mediate frequency dependent disynaptic inhibition (FDDI) (Le Bé et al., 2006; Silberberg and Markram, 2007). Similar to these results, more recent experiments performed in motor cortex demonstrated that, compared to IT L6 neurons, PT L6 neurons are able to more readily recruit local intralaminar inhibition (Yamawaki and Shepherd, 2015). My findings are in keeping with these observations in the sense that PT L5 subpopulations appear to selectively target L2/3 interneurons and thereby recruit greater relative inhibition.

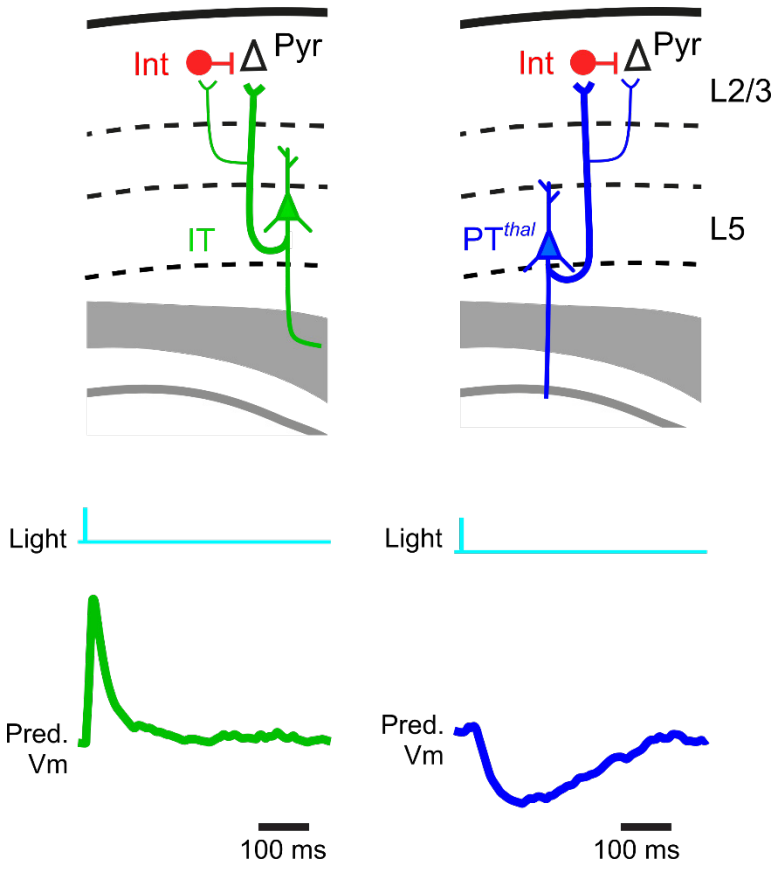


Figure 7.1 PT and IT L5 pyramidal neurons deliver opposing E/I signals to L2/3

In the proposed model, the selective translaminar connectivity of projection-defined L5 pyramidal neuron subpopulations means that they deliver opposing E/I signals to L2/3. Due to their weak recruitment of local interneurons, IT L5 neurons deliver fast excitatory signals (high E/I) to L2/3 pyramidal neurons (left). Whereas due to their strong recruitment of local interneurons, PT^{thal} L5 neurons deliver slower inhibitory signals (low E/I) to L2/3 pyramidal neurons (right).

Also in keeping with the observation of selective strong connectivity to local interneurons with translaminar output is the previous description of strong direct inhibition from L5b to L2/3 (Kätzel et al., 2011). Given this, it is interesting that I observed a limited contribution of direct translaminar inhibition (see Chapter 5). One potential explanation for this could be my limited exploration of FDDI. Due to the potential variability of ChR2 responses to a high frequency train of stimuli, I focused on the post-synaptic responses following single pre-synaptic stimuli. I found that L5 input to L2/3 SST neurons was uniformly weaker than the input to either local pyramidal neurons or PV interneurons. One potential avenue for future work could be to use high-speed optogenetic tools to explore how PT and IT L5 neurons differentially recruit local inhibition with different temporal patterns of pre-synaptic activity (Gunaydin et al., 2010; Klapoetke et al., 2014). Nevertheless, it remains the case that PT and IT L5 subpopulations differ in their relative targeting of L2/3 PV interneurons. This therefore raises the question, what mechanism might generate such connectivity patterns?

How might local L5 circuitry be established?

Whilst I have begun to dissect the circuits underlying differences in translaminar signaling, I have not explored the mechanisms that are responsible for generating these circuits. As with many cortical circuits, it remains an open question as to how much of the connectivity pattern seen in the adult brain reflects a molecular-genetic template, and how much is due to activity-dependent mechanisms. There are a number of reasons to believe that molecular-genetic mechanisms are responsible for the observed selective targeting. Firstly, recent transcriptomic work has identified that throughout L5, pyramidal neurons can be clustered into different subtypes based on gene expression (Tasic et al., 2016). Through a combination of retrograde tracing and single cell RNA sequencing, it has been shown that IT and PT pyramidal neurons have distinct gene expression patterns (Tasic et al., 2018; Scala et al., 2020). Some genes can be found

across all IT or PT neuronal subtypes, whereas the expression of other genes is more restricted and correlates with specific projection targets. There also appear to be distinct genetic expression patterns amongst subtypes of PV and SST interneurons (Tasic et al., 2016, 2018; Scala et al., 2020). Interestingly, the differential expression of genes that most clearly distinguish neuronal subtypes are those associated with various aspects of synaptic signaling, such as ion channels, neurotransmitter receptors, cell adhesion molecules, neuropeptide and vesicular release mechanisms (Paul et al., 2017).

For example, one potential family of genes that could mediate selective synaptic targeting are cell adhesion molecules (CAMs). The precise matching of pre- and post-synaptic CAMs is thought to play a role in providing structural support to synapses and thereby enable cell-specific connectivity. Previous work in the hippocampus has shown that CAM expression patterns are distinct between interneuron subtypes and pyramidal neurons in CA1 (Földy et al., 2016). In addition, whilst gene expression patterns were similar between regular spiking and intrinsically-bursting neurons in the subiculum, there were clear differences in CAM expression exhibited by CA1 pyramidal neurons. Indeed, a single CAM has recently been shown to be essential for the axo-axonic targeting of chandelier PV neurons (Tai et al., 2019). One possible mechanism for specific L5 to L2/3 connectivity is therefore through the selective expression of families of genes such as CAMs, which can mediate connectivity between excitatory and inhibitory neuronal subtypes.

It is also unknown whether the biased connectivity that I observe is present during early development, or whether it emerges over time. In potential support of the latter, there is already evidence that ascending connections from the infragranular layers form transiently during critical periods of cortical development, which are then refined to form the final adult circuit (Meng et al., 2020). It would therefore be interesting to investigate the development of L5 ascending collaterals, which to my knowledge, has not been explored for projection-defined subtypes. Such circuit refinement is usually associated with activity-dependent mechanisms and previous evidence suggests that formation of inhibitory cortical circuits is regulated by

activity. For instance, sensory deprivation experiments have revealed changes in translaminar inhibitory motifs (Kätzel and Miesenböck, 2014) and manipulations of pyramidal neuron activity lead to changes in the strength of inhibitory input that these neurons receive (Xue et al., 2014; Moore et al., 2018). One set of hypothetical future experiments could investigate the translaminar connectivity of PT and IT L5 pyramidal neurons in S1 of whisker-deprived mice. Or in cases where the activity of the pre-synaptic L5 neurons, or post-synaptic L2/3 neurons, have been selectively silenced during development via the targeted expression of potassium channels (Xue et al., 2014).

Potential functions for distinct translaminar L5 to L2/3 signals

Having considered some of the potential mechanisms that might generate selective L5-to-L2/3 connectivity, I will now use the remaining sections to consider what these circuits might do. I have observed that IT and PT L5 pyramidal neurons provide distinct and opposing translaminar signals in terms of the E/I ratios that they elicit within L2/3 pyramidal neurons (**Fig. 7.1**). The questions then arise: what roles might these signals serve in cortical computations and what might be achieved through having distinct and opposing E/I signals from two independent subpopulations, rather than equivalent signals from all L5 subtypes?

I will first explore how differences in the translaminar E/I signal might shape synaptic integration mechanisms that are fundamental to cortical function. Having discussed this, I will then explore how IT and PT subtypes may contribute to distinct information streams. And finally, I will consider how the information provided by ascending collaterals could be considered 'feedback' signals, which provide a local representation of the information that a cortical column sends to its long-range targets.

Signal processing implications for distinct translaminar L5 to L2/3 signals

Dynamic range refers to the range of input levels over which a neuron's input-output curve continues to operate. It is well known that activity levels vary greatly in cortex and the ability to control a neuron's gain, and therefore sensitivity to input, is fundamental to cortical function (Ferguson & Cardin, 2020). The mechanisms that solve such signal processing processes in the brain typically involve the interaction of excitatory and inhibitory signals. For instance, cortical circuits are known to transition between 'up' and 'down' states *in vivo* (Roux & Buzsáki, 2015) and these transitions require temporary shifts in the balance of excitation and inhibition, which have been linked to L5 (Beltramo et al., 2013). Hippocampal neurons under conditions of high background synaptic noise are thought to employ feedforward inhibitory mechanisms to maintain their dynamic range, modulating gain whilst decreasing the neuron's sensitivity to noise (Khubieh et al., 2016). At the same time, for information transfer to occur between a pre-synaptic and post-synaptic neuron, there must exist a dominance of excitatory input (Roux and Buzsáki, 2015). These imbalances in excitation and inhibition are thought to occur at the millisecond timescale, as has been shown to be the case during somatosensory processing (Kremkow et al., 2010).

By demonstrating that the two principal subtypes of L5 pyramidal neuron deliver distinct E/I signals to L2/3, I may have identified a circuit-based mechanism that contributes to cortical signal processing. As IT neurons can present an relatively greater excitatory signal to L2/3 pyramidal neurons, and PT neurons present a signal with greater relative inhibition, these can be considered opposing signals delivered by (somewhat) independent subpopulations. By varying both the timing and activity levels within each of the two subpopulations, one would predict that this would serve to increase the L2/3 neuron's dynamic range, and more so than if all L5 neurons provided an equivalent signal. To test these ideas, one would like to conduct experiments in which the two subpopulations could be independently stimulated in the same animal. Indeed, spectrally separate optogenetic activators are beginning to make this experimentally

feasible (Klapoetke et al., 2014). In addition, computational modelling approaches could be used to explore the signal processing effects of systematically varying the timing and activity levels of two subpopulations that exert opposing effects on a post-synaptic neuron.

Parallel information processing streams with distinct translaminar L5 to L2/3 signals

As discussed above, the fact that signals from IT and PT L5 neurons convey different E/I signals could modulate the integration of other inputs to L2/3 pyramidal neurons. Such differences could be related to how these subpopulations are recruited as part of parallel sensory processing streams. To explore this idea further, I will refer to what is known about the lemniscal and paralemniscal pathways in the rodent primary somatosensory cortex. Understanding when these pathways may be engaged will also help us to consider how and when either of the L5 subpopulations are likely to be active.

The large, layer-spanning apical dendrites of both IT and PT L5 pyramidal neurons, means that these neurons are well-placed to integrate inputs from other cortical regions and layers. However, these inputs can be non-overlapping between the two L5 subtypes, as is shown by differences in their inputs from thalamus. PT neurons in L5b are highly thalamorecipient for inputs from VPM and could therefore be considered part of the 'lemniscal' system (Petersen, 2007; Feldmeyer, 2012; Sermet et al., 2019). These neurons can be directly stimulated by thalamic inputs independent of other cortical layers (Constantinople and Bruno, 2013). The lemniscal pathway is thought to convey information regarding single whisker stimuli. In contrast IT neurons are thalamorecipient of the POm nucleus (Audette et al., 2018; Bureau et al., 2006; Dirk Schubert et al., 2001; Wimmer et al., 2010). There is some evidence in the barrel cortex that ascending collaterals from IT neurons are an extension of the paralemniscal pathway, the strength of this connection from IT L5 to L2/3 may rival those of L4 to L2/3, particularly over septal regions (Bureau et al., 2006; Shepherd & Svoboda, 2005). The paralemniscal pathway is thought to convey

more contextual information from multiple whiskers, as well as temporally important information (Ahissar et al., 2000).

During whisking, it has been demonstrated that PT neurons in L5b receive thalamic inputs with short latency and high sensitivity (Armstrong-James and Fox, 1987; Constantinople and Bruno, 2013; Reyes-Puerta et al., 2015). In contrast, IT L5 neurons appear to exhibit more delayed responses and to be associated with greater spread of activity to surrounding cortex (Lefort et al., 2009; Constantinople and Bruno, 2013; Reyes-Puerta et al., 2015). That these neurons may be part of distinct information streams and activated at separate times or independently, speaks to the fact that they likely play complementary roles.

The distinct E/I signals from PT and IT neurons could assist in information processing in these two parallel pathways. As part of the lemniscal pathway, the recruitment of inhibition by PT L5 neurons could be important in improving signal to noise within this pathway. Indeed, consistent with the idea that these neurons play an important role in sensory perception, recent work shows that activity in PT neurons is important for whisker stimulus detection at threshold intensities (Takahashi et al., 2020). It has also been shown that PT neuronal output from visual cortex is important for carrying task-specific information required for behavioral performance (Tang and Higley, 2020). As described previously, in another set of experiments it was demonstrated that L5 activation served to recruit local inhibition thereby sharpening the whisker-evoked response when optogenetic stimulation was delivered shortly after a sensory stimulus (Vecchia et al., 2020). In contrast, silencing L5 increased ongoing activity following whisker stimulation, while decreasing behavioral performance levels. Increased inhibitory recruitment (particularly by PV interneurons) can serve to sharpen the feature selectivity of cortical principal neurons and improve performance in perceptual tasks (Lee et al., 2012; Tanke et al., 2018).

In contrast to this, the paralemniscal pathway is thought to convey contextual information regarding multiple whiskers. Such processing of contextual information requires information to be integrated from a number of surrounding barrels (Hawkins et al., 2017). As part of this pathway, higher E/I signals from IT neurons could provide contextual information across a number of cortical columns. Whilst significant excitation by L5 pyramidal neurons is likely to recruit local inhibition within the home column (see Chapter 3; (Xue et al., 2014))**,** IT neurons have been demonstrated to project to surrounding columns, both in my work (see Chapter 4) and others' (de Kock and Sakmann, 2009; Oberlaender et al., 2011; Narayanan et al., 2017). Thus, when stimulating IT L5 neurons, neighboring columns may receive similar levels of excitation as the principal whisker column (see Chapter 5). L2/3 pyramidal neurons follow a sparse coding regime, enforced by local inhibition, It should also be reiterated that due to the sparse coding regime in L2/3 each spike contains a high value of mutual information(Yu et al., 2018), therefor small increases or decreases in the probability of spiking would likely have an outsize effect on columnar computation. Such excitatory input to a neighboring column from IT neurons, as I demonstrate could increase the spiking probability of L2/3 pyramidal neurons within it. As such, this could serve as a mechanism for facilitation in surrounding columns, providing a source of contextual somatosensory information.

Thus in summary, PT neurons could be considered to play an important role in the lemniscal pathway, where the lower translaminar E/I signal to L2/3 could be important for improving signal to noise. IT neurons are more strongly associated with the paralemniscal pathway, where a higher translaminar E/I signal could play an important role in integrating contextual information across a number of cortical columns. To further test these hypothesis, a number of experiments could be performed. Firstly, by performing more complex whisker stimulation in which the direction of the whisk is systematically varied, it would be possible to determine if either L5 subpopulation could change the tuning of the whisker response. To further interrogate this *in vivo*, patch clamp recording techniques could be used to evaluate

subthreshold inputs to L2/3 pyramidal neurons. Finally, and most complex, would be to perform these experiments in awake head-fixed mice that have been trained on a perceptual threshold task.

Distinct translaminar L5 to L2/3 communication as 'feedback' signals

The translaminar E/I signals from L5 subtypes could also be considered as a read-out of cortical output, which is relayed back to inform ongoing activity within other cortical layers. Such 'feedback' signals could play a role in generating an internal expected model of the sensory environment, which could be important for predictive coding, sensory-motor integration, or to gate synaptic plasticity mechanisms (Bastos et al., 2012; Keller & Mrsic-Flogel, 2018).

Such a framework for interpreting my findings draws on the idea that sensory-motor integration of information conveyed via the cortico-thalamocortical pathways, is fundamentally different to that conveyed via direct cortico-cortical connections (Sherman and Guillery, 2011; Mo and Sherman, 2019). In the case of PT L5 pyramidal neurons, in almost all cortical regions including sensory cortex, this subtype project to motor structures in the brainstem and spine (Guillery and Sherman, 2011; Sherman and Guillery, 2011; Sherman, 2016). Subcortical output from PT L5 in somatosensory cortex for example, is sufficient to elicit whisking (Matyas et al., 2010). Given that the long-range outputs of PT neurons are important for initiating or informing motor actions that are downstream of sensory perception (Takahashi et al., 2020), the feedback signal delivered via their local ascending collaterals conveys an 'efference' copy of a modulatory motor output signal (Guillery and Sherman, 2011).

Meanwhile, in the case of the IT L5 pyramidal neurons, the local representations of their long-range output is also likely to provide an important signal to local processing. Whilst these long-range projections do not initiate motor output, it is established that they provide important modulatory signals to other cortical areas (Aronoff et al., 2010; Mao et al., 2011). Interareal IT axonal projections appear to engage local disinhibitory (and thus net excitatory) motifs (Ayaz et al., 2019; Soohyun Lee et al., 2013). The

ascending collaterals of IT L5 neurons therefore provide a copy of these excitatory modulatory signals, which are fed back within the local column.

What role could such a local copy of the output signal play and how might the observed differences in E/I ratios contribute? Ascending collaterals of IT L5 neurons provide excitatory signals to local L2/3, similar to the disinhibitory motif that are elicited by their long-range interareal projections. This may enhance the integration of additional contextual information (Pouille and Scanziani, 2001; Williams and Holtmaat, 2019). In contrast, the recruitment of inhibition by the ascending collaterals of PT L5 neurons serves to limit ongoing local activity. Similar inhibitory mechanisms have been observed in auditory cortex, where motor outputs have been shown to reduce excitatory neuronal activity, in a manner that can reduce the sensitivity of the system to self-generated noise (Schneider et al., 2014). It would therefore be interesting to explore the contributions of IT and PT L5 neurons in sensory-motor integration. One could imagine examining the effects of stimulating primary motor cortex and a projection-defined L5 subpopulation, upon local L2/3 pyramidal neuron activity in S1. Stimulation of motor cortex could use either optogenetics, a more physiological stimulus such as locomotion on a treadmill, or pharmacological agents to excite or inhibit that region of cortex. Meanwhile, the modulatory effects upon local sensory responses, such as a whisker response, could be monitored.

In addition to sensory processing, local feedback representations of long-range outputs could be important as sources of 'error' in a predictive coding model of cortex. In such a scheme, each group of neurons compares an afferent sensory input from preceding stages of information processing, with an internally generated model of the expected environment that is delivered via 'top down' inputs (Bastos et al., 2012). L2/3 pyramidal neurons have been proposed to encode 'errors', which represent differences between 'bottom up' sensory afferents and the predicted model that is signaled by 'top down' higher-order inputs. Inhibitory neurons could play important roles in cancelling such error signals. Evidence for this has been demonstrated in visual cortex, where a subset of L2/3 neurons were found to strongly

respond to mismatch between locomotion speed and visual flow (Keller et al., 2012). Within such a model, PT L5 neurons could provide the local representation of the motor output (Guillery and Sherman, 2011; Brecht, 2017), serving to inhibit L2/3 responses to the expected sensory input, and thereby generating a 'positive prediction error response' (Keller and Mrsic-Flogel, 2018). Meanwhile, IT L5 neurons could be delivering a representation of contextual information to L2/3, and the excitatory nature of these signals would enhance the sensitivity to any unexpected or 'salient' inputs. This would therefore be part of a 'mismatch error' or 'negative prediction error' circuit (Keller and Mrsic-Flogel, 2018).

Finally, these local signals may serve to gate plasticity. Increasingly, it is being recognized that 'third factors' can modulate the sign and/or strength of synaptic plasticity. This can occur via neuromodulators such as dopamine or acetylcholine, which encode reward, attention or the aforementioned 'error' signals (Kuśmierz et al., 2017). Local inhibitory and disinhibitory cortical circuits in L2/3 have also been shown to gate synaptic plasticity(L. E. Williams & Holtmaat, 2019). Long-range projections from higher-order thalamus appear to engage a disinhibitory motif in supragranular layers of S1, which produce sustained depolarizations in L2/3 pyramidal neurons and allows these neurons to integrate inputs over a longer timescale (Ayaz et al., 2019; Zhang and Bruno, 2019). It has also been observed that higher-order thalamic inputs from POm can act to gate long-term synaptic plasticity between L4 and L2/3 (Gambino et al., 2014), through the engagement of the same disinhibitory circuit. One possibility is that the ascending collaterals of IT L5 pyramidal neurons also gate plasticity by increasing the excitatory drive to L2/3 pyramidal neurons. Whereas the local inhibitory signal elicited by the ascending collaterals of L5 PT neurons could serve to narrow the temporal window for coincidence detection and limit L2/3 plasticity. To test these possibilities, one could imagine using spike timing protocols to induce plasticity at the L4-to-L2/3 synapses, and then compare the effects of plasticity induction when either IT or PT L5 neurons are optogenetically activated.

Concluding remarks

Through this thesis I have explored the local reciprocal signaling from L5 pyramidal neurons to L2/3 pyramidal neurons. I have shown that L5 pyramidal neurons play a significant role in modulating activity within the supragranular layers. Furthermore, I have found that when L5 pyramidal neurons are subclassified according to their long-range axonal projection targets, significant differences are revealed in terms of how these L5 subpopulations signal locally via their ascending axonal collaterals. PT L5 neurons elicit significant levels of synaptic inhibition within L2/3. In contrast, IT L5 neurons evoke excitation in L2/3, but little inhibition. As a consequence, L5 subtypes exert opposing modulatory effects upon the input-output behavior of L2/3 pyramidal neurons, including their responses to sensory-driven input *in vivo.* In discussing the potential implications of these findings, I have considered the relevance of these L5-to-L2/3 signals in sensory processing, sensory-motor integration and synaptic plasticity mechanisms.

Page intentionally left blank

Chapter 8 : References

Acsády, L., Görcs, T. J., & Freund, T. F. (1996). Different populations of vasoactive intestinal polypeptide-immunoreactive interneurons are specialized to control pyramidal cells or interneurons in the hippocampus. *Neuroscience*, *73*(2), 317–334. https://doi.org/10.1016/0306-4522(95)00609-5

Adesnik, H. (2018). Layer-specific excitation/inhibition balances during neuronal synchronization in the visual cortex. *The Journal of Physiology*, *596*(9), 1639–1657. https://doi.org/10.1113/JP274986

Adesnik, H., & Naka, A. (2018). Cracking the Function of Layers in the Sensory Cortex. *Neuron*, *100*(5), 1028–1043. https://doi.org/10.1016/j.neuron.2018.10.032

Adesnik, H., & Scanziani, M. (2010). Lateral competition for cortical space by layer-specific horizontal circuits. *Nature*, *464*(7292), 1155–1160. https://doi.org/10.1038/nature08935

Agmon, A., & Connors, B. W. (1991). Thalamocortical responses of mouse somatosensory (barrel) cortexin vitro. *Neuroscience*, *41*(2), 365–379. https://doi.org/https://doi.org/10.1016/0306-4522(91)90333-J

Ahissar, E., Sosnik, R., & Haidarliu, S. (2000). Transformation from temporal to rate coding in a somatosensory thalamocortical pathway. *Nature*, *406*(6793), 302–306. https://doi.org/10.1038/35018568

Alloway, K. D. (2008). Information Processing Streams in Rodent Barrel Cortex: The Differential Functions of Barrel and Septal Circuits. *Cerebral Cortex*, *18*(5), 979–989. https://doi.org/10.1093/cercor/bhm138

Anastasiades, P. G., Marlin, J. J., & Carter, A. G. (2018). Cell-Type Specificity of Callosally Evoked Excitation and Feedforward Inhibition in the Prefrontal Cortex. *Cell Reports*, *22*(3), 679–692. https://doi.org/10.1016/j.celrep.2017.12.073

Anastasiades, P. G., Marques-Smith, A., & Butt, S. J. B. (2018). Studies of cortical connectivity using optical circuit mapping methods. *The Journal of Physiology*, *596*(2), 145–162. https://doi.org/10.1113/JP273463

Anderson, J. S., Carandini, M., & Ferster, D. (2000). Orientation Tuning of Input Conductance, Excitation, and Inhibition in Cat Primary Visual Cortex. *Journal of Neurophysiology*, *84*(2), 909–926. https://doi.org/10.1152/jn.2000.84.2.909

Armstrong-James, M, Fox, K., & Das-Gupta, A. (1992). Flow of excitation within rat barrel cortex on striking a single vibrissa. *Journal of Neurophysiology*, *68*(4), 1345–1358. https://doi.org/10.1152/jn.1992.68.4.1345

Armstrong-James, Michael, & Fox, K. (1987). Spatiotemporal convergence and divergence in the rat S1 "Barrel" cortex. *Journal of Comparative Neurology*, *263*(2), 265–281. https://doi.org/https://doi.org/10.1002/cne.902630209

Aronoff, R., Matyas, F., Mateo, C., Ciron, C., Schneider, B., & Petersen, C. C. H. (2010). Long-range connectivity of mouse primary somatosensory barrel cortex. *European Journal of Neuroscience*, *31*(12), 2221–2233. https://doi.org/10.1111/j.1460-9568.2010.07264.x

Ascoli, G. A., Alonso-Nanclares, L., Anderson, S. A., Barrionuevo, G., Benavides-Piccione, R., Burkhalter, A., Buzsáki, G., Cauli, B., DeFelipe, J., Fairén, A., Feldmeyer, D., Fishell, G., Fregnac, Y., Freund, T. F., Gardner, D., Gardner, E. P., Goldberg, J. H., Helmstaedter, M., Hestrin, S., … (PING), T. P. I. N. G. (2008). Petilla terminology: nomenclature of features of GABAergic interneurons of the cerebral cortex. *Nature Reviews Neuroscience*, *9*(7), 557–568. https://doi.org/10.1038/nrn2402

Atallah, B. V., Bruns, W., Carandini, M., & Scanziani, M. (2012). Parvalbumin-Expressing Interneurons Linearly Transform Cortical Responses to Visual Stimuli. *Neuron*, *73*(1), 159–170.

https://doi.org/10.1016/j.neuron.2011.12.013

Audette, N. J., Urban-Ciecko, J., Matsushita, M., & Barth, A. L. (2018). POm Thalamocortical Input Drives Layer-Specific Microcircuits in Somatosensory Cortex. *Cerebral Cortex (New York, N.Y. : 1991)*, *28*(4), 1312–1328. https://doi.org/10.1093/cercor/bhx044

Avermann, M., Tomm, C., Mateo, C., Gerstner, W., & Petersen, C. C. H. (2012). Microcircuits of excitatory and inhibitory neurons in layer 2/3 of mouse barrel cortex. *Journal of Neurophysiology*, *107*(11), 3116–3134. https://doi.org/10.1152/jn.00917.2011

Ayaz, A., Stäuble, A., Hamada, M., Wulf, M.-A., Saleem, A. B., & Helmchen, F. (2019). Layer-specific integration of locomotion and sensory information in mouse barrel cortex. *Nature Communications*, *10*(1), 2585. https://doi.org/10.1038/s41467-019-10564-8

Bagnall, M. W., Hull, C., Bushong, E. A., Ellisman, M. H., & Scanziani, M. (2011). Multiple Clusters of Release Sites Formed by Individual Thalamic Afferents onto Cortical Interneurons Ensure Reliable Transmission. *Neuron*, *71*(1), 180–194. https://doi.org/10.1016/j.neuron.2011.05.032

Barthó, P., Hirase, H., Monconduit, L., Zugaro, M., Harris, K. D., & Buzsáki, G. (2004). Characterization of Neocortical Principal Cells and Interneurons by Network Interactions and Extracellular Features. *Journal of Neurophysiology*, *92*(1), 600–608. https://doi.org/10.1152/jn.01170.2003

Bastos, A. M., Usrey, W. M., Adams, R. A., Mangun, G. R., Fries, P., & Friston, K. J. (2012). Canonical Microcircuits for Predictive Coding. *Neuron*, *76*(4), 695–711. https://doi.org/10.1016/j.neuron.2012.10.038

Bates, A. S., Manton, J. D., Jagannathan, S. R., Costa, M., Schlegel, P., Rohlfing, T., & Jefferis, G. S. X. E. (2020). The natverse, a versatile toolbox for combining and analysing neuroanatomical data. *ELife*, *9*, e53350. https://doi.org/10.7554/eLife.53350

Beltramo, R., D'Urso, G., Dal Maschio, M., Farisello, P., Bovetti, S., Clovis, Y., Lassi, G., Tucci, V., De Pietri Tonelli, D., & Fellin, T. (2013). Layer-specific excitatory circuits differentially control recurrent network dynamics in the neocortex. *Nature Neuroscience*, *16*, 227. http://dx.doi.org/10.1038/nn.3306

Berker, E. A., Berker, A. H., & Smith, A. (1986). Translation of Broca's 1865 Report: Localization of Speech in the Third Left Frontal Convolution. *Archives of Neurology*, *43*(10), 1065–1072. https://doi.org/10.1001/archneur.1986.00520100069017

Berndt, A., Schoenenberger, P., Mattis, J., Tye, K. M., Deisseroth, K., Hegemann, P., & Oertner, T. G. (2011). High-efficiency channelrhodopsins for fast neuronal stimulation at low light levels. *Proceedings of the National Academy of Sciences of the United States of America*, *108*(18), 7595–7600. https://doi.org/10.1073/pnas.1017210108

Binzegger, T., Douglas, R. J., & Martin, K. A. C. (2004). A quantitative map of the circuit of cat primary visual cortex. *The Journal of Neuroscience : The Official Journal of the Society for Neuroscience*, *24*(39), 8441–8453. https://doi.org/10.1523/JNEUROSCI.1400-04.2004

Bonin, V., Histed, M. H., Yurgenson, S., & Reid, R. C. (2011). Local Diversity and Fine-Scale Organization of Receptive Fields in Mouse Visual Cortex. *The Journal of Neuroscience*, *31*(50), 18506 LP – 18521. https://doi.org/10.1523/JNEUROSCI.2974-11.2011

Bortone, D. S. S., Olsen, S. R. R., & Scanziani, M. (2014). Translaminar Inhibitory Cells Recruited by Layer 6 Corticothalamic Neurons Suppress Visual Cortex. *Neuron*, *82*(2), 474–485. https://doi.org/10.1016/j.neuron.2014.02.021

Boyden, E. S. (2011). Optogenetics: using light to control the brain. *Cerebrum : The Dana Forum on Brain Science*, *2011*, 16.

Boyden, E. S., Zhang, F., Bamberg, E., Nagel, G., & Deisseroth, K. (2005). Millisecond-timescale, genetically targeted

optical control of neural activity. *Nature Neuroscience*, *8*(9), 1263–1268. https://doi.org/10.1038/nn1525

Brecht, M. (2017). The Body Model Theory of Somatosensory Cortex. *Neuron*, *94*(5), 985–992. https://doi.org/https://doi.org/10.1016/j.neuron.2017.05.018

Broca, P. (1861). Remarques sur le siège de la faculté du langage articulé, suivies d'une observation d'aphémie (perte de la parole). *Bulletin et Memoires de La Societe Anatomique de Paris*, *6*, 330–357.

Brodmann, K. (1907). *Beiträge zur histologischen Lokalisation der Grosshirnrinde: Die Cortexgliederung des Menschen. VI*. Verlag von Johann Ambrosius Barth.

Brodmann, K. (1909). *Vergleichende Lokalisationslehre der Grosshirnrinde in ihren Prinzipien dargestellt auf Grund des Zellenbaues*. Barth.

Brodmann, K. (1914). *Physiologie des gehirns*. Druck der Union deutsche Verlagsgesellschaft.

Brown, S. P., & Hestrin, S. (2009). Intracortical circuits of pyramidal neurons reflect their long-range axonal targets. *Nature*, *457*, 1133. http://dx.doi.org/10.1038/nature07658

Brumberg, J. C., Pinto, D. J., & Simons, D. J. (1999). Cortical Columnar Processing in the Rat Whisker-to-Barrel System. *Journal of Neurophysiology*, *82*(4), 1808–1817. https://doi.org/10.1152/jn.1999.82.4.1808

Bruno, R. M., & Simons, D. J. (2002). Feedforward mechanisms of excitatory and inhibitory cortical receptive fields. *The Journal of Neuroscience : The Official Journal of the Society for Neuroscience*, *22*(24), 10966–10975. https://doi.org/10.1523/JNEUROSCI.22-24-10966.2002

Buchanan, K. A., Blackman, A. V., Moreau, A. W., Elgar, D., Costa, R. P., Lalanne, T., Tudor Jones, A. A., Oyrer, J., & Sjöström, P. J. (2012). Target-Specific Expression of Presynaptic NMDA Receptors in Neocortical Microcircuits. *Neuron*, *75*(3), 451–466. https://doi.org/10.1016/j.neuron.2012.06.017

Bureau, I., von Saint Paul, F., & Svoboda, K. (2006). Interdigitated Paralemniscal and Lemniscal Pathways in the Mouse Barrel Cortex. *PLoS Biology*, *4*(12), e382. https://doi.org/10.1371/journal.pbio.0040382

Buskila, Y., Breen, P. P., Tapson, J., van Schaik, A., Barton, M., & Morley, J. W. (2014). Extending the viability of acute brain slices. *Scientific Reports*, *4*, 5309. https://doi.org/10.1038/srep05309

Butt, S. J. B., Fuccillo, M., Nery, S., Noctor, S., Kriegstein, A., Corbin, J. G., & Fishell, G. (2005). The Temporal and Spatial Origins of Cortical Interneurons Predict Their Physiological Subtype. *Neuron*, *48*(4), 591–604. https://doi.org/10.1016/j.neuron.2005.09.034

Cardin, J. A., Palmer, L. A., & Contreras, D. (2008). Cellular mechanisms underlying stimulus-dependent gain modulation in primary visual cortex neurons in vivo. *Neuron*, *59*(1), 150–160. https://doi.org/10.1016/j.neuron.2008.05.002

Chmielowska, J., Carvell, G. E., & Simons, D. J. (1989). Spatial organization of thalamocortical and corticothalamic projection systems in the rat SmI barrel cortex. *The Journal of Comparative Neurology*, *285*(3), 325–338. https://doi.org/10.1002/cne.902850304

Chow, B. Y., Han, X., & Boyden, E. S. (2012). Chapter 3 - Genetically encoded molecular tools for light-driven silencing of targeted neurons. In T. Knöpfel & E. S. B. T.-P. in B. R. Boyden (Eds.), *Optogenetics: Tools for Controlling and Monitoring Neuronal Activity* (Vol. 196, pp. 49–61). Elsevier. https://doi.org/https://doi.org/10.1016/B978-0-444-59426-6.00003-3

Colbert, C. M. (2006). *Preparation of Cortical Brain Slices for Electrophysiological Recording BT - Ion Channels: Methods and Protocols* (J. D. Stockand & M. S. Shapiro (eds.); pp. 117–125). Humana Press. https://doi.org/10.1385/1-59745-095-2:117

Connors, B. W., & Gutnick, M. J. (1990). Intrinsic firing patterns of diverse neocortical neurons. *Trends in*

Neurosciences, *13*(3), 99–104. https://doi.org/https://doi.org/10.1016/0166-2236(90)90185-D

Constantinople, C. M., & Bruno, R. M. (2013). Deep Cortical Layers Are Activated Directly by Thalamus. *Science*, *340*(6140), 1591–1594. https://doi.org/10.1126/science.1236425

Conte, W. L., Kamishina, H., & Reep, R. L. (2009a). Multiple neuroanatomical tract-tracing using fluorescent Alexa Fluor conjugates of cholera toxin subunit B in rats. *Nature Protocols*, *4*(8), 1157–1166. https://doi.org/10.1038/nprot.2009.93

Conte, W. L., Kamishina, H., & Reep, R. L. (2009b). The efficacy of the fluorescent conjugates of cholera toxin subunit B for multiple retrograde tract tracing in the central nervous system. *Brain Structure and Function*, *213*(4), 367–373. https://doi.org/10.1007/s00429-009-0212-x

Cruikshank, S. J., Lewis, T. J., & Connors, B. W. (2007). Synaptic basis for intense thalamocortical activation of feedforward inhibitory cells in neocortex. *Nature Neuroscience*, *10*, 462. https://doi.org/10.1038/nn1861

Cruikshank, S. J., Urabe, H., Nurmikko, A. V, & Connors, B. W. (2010). Pathway-Specific Feedforward Circuits between Thalamus and Neocortex Revealed by Selective Optical Stimulation of Axons. *Neuron*, *65*(2), 230–245. https://doi.org/10.1016/j.neuron.2009.12.025

D'Souza, R. D., Meier, A. M., Bista, P., Wang, Q., & Burkhalter, A. (2016). Recruitment of inhibition and excitation across mouse visual cortex depends on the hierarchy of interconnecting areas. *ELife*, *5*, e19332. https://doi.org/10.7554/eLife.19332

Daigle, T. L., Madisen, L., Hage, T. A., Valley, M. T., Knoblich, U., Larsen, R. S., Takeno, M. M., Huang, L., Gu, H., Larsen, R., Mills, M., Bosma-Moody, A., Siverts, L. A., Walker, M., Graybuck, L. T., Yao, Z., Fong, O., Nguyen, T. N., Garren, E., … Zeng, H. (2018). A Suite of Transgenic Driver and Reporter Mouse Lines with Enhanced Brain-Cell-Type Targeting and Functionality. *Cell*, *174*(2), 465-480.e22. https://doi.org/10.1016/j.cell.2018.06.035

Dantzker, J. L., & Callaway, E. M. (2000). Laminar sources of synaptic input to cortical inhibitory interneurons and pyramidal neurons. *Nature Neuroscience*, *3*(7), 701–707. https://doi.org/10.1038/76656

De Kock, C P J, Bruno, R. M., Spors, H., & Sakmann, B. (2007). Layer- and cell-type-specific suprathreshold stimulus representation in rat primary somatosensory cortex. *The Journal of Physiology*, *581*(1), 139–154. https://doi.org/https://doi.org/10.1113/jphysiol.2006.124321

de Kock, Christiaan P J, & Sakmann, B. (2009). Spiking in primary somatosensory cortex during natural whisking in awake head-restrained rats is cell-type specific. *Proceedings of the National Academy of Sciences*, *106*(38), 16446–16450. https://doi.org/10.1073/pnas.0904143106

DeFelipe, J., López-Cruz, P. L., Benavides-Piccione, R., Bielza, C., Larrañaga, P., Anderson, S., Burkhalter, A., Cauli, B., Fairén, A., Feldmeyer, D., Fishell, G., Fitzpatrick, D., Freund, T. F., González-Burgos, G., Hestrin, S., Hill, S., Hof, P. R., Huang, J., Jones, E. G., … Ascoli, G. A. (2013). New insights into the classification and nomenclature of cortical GABAergic interneurons. *Nature Reviews Neuroscience*, *14*(3), 202–216. https://doi.org/10.1038/nrn3444

Deneris, E. S., & Hobert, O. (2014). Maintenance of postmitotic neuronal cell identity. *Nature Neuroscience*, *17*(7), 899–907. https://doi.org/10.1038/nn.3731

Deschênes, M., Bourassa, J., & Pinault, D. (1994). Corticothalamic projections from layer V cells in rat are collaterals of long-range corticofugal axons. *Brain Research*, *664*(1–2), 215–219. https://doi.org/http://dx.doi.org/10.1016/0006-8993(94)91974-7

Devonshire, I. M., Grandy, T. H., Dommett, E. J., & Greenfield, S. A. (2010). Effects of urethane anaesthesia on sensory processing in the rat barrel cortex revealed by combined optical imaging and electrophysiology. *The European Journal of Neuroscience*, *32*(5), 786–797. https://doi.org/10.1111/j.1460-9568.2010.07322.x

Diamond, M. E., Armstrong-James, M., Budway, M. J., & Ebner, F. F. (1992). Somatic sensory responses in the rostral sector of the posterior group (POm) and in the ventral posterior medial nucleus (VPM) of the rat thalamus:

Dependence on the barrel field cortex. *Journal of Comparative Neurology*, *319*(1), 66–84. https://doi.org/https://doi.org/10.1002/cne.903190108

Diamond, M. E., von Heimendahl, M., Knutsen, P. M., Kleinfeld, D., & Ahissar, E. (2008). "Where" and "what" in the whisker sensorimotor system. *Nature Reviews Neuroscience*, *9*(8), 601–612. https://doi.org/10.1038/nrn2411

Douglas, R J, & Martin, K. A. (1991). A functional microcircuit for cat visual cortex. *The Journal of Physiology*, *440*, 735–769. https://doi.org/10.1113/jphysiol.1991.sp018733

Douglas, Rodney J, & Martin, K. A. C. (2004). Neuronal Circuits of the Neocortex. *Annual Review of Neuroscience*, *27*(1), 419–451. https://doi.org/10.1146/annurev.neuro.27.070203.144152

Douglas, Rodney J, Martin, K. A. C., & Whitteridge, D. (1989). A Canonical Microcircuit for Neocortex. *Neural Computation*, *1*(4), 480–488. https://doi.org/10.1162/neco.1989.1.4.480

Einevoll, G. T., Kayser, C., Logothetis, N. K., & Panzeri, S. (2013). Modelling and analysis of local field potentials for studying the function of cortical circuits. *Nature Reviews Neuroscience*, *14*(11), 770–785. https://doi.org/10.1038/nrn3599

Ellender, T. J., Avery, S. V, Mahfooz, K., Scaber, J., von Klemperer, A., Nixon, S. L., Buchan, M. J., van Rheede, J. J., Gatti, A., Waites, C., Pavlou, H. J., Sims, D., Newey, S. E., & Akerman, C. J. (2019). Embryonic progenitor pools generate diversity in fine-scale excitatory cortical subnetworks. *Nature Communications*, *10*(1), 5224. https://doi.org/10.1038/s41467-019-13206-1

Erchova, I. A., Lebedev, M. A., & Diamond, M. E. (2002). Somatosensory cortical neuronal population activity across states of anaesthesia. *European Journal of Neuroscience*, *15*(4), 744–752. https://doi.org/https://doi.org/10.1046/j.0953-816x.2002.01898.x

Espinosa, J. S., & Stryker, M. P. (2012). Development and Plasticity of the Primary Visual Cortex. *Neuron*, *75*(2), 230–249. https://doi.org/https://doi.org/10.1016/j.neuron.2012.06.009

Fanselow, E. E., Richardson, K. A., & Connors, B. W. (2008). Selective, State-Dependent Activation of Somatostatin-Expressing Inhibitory Interneurons in Mouse Neocortex. *Journal of Neurophysiology*, *100*(5), 2640–2652. https://doi.org/10.1152/jn.90691.2008

Feldmeyer, D. (2012). Excitatory neuronal connectivity in the barrel cortex. *Frontiers in Neuroanatomy*, *6*, 24. https://doi.org/10.3389/fnana.2012.00024

Feldmeyer, D., Lübke, J., & Sakmann, B. (2006). Efficacy and connectivity of intracolumnar pairs of layer 2/3 pyramidal cells in the barrel cortex of juvenile rats. *The Journal of Physiology*, *575*(Pt 2), 583–602. https://doi.org/10.1113/jphysiol.2006.105106

Feldmeyer, D., Lübke, J., Silver, R. A., & Sakmann, B. (2002). Synaptic connections between layer 4 spiny neurone-layer 2/3 pyramidal cell pairs in juvenile rat barrel cortex: physiology and anatomy of interlaminar signalling within a cortical column. *The Journal of Physiology*, *538*(3), 803–822. https://doi.org/https://doi.org/10.1113/jphysiol.2001.012959

Fenno, L. E., Mattis, J., Ramakrishnan, C., Hyun, M., Lee, S. Y., He, M., Tucciarone, J., Selimbeyoglu, A., Berndt, A., Grosenick, L., Zalocusky, K. A., Bernstein, H., Swanson, H., Perry, C., Diester, I., Boyce, F. M., Bass, C. E., Neve, R., Huang, Z. J., & Deisseroth, K. (2014). Targeting cells with single vectors using multiple-feature Boolean logic. *Nature Methods*, *11*(7), 763–772. https://doi.org/10.1038/nmeth.2996

Ferguson, K. A., & Cardin, J. A. (2020). Mechanisms underlying gain modulation in the cortex. *Nature Reviews Neuroscience*, *21*(2), 80–92. https://doi.org/10.1038/s41583-019-0253-y

Fino, E., & Yuste, R. (2011). Dense Inhibitory Connectivity in Neocortex. *Neuron*, *69*(6), 1188–1203. https://doi.org/10.1016/j.neuron.2011.02.025

Földy, C., Darmanis, S., Aoto, J., Malenka, R. C., Quake, S. R., & Südhof, T. C. (2016). Single-cell RNAseq reveals cell adhesion molecule profiles in electrophysiologically defined neurons. *Proceedings of the National Academy of Sciences*, *113*(35), E5222 LP-E5231. https://doi.org/10.1073/pnas.1610155113

Frandolig, J. E., Matney, C. J., Lee, K., Kim, J., Chevée, M., Kim, S.-J., Bickert, A. A., & Brown, S. P. (2019). The Synaptic Organization of Layer 6 Circuits Reveals Inhibition as a Major Output of a Neocortical Sublamina. *Cell Reports*, *28*(12), 3131-3143.e5. https://doi.org/10.1016/j.celrep.2019.08.048

Franklin, K., & Paxinos, G. (2007). The Mouse Brain Atlas in Stereotaxic Coordinates. In *The Mouse Brain Atlas* (3rd ed., p. xv). Elsevier. https://doi.org/10.1016/B978-0-12-374247-6.50004-3

Gambino, F., Pagès, S., Kehayas, V., Baptista, D., Tatti, R., Carleton, A., & Holtmaat, A. (2014). Sensory-evoked LTP driven by dendritic plateau potentials in vivo. *Nature*, *515*(7525), 116–119. https://doi.org/10.1038/nature13664

Gao, W.-J., & Zheng, Z.-H. (2004). Target-specific differences in somatodendritic morphology of layer V pyramidal neurons in rat motor cortex. *Journal of Comparative Neurology*, *476*(2), 174–185. https://doi.org/10.1002/cne.20224

Gentet, L. (2012). Functional diversity of supragranular GABAergic neurons in the barrel cortex . In *Frontiers in Neural Circuits* (Vol. 6, p. 52). https://www.frontiersin.org/article/10.3389/fncir.2012.00052

Gentet, L. J., Avermann, M., Matyas, F., Staiger, J. F., & Petersen, C. C. H. (2010). Membrane Potential Dynamics of GABAergic Neurons in the Barrel Cortex of Behaving Mice. *Neuron*, *65*(3), 422–435. https://doi.org/10.1016/j.neuron.2010.01.006

Gerfen, C. R., Paletzki, R., & Heintz, N. (2013). GENSAT BAC Cre-Recombinase Driver Lines to Study the Functional Organization of Cerebral Cortical and Basal Ganglia Circuits. *Neuron*, *80*(6), 1368–1383. https://doi.org/https://doi.org/10.1016/j.neuron.2013.10.016

Gilbert, C. D. (1983). Microcircuitry of the Visual Cortex. *Annual Review of Neuroscience*, *6*(1), 217–247. https://doi.org/10.1146/annurev.ne.06.030183.001245

Gilbert, C. D., & Kelly, J. P. (1975). The projections of cells in different layers of the cat's visual cortex. *Journal of Comparative Neurology*, *163*(1), 81–105. https://doi.org/https://doi.org/10.1002/cne.901630106

Glickstein, M. (2006). Golgi and Cajal: The neuron doctrine and the 100th anniversary of the 1906 Nobel Prize. *Current Biology*, *16*(5), R147–R151.

Gong, S., Doughty, M., Harbaugh, C. R., Cummins, A., Hatten, M. E., Heintz, N., & Gerfen, C. R. (2007). Targeting Cre Recombinase to Specific Neuron Populations with Bacterial Artificial Chromosome Constructs. *The Journal of Neuroscience*, *27*(37), 9817 LP – 9823. http://www.jneurosci.org/content/27/37/9817.abstract

Gouwens, N. W., Sorensen, S. A., Berg, J., Lee, C., Jarsky, T., Ting, J., Sunkin, S. M., Feng, D., Anastassiou, C. A., Barkan, E., Bickley, K., Blesie, N., Braun, T., Brouner, K., Budzillo, A., Caldejon, S., Casper, T., Castelli, D., Chong, P., … Koch, C. (2019). Classification of electrophysiological and morphological neuron types in the mouse visual cortex. *Nature Neuroscience*, *22*(7), 1182–1195. https://doi.org/10.1038/s41593-019-0417-0

Guan, D., Armstrong, W. E., & Foehring, R. C. (2015). Electrophysiological properties of genetically identified subtypes of layer 5 neocortical pyramidal neurons: Ca2+ dependence and differential modulation by norepinephrine. *Journal of Neurophysiology*, *113*(7), 2014–2032. https://doi.org/10.1152/jn.00524.2014

Guillery, R. W., & Sherman, S. M. (2011). Branched thalamic afferents: What are the messages that they relay to the cortex? *Brain Research Reviews*, *66*(1), 205–219. https://doi.org/https://doi.org/10.1016/j.brainresrev.2010.08.001

Gunaydin, L. A., Yizhar, O., Berndt, A., Sohal, V. S., Deisseroth, K., & Hegemann, P. (2010). Ultrafast optogenetic control. *Nature Neuroscience*, *13*(3), 387–392. https://doi.org/10.1038/nn.2495

Guo, K., Yamawaki, N., Barrett, J. M., Tapies, M., & Shepherd, G. M. G. (2020). Cortico-Thalamo-Cortical Circuits of Mouse Forelimb S1 Are Organized Primarily as Recurrent Loops. *The Journal of Neuroscience*, *40*(14), 2849–2858. https://doi.org/10.1523/JNEUROSCI.2277-19.2020

Guy, J., & Staiger, J. F. (2017). The Functioning of a Cortex without Layers . In *Frontiers in Neuroanatomy* (Vol. 11, p. 54). https://www.frontiersin.org/article/10.3389/fnana.2017.00054

Hafner, G., Witte, M., Guy, J., Subhashini, N., Fenno, L. E., Ramakrishnan, C., Kim, Y. S., Deisseroth, K., Callaway, E. M., Oberhuber, M., Conzelmann, K. K., & Staiger, J. F. (2019). Mapping Brain-Wide Afferent Inputs of Parvalbumin-Expressing GABAergic Neurons in Barrel Cortex Reveals Local and Long-Range Circuit Motifs. *Cell Reports*, *28*(13), 3450-3461.e8. https://doi.org/10.1016/j.celrep.2019.08.064

Hardingham, N. R., Read, J. C. A., Trevelyan, A. J., Nelson, J. C., Jack, J. J. B., & Bannister, N. J. (2010). Quantal Analysis Reveals a Functional Correlation between Presynaptic and Postsynaptic Efficacy in Excitatory Connections from Rat Neocortex. *The Journal of Neuroscience*, *30*(4), 1441 LP – 1451. https://doi.org/10.1523/JNEUROSCI.3244-09.2010

Harris, K. D., & Mrsic-Flogel, T. D. (2013). Cortical connectivity and sensory coding. *Nature*, *503*(7474), 51–58. https://doi.org/10.1038/nature12654

Harris, K. D., & Shepherd, G. M. G. (2015). The neocortical circuit: themes and variations. *Nature Neuroscience*, *18*, 170. http://dx.doi.org/10.1038/nn.3917

Hattox, A. M., & Nelson, S. B. (2007a). Layer V Neurons in Mouse Cortex Projecting to Different Targets Have Distinct Physiological Properties. *Journal of Neurophysiology*, *98*(6), 3330–3340. https://doi.org/10.1152/jn.00397.2007

Hattox, A. M., & Nelson, S. B. (2007b). Layer V Neurons in Mouse Cortex Projecting to Different Targets Have Distinct Physiological Properties. *Journal of Neurophysiology*, *98*(6), 3330–3340. https://doi.org/10.1152/jn.00397.2007

Hawkins, J., Ahmad, S., & Cui, Y. (2017). A Theory of How Columns in the Neocortex Enable Learning the Structure of the World . In *Frontiers in Neural Circuits* (Vol. 11, p. 81). https://www.frontiersin.org/article/10.3389/fncir.2017.00081

Helmstaedter, M., Staiger, J. F., Sakmann, B., & Feldmeyer, D. (2008). Efficient Recruitment of Layer 2/3 Interneurons by Layer 4 Input in Single Columns of Rat Somatosensory Cortex. *The Journal of Neuroscience*, *28*(33), 8273 LP – 8284. https://doi.org/10.1523/JNEUROSCI.5701-07.2008

Hildebrandt, K. J., Sahani, M., & Linden, J. F. (2017). The Impact of Anesthetic State on Spike-Sorting Success in the Cortex: A Comparison of Ketamine and Urethane Anesthesia . In *Frontiers in Neural Circuits* (Vol. 11, p. 95). https://www.frontiersin.org/article/10.3389/fncir.2017.00095

Holmberg, J., & Perlmann, T. (2012). Maintaining differentiated cellular identity. *Nature Reviews Genetics*, *13*(6), 429–439. https://doi.org/10.1038/nrg3209

House, D. R. C., Elstrott, J., Koh, E., Chung, J., & Feldman, D. E. (2011). Parallel Regulation of Feedforward Inhibition and Excitation during Whisker Map Plasticity. *Neuron*, *72*(5), 819–831. https://doi.org/10.1016/j.neuron.2011.09.008

Hu, H., Gan, J., & Jonas, P. (2014). Fast-spiking, parvalbumin+ GABAergic interneurons: From cellular design to microcircuit function. *Science*, *345*(6196), 1255263–1255263. https://doi.org/10.1126/science.1255263

Hubel, D. H., & Wiesel, T. N. (1959). Receptive fields of single neurones in the cat's striate cortex. *The Journal of Physiology*, *148*(3), 574–591. https://doi.org/https://doi.org/10.1113/jphysiol.1959.sp006308

Hubel, D. H., & Wiesel, T. N. (1962). Receptive fields, binocular interaction and functional architecture in the cat's visual cortex. *The Journal of Physiology*, *160*(1), 106–154. https://doi.org/10.1113/jphysiol.1962.sp006837

Hubel, D. H., & Wiesel, T. N. (1977). Ferrier lecture. Functional architecture of macaque monkey visual cortex.

Proceedings of the Royal Society of London. Series B, Biological Sciences, *198*(1130), 1–59. https://doi.org/10.1098/rspb.1977.0085

Hull, C., Isaacson, J. S., & Scanziani, M. (2009). Postsynaptic Mechanisms Govern the Differential Excitation of Cortical Neurons by Thalamic Inputs. *The Journal of Neuroscience*, *29*(28), 9127 LP – 9136. https://doi.org/10.1523/JNEUROSCI.5971-08.2009

Inoue, T., & Imoto, K. (2006). Feedforward inhibitory connections from multiple thalamic cells to multiple regular-spiking cells in layer 4 of the somatosensory cortex. *Journal of Neurophysiology*, *96*(4), 1746–1754. https://doi.org/10.1152/jn.00301.2006

Isaacson, J. S., & Scanziani, M. (2011). How Inhibition Shapes Cortical Activity. *Neuron*, *72*(2), 231–243. https://doi.org/10.1016/j.neuron.2011.09.027

Ivanov, A., & Zilberter, Y. (2011). Critical state of energy metabolism in brain slices: the principal role of oxygen delivery and energy substrates in shaping neuronal activity. *Frontiers in Neuroenergetics*, *3*, 9. https://doi.org/10.3389/fnene.2011.00009

Jackson, J. H. (1867). Remarks on the disorderly movements of chorea and convulsion, and on localisation. *Med Times Gazette*, *2*, 669–670.

Jackson, J. H. (1868). Notes on the physiology and pathology of the nervous system. *Med Times Gaz*, *2*, 696.

Jouhanneau, J.-S., Kremkow, J., & Poulet, J. F. A. (2018). Single synaptic inputs drive high-precision action potentials in parvalbumin expressing GABA-ergic cortical neurons in vivo. *Nature Communications*, *9*(1), 1540. https://doi.org/10.1038/s41467-018-03995-2

Junyent, F., & Kremer, E. J. (2015). CAV-2 - Why a canine virus is a neurobiologist's best friend. *Current Opinion in Pharmacology*, *24*, 86–93. https://doi.org/10.1016/j.coph.2015.08.004

Kaas, J. H. (2011). Neocortex in early mammals and its subsequent variations. *Annals of the New York Academy of Sciences*, *1225*, 28–36. https://doi.org/10.1111/j.1749-6632.2011.05981.x

Kajikawa, Y., & Schroeder, C. E. (2011). How Local Is the Local Field Potential? *Neuron*, *72*(5), 847–858. https://doi.org/https://doi.org/10.1016/j.neuron.2011.09.029

Kampa, B. M., Letzkus, J. J., & Stuart, G. J. (2006). Cortical feed-forward networks for binding different streams of sensory information. *Nature Neuroscience*, *9*(12), 1472–1473. https://doi.org/10.1038/nn1798

Kandel, E. R., Schwartz, J. H., Jessell, T. M., Siegelbaum, S., & Hudspeth, A. J. (2013). *Principles of neural science* (5th ed.). McGraw-Hill.

Karnani, M. M., Agetsuma, M., & Yuste, R. (2014). A blanket of inhibition: functional inferences from dense inhibitory connectivity. *Current Opinion in Neurobiology*, *26*, 96–102. https://doi.org/https://doi.org/10.1016/j.conb.2013.12.015

Karnani, M. M., Jackson, J., Ayzenshtat, I., Hamzehei Sichani, A., Manoocheri, K., Kim, S., & Yuste, R. (2016). Opening Holes in the Blanket of Inhibition: Localized Lateral Disinhibition by VIP Interneurons. *The Journal of Neuroscience*, *36*(12), 3471 LP – 3480. https://doi.org/10.1523/JNEUROSCI.3646-15.2016

Kätzel, D., & Miesenböck, G. (2014). Experience-Dependent Rewiring of Specific Inhibitory Connections in Adult Neocortex. *PLoS Biology*, *12*(2), e1001798. https://doi.org/10.1371/journal.pbio.1001798

Kätzel, D., Zemelman, B. V, Buetfering, C., Wölfel, M., & Miesenböck, G. (2011). The columnar and laminar organization of inhibitory connections to neocortical excitatory cells. *Nature Neuroscience*, *14*(1), 100–107. https://doi.org/10.1038/nn.2687

Kawaguchi, Y, & Kubota, Y. (1996). Physiological and morphological identification of somatostatin- or vasoactive

intestinal polypeptide-containing cells among GABAergic cell subtypes in rat frontal cortex. *The Journal of Neuroscience : The Official Journal of the Society for Neuroscience*, *16*(8), 2701–2715. https://doi.org/10.1523/JNEUROSCI.16-08-02701.1996

Kawaguchi, Y, & Kubota, Y. (1997). GABAergic cell subtypes and their synaptic connections in rat frontal cortex. *Cerebral Cortex*, *7*(6), 476–486. https://doi.org/10.1093/cercor/7.6.476

Kawaguchi, Yasuo. (2017). Pyramidal Cell Subtypes and Their Synaptic Connections in Layer 5 of Rat Frontal Cortex. *Cerebral Cortex*, *27*(12), 5755–5771. https://doi.org/10.1093/cercor/bhx252

Keller, G. B., Bonhoeffer, T., & Hübener, M. (2012). Sensorimotor Mismatch Signals in Primary Visual Cortex of the Behaving Mouse. *Neuron*, *74*(5), 809–815. https://doi.org/10.1016/j.neuron.2012.03.040

Keller, G. B., & Mrsic-Flogel, T. D. (2018). Predictive Processing: A Canonical Cortical Computation. *Neuron*, *100*(2), 424–435. https://doi.org/10.1016/j.neuron.2018.10.003

Khubieh, A., Ratté, S., Lankarany, M., & Prescott, S. A. (2016). Regulation of Cortical Dynamic Range by Background Synaptic Noise and Feedforward Inhibition. *Cerebral Cortex*, *26*(8), 3357–3369. https://doi.org/10.1093/cercor/bhv157

Khurana, S., & Li, W.-K. (2013). Baptisms of fire or death knells for acute-slice physiology in the age of “omics” and light? *Reviews in the Neurosciences*, *24*, 527–536. https://doi.org/10.1515/revneuro-2013-0028

Killackey, H. P., Koralek, K.-A., Chiaia, N. L., & Rhoades, R. W. (1989). Laminar and areal differences in the origin of the subcortical projection neurons of the rat somatosensory cortex. *Journal of Comparative Neurology*, *282*(3), 428–445. https://doi.org/https://doi.org/10.1002/cne.902820309

Kim, E. J. J., Juavinett, A. L. L., Kyubwa, E. M. M., Jacobs, M. W. W., & Callaway, E. M. M. (2015). Three Types of Cortical Layer 5 Neurons That Differ in Brain-wide Connectivity and Function. *Neuron*, *88*(6), 1253–1267. https://doi.org/10.1016/j.neuron.2015.11.002

Kim, M.-H., Znamenskiy, P., Iacaruso, M. F., & Mrsic-Flogel, T. D. (2018). Segregated Subnetworks of Intracortical Projection Neurons in Primary Visual Cortex. *Neuron*, *100*(6), 1313-1321.e6. https://doi.org/10.1016/j.neuron.2018.10.023

Kim, T., Oh, W. C., Choi, J. H., & Kwon, H.-B. (2016). Emergence of functional subnetworks in layer 2/3 cortex induced by sequential spikes in vivo. *Proceedings of the National Academy of Sciences* , *113*(10), E1372–E1381. https://doi.org/10.1073/pnas.1513410113

Kiritani, T., Wickersham, I. R., Seung, H. S., & Shepherd, G. M. G. (2012). Hierarchical Connectivity and Connection-Specific Dynamics in the Corticospinal–Corticostriatal Microcircuit in Mouse Motor Cortex. *The Journal of Neuroscience*, *32*(14), 4992 LP – 5001. https://doi.org/10.1523/JNEUROSCI.4759-11.2012

Klapoetke, N. C., Murata, Y., Kim, S. S., Pulver, S. R., Birdsey-Benson, A., Cho, Y. K., Morimoto, T. K., Chuong, A. S., Carpenter, E. J., Tian, Z., Wang, J., Xie, Y., Yan, Z., Zhang, Y., Chow, B. Y., Surek, B., Melkonian, M., Jayaraman, V., Constantine-Paton, M., … Boyden, E. S. (2014). Independent optical excitation of distinct neural populations. *Nature Methods*, *11*(3), 338–346. https://doi.org/10.1038/nmeth.2836

Klausberger, T., & Somogyi, P. (2008). Neuronal diversity and temporal dynamics: the unity of hippocampal circuit operations. *Science (New York, N.Y.)*, *321*(5885), 53–57. https://doi.org/10.1126/science.1149381

Kremkow, J., Aertsen, A., & Kumar, A. (2010). Gating of Signal Propagation in Spiking Neural Networks by Balanced and Correlated Excitation and Inhibition. *The Journal of Neuroscience*, *30*(47), 15760 LP – 15768. https://doi.org/10.1523/JNEUROSCI.3874-10.2010

Kristensson, K., & Olsson, Y. (1971a). Uptake and retrograde axonal transport of peroxidase in hypoglossal neurones. *Acta Neuropathologica*, *19*(1), 1–9. https://doi.org/10.1007/BF00690948

Kristensson, K., & Olsson, Y. (1971b). Retrograde axonal transport of protein. *Brain Research*, *29*(2), 363–365. https://doi.org/10.1016/0006-8993(71)90044-8

Krook-Magnuson, E., Varga, C., Lee, S.-H., & Soltesz, I. (2012). New dimensions of interneuronal specialization unmasked by principal cell heterogeneity. *Trends in Neurosciences*, *35*(3), 175–184. https://doi.org/https://doi.org/10.1016/j.tins.2011.10.005

Kubota, Y. (2014). Untangling GABAergic wiring in the cortical microcircuit. *Current Opinion in Neurobiology*, *26*, 7–14. https://doi.org/10.1016/j.conb.2013.10.003

Kuśmierz, Ł., Isomura, T., & Toyoizumi, T. (2017). Learning with three factors: modulating Hebbian plasticity with errors. *Current Opinion in Neurobiology*, *46*, 170–177. https://doi.org/https://doi.org/10.1016/j.conb.2017.08.020

Lam, Y.-W., & Sherman, S. M. (2010). Functional organization of the somatosensory cortical layer 6 feedback to the thalamus. *Cerebral Cortex (New York, N.Y. : 1991)*, *20*(1), 13–24. https://doi.org/10.1093/cercor/bhp077

Lanciego, J. L., & Wouterlood, F. G. (2020). Neuroanatomical tract-tracing techniques that did go viral. In *Brain Structure and Function* (Vol. 225, Issue 4). Springer Berlin Heidelberg. https://doi.org/10.1007/s00429-020-02041-6

Larsen, Delaine D. (2008). Retrograde tracing with recombinant rabies virus reveals correlations between projection targets and dendritic architecture in layer 5 of mouse barrel cortex. *Frontiers in Neural Circuits*, *1*, 5. https://doi.org/10.3389/neuro.04.005.2007

Larsen, DeLaine D, & Callaway, E. M. (2006). Development of layer-specific axonal arborizations in mouse primary somatosensory cortex. *Journal of Comparative Neurology*, *494*(3), 398–414. https://doi.org/10.1002/cne.20754

Le Bé, J.-V., Silberberg, G., Wang, Y., & Markram, H. (2006). Morphological, Electrophysiological, and Synaptic Properties of Corticocallosal Pyramidal Cells in the Neonatal Rat Neocortex. *Cerebral Cortex*, *17*(9), 2204–2213. https://doi.org/10.1093/cercor/bhl127

Lee, S.-H., Kwan, A. C., Zhang, S., Phoumthipphavong, V., Flannery, J. G., Masmanidis, S. C., Taniguchi, H., Huang, Z. J., Zhang, F., Boyden, E. S., Deisseroth, K., & Dan, Y. (2012). Activation of specific interneurons improves V1 feature selectivity and visual perception. *Nature*, *488*(7411), 379–383. https://doi.org/10.1038/nature11312

Lee, SooHyun, Hjerling-Leffler, J., Zagha, E., Fishell, G., & Rudy, B. (2010). The largest group of superficial neocortical GABAergic interneurons expresses ionotropic serotonin receptors. *The Journal of Neuroscience : The Official Journal of the Society for Neuroscience*, *30*(50), 16796–16808. https://doi.org/10.1523/JNEUROSCI.1869-10.2010

Lee, Soohyun, Kruglikov, I., Huang, Z. J., Fishell, G., & Rudy, B. (2013). A disinhibitory circuit mediates motor integration in the somatosensory cortexLee, S., Kruglikov, I., Huang, Z. J., Fishell, G., & Rudy, B. (2013). A disinhibitory circuit mediates motor integration in the somatosensory cortex. Nature Neuroscience, 16(11). *Nature Neuroscience*, *16*(11), 1662–1670. https://doi.org/10.1038/nn.3544

Lefort, S., Tomm, C., Floyd Sarria, J.-C., & Petersen, C. C. H. (2009). The Excitatory Neuronal Network of the C2 Barrel Column in Mouse Primary Somatosensory Cortex. *Neuron*, *61*(2), 301–316. https://doi.org/10.1016/j.neuron.2008.12.020

Li, B., Nguyen, T. P., Ma, C., & Dan, Y. (2020). Inhibition of impulsive action by projection-defined prefrontal pyramidal neurons. *Proceedings of the National Academy of Sciences*, *117*(29), 17278 LP – 17287. https://doi.org/10.1073/pnas.2000523117

Lin, J. Y., Lin, M. Z., Steinbach, P., & Tsien, R. Y. (2009). Characterization of Engineered Channelrhodopsin Variants with Improved Properties and Kinetics. *Biophysical Journal*, *96*(5), 1803–1814. https://doi.org/10.1016/j.bpj.2008.11.034

Llinás, R. R. (2014). Intrinsic electrical properties of mammalian neurons and CNS function: a historical perspective . In *Frontiers in Cellular Neuroscience* (Vol. 8, p. 320). https://www.frontiersin.org/article/10.3389/fncel.2014.00320

Lodato, S., Rouaux, C., Quast, K. B., Jantrachotechatchawan, C., Studer, M., Hensch, T. K., & Arlotta, P. (2011). Excitatory Projection Neuron Subtypes Control the Distribution of Local Inhibitory Interneurons in the Cerebral Cortex. *Neuron*, *69*(4), 763–779. https://doi.org/10.1016/j.neuron.2011.01.015

Longair, M. H., Baker, D. A., & Armstrong, J. D. (2011). Simple Neurite Tracer: open source software for reconstruction, visualization and analysis of neuronal processes. *Bioinformatics*, *27*(17), 2453–2454. https://doi.org/10.1093/bioinformatics/btr390

Lőrincz, M. L., Gunner, D., Bao, Y., Connelly, W. M., Isaac, J. T. R., Hughes, S. W., & Crunelli, V. (2015). A Distinct Class of Slow (~0.2–2 Hz) Intrinsically Bursting Layer 5 Pyramidal Neurons Determines UP/DOWN State Dynamics in the Neocortex. *The Journal of Neuroscience*, *35*(14), 5442 LP – 5458. https://doi.org/10.1523/JNEUROSCI.3603-14.2015

Lu, S.-M., & Lin, R. C.-S. (1993). Thalamic Afferents of the Rat Barrel Cortex: A Light-and Electron-Microscopic Study Using Phaseolus vulgaris Leucoagglutinin as an Anterograde Tracer. *Somatosensory & Motor Research*, *10*(1), 1–16. https://doi.org/10.3109/08990229309028819

Lübke, J., Egger, V., Sakmann, B., & Feldmeyer, D. (2000). Columnar Organization of Dendrites and Axons of Single and Synaptically Coupled Excitatory Spiny Neurons in Layer 4 of the Rat Barrel Cortex. *The Journal of Neuroscience*, *20*(14), 5300 LP – 5311. https://doi.org/10.1523/JNEUROSCI.20-14-05300.2000

Ma, P. M. (1991). The barrelettes—architectonic vibrissal representations in the brainstem trigeminal complex of the mouse. Normal structural organization. *Journal of Comparative Neurology*, *309*(2), 161–199. https://doi.org/https://doi.org/10.1002/cne.903090202

Ma, Y. (2006). Distinct Subtypes of Somatostatin-Containing Neocortical Interneurons Revealed in Transgenic Mice. *Journal of Neuroscience*, *26*(19), 5069–5082. https://doi.org/10.1523/JNEUROSCI.0661-06.2006

Madisen, L., Mao, T., Koch, H., Zhuo, J., Berenyi, A., Fujisawa, S., Hsu, Y.-W. A., Garcia III, A. J., Gu, X., Zanella, S., Kidney, J., Gu, H., Mao, Y., Hooks, B. M., Boyden, E. S., Buzsáki, G., Ramirez, J. M., Jones, A. R., Svoboda, K., … Zeng, H. (2012). A toolbox of Cre-dependent optogenetic transgenic mice for light-induced activation and silencing. *Nature Neuroscience*, *15*, 793. http://dx.doi.org/10.1038/nn.3078

Madisen, L., Zwingman, T. A., Sunkin, S. M., Oh, S. W., Zariwala, H. A., Gu, H., Ng, L. L., Palmiter, R. D., Hawrylycz, M. J., Jones, A. R., Lein, E. S., & Zeng, H. (2010). A robust and high-throughput Cre reporting and characterization system for the whole mouse brain. *Nature Neuroscience*, *13*(1), 133–140. https://doi.org/10.1038/nn.2467

Mao, T., Kusefoglu, D., Hooks, B. M. M., Huber, D., Petreanu, L., & Svoboda, K. (2011). Long-Range Neuronal Circuits Underlying the Interaction between Sensory and Motor Cortex. *Neuron*, *72*(1), 111–123. https://doi.org/10.1016/j.neuron.2011.07.029

Marín, O., & Müller, U. (2014). Lineage origins of GABAergic versus glutamatergic neurons in the neocortex. *Current Opinion in Neurobiology*, *26*, 132–141. https://doi.org/10.1016/j.conb.2014.01.015

Markram, H., Toledo-Rodriguez, M., Wang, Y., Gupta, A., Silberberg, G., & Wu, C. (2004). Interneurons of the neocortical inhibitory system. *Nature Reviews Neuroscience*, *5*(10), 793–807. https://doi.org/10.1038/nrn1519

Mateo, C., Avermann, M., Gentet, L. J., Zhang, F., Deisseroth, K., & Petersen, C. C. H. (2011). In Vivo Optogenetic Stimulation of Neocortical Excitatory Neurons Drives Brain-State-Dependent Inhibition. *Current Biology*, *21*(19), 1593–1602. https://doi.org/10.1016/j.cub.2011.08.028

Matyas, F., Sreenivasan, V., Marbach, F., Wacongne, C., Barsy, B., Mateo, C., Aronoff, R., & Petersen, C. C. H. (2010). Motor Control by Sensory Cortex. *Science*, *330*(6008), 1240–1243. https://doi.org/10.1126/science.1195797

McClellan, A. M., & Twyman, R. E. (1999). Receptor system response kinetics reveal functional subtypes of native murine and recombinant human GABAA receptors. *The Journal of Physiology*, *515 (Pt 3*(Pt 3), 711–727. https://doi.org/10.1111/j.1469-7793.1999.711ab.x

McCormick, D. A., Connors, B. W., Lighthall, J. W., & Prince, D. A. (1985). Comparative electrophysiology of pyramidal and sparsely spiny stellate neurons of the neocortex. *Journal of Neurophysiology*, *54*(4), 782–806.

Mease, R. A., Sumser, A., Sakmann, B., & Groh, A. (2016a). Cortical Dependence of Whisker Responses in Posterior Medial Thalamus In Vivo. *Cerebral Cortex*, *26*(8), 3534–3543. https://doi.org/10.1093/cercor/bhw144

Mease, R. A., Sumser, A., Sakmann, B., & Groh, A. (2016b). Corticothalamic Spike Transfer via the L5B-POm Pathway in vivo. *Cerebral Cortex*, *26*(8), 3461–3475. https://doi.org/10.1093/cercor/bhw123

Meinecke, D. L., & Peters, A. (1987). GABA immunoreactive neurons in rat visual cortex. *The Journal of Comparative Neurology*, *261*(3), 388–404. https://doi.org/10.1002/cne.902610305

Meng, X., Solarana, K., Bowen, Z., Liu, J., Nagode, D. A., Sheikh, A., Winkowski, D. E., Kao, J. P. Y., & Kanold, P. O. (2020). Transient Subgranular Hyperconnectivity to L2/3 and Enhanced Pairwise Correlations During the Critical Period in the Mouse Auditory Cortex. *Cerebral Cortex*, *30*(3), 1914–1930. https://doi.org/10.1093/cercor/bhz213

Meng, X., Winkowski, D. E., Kao, J. P. Y., & Kanold, P. O. (2017). Sublaminar Subdivision of Mouse Auditory Cortex Layer 2/3 Based on Functional Translaminar Connections. *The Journal of Neuroscience*, *37*(42), 10200–10214. https://doi.org/10.1523/JNEUROSCI.1361-17.2017

Meyer, H. S., Schwarz, D., Wimmer, V. C., Schmitt, A. C., Kerr, J. N. D., Sakmann, B., & Helmstaedter, M. (2011). Inhibitory interneurons in a cortical column form hot zones of inhibition in layers 2 and 5A. *Proceedings of the National Academy of Sciences*, *108*(40), 16807 LP – 16812. https://doi.org/10.1073/pnas.1113648108

Mi, D., Li, Z., Lim, L., Li, M., Moissidis, M., Yang, Y., Gao, T., Hu, T. X., Pratt, T., Price, D. J., Sestan, N., & Marín, O. (2018). Early emergence of cortical interneuron diversity in the mouse embryo. *Science*, *360*(6384), 81 LP – 85. https://doi.org/10.1126/science.aar6821

Miles, R. (1990). Synaptic excitation of inhibitory cells by single CA3 hippocampal pyramidal cells of the guinea-pig in vitro. *The Journal of Physiology*, *428*(1), 61–77. https://doi.org/https://doi.org/10.1113/jphysiol.1990.sp018200

Mitchell, S. J., & Silver, R. A. (2003). Shunting inhibition modulates neuronal gain during synaptic excitation. *Neuron*, *38*(3), 433–445.

Miyoshi, G., Hjerling-Leffler, J., Karayannis, T., Sousa, V. H., Butt, S. J. B., Battiste, J., Johnson, J. E., Machold, R. P., & Fishell, G. (2010). Genetic Fate Mapping Reveals That the Caudal Ganglionic Eminence Produces a Large and Diverse Population of Superficial Cortical Interneurons. *The Journal of Neuroscience*, *30*(5), 1582 LP – 1594. https://doi.org/10.1523/JNEUROSCI.4515-09.2010

Mo, C., & Sherman, S. M. (2019). A Sensorimotor Pathway via Higher-Order Thalamus. *The Journal of Neuroscience*, *39*(4), 692–704. https://doi.org/10.1523/JNEUROSCI.1467-18.2018

Molyneaux, B. J., Arlotta, P., Menezes, J. R. L., & Macklis, J. D. (2007). Neuronal subtype specification in the cerebral cortex. *Nature Reviews Neuroscience*, *8*(6), 427–437. https://doi.org/10.1038/nrn2151

Monier, C., Chavane, F., Baudot, P., Graham, L. J., & Frégnac, Y. (2003). Orientation and Direction Selectivity of Synaptic Inputs in Visual Cortical Neurons: A Diversity of Combinations Produces Spike Tuning. *Neuron*, *37*(4), 663–680. https://doi.org/10.1016/S0896-6273(03)00064-3

Moore, A. K., Weible, A. P., Balmer, T. S., Trussell, L. O., & Wehr, M. (2018). Rapid Rebalancing of Excitation and Inhibition by Cortical Circuitry. *Neuron*, *97*(6), 1341-1355.e6. https://doi.org/10.1016/j.neuron.2018.01.045

Morishima, M., & Kawaguchi, Y. (2006). Recurrent Connection Patterns of Corticostriatal Pyramidal Cells in Frontal Cortex. *The Journal of Neuroscience*, *26*(16), 4394 LP – 4405.

http://www.jneurosci.org/content/26/16/4394.abstract

Mountcastle, V. B. (1957). Modality and Topographic properties of single neurons of cat's somatic sensory cortex. *Journal of Neurophysiology*, *20*(4), 408–434.

Mountcastle, V. B. (1997). The columnar organization of the neocortex. *Brain: A Journal of Neurology*, *120*(4), 701–722.

Muñoz, W., Tremblay, R., Levenstein, D., & Rudy, B. (2017). Layer-specific modulation of neocortical dendritic inhibition during active wakefulness. *Science*, *355*(6328), 954–959. https://doi.org/10.1126/science.aag2599

Nagel, G., Szellas, T., Huhn, W., Kateriya, S., Adeishvili, N., Berthold, P., Ollig, D., Hegemann, P., & Bamberg, E. (2003). Channelrhodopsin-2, a directly light-gated cation-selective membrane channel. *Proceedings of the National Academy of Sciences of the United States of America*, *100*(24), 13940–13945. https://doi.org/10.1073/pnas.1936192100

Naka, A., & Adesnik, H. (2016). Inhibitory Circuits in Cortical Layer 5 . In *Frontiers in Neural Circuits* (Vol. 10, p. 35). https://www.frontiersin.org/article/10.3389/fncir.2016.00035

Narayanan, R. T., Udvary, D., & Oberlaender, M. (2017). Cell Type-Specific Structural Organization of the Six Layers in Rat Barrel Cortex. *Frontiers in Neuroanatomy*, *11*. https://doi.org/10.3389/fnana.2017.00091

Nieus, T. R., Mapelli, L., & D'Angelo, E. (2014). Regulation of output spike patterns by phasic inhibition in cerebellar granule cells . In *Frontiers in Cellular Neuroscience* (Vol. 8, p. 246). https://www.frontiersin.org/article/10.3389/fncel.2014.00246

Nigro, M. J., Hashikawa-Yamasaki, Y., & Rudy, B. (2018). Diversity and Connectivity of Layer 5 Somatostatin-Expressing Interneurons in the Mouse Barrel Cortex. *The Journal of Neuroscience*, *38*(7), 1622 LP – 1633. https://doi.org/10.1523/JNEUROSCI.2415-17.2017

O'Connor, D. H., Peron, S. P., Huber, D., & Svoboda, K. (2010). Neural Activity in Barrel Cortex Underlying Vibrissa-Based Object Localization in Mice. *Neuron*, *67*(6), 1048–1061. https://doi.org/10.1016/j.neuron.2010.08.026

Oberlaender, M., Boudewijns, Z. S. R. M., Kleele, T., Mansvelder, H. D., Sakmann, B., & de Kock, C. P. J. (2011). Three-dimensional axon morphologies of individual layer 5 neurons indicate cell type-specific intracortical pathways for whisker motion and touch. *Proceedings of the National Academy of Sciences*, *108*(10), 4188–4193. https://doi.org/10.1073/pnas.1100647108

Okun, M., & Lampl, I. (2008). Instantaneous correlation of excitation and inhibition during ongoing and sensory-evoked activities. *Nature Neuroscience*, *11*(5), 535–537. https://doi.org/10.1038/nn.2105

Okun, M., Steinmetz, N. A., Cossell, L., Iacaruso, M. F., Ko, H., Barthó, P., Moore, T., Hofer, S. B., Mrsic-Flogel, T. D., Carandini, M., & Harris, K. D. (2015). Diverse coupling of neurons to populations in sensory cortex. *Nature*, *521*(7553), 511–515. https://doi.org/10.1038/nature14273

Olsen, S. R., Bortone, D. S., Adesnik, H., & Scanziani, M. (2012). Gain control by layer six in cortical circuits of vision. *Nature*, *483*(7387), 47–52. https://doi.org/10.1038/nature10835

Oswald, M., Tantirigama, M., Sonntag, I., Hughes, S., & Empson, R. (2013). Diversity of layer 5 projection neurons in the mouse motor cortex. In *Frontiers in Cellular Neuroscience* (Vol. 7, p. 174). https://www.frontiersin.org/article/10.3389/fncel.2013.00174

Pachitariu, M, Steinmetz, N., Kadir, S., Carandini, M., & Harris, K. (2016). *Fast and accurate spike sorting of high-channel count probes with KiloSort*.

Pachitariu, Marius, Lyamzin, D. R., Sahani, M., & Lesica, N. A. (2015). State-Dependent Population Coding in Primary Auditory Cortex. *The Journal of Neuroscience*, *35*(5), 2058 LP – 2073. https://doi.org/10.1523/JNEUROSCI.3318-14.2015

Packer, A. M., & Yuste, R. (2011). Dense, Unspecific Connectivity of Neocortical Parvalbumin-Positive Interneurons: A Canonical Microcircuit for Inhibition? *The Journal of Neuroscience*, *31*(37), 13260 LP – 13271. https://doi.org/10.1523/JNEUROSCI.3131-11.2011

Paul, A., Crow, M., Raudales, R., He, M., Gillis, J., & Huang, Z. J. (2017). Transcriptional Architecture of Synaptic Communication Delineates GABAergic Neuron Identity. *Cell*, *171*(3), 522-539.e20. https://doi.org/10.1016/j.cell.2017.08.032

Pauzin, F. P., Schwarz, N., & Krieger, P. (2019). Activation of Corticothalamic Layer 6 Cells Decreases Angular Tuning in Mouse Barrel Cortex . In *Frontiers in Neural Circuits* (Vol. 13, p. 67). https://www.frontiersin.org/article/10.3389/fncir.2019.00067

Petersen, C. C. H. (2007). The Functional Organization of the Barrel Cortex. *Neuron*, *56*(2), 339–355. https://doi.org/10.1016/j.neuron.2007.09.017

Petersen, C. C. H. (2019). Sensorimotor processing in the rodent barrel cortex. *Nature Reviews Neuroscience*, *20*(9), 533–546. https://doi.org/10.1038/s41583-019-0200-y

Petersen, C. C. H., & Crochet, S. (2013). Synaptic Computation and Sensory Processing in Neocortical Layer 2/3. *Neuron*, *78*(1), 28–48. https://doi.org/10.1016/j.neuron.2013.03.020

Petreanu, L., Huber, D., Sobczyk, A., & Svoboda, K. (2007). Channelrhodopsin-2–assisted circuit mapping of long-range callosal projections. *Nature Neuroscience*, *10*, 663. https://doi.org/10.1038/nn1891

Petreanu, L., Mao, T., Sternson, S. M., & Svoboda, K. (2009). The subcellular organization of neocortical excitatory connections. *Nature*, *457*, 1142. http://dx.doi.org/10.1038/nature07709

Pfeffer, C. K., Xue, M., He, M., Huang, Z. J., & Scanziani, M. (2013). Inhibition of inhibition in visual cortex: the logic of connections between molecularly distinct interneurons. *Nature Neuroscience*, *16*(8), 1068–1076. https://doi.org/10.1038/nn.3446

Pi, H.-J., Hangya, B., Kvitsiani, D., Sanders, J. I., Huang, Z. J., & Kepecs, A. (2013). Cortical interneurons that specialize in disinhibitory control. *Nature*, *503*(7477), 521–524. https://doi.org/10.1038/nature12676

Pierret, T., Lavallée, P., & Deschênes, M. (2000). Parallel Streams for the Relay of Vibrissal Information through Thalamic Barreloids. *The Journal of Neuroscience*, *20*(19), 7455 LP – 7462. https://doi.org/10.1523/JNEUROSCI.20-19-07455.2000

Piersanti, S., Astrologo, L., Licursi, V., Costa, R., Roncaglia, E., Gennetier, A., Ibanes, S., Chillon, M., Negri, R., Tagliafico, E., Kremer, E. J., & Saggio, I. (2013). Differentiated Neuroprogenitor Cells Incubated with Human or Canine Adenovirus, or Lentiviral Vectors Have Distinct Transcriptome Profiles. *PLOS ONE*, *8*(7), e69808. https://doi.org/10.1371/journal.pone.0069808

Pouille, F., Marin-Burgin, A., Adesnik, H., Atallah, B. V, & Scanziani, M. (2009). Input normalization by global feedforward inhibition expands cortical dynamic range. *Nature Neuroscience*, *12*(12), 1577–1585. https://doi.org/10.1038/nn.2441

Pouille, F., & Scanziani, M. (2001). Enforcement of Temporal Fidelity in Pyramidal Cells by Somatic Feed-Forward Inhibition. *Science*, *293*(5532), 1159 LP – 1163. https://doi.org/10.1126/science.1060342

Pouille, F., & Scanziani, M. (2004). Routing of spike series by dynamic circuits in the hippocampus. *Nature*, *429*(6993), 717–723. https://doi.org/10.1038/nature02615

Quiroga, R. Q., Nadasdy, Z., & Ben-Shaul, Y. (2004). Unsupervised spike detection and sorting with wavelets and superparamagnetic clustering. *Neural Computation*, *16*(8), 1661–1687. https://doi.org/10.1162/089976604774201631

Ramaswamy, S., & Markram, H. (2015). Anatomy and physiology of the thick-tufted layer 5 pyramidal neuron.

Frontiers in Cellular Neuroscience, *9*, 233. https://doi.org/10.3389/fncel.2015.00233

Ranjbar-Slamloo, Y., & Arabzadeh, E. (2016). High-velocity stimulation evokes “dense” population response in layer 2/3 vibrissal cortex. *Journal of Neurophysiology*, *117*(3), 1218–1228. https://doi.org/10.1152/jn.00815.2016

Reardon, T. R., Murray, A. J., Turi, G. F., Wirblich, C., Croce, K. R., Schnell, M. J., Jessell, T. M., & Losonczy, A. (2016). Rabies Virus CVS-N2cΔG Strain Enhances Retrograde Synaptic Transfer and Neuronal Viability. *Neuron*, *89*(4), 711–724. https://doi.org/https://doi.org/10.1016/j.neuron.2016.01.004

Reyes-Puerta, V., Sun, J.-J., Kim, S., Kilb, W., & Luhmann, H. J. (2015). Laminar and Columnar Structure of Sensory-Evoked Multineuronal Spike Sequences in Adult Rat Barrel Cortex In Vivo. *Cerebral Cortex*, *25*(8), 2001–2021. https://doi.org/10.1093/cercor/bhu007

Reyes, A., & Sakmann, B. (1999). Developmental Switch in the Short-Term Modification of Unitary EPSPs Evoked in Layer 2/3 and Layer 5 Pyramidal Neurons of Rat Neocortex. *The Journal of Neuroscience*, *19*(10), 3827 LP – 3835. https://doi.org/10.1523/JNEUROSCI.19-10-03827.1999

Rice, M. E. (1999). Use of Ascorbate in the Preparation and Maintenance of Brain Slices. *Methods*, *18*(2), 144–149. https://doi.org/https://doi.org/10.1006/meth.1999.0767

Riedemann, T. (2019). Diversity and Function of Somatostatin-Expressing Interneurons in the Cerebral Cortex. *International Journal of Molecular Sciences*, *20*(12), 2952. https://doi.org/10.3390/ijms20122952

Robinson, R. B., & Siegelbaum, S. A. (2003). Hyperpolarization-Activated Cation Currents: From Molecules to Physiological Function. *Annual Review of Physiology*, *65*(1), 453–480. https://doi.org/10.1146/annurev.physiol.65.092101.142734

Rojas-Piloni, G., Guest, J. M., Egger, R., Johnson, A. S., Sakmann, B., & Oberlaender, M. (2017). Relationships between structure, in vivo function and long-range axonal target of cortical pyramidal tract neurons. *Nature Communications*, *8*(1), 870. https://doi.org/10.1038/s41467-017-00971-0

Roth, B. L. (2016). DREADDs for Neuroscientists. *Neuron*, *89*(4), 683–694. https://doi.org/10.1016/j.neuron.2016.01.040

Roux, L., & Buzsáki, G. (2015). Tasks for inhibitory interneurons in intact brain circuits. *Neuropharmacology*, *88*, 10–23. https://doi.org/https://doi.org/10.1016/j.neuropharm.2014.09.011

Rudy, B., Fishell, G., Lee, S., & Hjerling-Leffler, J. (2011). Three groups of interneurons account for nearly 100% of neocortical GABAergic neurons. *Developmental Neurobiology*, *71*(1), 45–61. https://doi.org/10.1002/dneu.20853

Sakata, S., & Harris, K. D. (2009). Laminar structure of spontaneous and sensory-evoked population activity in auditory cortex. *Neuron*, *64*(3), 404–418. https://doi.org/10.1016/j.neuron.2009.09.020

Scala, F., Kobak, D., Bernabucci, M., Bernaerts, Y., Cadwell, C. R., Castro, J. R., Hartmanis, L., Jiang, X., Laturnus, S., Miranda, E., Mulherkar, S., Tan, Z. H., Yao, Z., Zeng, H., Sandberg, R., Berens, P., & Tolias, A. S. (2020). Phenotypic variation of transcriptomic cell types in mouse motor cortex. *Nature*. https://doi.org/10.1038/s41586-020-2907-3

Schindelin, J., Arganda-Carreras, I., Frise, E., Kaynig, V., Longair, M., Pietzsch, T., Preibisch, S., Rueden, C., Saalfeld, S., Schmid, B., Tinevez, J.-Y., White, D. J., Hartenstein, V., Eliceiri, K., Tomancak, P., & Cardona, A. (2012). Fiji: an open-source platform for biological-image analysis. *Nature Methods*, *9*(7), 676–682. https://doi.org/10.1038/nmeth.2019

Schmued, L. C., & Fallon, J. H. (1986). Fluoro-gold: a new fluorescent retrograde axonal tracer with numerous unique properties. *Brain Research*, *377*(1), 147–154. https://doi.org/10.1016/0006-8993(86)91199-6

Schneider, D. M., Nelson, A., & Mooney, R. (2014). A synaptic and circuit basis for corollary discharge in the auditory

cortex. *Nature*, *513*(7517), 189–194. https://doi.org/10.1038/nature13724

Schnell, M. J., McGettigan, J. P., Wirblich, C., & Papaneri, A. (2010). The cell biology of rabies virus: using stealth to reach the brain. *Nature Reviews Microbiology*, *8*(1), 51–61. https://doi.org/10.1038/nrmicro2260

Schoonover, C. E., Tapia, J. C., Schilling, V. C., Wimmer, V., Blazeski, R., Zhang, W., Mason, C. A., & Bruno, R. M. (2014). Comparative strength and dendritic organization of thalamocortical and corticocortical synapses onto excitatory layer 4 neurons. *Journal of Neuroscience*, *34*(20), 6746–6758. https://doi.org/10.1523/JNEUROSCI.0305-14.2014

Schubert, D, Kötter, R., Luhmann, H. J., & Staiger, J. F. (2006). Morphology, Electrophysiology and Functional Input Connectivity of Pyramidal Neurons Characterizes a Genuine Layer Va in the Primary Somatosensory Cortex. *Cerebral Cortex*, *16*(2), 223–236. https://doi.org/10.1093/cercor/bhi100

Schubert, Dirk, Kötter, R., Zilles, K., Luhmann, H. J., & Staiger, J. F. (2003). Cell Type-Specific Circuits of Cortical Layer IV Spiny Neurons. *The Journal of Neuroscience*, *23*(7), 2961 LP – 2970. https://doi.org/10.1523/JNEUROSCI.23-07-02961.2003

Schubert, Dirk, Staiger, J. F., Cho, N., Kötter, R., Zilles, K., & Luhmann, H. J. (2001). Layer-Specific Intracolumnar and Transcolumnar Functional Connectivity of Layer V Pyramidal Cells in Rat Barrel Cortex. *The Journal of Neuroscience*, *21*(10), 3580 LP – 3592. https://doi.org/10.1523/JNEUROSCI.21-10-03580.2001

Sellers, K. K., Bennett, D. V, Hutt, A., Williams, J. H., & Fröhlich, F. (2015). Awake vs. anesthetized: layer-specific sensory processing in visual cortex and functional connectivity between cortical areas. *Journal of Neurophysiology*, *113*(10), 3798–3815. https://doi.org/10.1152/jn.00923.2014

Sempere-Ferràndez, A., Martínez, S., & Geijo-Barrientos, E. (2019). Synaptic mechanisms underlying the intense firing of neocortical layer 5B pyramidal neurons in response to cortico-cortical inputs. *Brain Structure and Function*, *224*(4), 1403–1416. https://doi.org/10.1007/s00429-019-01842-8

Sengupta, B., Laughlin, S. B., & Niven, J. E. (2013). Balanced excitatory and inhibitory synaptic currents promote efficient coding and metabolic efficiency. *PLoS Computational Biology*, *9*(10), e1003263–e1003263. https://doi.org/10.1371/journal.pcbi.1003263

Sermet, B. S., Truschow, P., Feyerabend, M., Mayrhofer, J. M., Oram, T. B., Yizhar, O., Staiger, J. F., & Petersen, C. C. (2019). Pathway-, layer- and cell-type-specific thalamic input to mouse barrel cortex. *ELife*, *8*. https://doi.org/10.7554/eLife.52665

Seung, H. S., & Sümbül, U. (2014). Neuronal Cell Types and Connectivity: Lessons from the Retina. *Neuron*, *83*(6), 1262–1272. https://doi.org/https://doi.org/10.1016/j.neuron.2014.08.054

Shepherd, G. M. G., & Svoboda, K. (2005). Laminar and columnar organization of ascending excitatory projections to layer 2/3 pyramidal neurons in rat barrel cortex. *The Journal of Neuroscience : The Official Journal of the Society for Neuroscience*, *25*(24), 5670–5679. https://doi.org/10.1523/JNEUROSCI.1173-05.2005

Sherman, S. M. (2007). THE THALAMUS IS MORE THAN JUST A RELAY. *Current Opinion in Neurobiology*, *17*(4), 417–422. https://doi.org/10.1016/j.conb.2007.07.003

Sherman, S. M. (2016). Thalamus plays a central role in ongoing cortical functioning. In *Nature Neuroscience*. https://doi.org/10.1038/nn.4269

Sherman, S. M., & Guillery, R. W. (1998). On the actions that one nerve cell can have on another: Distinguishing "drivers" from "modulators." *Proceedings of the National Academy of Sciences of the United States of America*. https://doi.org/10.1073/pnas.95.12.7121

Sherman, S. M., & Guillery, R. W. (2011). Distinct functions for direct and transthalamic corticocortical connections. *Journal of Neurophysiology*, *106*(3), 1068–1077. https://doi.org/10.1152/jn.00429.2011

Silberberg, G., & Markram, H. (2007). Disynaptic Inhibition between Neocortical Pyramidal Cells Mediated by Martinotti Cells. *Neuron*, *53*(5), 735–746. https://doi.org/10.1016/j.neuron.2007.02.012

Simão, D., Pinto, C., Fernandes, P., Peddie, C. J., Piersanti, S., Collinson, L. M., Salinas, S., Saggio, I., Schiavo, G., Kremer, E. J., Brito, C., & Alves, P. M. (2016). Evaluation of helper-dependent canine adenovirus vectors in a 3D human CNS model. *Gene Therapy*, *23*(1), 86–94. https://doi.org/10.1038/gt.2015.75

Simons, D. J. (1978). Response properties of vibrissa units in rat SI somatosensory neocortex. *Journal of Neurophysiology*, *41*(3), 798–820. https://doi.org/10.1152/jn.1978.41.3.798

Somogyi, P., & Klausberger, T. (2005). Defined types of cortical interneurone structure space and spike timing in the hippocampus. *The Journal of Physiology*, *562*(Pt 1), 9–26. https://doi.org/10.1113/jphysiol.2004.078915

Staiger, J. F., Bojak, I., Miceli, S., & Schubert, D. (2015). A gradual depth-dependent change in connectivity features of supragranular pyramidal cells in rat barrel cortex. *Brain Structure and Function*, *220*(3), 1317–1337. https://doi.org/10.1007/s00429-014-0726-8

Staiger, J. F., Loucif, A. J. C., Schubert, D., & Möck, M. (2016). Morphological Characteristics of Electrophysiologically Characterized Layer Vb Pyramidal Cells in Rat Barrel Cortex. *PLOS ONE*, *11*(10), e0164004. https://doi.org/10.1371/journal.pone.0164004

Staiger, J. F., Masanneck, C., Schleicher, A., & Zuschratter, W. (2004). Calbindin-containing interneurons are a target for VIP-immunoreactive synapses in rat primary somatosensory cortex. *The Journal of Comparative Neurology*, *468*(2), 179–189. https://doi.org/10.1002/cne.10953

Stokes, C. C. A., & Isaacson, J. S. (2010). From dendrite to soma: dynamic routing of inhibition by complementary interneuron microcircuits in olfactory cortex. *Neuron*, *67*(3), 452–465. https://doi.org/10.1016/j.neuron.2010.06.029

Swadlow, H. A. (2003). Fast-spike Interneurons and Feedforward Inhibition in Awake Sensory Neocortex. *Cerebral Cortex*, *13*(1), 25–32. https://doi.org/10.1093/cercor/13.1.25

Swadlow, H. A., & Gusev, A. G. (2002). Receptive-field construction in cortical inhibitory interneurons. *Nature Neuroscience*, *5*(5), 403–404. https://doi.org/10.1038/nn847

Swanson, O. K., & Maffei, A. (2019). From Hiring to Firing: Activation of Inhibitory Neurons and Their Recruitment in Behavior. *Frontiers in Molecular Neuroscience*, *12*, 168. https://doi.org/10.3389/fnmol.2019.00168

Tai, Y., Gallo, N. B., Wang, M., Yu, J.-R., & Van Aelst, L. (2019). Axo-axonic Innervation of Neocortical Pyramidal Neurons by GABAergic Chandelier Cells Requires AnkyrinG-Associated L1CAM. *Neuron*, *102*(2), 358-372.e9. https://doi.org/10.1016/j.neuron.2019.02.009

Takahashi, N., Ebner, C., Sigl-Glöckner, J., Moberg, S., Nierwetberg, S., & Larkum, M. E. (2020). Active dendritic currents gate descending cortical outputs in perception. *Nature Neuroscience*, *23*(10), 1277–1285. https://doi.org/10.1038/s41593-020-0677-8

Tan, A. Y. Y., Zhang, L. I., Merzenich, M. M., & Schreiner, C. E. (2004). Tone-Evoked Excitatory and Inhibitory Synaptic Conductances of Primary Auditory Cortex Neurons. *Journal of Neurophysiology*, *92*(1), 630–643. https://doi.org/10.1152/jn.01020.2003

Tang, L., & Higley, M. J. (2020). Layer 5 Circuits in V1 Differentially Control Visuomotor Behavior. *Neuron*, *105*(2), 346-354.e5. https://doi.org/10.1016/j.neuron.2019.10.014

Taniguchi, H., He, M., Wu, P., Kim, S., Paik, R., Sugino, K., Kvitsani, D., Fu, Y., Lu, J., Lin, Y., Miyoshi, G., Shima, Y., Fishell, G., Nelson, S. B., & Huang, Z. J. (2011). A Resource of Cre Driver Lines for Genetic Targeting of GABAergic Neurons in Cerebral Cortex. *Neuron*, *71*(6), 995–1013. https://doi.org/10.1016/j.neuron.2011.07.026

Tanke, N., Borst, J. G. G., & Houweling, A. R. (2018). Single-Cell Stimulation in Barrel Cortex Influences Psychophysical

Detection Performance. *The Journal of Neuroscience*, *38*(8), 2057 LP – 2068. https://doi.org/10.1523/JNEUROSCI.2155-17.2018

Tasic, B., Menon, V., Nguyen, T. N., Kim, T. K., Jarsky, T., Yao, Z., Levi, B., Gray, L. T., Sorensen, S. A., Dolbeare, T., Bertagnolli, D., Goldy, J., Shapovalova, N., Parry, S., Lee, C., Smith, K., Bernard, A., Madisen, L., Sunkin, S. M., … Zeng, H. (2016). Adult mouse cortical cell taxonomy revealed by single cell transcriptomics. *Nature Neuroscience*, *19*(2), 335–346. https://doi.org/10.1038/nn.4216

Tasic, B., Yao, Z., Graybuck, L. T., Smith, K. A., Nguyen, T. N., Bertagnolli, D., Goldy, J., Garren, E., Economo, M. N., Viswanathan, S., Penn, O., Bakken, T., Menon, V., Miller, J., Fong, O., Hirokawa, K. E., Lathia, K., Rimorin, C., Tieu, M., … Zeng, H. (2018). Shared and distinct transcriptomic cell types across neocortical areas. *Nature*, *563*(7729), 72–78. https://doi.org/10.1038/s41586-018-0654-5

Tervo, D. G. R., Hwang, B.-Y., Viswanathan, S., Gaj, T., Lavzin, M., Ritola, K. D., Lindo, S., Michael, S., Kuleshova, E., Ojala, D., Huang, C.-C., Gerfen, C. R., Schiller, J., Dudman, J. T., Hantman, A. W., Looger, L. L., Schaffer, D. V., & Karpova, A. Y. (2016). A Designer AAV Variant Permits Efficient Retrograde Access to Projection Neurons. *Neuron*, *92*(2), 1–11. https://doi.org/10.1016/j.neuron.2016.09.021

Thomson, A. M., & Bannister, A. P. (2003). Interlaminar Connections in the Neocortex. *Cerebral Cortex*, *13*(1), 5–14. https://doi.org/10.1093/cercor/13.1.5

Ting, J. T., Lee, B. R., Chong, P., Soler-Llavina, G., Cobbs, C., Koch, C., Zeng, H., & Lein, E. (2018). Preparation of Acute Brain Slices Using an Optimized N-Methyl-D-glucamine Protective Recovery Method. *Journal of Visualized Experiments : JoVE*, *132*, 53825. https://doi.org/10.3791/53825

Tremblay, R., Lee, S., & Rudy, B. (2016). GABAergic Interneurons in the Neocortex: From Cellular Properties to Circuits. *Neuron*, *91*(2), 260–292. https://doi.org/10.1016/j.neuron.2016.06.033

van Aerde, K. I., & Feldmeyer, D. (2015). Morphological and Physiological Characterization of Pyramidal Neuron Subtypes in Rat Medial Prefrontal Cortex. *Cerebral Cortex*, *25*(3), 788–805. https://doi.org/10.1093/cercor/bht278

Van der Loos, H., & Woolsey, T. A. (1973). Somatosensory cortex: structural alterations following early injury to sense organs. *Science*, *179*(4071), 395–398.

Vecchia, D., Beltramo, R., Vallone, F., Chéreau, R., Forli, A., Molano-Mazón, M., Bawa, T., Binini, N., Moretti, C., Holtmaat, A., Panzeri, S., & Fellin, T. (2020). Temporal Sharpening of Sensory Responses by Layer V in the Mouse Primary Somatosensory Cortex. *Current Biology : CB*, *30*(9), 1589-1599.e10. https://doi.org/10.1016/j.cub.2020.02.004

Veinante, P., Jacquin, M. F., & Deschênes, M. (2000). Thalamic projections from the whisker-sensitive regions of the spinal trigeminal complex in the rat. *Journal of Comparative Neurology*, *420*(2), 233–243. https://doi.org/https://doi.org/10.1002/(SICI)1096-9861(20000501)420:2<233::AID-CNE6>3.0.CO;2-T

Wang, Y., Toledo-Rodriguez, M., Gupta, A., Wu, C., Silberberg, G., Luo, J., & Markram, H. (2004). Anatomical, physiological and molecular properties of Martinotti cells in the somatosensory cortex of the juvenile rat. *The Journal of Physiology*, *561*(Pt 1), 65–90. https://doi.org/10.1113/jphysiol.2004.073353

Wang, Y., Ye, M., Kuang, X., Li, Y., & Hu, S. (2018). A simplified morphological classification scheme for pyramidal cells in six layers of primary somatosensory cortex of juvenile rats. *IBRO Reports*, *5*, 74–90. https://doi.org/10.1016/j.ibror.2018.10.001

Wehr, M., & Zador, A. M. (2003). Balanced inhibition underlies tuning and sharpens spike timing in auditory cortex. *Nature*, *426*, 442. http://dx.doi.org/10.1038/nature02116

Welker, C. (1971). Microelectrode delineation of fine grain somatotopic organization of (SmI) cerebral neocortex in albino rat. *Brain Research*, *26*(2), 259–275.

Wernicke, C. (1969). The symptom complex of aphasia. *Proceedings of the Boston Colloquium for the Philosophy of Science 1966/1968*, 34–97.

Wilent, W. B., & Contreras, D. (2005). Dynamics of excitation and inhibition underlying stimulus selectivity in rat somatosensory cortex. *Nature Neuroscience*, *8*(10), 1364–1370. https://doi.org/10.1038/nn1545

Williams, L. E., & Holtmaat, A. (2019). Higher-Order Thalamocortical Inputs Gate Synaptic Long-Term Potentiation via Disinhibition. *Neuron*, *101*(1), 91-102.e4. https://doi.org/10.1016/j.neuron.2018.10.049

Williams, M. N., Zahm, D. S., & Jacquin, M. F. (1994). Differential Foci and Synaptic Organization of the Principal and Spinal Trigeminal Projections to the Thalamus in the Rat. *European Journal of Neuroscience*, *6*(3), 429–453. https://doi.org/https://doi.org/10.1111/j.1460-9568.1994.tb00286.x

Wimmer, V. C., Bruno, R. M., de Kock, C. P. J., Kuner, T., & Sakmann, B. (2010). Dimensions of a Projection Column and Architecture of VPM and POm Axons in Rat Vibrissal Cortex. *Cerebral Cortex*, *20*(10), 2265–2276. https://doi.org/10.1093/cercor/bhq068

Wise, S. P., & Jones, E. G. (1977). Cells of origin and terminal distribution of descending projections of the rat somatic sensory cortex. *Journal of Comparative Neurology*, *175*(2), 129–157. https://doi.org/https://doi.org/10.1002/cne.901750202

Woolsey, T. A., & Van der Loos, H. (1970). The structural organization of layer IV in the somatosensory region (S I) of mouse cerebral cortex. *Brain Research*, *17*(2), 205–242. https://doi.org/10.1016/0006-8993(70)90079-X

Wu, G. K., Arbuckle, R., Liu, B., Tao, H. W., & Zhang, L. I. (2008). Lateral Sharpening of Cortical Frequency Tuning by Approximately Balanced Inhibition. *Neuron*, *58*(1), 132–143. https://doi.org/10.1016/j.neuron.2008.01.035

Xu, H., Jeong, H.-Y., Tremblay, R., & Rudy, B. (2013). Neocortical Somatostatin-Expressing GABAergic Interneurons Disinhibit the Thalamorecipient Layer 4. *Neuron*, *77*(1), 155–167. https://doi.org/10.1016/j.neuron.2012.11.004

Xu, Q., Cobos, I., De La Cruz, E., Rubenstein, J. L., & Anderson, S. A. (2004). Origins of Cortical Interneuron Subtypes. *The Journal of Neuroscience*, *24*(11), 2612 LP – 2622. https://doi.org/10.1523/JNEUROSCI.5667-03.2004

Xu, X., & Callaway, E. M. (2009). Laminar specificity of functional input to distinct types of inhibitory cortical neurons. *The Journal of Neuroscience : The Official Journal of the Society for Neuroscience*, *29*(1), 70–85. https://doi.org/10.1523/JNEUROSCI.4104-08.2009

Xu, X., Olivas, N. D., Ikrar, T., Peng, T., Holmes, T. C., Nie, Q., & Shi, Y. (2016). Primary visual cortex shows laminar-specific and balanced circuit organization of excitatory and inhibitory synaptic connectivity. *The Journal of Physiology*, *594*(7), 1891–1910. https://doi.org/10.1113/JP271891

Xu, X., Roby, K. D., & Callaway, E. M. (2010). Immunochemical characterization of inhibitory mouse cortical neurons: three chemically distinct classes of inhibitory cells. *The Journal of Comparative Neurology*, *518*(3), 389–404. https://doi.org/10.1002/cne.22229

Xue, M., Atallah, B. V, & Scanziani, M. (2014). Equalizing excitation–inhibition ratios across visual cortical neurons. *Nature*, *511*, 596. http://dx.doi.org/10.1038/nature13321

y Cajal, S. R. (1891). *Sur la structure de l'écorce cérébrale de quelques mammifères*. Typ. de Joseph Van In.

y Cajal, S. R. (1911). Cajal S (1911) Histologie du systéme nerveux de l'Homme et des Vertébrés. *Paris: Maloine*.

Yamamura, D., Sano, A., & Tateno, T. (2017). An analysis of current source density profiles activated by local stimulation in the mouse auditory cortex in vitro. *Brain Research*, *1659*, 96–112. https://doi.org/https://doi.org/10.1016/j.brainres.2017.01.021

Yamashita, T., Pala, A., Pedrido, L., Kremer, Y., Welker, E., & Petersen, C. C. H. C. H. (2013). Membrane Potential Dynamics of Neocortical Projection Neurons Driving Target-Specific Signals. *Neuron*, *80*(6), 1477–1490.

https://doi.org/10.1016/J.NEURON.2013.10.059

Yamashita, T., Vavladeli, A., Pala, A., Galan, K., Crochet, S., Petersen, S. S. A., & Petersen, C. C. H. (2018). Diverse Long-Range Axonal Projections of Excitatory Layer 2/3 Neurons in Mouse Barrel Cortex . In *Frontiers in Neuroanatomy* (Vol. 12, p. 33). https://www.frontiersin.org/article/10.3389/fnana.2018.00033

Yamawaki, N., & Shepherd, G. M. G. (2015). Synaptic Circuit Organization of Motor Corticothalamic Neurons. *Journal of Neuroscience*, *35*(5), 2293–2307. https://doi.org/10.1523/JNEUROSCI.4023-14.2015

Yang, W., & Sun, Q.-Q. (2018). Circuit-specific and neuronal subcellular-wide E-I balance in cortical pyramidal cells. *Scientific Reports*, *8*(1), 3971. https://doi.org/10.1038/s41598-018-22314-9

York III, G. K., & Steinberg, D. A. (2011). Hughlings Jackson's neurological ideas. *Brain*, *134*(10), 3106–3113. https://doi.org/10.1093/brain/awr219

Yoshimura, Y., Dantzker, J. L. M., & Callaway, E. M. (2005). Excitatory cortical neurons form fine-scale functional networks. *Nature*, *433*, 868. http://dx.doi.org/10.1038/nature03252

Yu, L., Shen, Z., Wang, C., & Yu, Y. (2018). Efficient Coding and Energy Efficiency Are Promoted by Balanced Excitatory and Inhibitory Synaptic Currents in Neuronal Network . In *Frontiers in Cellular Neuroscience* (Vol. 12, p. 123). https://www.frontiersin.org/article/10.3389/fncel.2018.00123

Zeng, H., & Sanes, J. R. (2017). Neuronal cell-type classification: challenges, opportunities and the path forward. *Nature Reviews Neuroscience*, *18*, 530. https://doi.org/10.1038/nrn.2017.85

Zhang, W., & Bruno, R. M. (2019). High-order thalamic inputs to primary somatosensory cortex are stronger and longer lasting than cortical inputs. *ELife*, *8*, 1–22. https://doi.org/10.7554/eLife.44158